The content and stable isotopic composition of carbon in spherical micrometeorites

Thesis

The Content and Stable Isotopic Composition of Carbon in Spherical Micrometeorites.

A thesis submitted for the degree of
Doctor of Philosophy

by

Paul David Yates
B.Sc. Hons. (Leicester, 1986)
Cert.Ed. (Bath, 1987)

April 1992

Department of Earth Sciences
The Open University

The Content and Stable Isotopic Composition of Carbon in Spherical Micrometeorites.

A thesis submitted for the degree of
Doctor of Philosophy

by

Paul David Yates
B.Sc. Hons. (Leicester, 1986)
Cert.Ed. (Bath, 1987)

April 1992
Department of Earth Sciences
The Open University

For Sara

EX12

HIGHER DEGREES OFFICE

LIBRARY AUTHORISATION FORM

STUDENT: PAUL YATES SERIAL NO: _____

DEGREE: DOCTOR OF PHILOSOPHY

TITLE OF THESIS: THE CONTENT AND STABLE ISOTOPIC COMPOSITION OF CARBON IN SPHERICAL MICROMETEORITES

I confirm that I am willing that my thesis be made available to readers and maybe photocopied, subject to the discretion of the Librarian.

SIGNED: _____ DATE: 7/4/92.

Abstract

Micrometeorites are extraterrestrial bodies that have survived atmospheric entry to be found on Earth as grains <1mm in diameter. Of the annual flux of extraterrestrial material to the Earth *ca.*99% is supplied by the micrometeorites. The lifetime of the micrometeroids in the interplanetary medium in extremely ephemeral, but their population is maintained largely by ejection of particles from cometary nuclei and from collisional debris from the asteroid belt. As such, the micrometeorites are of fundemental importance to cosmogony, because they may provide the only means, at present, to directly study cometary material, and sample a far less biased cross section of the asteroid belt than conventional meteorites.

A static gas source mass spectrometer for carbon isotope measurements built in the Planetary Sciences Unit has been tested and shown capable of routinely analysing *ca.*1 nanogram of carbon (as carbon dioxide) to precisions of *ca.*±1‰. To enable this gain in sensitivity to be exploited, a sample preparation and carbon dioxide extraction system has been devised that typically imparts a total of less than 20 nanograms of extraneous carbon contamination to the samples. An advantage of the mass spectrometer is its ability to make accurate isotopic abundance measurements of the blank contribution for the purpose of making corrections to the analytical data. The instrument and inlet system has been applied to studies of micrometeorites >200∝m in diameter.

A procedure has been developed involving three analytical techniques (chemical/petrographic, X-ray diffraction and stable carbon isotope). Carbon isotopic analyses of multiple-sample aliquots of deep-sea, and individual Greenland and Antarctic micrometeorites has enabled the identification of components that are similar to those within the stony chondritic meteorites. More specifically, components have been revealed that may indicate a generic connection to primitive chondrites. Carbon isotopic characterisation of acid-resistant residues prepared from micrometeorite-rich Greenland cryoconite suggested that the micrometeorites contain pre-solar dust grains of silicon carbide, graphite and diamond, which provides an additional indication of the primitive nature of some micrometeorites. Experiments to produce micrometeorite analogues by pulse-heating microgram-sized samples of whole-rock meteorites showed that indigenous carbonaceous species can survive pulse-heating above their normal combustion temperatures. The overall conclusion of the investigation is that the flux of >200∝m micrometeorites is dominated by asteroidal material and that the atmospheric entry heating process is poorly understood.

Acknowledgements

My sojurn at the Open University and foray into the field of cosmic dust has bought me into contact with a variety of interesting and sometimes unusual people. The execution of the study described within this thesis has been a challenging (and sometimes distressing) time, but it is my pleasure to be able to acknowledge here all those colleagues and friends who have enabled me to endure the last four (or five?) years.

Firstly my thanks go to my supervisors, Colin Pillinger and Bob Hutchison, for both having the imagination (and sense of humour) to initiate this project and then see it through to its conclusion. I would especially like to express my gratitude to Ian Wright, who managed to wade through the early drafts of this thesis and still provide (largely) constructive criticism. I am especially grateful for his use of multi-coloured pens to heighten my enjoyment of deciphering his scribblings. The first six months of my research career were spent at the Natural History Museum; Terry, Frances, John, Steve, Don and Gordon are all acknowledged for their patience in explaining the workings of several intimidating-looking machines. In particular Valerie Jones contributed to my enjoyment of museum life (!) with her ubiquitous cheerful nature and fathomless store of museum scandal and gossip.

Working within the Planetary Sciences Unit makes apparently rational people behave in strange ways. It is difficult to be able to convey my individual thanks to all the members of the PSU, both past and present, but the following have helped to alleviate the day-to-day laboratory tedium and countless hours spent in T24 staring at blank sheets of paper. Richard is thanked for showing me how to clear the Mac room with a cunningly placed 'eggy-hummer', Sara R. for providing hours of entertainment guessing what she had eaten for lunch by examining the stains on her jumper, and Leon for initiating me into the technique of thesis-writing whilst *appearing* to be asleep at your desk (*i.e.* eyes closed, feet up and snoring). Andy is thanked for countless 'hob-nobs' and 'jelly babies', and for liasing with the local constabulary. In the early days Nathan and Alan are acknowledged respectively for the 'mail order' catalogue (my wife Sara still hasn't found a use for the 'lip-dick'.....) and 'top-tips' on the delivery of seminars and the use of abusive language in public houses. Special thanks must go to Simon for helping me to secure a mortgage by applying a marmite poultice

to my head ten minutes before my interview with the Building Society. Ian F. is gratefully acknowledged for his cryoconite collection efforts and fending off the furry-arctic-killer-frogs. Monica provided much helpful guidance in the laboratory and clean room, but I have yet to take her advice on the use of a firm kulfi (Mon - does Ian have to take pain killers afterwards?). Jez and Phil are thanked for their ridiculous haircuts and appalling fashion sense. Jason (Suede-head) deserves special recognition for prolonging the preparation of this thesis by super-glueing all my stationary to my desk and giving me a stomach upset after his conker-in-the-kettle jape. I am likewise indebted to the cheerful and happy-go-lucky O.U. estates men who were dispatched to sweep the transline roof after each time it rained. Their ability to convey such depth of resentment at being 'called out yet again' using an alarmingly wide selection of expletives supplied me with many hours of dictionary and thesaurus practice. Outside of the PSU, the 'Earth Science Squash Clique' (Phil, Jon, Ben, Tim *etc.*) are thanked for many hours of much needed thesis evasion. Phil is especially thanked for his frequent (and largely incorrect) discussions on the weather.

Throughout my academic career my family have provided constant support and encouragement in achieving my goals. My Mother, Grandparents, and in latter years, Step-Father, have all made sacrifices to ensure that I have been able to pursue my ambitions; this thesis is a reflection of your love and commitment. Over the past five years a great deal of this burden has been shared with my wife, Sara, and her family. Without her patience and unstinting support throughout its preparation, this thesis would not have been completed, and it is for this reason that I dedicate it to Sara.

Funding for this study was provided by the Open University and the British Museum (Natural History). I am also grateful to the Wolfson Foundation and the Meteoritical Society to allow me to collect Greenland cryoconite and attend the 52nd Met.Soc in Vienna.

Contents

Chapter 1: Introduction.

Chapter 2: The Analysis Protocol and Stable Isotope Mass Spectrometry.

Chapter 3: Major Element Chemistry and Mineralogic Studies.

Chapter 4: Evaluation of the Sample Handling Protocol and Attempts to Elucidate the Carbon Isotopic Composition of the Stepped Combustion Experiment Blank.

Chapter 5: Carbon Stable Isotopic Analyses of Multiple Aliquots of Deep-Sea and Individual Greenland and Antarctic micrometeorites.

Chapter 6: The Preparation and Analysis of Cryoconite Acid-Resistant Residues.

Chapter 7: Small Sample Bulk Meteorite and Pulse Heating Experiments.

Chapter 8: Summary and Further Work.

Appendices:

Appendix A1: Stepped Combustion Data.

List of Figures

List of Tables

List of Plates

Chapter 1

Introduction.

'Much careful research yet remains to be done along the lines of refining the methods of collecting , of analyses and separation of meteoritic from terrestrial dust, of seasonal and geographic distribution of fall, etc. Years must be devoted to the task , but the final results are of profound importance to astronomy and geology, as well as to meteorology and meteoritics'

H.H.Nininger (1940).

1.1. Transient phenomena: Harbingers of bad tidings?

Throughout time, movements in the heavens have held the attention of mankind. The repetition of each day, the rising and setting of the Sun, the monthly phases of the Moon and cycle of the seasons, coupled with the orderly movements of the stars and erratic wanderings of the planets, have provided the stimulus for early philosophers and scholars in their attempts to comprehend our place in the Universe.

Such predictable phenomena were benevolent; interpretation of the apparent movement of the Sun, and the length and direction of shadows cast by it, allowed man to measure time and chart the seasons. Furthermore, the meticulous observation of the celestial dome during darkness facilitated the evolution of the art of navigation by which he could further explore his environment. Notwithstanding this, such heavenly activity was perceived as being under the control of supernatural forces, and in particular any sudden and unexpected celestial event viewed as a malediction. In 1456 the spectacular appearance of Halley's Comet provoked Pope Calixtus III to issue a declaration against 'the Devil, the Turk and the Comet' (Moore and Hunt, 1990). The 1066 perihelion passage of Halley is depicted in the 'Bayeux Tapestry', and shows King Harold and his courtiers staring up at the comet in terror whilst across the

Channel, William of Normandy prepares for the forthcoming invasion of Britain (*e.g.* Tauber, 1979). Such events are not confined to ancient times, for as recent as 1970 Comet Bennett caused alarm in many Arab states as it was mistaken for a new Israeli weapon (Moore and Hunt, 1990).

Comets, however, are not the sole such 'transient phenomena' to which such attention is given, but their global audience tends to guarantee recognition in the history books. The arrival of meteorites (with frequently accompanying bolide) although often being a more locally witnessed event, are equally well documented and often cause equivalent, or even more distress. The earliest such reports are recorded on Egyptian paparus in *ca.* 2000 BC, and the Sacred Stone in Kaaba is probably a meteorite (Moore and Hunt, 1990). The oldest meteorite whose fall can precisely be dated fell in Ensisheim in Switzerland on the 16th of November 1492, where on its arrival the Roman Emperor Maximilian I ordered it to be placed in the local church where it still remains today, as he believed it represented an omen of divine protection against threat of Turkish invasion (*e.g.* McSween, 1987).

As comprehension of the Earths' place in the Solar System and the Universe has evolved , so has the realisation that these rare celestial occurences are far from being adverse, and indeed it would appear that the situation is now reversed. Witnessing the passage of a comet, the arrival of a meteorite or the experience of a meteor shower still remains one of the most spectacular and awe inspiring natural phenomena, but today such events are eagerly awaited by meteoriticists within the scientific community as each event heralds the potential delivery of extraterrestrial material to our planet. There are many theories as to the origin and evolution of the Earth and Solar System, but proving them is difficult because geologic activity on Earth has all but erased the initial stages of our planets evolution. It is only by the careful and painstaking characterisation of the extraterrestrial material that is delivered to us as a result of these 'transient phenomena', that we can ever hope to fully unravel, and comprehend, that crucial period in the life of our planet and the Solar System.

The discovery by Aumann (1984) of an infrared (IR) excess around the star α Lyrae (Vega) was amongst the most exciting astronomical events of recent years, as it was the first direct confirmation of the probable existence of a planetary system outside of our own. Subsequently, the other nearby stars β Pictoris, α Piscis Austrini and ϵ Eridani were also found to possess clouds of solid grains emitting strongly in the far

(IR) (*e.g.* Beichman, 1987), and recent detailed studies of IR data have revealed that possibly in excess of a further 100 other stars exhibit similar IR features (Backman and Paresce, 1992). These observations captured scientific and popular imagination and initiated a series of investigations by astronomers to locate the final prize; the location of a planet outside of the solar system. Such a task has pushed observational techniques to their limits, but both Bailes *et al.*, (1991) and Rasio *et al.*, (1992) have reported the prescence of such planetary companions orbiting the pulsars PSR1829-10 and PSR1257+12. Even though the identification of the first planet is now in doubt (Lyne and Bailes, 1992), and the origin and relation of such bodies to our solar system is poorly understood (*e.g.* Podsiadlowski *et al.*, 1991), such observations serve as a catalyst to learn more about how our own Earth and the other solar system planets formed, as it is only from this position that we can possibly begin to understand the evolution of any extraterrestrial planetary systems and then engage in what is probably the greatest pursuit for mankind: the search for life elsewhere in the Universe.

1.1.1. The flux of extra-terrestrial material to the Earth.

As the Earth moves around the Sun it is bombarded with extra-terrestrial material ranging from objects in mass from less than 10^{-12}g to over 10^{10}g. Typical encounter velocities between the Earth and this impinging material are 5 to 11kms^{-1} (Flynn, 1989), and in the first instance, if the object is to survive destruction upon impact with the Earths' surface, this energy must be dissapated by deceleration in the atmosphere. Meteors are the product of this interaction, their incandescent trails testifying to the frictional heating that results from this deceleration. By monitoring the frequency of meteors by visual, radio, radar and satellite techniques (*e.g.* Hughes, 1978), it has been possible to calculate the amount of extraterrestrial material the Earth accretes. Considering the differing methods used, and corresponding uncertainities involved in these calculations, it is remarkable that in each case a figure for the annual flux for the entire Earth of *ca.*10^{10}g has consistently been obtained (*e.g.* Whipple, 1967; Dohnanyi, 1971; Millman, 1975; Hughes, 1978; Thomas *et al.*, 1986). Of equal importance is in which size range the majority of this material arrives. Horz *et al.* (1975) calculated that for each square meter at the top of the atmosphere, the flux of material from the interplanetary medium (IPM) would be as follows; one 10$\propto$m diameter particle per day, three 100$\propto$m per year and three 1cm grains per 10^7 years. Considering giant meteoroids, Shoemaker (1977) estimated a flux of one >700m

diameter body every 300,000 years for the entire Earth. From these estimates it is apparent that the bulk of the material accreted by the Earth is in the form of the smaller particles, *i.e.* Hughes (1978), in a review of meteor studies, calculated that out of the *ca.* 1.6 x 10^{10}g that arrive each year, *ca.*99% lies within the 10^{-10} to 10^{1}g size range. Olsson-Steele (1988), using sensitive radar meteor detection methods and detailed modelling of height distribution, has enabled an even tighter constraint to be placed upon this flux, and has calculated that *ca.*85% of the total is within the 10^{-9} to 10^{-5}g range.

In view of such domination of the total flux by small particles, the neccessity to develop techniques to collect, curate and study these analytically challenging particles becomes obvious. Neglecting data aquired from Earth based remote observations and space probe visits to other planets, to date, the majority of our knowledge of the solar system is based on the results of work carried out on the extraterrestrial material that has been delivered to us by natural means. Such work has concentrated on the larger (>gram sized) objects, which represent less than 1% of the total available. The remainder of this chapter is divided into assessing the possible sources, nature and collection of the remaining *ca.*99%, and to facilitate this the term 'dust' is used and is defined (Brownlee, 1985) as particulate material that exists, or has existed, in the IPM as bodies smaller than 1mm in diameter.

1.2. Dust in Interstellar Space.

In 1823 H.W.M.Olbers wrote a paper entitled 'On the transparency of Space' in which he posed a remarkable paradox (*e.g.*Tauber, 1979). In attempting to calculate the total amount of starlight that reaches the Earth, he found that contrary to the overall darkness studded by numerous pinpoints of starlight we observe, the night sky should be flooded with light[1]. Despite making several incorrect assumptions in arriving at his result, to resolve the problem he correctly suggested that some sort of 'interstellar fog' was partly responsible for obscuring the starlight. Olbers was correct in assuming that the space between the stars is not quite a perfect vacuum, as subsequent astronomical

[1] Olbers was not in fact the first to have noticed this problem (commonly referred to as 'Olber's Paradox'); In 1744 the Swiss astronomer P.Loys de Cheseaux alluded to the same question in the appendix of his book on the comet of 1743 (*e.g.* Tauber, 1979).

observations have led to the identification of several components within it. Perhaps not surprisingly, considering its cosmic abundance, hydrogen (as H_2, H and H^+) dominates this ISM material, although other atoms and molecules of gas and solid 'dust grains' have been identified. Even though these grains are microscopic and lie hundreds of light years away (1 light year = 9.46×10^{12}km), astronomers have still been able to deduce a great deal about them, including their shape, size and chemical composition (*e.g.* Mathis, 1988). These properties are deduced by the various effects that dust exerts on the starlight which passes through it, and such observations of the ISM have also revealed that the dust distribution is not uniform, in places there are denser concentrations which are called 'interstellar clouds'. It is noteworthy here to mention that observations show that dust is not actually more abundant in these clouds; the ratio of dust to gas remains the same both inside and outside of them, with the dust constituting about 1% of the total by mass (Spitzer, 1968). The local interstellar gas density is one H_2 molecule for each cm^3 (Kerr, 1962), and assuming 1% mass is in solid particles, then the local ISM dust density is *ca.* 2×10^{-26} g cm^{-3} (Sandford, 1987), which translates into *ca.*10% of the total mass of the ISM (*e.g.* Harding, 1985).

Much of the recent work on interstellar dust has been concerned with formation and destruction processes and the chemical composition of the dust grains (*e.g.* Bailey and Williams, 1988). Such work has shown that interstellar dust is an extremely important component of the ISM as it is crucial in the heating and cooling process of clouds through gas-grain collisions and the emission and absorption of radiation. In addition, the solid grains are important in determining the gas phase composition of interstellar clouds, because they act as catalysts in reactions occuring on their grain surfaces. The chemical compostion of the dust itself has been deduced by examining starlight that has passed through it to produce the 'interstellar extinction curve'. In the last years several models have been developed to determine the composition of dust required to produce this extinction curve (*e.g.* Mathis *et al.*, 1977; Draine and Lee, 1984; Greenberg and Chlewicki, 1984), and many different dust components have been proposed, including solid carbonaceous materials (graphite, amorphous carbon), silicates, silicon carbide, metallic oxides and polycyclic aromatic hydrocarbons (PAHs). To compliment these observational interpretations, there has also been a considerable effort to replicate the observed spectra by laboratory simulations (*e.g.* Allamandola and Sandford, 1988), and although only being in its infancy, the results

of such work are both confirming the observations and facilitating a better insight into the chemical composition of the dust.

With respect to the physical dimensions of the interstellar dust, Trumpler (1930) found that it preferentially absorbed starlight at the blue end of the visible spectrum, thus indicating that the grains were smaller than the wavelength of red light (*ca.*0.7μm) and closer to that of blue (*ca.*0.4μm), although satellite based IR observations have shown some ISM dust exists as grains as large as *ca.*100μm (Hauser *et al.*, 1984). The light is also occasionally polarised, showing that the grains possess a non-spherical/elongated shape as they are capable of having a preferred orientation in response to interstellar magnetic fields to produce this effect (Heiles, 1976). Furthermore, light that manages to pass through regions of interstellar cloud show IR absorptions associated with the presence of the ices of water (H_2O), ammonia (NH_3), methane (CH_4) and carbon monoxide/dioxide (CO/CO_2). It would appear that the grains in the clouds are mantled with these ices, and the action of the cloud allows protection of such volatile material from the rigours of the ISM where exposure to cosmic/galactic rays would sputter it away. Although being shrouded in this way, UV light can still penetrate the clouds, and experimental work has shown that such irradiation of the ices is capable of initiating complex chemical reactions leading in turn to the formation of complicated organic molecules within the mantles (*e.g.* Williams, 1988). Incorporating all this information together allows models of the structure and chemical composition of the dust grains to be constructed and accordingly Figure 1.1 illustrates the structure and composition of the postulated interstellar grain.

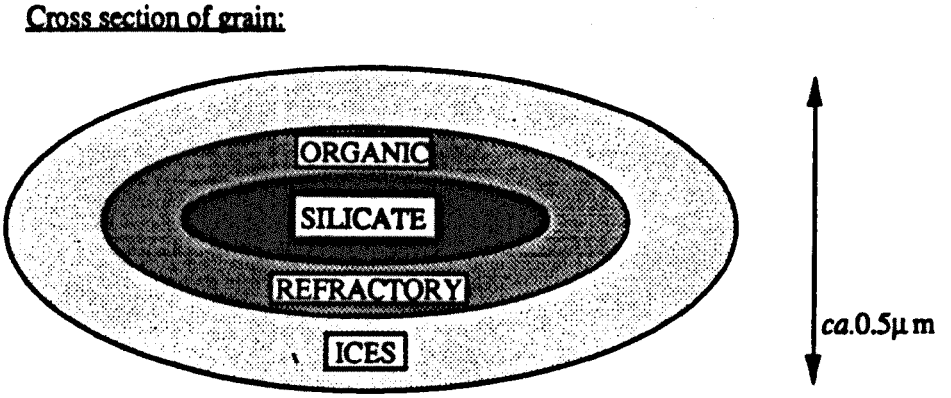

Component	Mass fraction	Composition
Silicates	0.20	'Amorphous' Mg, Si and Fe silicates
Organic refractory	0.25	'Complex organic' molecules composed mainly of H, C, N and O
Ices	0.55	Mainly CO and H_2O, but also NH_3, CH_4, CO_2 and H_2CO

Figure 1.1. A schematic illustration of an interstellar dust grain at the final stages of interstellar cloud condensation. This structure and composition is probably similar to that of the grains that seeded the pre-solar nebula (after Greenberg, 1988).

1.3 Dust in the Solar System

Proving the existence of dust in the IPM of the Solar System is easily accomplished by a simple observation of the sky shortly before sunset or after sunrise, where with reasonably clear conditions, a cone of light can be seen extending upwards from the horizon which passes through the constellations of the Zodiac to the other horizon. This is the 'zodiacal light' (or 'gengenschein') and was first observed in the 18th century by Cassini (*e.g.* Sandford, 1987). A later inspection of the solar corona by Van de Hulst (1947) revealed the presence of Fraunhofer lines[2] that led him to suggest that this light was the product of the Sun illuminating the dust that orbits between it and the Earth. Studies of impact micro-craters produced in mineral grains within lunar rocks by this dust show that the cloud is not a transient feature, and has been stable for at least the last *ca.*10^9 years (Morrison and Zinner, 1976; Pompeau *et al.*, 1977). Ney (1982) found that the spectra of the zodiacal light in the visible wavelengths matches that of the Sun, so illustrating that the grains are large compared to optical wavelengths (*i.e.* >1μm), and Hodge (1981) detected a slight reddening in this spectra showing the presence of grains as large as 100μm. Laboratory experiments on the scattering of light by small grains by Weiss-Wrana (1983) showed that the principal properties that

[2] Careful examination of the Sun's spectrum reveals that it is crossed by a large number of dark lines. These lines were discovered in 1814 by Fraunhofer and, accordingly, are known as Fraunhofer lines. Most of the lines are due to cool gases in the outer regions of the Sun absorbing certain of the wavelengths radiated by the interior (*e.g.* Muncaster, 1981).

are observed in the zodiacal light can be accounted for by opaque, irregular shaped particles in the size range 20 to 120μm. Direct evidence of the zodiacal cloud dust size range has been obtained by detailed examination of micro-craters in lunar rocks (*e.g.* Fechtig *et al.*, 1974) and in-situ measurements in space (Giese and Grun, 1976), and reveal that 80% of the zodiacal light can be explained by scattering from particles >10μm in size. Furthermore, satellite based IR observations (Dermott *et al.*, 1984) and direct space probe measurements (Leinert *et al.*, 1983) show that the dust cloud permeates throughout the Inner Solar System and at least out to 3 Astronomical Units (A.U.)[3] distance from the Sun.

When initially considering this dust it would not seem unreasonable as a first approximation to assume that it is the same as the material that is known to pervade the ISM, either left over as remnant dust after the formation of the solar system, or as material entering the solar system from the ISM at the present day. To address this hypothesis it is necessary first to briefly examine the origins of the solar system, and then to take a closer look at the present day situation in terms of its effect upon the dust population.

1.3.1. The origin of the Solar System.

The general scenario envisaged for the formation of the solar system is that the Sun formed by collapse of a region of interstellar gas and dust, and then some of this material formed an accretion disk (usually called the 'primitive solar nebula') from which the planets and many smaller bodies of the solar system were formed. Although only representing a simple overview, such a model as this appears to succinctly account for the formation of the solar system, but on closer examination there are a multitude problems inherent within it, and these have kept the debate of the exact mechanisms of solar system formation fuelled for over two centuries.

A fundemental problem is why an interstellar cloud would undergo collapse in the first instance as, unless some sort of pressure was applied to initiate the collapse, such a cloud would theoretically expand into surrounding less dense regions of the ISM. A possible explanation was offered when evidence for the presence of short lived

---

[3] 1 A.U. = 1.50×10^{11}m, and is defined as the distance betwen the Sun and the Earth.

radionuclides in early solar system material was found (*e.g.* Wasserburg, 1985). These radionuclides are produced in stellar nucleosynthesis, so any proposed model needs to allow for their formation within a star, ejection, and incorporation into the evolving solar nebula before they were lost through natural radioactive decay processes. In particular, the presence of ^{26}Al required that this process took place in less than 3 x 10^6years, and such a short time span led to the evolution of the 'supernova trigger hypothesis' by Cameron and Truran (1977). This model invoked that an interstellar cloud would exist close to a star which would then undergo supernova, and this would rapidly initiate the collapse of the cloud and at the same time seed the evolving nebula with the products of nucleosynthesis. However, subsequent detailed IR observations of interstellar clouds (*e.g.* Elmegreen, 1985) showed that many clouds contained 'cores' where the local gas and dust density was up to 30 times that of the bulk cloud, and more specifically, that more than half of these cores had a primitive stellar object at their centre. This finding did not fit with the supernova trigger hypothesis, as it was incapable of producing collapse within isolated regions of the interstellar cloud it was acting upon. In an attempt to reconcile these observations with the already discussed need to incorporate short lived radionuclides, Cameron (1984) constructed the following model. He postulated that instead of the supernova trigger, the cloud core formation collapse was initiated by injection of material from the shells of nearby ageing 'red giant' stars (see 1.6.1), and produced a model that utilised magnetic field lines associated with this ejected material to channel it into the cloud, whilst at the same time sweeping up cloud material into localised cores, which would then undergo further collapse to form the stellar objects. Such an event would also seed the clouds with the radionuclides, but with the red giant stars also being a major site for the condensation of solid dust grains (see 1.6.1), the primitive solar nebula would also be seeded with this distinctive material.

Which ever is the correct hypothesis, after the initial collapse of the cloud and the formation of the young Sun, the problem then becomes one of explaining the contemporary structure of the solar system both in terms of chemical composition and distribution of mass and angular momentum within it. Of the models developed, one in particular has proved to be flexible enough to accomodate these criteria and has remained popular (to a lesser or greater extent) ever since its conception by Laplace in 1796 (*e.g.* Tauber, 1979). His ideas have become the basis for the 'nebula theories' and the basic principles have survived to become the framework of most contemporary models (*e.g.* Wood and Morfill, 1988).

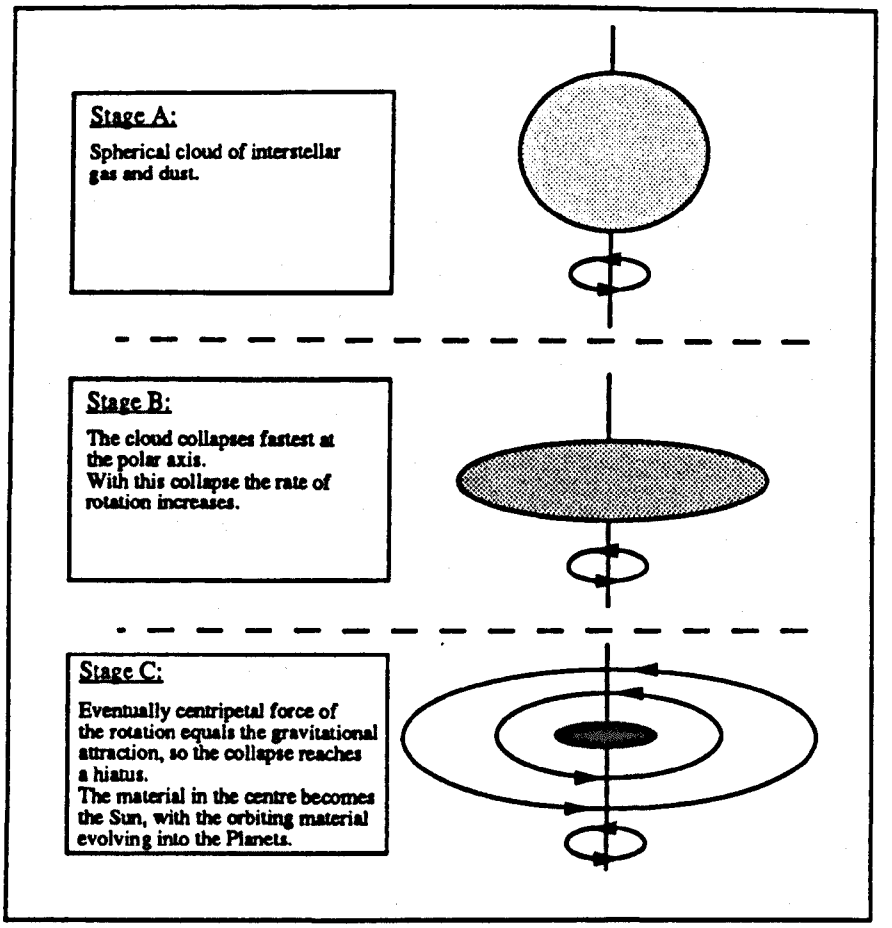

Figure 1.2. The initial stages of gravitational collapse of the pre-solar nebula. For a review of nebula models see Jones, (1985) and Wood and Morfill, (1988).

Figure 1.2 illustrates the initial development of this nebula. The cloud begins to collapse (moving from A to B), and does so fastest at the polar axis. The reasons for this are complicated but essentially are due to the relative interaction of gravitational and centripetal forces within the rotating material. The centripetal force is itself derived from the gravitational force, but because there is no rotation at the polar axis, there is in turn no centripetal force. Moving away from the axis the centripetal force increases, thereby reducing the overall gravitational force, so the collapse is slower. As the body shrinks further (B to C), its rate of rotation increases as angular momentum is conserved, until eventually the centripetal force equals that of the gravitational, so the orbiting material can move no further inwards. In this way material is left in stable circular orbits and it is from these rings of dust and gas that Laplace proposed that the planets were formed, with the Sun forming in the central region.

It is estimated that *ca.*10^{46} grains of interstellar dust were involved in the initial interstellar cloud that became the Solar System (Brownlee, 1987) so it is desirable to examine how the evolution of the nebula effected these grains to explore the possibility that they have survived to form the modern day zodiacal cloud. As such, a summary of the major evolutionary stages of a typical contemporary nebula model (the 'Kyoto Low Mass Nebular Theory' taken from Jones, 1985) is presented below:

(i) Stage 1; Contraction of the interstellar cloud.

(ii) Stage 2; Period of 'sedimentation'. (This involves growth of the dust grains after the turbulence associated with Stage 1 has died away. In this way it is possible to produce grains of millimeter size, thousands of times larger than the original ISM precursors).

(iii) Stage 3; As sedimentation proceeds then the dust sheet produced (on the equatorial region of Figure 1.2) begins to gravitationally break-up into *ca.*10^{12} solid 'planetisimals' each of mass *ca.*10^{15}kg (Safronov, 1969).

(iv) Stage 4; These planetisimals themselves then begin to accrete to form planets (*e.g.* Wetherill and Stewart, 1989).

(v) Stage 5; The young Sun, which has already begun internal nuclear reactions and has been shining for some time, suddenly begins to emit a powerful stellar wind (Herbig, 1977). This wind is essentially a plasma of large numbers of protons and electrons (with a smaller number of heavier ions) and has the effect of removing the remaining gas and dust back to the ISM.

The implications for the survival of presolar dust grains in the IPM would not appear good. Stage 5 effectively precludes that the dust observed today is that remaining from the initial solar nebula, so it would appear that the only pathway such dust can return to the IPM is if it can incorporated into a solar system body, remain effectively unchanged, and then be re-emitted at a later stage. Although such a complex sequence of steps appears unlikely, it is nethertheless feasible. During stages 2, 3 and 4, a proportion of the ISM grains aggregate together into larger bodies that will then in turn be able to survive Stage 5. Cameron (1973) estimated that clumps of interstellar grains of the order of 1cm in diameter could grow by the time that the infalling fragment of cloud reached the outer primitive solar nebula. This aggregation could take place because there was unlikely to have been any significant chemical alteration to the infalling grains until the late stages of the collapse, when the cloud becomes optically thick and ambient temperature rises, and with the icy molecules in the grain mantles not being at a chemical equilibrium, if the grains encountered each

other, there was a good chance that they would stick due to chemical bonding at the point of contact. The state of preservation and ultimate fate of these grains is dependent upon position within the nebula and exactly what size the bodies achieve. During the initial contraction the temperature within the nebula is controlled by a balance between radiative heating from the Sun and cooling to the ISM, and is therefore extremely variable depending upon position relative to the Sun and within the nebula with regard to the ISM/nebula interface. However, it is possible to generalise that a temperature gradient exists outwards with decreasing temperature from the Sun; dust within and in close proximity to the Sun will be vaporized, whilst in the outer regions of the solar system it will remain relatively unchanged. The final aggregation phases into planetisimals and planets (stages 3 and 4) bring a new set of possibilities for the fate of the dust. Neglecting collisional destruction, it is the size of the body to which the dust accretes to that is crucial for its survival, because generally speaking it is this parameter that controls the subsequent internal temperatures the body achieves, the rate of cratering it suffers (after initial accretion), and whether an atmosphere is retained. The internal temperatures are governed mainly by the decay of inherited short-lived radionucides, and if the heat thus generated is not able to be radiated away then it accumulates resulting in an elevation of temperature (*e.g.* McSween *et al.*, 1988). We know that planetary sized bodies underwent total melting and differentiation in this way, our own planet is graphic evidence of this. The smaller the body, the greater its surface area to mass ratio, so allowing increased efficiency in radiating away this energy. Whether melting occurs is also dependent to a certain degree upon other extraneous factors; such as the initial temperature of accretion and concentration of radionuclides, but it would appear that size is the controlling parameter.

The presence of an atmosphere is also of relevance as it could be argued that even if the inside of the body is heated then the outside will remain cool, thereby allowing the survival of pristine material at the surface. If the body can retain an atmosphere, the surface will be subjected to reworking by the action of erosion *etc.*, destroying its original character. In actual fact, this argument is of little relevance because if the body is large enough to have the gravitational attraction to hold an atmosphere, then it will probably also undergone internal melting and differentiation. However, the absence of an atmosphere does not guarantee that the surface will escape without any reworking; the face of our own moon testifies to the bombardment it suffered by impacting bodies even after initial accretion and differentiation. These impacts deliver a considerable

amount of kinetic energy to the surface rocks resulting in vaporization, melting, brecciation and formation of high pressure mineral polymorphs within them (*e.g.* Housen and Wilkening, 1982), and so again the survival of pristine material appears unlikely.

All this evidence points towards the conclusion that only the smallest solar system bodies that formed in the outer regions of the evolving nebula can harbour pristine ISM dust, as they would suffer only minimal internal heating, retain no atmosphere, and their small gravitational attraction and corresponding cross-sectional area reduces the chances of later bombardment. Of equal importance, this small gravitational attraction allows easy subsequent ejection from the bodies which is of paramount importance to be able to return the dust to the IPM unaltered.

1.3.2. Minor solar system bodies: Reservoirs of Pre-Solar material?

In examining the postulated retention of ISM dust it is necessary to view the grains as being composed of two distinct phases; refractory silicates and volatile ices. Intuitively it is easier to preserve the refractory phase as it is more resistant to both increases in temperature and mechanical abrasion, however, if retention of the ices is achieved then it can be assumed that the silicate phase has undergone only minimal alteration.

The asteroid belt lies between the orbits of Mars and Jupiter. Various lines of reasoning following an initial interpretation by Titius von Wittenburg in 1766[4] of the spacings between planets (*e.g.*McSween, 1987) suggest that they represent either planetisimals that failed to accrete into a planet or the remnant of one that has since been destroyed. Astronomical observations of the belt (there are now >3000 named asteroids) show a wide variety of shapes and sizes of bodies, ranging from spherical

---

[4] He noted a pattern in the spacings between the planets where;

$$r = 0.4 + (0.3 \times 2^n)$$

r = radius of the orbit.

n = numerical order of the planet outward from the Sun.

J.E.Bode used this rule to argue for a missing planet between Mars and Jupiter, and this relationship became known as the 'Titius-Bode law'.

(and therefore presumably melted/differentiated) ones with diameters of *ca.*1000km to irregular (unmelted) bodies with dimensions as small as *ca.*10km (Moore and Hunt, 1990). Spectrographic studies (*e.g.* Gaffey and McCord, 1978) show that they are predominately of silicate composition with little evidence of ices, indicating that they have lost their volatiles (at least at the surface).

Petrologic studies of meteorites would seem to substantiate these observations as they indicate that their major constituent components are the product of condensation from a hot nebula (*e.g.* Dodd, 1981). Additionally, there is evidence for secondary thermal and aqueous alteration within some meteorites (*e.g.* McSween *et al.*, 1988; Zolensky and McSween, 1988), so even if ISM grains could survive heating within the nebula before accretion, they would likely have been subsequently destroyed. This being said it has been possible to identify and isolate the most refractory components of the ISM dust parents (*e.g.* Anders, 1988; Zinner, 1988), but although the asteroids may still be a potential source for IPM dust of a differing nature, we must look elsewhere for the retention of ISM dust.

The comets are probably the most enigmatic bodies within the Solar System, in as much as although much work a has been carried out on determining their orbits and obtaining detailed spectral information from them, it is not possible to directly view cometary nuclei from Earth. Until recently , when in 1986 spacecraft flew through the coma of Comet P/Halley and passed in close proximity to the nucleus (Sagdeev *et al*, 1986; Hirao and Itoh, 1986; Reinhard, 1986), our understanding was limited to theoretical work and ground or satellite based observations of their coma and tail complexes. Questions as to the origin and formation of comets have been debated ever since the first hypotheses for the origin of the Solar System were conceived (for a historical review see Bailey *et al*, 1986 and 1990), but a watershed with regard to the problem occured when Whipple (1950a) presented a 'dirty snowball' model for the cometary nucleus. He proposed that the nucleus was constructed of a mixture of 'ice' and 'rocky' (silicate) dust and correspondingly represented very pristine solar system material that had somehow managed to escape the rigours of inner solar system nebula heating and planetary formation processes. Since the conception of this model, the debate as to the exact nature of comet nuclei and cometary origin processes has continued, with the evolution of the 'rubble-pile' model (Weissman, 1986) of a more loosley bound agglomeration of ice and dust, and the 'icy-glue' model of Gombosi and Houpis (1986) which attempted to explain the spaceprobe observations of Comet

Halley's nucleus and suggested that refractory boulders up to several tens of meters in diameter were 'glued' together by a much finer grained ice-dust mixture. With regard to cometary origin, there have been arguments presented as to whether comets are actually of a solar system origin, or if they represent captured material from interstellar clouds as the solar system moves through inter-galactic space (Clube and Napier, 1984).

The spacecraft that visited Halley carried a plethora of scientific hardware, and included instruments to analyse the chemistry of the dust grains emitted from the nucleus. The data thus aquired have not only shown the model of Whipple to be largely correct, but have also opened up many new intriguing questions as to the nature of the nucleus (Huebner and McKay, 1990). The dust was found to be of three main types; grains composed of silicate only, of silicate plus 'organics' (predominately ices of C, H, O and N) and those of 'organics' alone, and in relative abundances as shown in table 1.1.

Abundance (% of events measured)			Key
Silicate	Silicate/Organic	Organic	
33	33	33	1
20	40	40	2
10	70	6	3*
	28	72	4

* The remaining 14% were difficult to interpret.
(1) Langevin *et al.*, (1987).
(2) Clark *et al.*, (1986).
(3) Solc *et al.*, (1987).
(4) Jessberger *et al.*, (1988).

Table 1.1. The relative abundances of cometary dust types as detected from in-situ measurements of Comet P/Halley.

The different values given by the various authors in table 1.1 are mostly due to different definitions of the particle types, but common to all is the clear evidence that the cometary dust is a mixture of CHON-rich and silicate-rich material in highly variable proportions. It would appear that not only has the refractory silicate component of the ISM dust survived, but also the observed 'organics' are likely to represent the original volatile dust mantles. In addition, the observations revealed that

the nucleus was irregular in shape and only a few kilometers is size, this small size and non-spherical shape suggesting that the body has suffered little internal heating. Interpretation of the data has since revealed that the dust component is chemically very primitive and is closer to the composition of the Sun than even the carbonaceous and unequilibrated ordinary chondritic meteorites (Grun and Jessberger, 1990).

The most important criteria to address in searching for a suitable locality for comet formation is preservation of the ices, and if a Solar System origin is correct, then formation is limited to areas beyond Jupiter, as the initial nebula accretion temperatures inside of this precluded the survival of ices, but exactly how far beyond is still a question of debate (Rickman and Huebner, 1990). Within the nebula models comets are held to be small planetisimals that approached the young planets closely enough to have their orbits perturbed, but not close enough to be captured. In this way they were removed from the main Solar System and escaped incorporation into a planet or further inter-planetisimal accretion. Present day observational data on the orbits of comets indicate that most lie in a spherical shell well beyond Pluto (Oort, 1990), and this shell (or 'cloud') is postulated to contain 10^{12} - 10^{13} members (Weissman, 1990). Examination of the postulated protoplanetary disks around nearby stars (see 1.1) shows that the role of comets in the evolution of planetary systems may have been underestimated. Telesco and Knacke (1991) have found that the dust within the disk around β Pictoris shows a sriking similarity to that of Comet P/Halley, so suggesting a cometary origin for the dust, and circumstellar gas flowing inwards to the young star (Bruhweiler *et al.*, 1991) can be explained most readily by invoking a high flux (10-100 each year) of 'star-grazing' comets that release large amounts of gas on their perihelion passages. Consequent re-evaluation of the role of comets has shown that if such clouds are common (although a IR search of 17 nearby stars proved negative (Stern *et al.*, 1991)), then as much dust could be locked into comet clouds as there is in the entire ISM (Stern and Shull, 1990).

In conclusion it would appear that the comets may indeed present the almost perfect vehicle for the preservation of the ISM dust that seeded the presolar interstellar cloud. It is remarkable to consider that comets not only offer the chance to further study the refractory components already identified in meteorites, but also the more volatile ones that probably have not survived elsewhere. Until such a time that direct sampling of a comet nucleus is possible (Schwehm, 1989; Huebner,1990), the study of the dust released from comets that have been perturbed from 'cold storage' within the Oort

cloud to the inner Solar System, is the only way to examine this cosmogonically irreplaceable material. Equally there is no doubt that this cometary input of dust to the IPM constitutes an important reservoir (see 1.4), but of even greater importance it is necessary to examine the interaction of such dust with the present day Solar System environment to assess the possibilities for successful capture of the material by the Earth.

1.4. Dust in the Solar System today.

The solar system was born out of a dust laden cloud, but events that immediately followed its formation led to the expulsion of any dust and gas that had initially escaped incorporation into the evolving solar system bodies (section 1.3.1). Even though the primordial dust was thus removed (although the comets may have retained some relatively unaltered material as discussed in 1.3.2), observations today show the IPM remains dusty. The combined action of the Sun and planets still make the IPM an extremely inhospitable environment for such material (*e.g.* Dohnanyi, 1978). In the first instance, the radiation pressure of the Sun remains strong enough push all particles with diameters less than *ca.*1μm from the Inner Solar System, and whilst investigating such effects Poynting (1903) discovered a secondary action of this radiation that is instrumental in the removal of larger bodies. He examined the consequences of absorption and re-radiation of solar radiation upon the motion of bodies within the Solar System, and discovered this interaction caused a tangential drag, which in turn gave rise to a decrease in the orbiting bodies angular momentum. In this way the orbit of the body would decay, eventually causing it to spiral into the Sun. This phenomena, later confirmed and quantified by Robertson (1937), and subsequently known as the Poynting-Robertson (P-R) effect, acts upon all orbiting bodies, but because it is relatively weak (Russell, 1937, estimated its effect as *ca.*0.5 kg m^{-2}) is more pronounced in small bodies where the surface area/mass ratio is greatest. Russell (1937) also calculated that all masses of stony material of less than 2.5m in diameter that were originally orbiting at the same distance as the Earth would have fallen into the Sun within the lifetime of the Solar System, and likewise all particles below *ca.*6mm in diameter been absorbed from as far as the orbit of Neptune. Under such action it seems feasible that the IPM dust within the inner Solar System today represents primordial dust that is only today evolving under P-R drag from the outer regions. Harwit (1964) suggested that the same mechanisms that operated to

expel the cometary nuclei from the Inner Solar System would have also put dust into similar orbits, and it is this material that is now returning under P-R drag. Unfortunately the model fails because the P-R effect is not the only limiting factor for dust lifetime in the Solar System, as the gravitational fields of the planets are also efficient in the removal of dust in their immediate vicinities; our own planet has been shown to be effective at capturing dust (*e.g.* Gustafson and Misconi, 1986; Jackson and Zook, 1988).

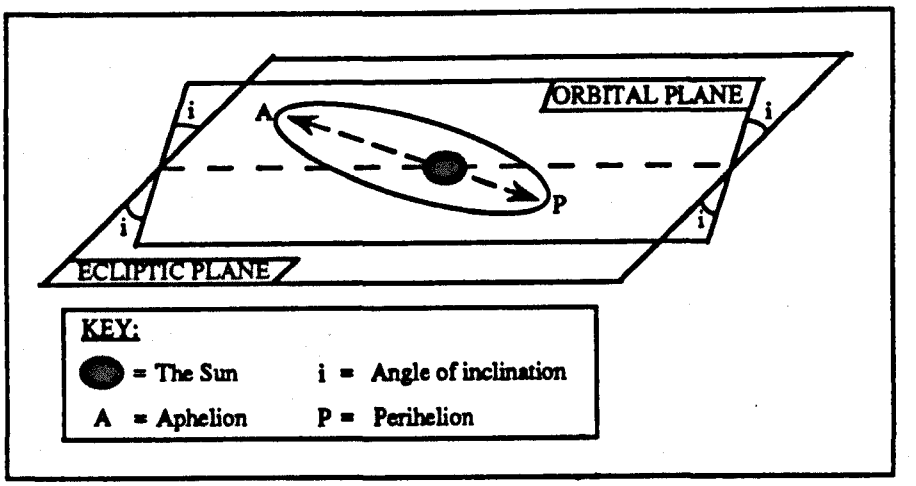

Figure 1.3. A schematic to illustrate the orbital elements of an object moving in the gravitational field of the Sun (after Dohnanyi, 1978).

P-R drag not only results in the decay of an orbit with respect to its distance to the Sun, but also reduces its eccentricity and inclination (see figure 1.3), so after a period of P-R influence the dust describes increasingly circular orbits close to the ecliptic plane, and it is hard to believe that such dust could then manage to escape the huge gravitational fields of the outer Jovian Planets as it evolves into the Inner Solar System. Inter-particle collisions further limit the lifetime of IPM dust and on astronomical timespans is the most important factor for consideration; typical lifetimes dictated by collisions are only *ca.* 10^4 to 10^6 years (Grun *et al.*, 1985), and this is not long enough for dust to evolve under P-R drag from the outer Solar System. From this evidence it is apparent that the IPM dust not only requires constant replenishment, but its sources must be in close proximity to any observed dust, because even though the mechanisms to transport dust through the IPM exist, dust lifetimes are prohibitive in allowing long term evolution.

1.4.1. Contemporary dust sources within the inner Solar System.

In searching for potential sources for the IPM dust, and with particular reference to that within the inner Solar System where collection by Earth is possible, there would appear to be only a limited number of candidates. The capture of fresh ISM dust would not appear to be feasible mechanism; in the first instance the density of the ISM in the local region is too low to supply the zodiacal cloud (Hodge, 1981), and even by taking into account the movement of the Solar System through the ISM Sandford (1987) calculated that the corresponding flux is still at least two orders of magnitude too low. Even accepting that it is possible that there may be a limited input of ISM dust to the zodiacal cloud, there are problems with its capture. Observations of neutral gas in the solar vicinity suggest that the Solar System is moving relative to the local ISM at a velocity of *ca.*20km s^{-1} (*e.g.* Gustafson and Misconi, 1979). As a result any ISM dust approaching the Solar System will be travelling at such a high relative velocity that only a close encounter with the Sun (and its gravitational field) would enable successful capture, and such a close passage to the Sun would undoubtedly be catastrophic (Harwit,1964). Gustafson and Misconi (1979) investigated the interaction of such approaching grains with the solar wind and interplanetary magnetic field, and concluded that some streaming of ISM dust into the Solar System does occur, but were not certain to what extent. Recent work by Brophy (1991) examining impact craters on the Long Duration Exposure Facility (LDEF) satellite has indicated that a proportion of the impactors were travelling at velocities in excess of the Solar System escape velocity, indicating that material from the ISM does indeed pass through the IPM. The situation may not have always have been as at present, because when the Solar System is passing through an interstellar cloud, the major dust source then may infact be the ISM (Newman and Talbot, 1976), but usually, as at the present, the major suppliers are sources within the Solar System. As a result it appears the IPM dust must be supplied by Solar System bodies, and considering the gravitational problems of ejecting material from planetary sized bodies (*e.g.* Urey and Craig, 1953), and although it has been suggested that the Sun itself may supply a limited number of sub-micron refractory particles (Hemenway *et al.*, 1972), the minor bodies provide the most likely candidates, thereby narrowing down the choice between the asteroids and comets. It is noteworthy to mention that the ring systems of Jupiter, Saturn, Uranus and Neptune could represent a considerable reservoir of dust; the rings of Saturn alone contain *ca.*3 x 10^{22}g of dust (Cuzzi *et al.*, 1984) which is more than enough to

supply the needs of the zodiacal cloud, but the feasibility and dynamics of ejection of such material to the IPM have not been investigated (Sandford, 1987).

Inter-asteroidal collisions have long been evoked as the ejection mechanism by which meteorites begin their journey to Earth (*e.g.* Wetherill, 1985), and equally have been suspected as being a source of IPM dust. Piotrowski (1953) closely examined the mechanism and probability of asteroidal collisions and concluded that their observed size distribution within the belt show that collisions have dominated their history, and also that such activity could supply the majority of the dust required to maintain the IPM dust population. The formation of cometary dust tails was first discussed by Bessell (1836) and confirmation of the link between comets and IPM dust occured as early as the 1860s when the annual meteor streams of the Leonids and Perseids were first associated specifically with their parent comets (Bailey *et al.*, 1986 and 1990). In 1820, Drago had recognised that the light from a comet is mostly scattered sunlight (*e.g.* Grun and Jessberger, 1990), and concluded that the tail must have a considerable dust content, but the question as to exactly how much dust the comets supply to the IPM has been debated ever since (*e.g.* Delsemme, 1976; Fechtig, 1982; Whipple, 1987). Even after the spacecraft visits to Halley, the question has not been fully resolved as although it proved possible to obtain comprehensive data on dust size distributions and chemistry, absolute determinations of the total dust production proved problematical (Grun and Jessberger, 1990). Additionally, it is not only the individual comet production rates that are required to solve the problem, but the overall cometary input. In contrast to the asteroids, which can be assumed to provide a relatively steady flux of dust to the IPM through collisions, it is probable that the total cometary input varies considerably, depending upon the number, size, and age of comets as they are perturbed into the Inner Solar System (Delsemme, 1976). The recent observations of IPM dust by the Infrared Astronomy Satellite (IRAS) (Dermott *et al.*, 1984), a satellite based IR telescope (Neugebauer *et al.*, 1984), show dust bands within the IPM that can be directly connected to an origin from the asteroid belt (Low *et al.*, 1984) and also to cometary orbits (Sykes *et al.*, 1986), thereby confirming these two as IPM dust sources, but highlighting the problem as to which is the major supplier.

1.4.2. Why is asteriod dust of interest?

The possible importance of comet dust in cosmogony has been previously discussed in 1.3.2, but if a proportion of the dust being collected by the Earth is of asteroidal origin, then this is of equal precedence. There would appear to be no reason why such asteroidal dust is any different from the asteroidal material collected at the Earth in the form of meteorites, however, on closer examination it appears that the meteorites represent a highly biassed sampling of the asteroid belt. Spectrophotometric studies of meteorites and asteroids allow direct linkage of the distinct meteorite chemical classes (as deduced by laboratory study) to parent asteroids, based on simularities in albedo, IR reflectance, radiometry, polarimetry and speckle interferometry (*e.g.* Gaffey and McCord, 1978). The results of these studies are shown in figure 1.4. Although only suggestive, they serve to illustrate the apparent disparity between the relative abundance of meteorite types arriving at the Earth with their probable parent body distribution within the asteroid belt.

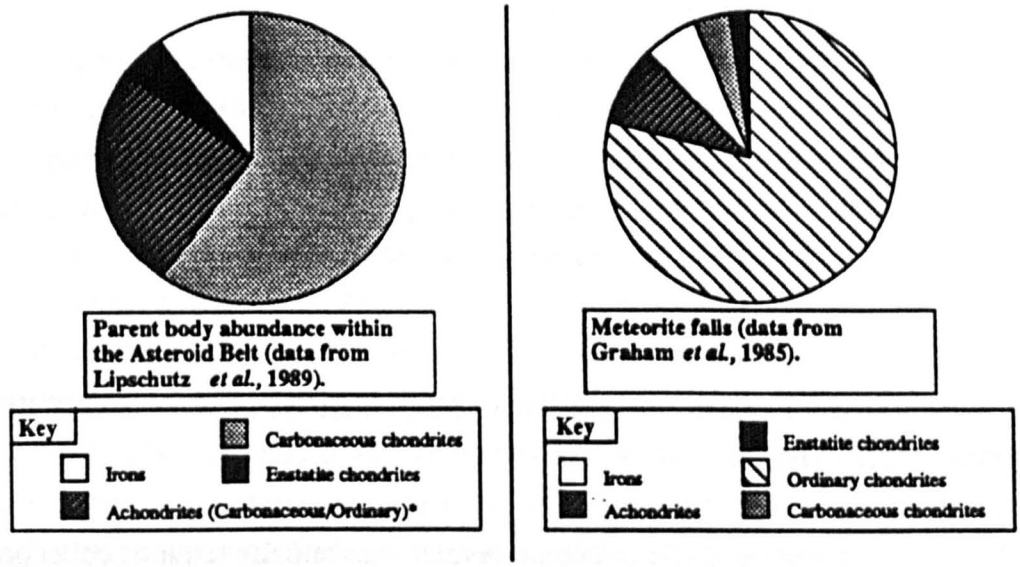

Figure 1.4. A comparison between the abundance of meteorite types (see 1.6.3) that are observed as 'falls' to their corresponding parent body abundance within the Asteroid Belt. (* The meteoritical association of the S-class asteroids is undetermined, but connections have been suggested to the stony-irons, ordinary chondrites and 'carbon-less' carbonaceous chondrites, but at the present, the stony-irons are favoured - Bell, 1991)

Such a comparison substantiates the observation that meteorite collections afford only a restricted sample of the belt, because they are expelled from areas where orbital resonance with Jupiter initiates asteroid collision and then rely on an almost unique set of further gravitational perturbances to deliver the meteorite to Earth (Wetherill, 1985). On the contrary, dust produced within virtually any position within the belt and under the influence of P-R drag, can evolve into an orbit suitable for Earth collection (Dohnanyi, 1978; Flynn, 1991), and in this way the dust gives a more representative view of the asteriod belt.

1.4.3. Conclusions.

Meteorites have been the focus of the study of extra-terrestrial material for many decades (reviews of much of this work are provided by Dodd, 1981 and Kerridge and Matthews, 1988), and as a result almost all our understanding as to origins and particularily the early evolution of the Solar System stem from this work. It is nethertheless apparent by studying meteorites alone, that we might be attempting to comprehend this crucial period based on only a fraction of the total material potentially available. In view of this, the study of dust assumes an even greater importance. Not only may such work provide the sole means of examining cometary, and thereby IPM/primordial dust, but dust arriving at the Earth from the asteriods not only compliments the meteorites, it potentially supplies an unbiassed and more representative sample of the asteriod belt.

1.5. The collection and analysis of extraterrestrial dust particles.

Direct analysis of extraterrestrial dust initially requires collection of particles and their subsequent return to the laboratory where suitable analytical procedures can be applied. When considering collection there would appear to be two options; either to attempt collection in directly from the IPM or alternately to isolate any accreted dust from the Earth's surface.

1.5.1. Space collection.

Intuitively the most straightforward approach to dust collection is simply to expose a surface to the IPM, and then after a period of time return it to Earth and examine the surface for the particles that will impinged on it during its sojourn. Such a collection would not have to be made at a great distance from the Earth, as long as collection was made in Earth orbit at an altitude greater than a few hundred kilometers, to avoid the orbiting anthropogenic debris (*e.g.* Kessler and Cour-Palais, 1978). The results of such studies are not only of interest in terms of the flux and type of material encountered, but with the design of future satellites and manned spacecraft/stations in mind, the damage caused by IPM dust to these surfaces has also been of considerable interest. As a result of this there has been substantial effort in both executing experiments specifically designed for this purpose; *e.g.* Gemini (Hemenway *et al.*, 1964), Skylab (Hallgren and Hemenway, 1976; Nagel *et al.*, 1976) and LDEF (Clark *et al.*, 1984). Additionally, investigations have been carried out on a variety of retrieved spacecraft surfaces which were not specifically designed for such purposes; Mercury (Hemenway and Linscott, 1964), Surveyor (Brownlee *et al.*, 1971), Apollo (Cour-Palais *et al.*, 1972), Skylab (Brownlee *et al.*, 1974) and Solar Max (Kessler *et al.*, 1985).

These experiments have proved extremely useful in evolving spacecraft design and in calculating the total flux of dust encountered, but have shed little light on the chemical composition or sources of the material. The problem with this collection mechanism is the sudden deceleration upon impact with the collector surface causes melting and vaporization of the impactor and associated crater formation. For absolute flux studies this is an advantage because all extraterrestrial dust impacts produce a crater (the impact velocity being *ca.*3kms^{-1} minimum[5]), whilst terrestrial contaminants in low Earth orbit possess lower velocities and as such are non-crater forming. However, attempts to determine the chemical composition of the impactor have resulted in only limited success(*e.g.* Horz *et al.*, 1983; Schramm and McKay, 1986).

---

[5] This occurs when a dust particle approaches the collector at the minimum velocity possible (the Earths' escape velocity) and impacts the trailing edge of the collector vehicle whilst on a trajectory that is parallel to the collector vehicles' orbit (*e.g.* Brownlee, 1985).

Development of capture cells allowing non-destructive collection and associated orbit determination of impactors (*e.g.* Mackinnon and Carey, 1988 and references therein) would appear to rectify this situation, but preliminary studies on the proposed capture medium, silica aerogel, reveal that for stable carbon isotope studies contamination may be prohibitive (Gibson *et al.*, 1991). It is evident that for the study proposed here, involving chemical and stable carbon isotopic characterisation of the dust particles, it is necessary to look towards alternative methods of sample collection.

1.5.2. Dust collection on Earth.

It is apparent from the discussion of space collection efforts in the previous section that all dust particles entering the atmosphere possess kinetic energies sufficient to cause total vaporization if deceleration occurs on a short enough time scale. However, impinging dust grains are typically decelerated over a distance of several kilometers at altitudes of about 100km, and because the atmospheric pressure at such altitudes is so tenuous (*ca.*10^{-3} mb, *e.g.* Weast, 1987) this deceleration is relatively gentle. In direct contrast to space collections, the frictional heat generated may be small enough to prevent melting of the incoming particles (Opik, 1937; Whipple, 1950b, 1951; Fraundorf, 1980; Love and Brownlee, 1991). Essentially, the small size of the dust particles means that any heating experienced is uniform throughout, which is in contrast to larger meteoritic bodies where temperature gradients can be sustained with molten exteriors existing alongside cool interiors. The fate of each individual is dependent upon several variables, but mainly the mass of the grain and its velocity and angle of incidence with the atmosphere. Love and Brownlee (1991) numerically modelled solutions for >50,000 such impacts of dust (between 10μm and 1 mm in diameter) with the atmosphere using random velocities and angles of incidence. It was found that of the particles which survived total vaporization, only *ca.*1% of those <70μm were completely melted, rising to 50% within the 70μm to 300μm range, and above 300μm less than 1% survived total vaporization.

1.5.3. Atmospheric collections.

Once the micrometeorites have been decelerated over several kilometers at altitudes of about 100km, they settle under gravity towards the surface of the Earth and

depending upon their size and density, typically have a residence time in the upper atmosphere (>20km) of between 1 and 60 days (Kasten, 1968). An interesting effect of this deceleration mechanism is that, on average, the spatial density of particles infalling through the atmosphere below *ca.*100km is enhanced over the flux in space by six orders of magnitude (*e.g.* Brownlee, 1978), and so provides an ideal opportunity for collection. The major difficulty with atmospheric collections is that of terrestrial contamination, and as a result of this, the protocol for atmospheric collections has been to collect at as high an altitude as possible, therefore presumably above wind blown terrestrial dust. Early collections were made by ballon (Fireman and Kistner, 1961) or by recoverable sounding rockets (Hemenway and Soberman, 1962), but the ballons were generally limited to altitudes of only a few kilometers, where terrestrial wind blown dust heavily dilutes the extraterrestrial material, and the sounding rockets, although achieving altitudes of tens of kilometers, only enabled the exposure of small (*ca.*<10cm^2) collection surfaces for short periods of time (*ca.*1 minute), so the potential for collection was poor. In addition to these problems, such early collection efforts suffered from contamination problems both during the construction of capture cells and on recovery from the ballon or rocket (*e.g.* Parkin and Tilles, 1968). Contemporaneous collections are made by aircraft flying at altitudes of 18 to 20km and the collection plates are exposed for several hours of flying time, so typically sample *ca.*80,000m^3 of air (Brownlee *et al.*, 1976). To overcome the problems of contamination, the construction and examination of the capture cells is carried out in specially constructed clean rooms with scrupulously clean equipment (*e.g.* Sandford, 1987). Actual collection on the aircraft is by impact onto exposed collector plates coated with silicon oil positioned under the wings. However, this inertial impaction techique leads to a considerable bias in the size of particles collected, since small particles (with large area to mass ratios) being strongly coupled to to the air flow, follow flow lines around the collection surfaces and are thus lost. In contrast, the larger particles possess sufficient inertia to cross flow lines and impact onto the surface. In addition, the differential infall rates of particles effect their collection, with a further bias existing towards the smaller grains because they fall more slowly through the atmosphere and so have a higher spatial concentration. Combining these together results in the collection method being extremely efficient at collecting particles in the 2 to 50μm size range; below this the grains flow around the collectors and above it the high fall speeds mean that very few large particles are collected.

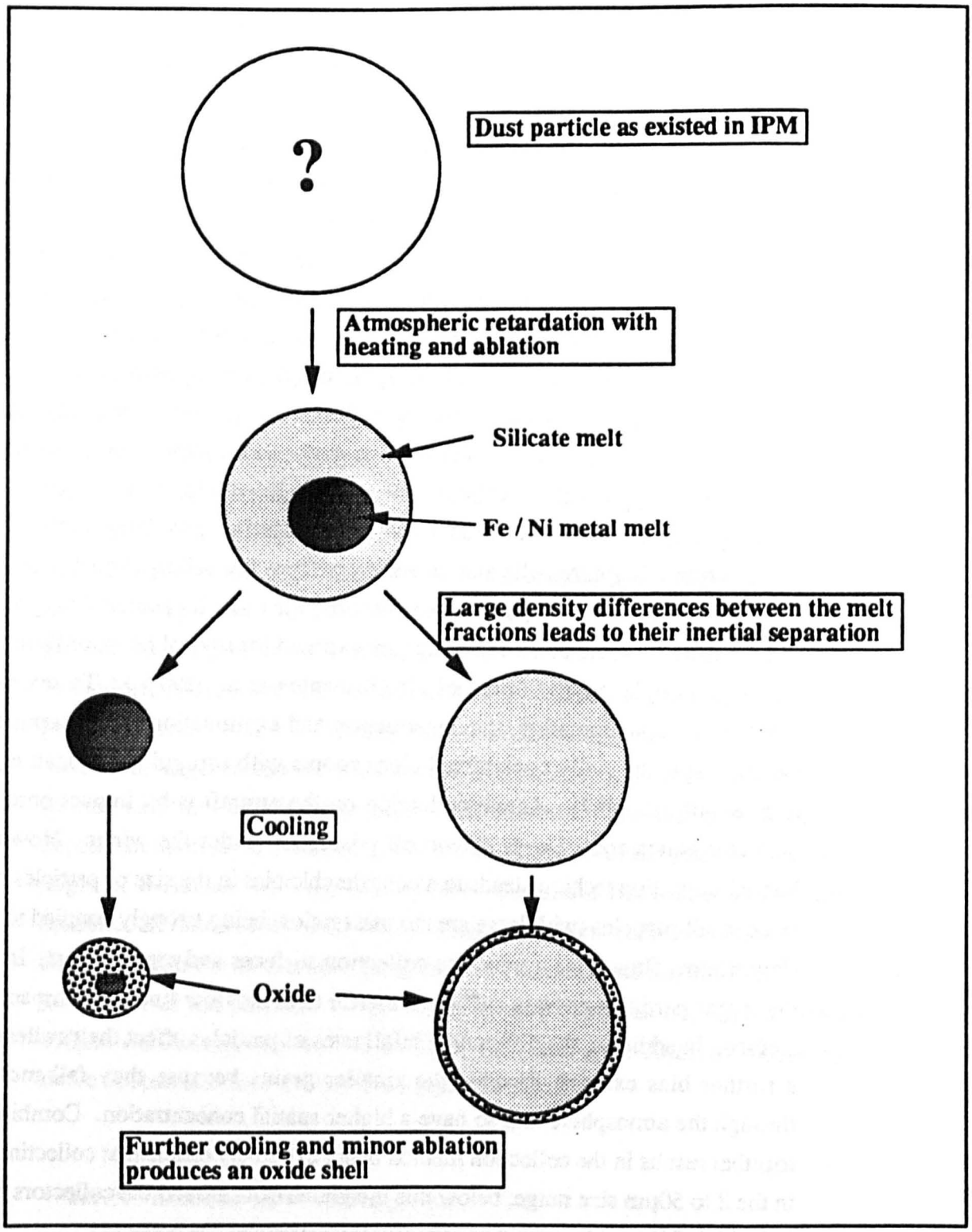

Figure 1.5. A schematic for a hypothetical set of events leading to the production of the distinctive spherical morpholgy of the micrometeorite shown within plate 1.1.

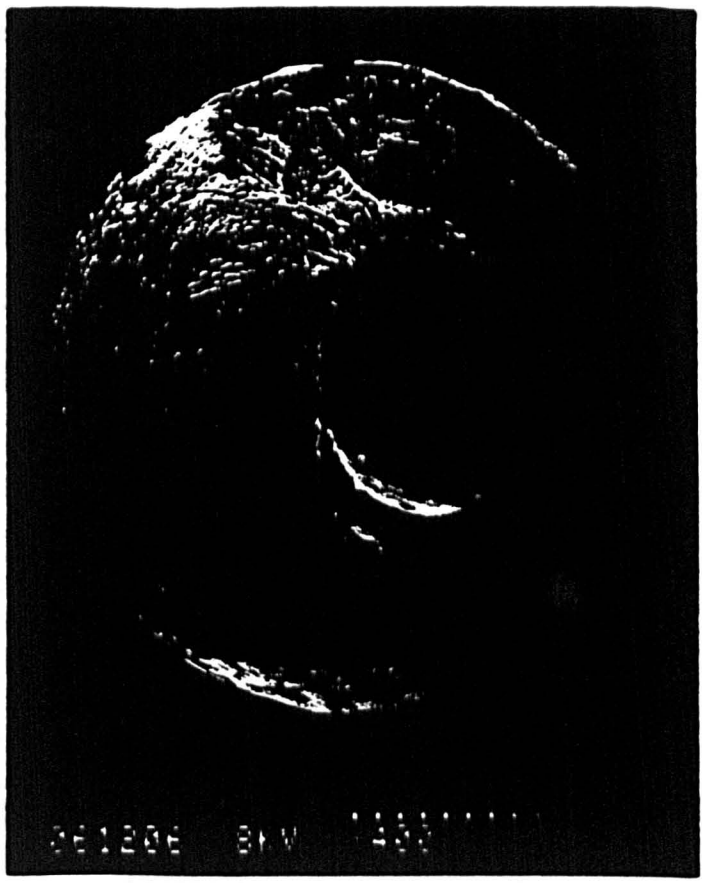

Plate 1.1. The typical morphology of an extraterrestrial dust particle that has suffered total or partial melting. This micrograph illustrates the characteristic shape which led to their naming as 'cosmic spherules' by Murray and Renard (1884), who were the first scientists to isolate these particles from deep-sea sediment and recognise their extraterrestrial nature.

1.5.4. Surface collections.

Extraterrestrial particles that survive entry into the atmosphere eventually reach the Earths' surface where they become mixed with an enormous complex of terrestrial particulates. Isolating and collecting the extraterrstrial material is a daunting task, but successes have been achieved by either confining investigations to particles with distinctive physical properties, or by looking for localities where either concentration mechanisms operate, or that occur distant from sources of terrestrial contamination.

An example of a micrometeorite that was collected on the basis of its morphology is presented in plate 1.1. These spherical particles are most likely produced by melting during atmospheric retardation (as explained in the schematic diagram in figure 1.5), but their morphology, coupled to the formation of iron oxides and corresponding magnetic nature of the particles, facilitates relatively easy identification and collection from the terrestrial environment. Since the discovery of this type of dust particle by scientists examining deep-sea oceanic sediments collected during the 1872 to 1876 voyage of HMS Challenger (Murray, 1876; Murray and Renard,1884), they have been isolated from a variety of diverse terrestrial environments, and a summary is presented in table 1.2.

Locality / Type of deposit	Reference*
Ocean sediment.	Murray, (1876).
Manganese nodules.	Murray, (1876); Finkleman, (1972).
Beach sands.	Marvin and Einaudi, (1967).
Desert sands.	Fredrikkson and Gowdy, (1963).
Roof tops.	Shima and Kimoto, (1966).
Greenland Ice.	Fireman and Langway, (1965); Maurette *et al*, (1986).
Antarctic Ice.	Schimdt, (1964); Harvey and Maurette, (1990).
Tertiary sediment.	Hunter and Parkin, (1961).
Palaeozoic salt deposits.	Mutch, (1964).

* References given represent either the chronologically first example of a positive identification of the melted particles, and if more than one reference is available, then a more comprehensive example may also be included

Table 1.2. Terrestrial environments where spherical micrometeorites have been isolated.

Buddhue (1950) gives an excellent review of collection efforts spanning from 1819 to 1950, whilst Schimdt (1965) and Parkin and Tilles (1968) cover the frenetic dust collection attempts of the 1960s. Murray and Renard (1884) discovered these morphologically distinctive melted micrometeorites by examining magnetic residues extracted from deep-sea sediments, where reduced terrestrial input of dust has enhanced the concentration of the extraterrestrial component to levels conducive for

collection. Magnetic raking of sediments has been used in more recent times to collect particles (*e.g.* Brownlee *et al.*, 1979), but there are several severe disadvantages with this approach. Most importantly, only those particles that are ferro-magnetic are collected, limiting particles to those grains that have experienced melting/ablation to form iron oxides, or to those with a high native-iron concentration. Additionally, the seawater surrounding the particles tends to etch the particles, and although weathering in the deep-sea oceanic environment is poorly understood, several workers, whilst undertaking petrologic surveys of collected particles, have noted weathering effects; *e.g.*, enhancement of the Fe/Si ratio (Brownlee *et al.*, 1980), dissolution of Mg-rich cores of olivine crystals and depletion of the bulk sample Ca and Al content (Brownlee, 1981) and alteration of concentrations of light rare earth elements (LREE) and certain other trace elements (Misawa *et al.*, 1989).

The recognition that *ca.*10% of the collected spherules were only partially melted (Brownlee, 1981), and the discovery of totally unmelted (probably extraterrestrial) particles during a painstaking examination of >2,500 oceanic particles (Brownlee *et al.*, 1980), provided the impetus to search for other collection environments that avoided magnetic collection protocols and enjoyed improved preservation potential.

1.5.5. Cryoconite deposits.

Cryoconite was discovered by Nordenskiold in 1870 (Buddhue, 1950), when during a journey 30 miles inland over a portion of the Greenland Icecap he noted that wherever the snow from the previous winter had melted away there remained a fine grey dust. He named this dust *kryokonit* (literally,'ice-dust'), but this has since been Anglicized to 'cryoconite'. During the 1980s an examination of the temporary glacial melt lakes and streams that form annually on the Greenland ice sheet, showed them to contain concentrations of the melted spherical type of extraterrestrial dust several orders of magnitude greater than those found in deep-sea sediments (Maurette *et al.*, 1986). These cryoconite deposits contain extraterrestrial dust particles that have fallen onto the icesheet and then become concentrated by seasonal meltwater runoff, much the same way as placer deposits of gold and diamond *etc.* are found in stream beds. Cryoconite collection is by a simple water suction technique from the pools and streams, and so removes the bias from the magnetic methods used on deep-sea deposits. In comparison to the oceanic sediments these streams and pools have the

advantage that their beds are solid ice and the only terrestrial dust contamination is wind blown. This is illustrated in section 6.2, where a comparison of the concentration of micrometeorites >200μm in diameter within a typical cryoconite deposit has been made to deep-sea sediment, and the results show the cryoconite to contain at least an order of magnitude higher dust concentration than the most enriched sediment analysed. However, one potential disadvantage of the cryoconite deposits is that the seasonal melting is associated with an algal bloom, and although the filaments of the algae act as a filter to trap and concentrate the dust, they are a potential source of contamination (see chapter 3). Examination of the collected particles have revealed that not only do they contain samples which are better preserved than those already isolated from oceanic deposits (Maurette *et al.*, 1987), but also an (unquantified) number of unmelted particles of types not seen before (Robin *et al.*, 1990). In common with deep-sea collections it is relatively easy to isolate melted spherules based on their morphology, but more importantly, spherical particles within the 200-500μm size range, which are exceedingly rare in oceanic deposits, are extractable with little effort. Identifying the unmelted particles is more problematic; optical characteristics alone do not serve as reliable selection criteria and it is only by subsequent detailed analytical work (*e.g.* noble gas content, Sarda *et al.*, 1991, or mineralogical characterisation, Steele, 1991) that their extraterrestrial nature can be confirmed.

Since the discovery of cryoconite in Greenland, similar deposits have been located both in Antarctica (Harvey and Maurette, 1990) and the Northern Canadian Territories (Robin *et al.*, 1990). In addition to these deposits, both melted and unmelted micrometeorites have been collected by the *in-situ* melting of Antarctic ice, where Maurette *et al.*, (1991) isolated *ca.*7500 probably unmelted and *ca.*1500 melted extraterrestrial particles of >100μm in diameter from *ca.*100 tonnes of ice at a locality near Cap Prudhomme in Antarctica. These samples extracted from the ice of Antarctica appear to be the least contaminated available to date, Robin *et al.*, (1990) discovered that whereas the Greenland samples show chemical evidence of their exposure to algal micro-organisms, the Antarctic analogs do not show any evidence of weathering or alteration.

1.5.6. Selection of particle types for carbon isotope studies.

In the choice of particle types most suitable for analysis there were several selection criteria to consider;

a) Whether samples are representative of the micrometeroid flux as a whole.
b) Confidence of extraterrestrial origin.
c) Availability of samples (ease of collection).
d) Suitability for analysis for stable carbon isotopes in terms of carbon content and terrestrial contamination.

Perhaps most importantly, the peak of the micrometeroid mass distribution range as measured by *in-situ* space and meteor studies (and discussed in section 1.1.1.) occurs in the microgram size range. Microgram sized particles entering the atmosphere are most likely to be heated to above their melting points (*e.g.* Love and Brownlee, 1991), and so correspondingly, the most representative particle type would be the spherical (melted) samples, but intuitively, such samples would have lost the majority of thier original carbon inventory. With respect to carbon content in particular, the smaller, largely unmelted, particles collected by the high flying aircraft would appear to be better candidates. Their altitude of collection is evidence to their extraterrestrial nature, and detailed mineralogical studies have shown them to be rich in carbonaceous species; *e.g.* amorphous carbon and carbides (Bradley *et al.*, 1984), aromatic hydrocarbons (Allamandola *et al.*, 1987), Fe and Mg carbonates (Tomeoka and Buseck, 1986) and poorly crystalline graphitic carbon (Rietmeijer and Mackinnon, 1985). Blanford *et al.*, (1988), using a microbeam analysis technique, directly determined the average carbon concentration within 'chondritic' atmospheric particles to be equal to *ca.*7.7wt%. However, there are several severe disadvantages (in addition to not representing the most abundant IPM particles) that render these atmospherically collected particles unsuitable for analysis. Firstly, the silicon oil used on the collector plates has been shown to produce contamination problems, evident in major element chemistry (*e.g.* Brownlee,1978; Schramm *et al.*,1989; Thomas *et al.*, 1990) and volatiles, including carbon (Carr *et al.*, 1986a; Hartmetz *et al.*, 1991a). Even without these contamination problems, the small size of the atmospherically collected particles (<50μm in diameter) means that even with such high carbon contents they only yield picogram amounts for analysis. At present this is not sufficient to allow analysis using stepped combustion

by static vacuum mode mass spectrometry (see chapter 2) with the neccessary precision to isolate indigenous species.

The large (*ca.*100μm) unmelted micrometeorites from Greenland Cryoconite and Antarctic Ice would appear to be the ideal candidates for analysis. Not only have they been spared the melting episode that produced the distinctive morphology of their similar sized spherical counterparts, but their relatively large size means that in contrast to the <50μm diameter unmelted samples collected in the atmosphere, they could provide enough carbon (*ca.*100ng) for isotopic analysis. However, isolation of unmelted particles from either oceanic sediments (Brownlee, 1980) or the ice of Greenland and Antarctica (*e.g.* Maurette *et al.*, 1986; 1991), has proved extremely laborious and largely dependent upon the experience of the individual collector. In particular, because of the similarity of the large unmelted extraterrestrial particles to terrestrial dust, until the relevant analytical procedures have been applied (see 1.5.5), proof of an extraterrestrial provenance cannot be determined. This raises the problem that sample manipulation and concomittant organic contamination associated with implementing the required analytical procedures would render analysis for indigenous carbon isotopes pointless. In contrast, the distinctive spherical morphology of the more strongly heated particles is direct testimony to the atmospheric ablation process, and good proof of an extraterrestrial origin. This being said, King (1982) showed that contemporary industrial processes can produce analogues almost identical to the extraterrestrial spherical particles, but as long as the samples are collected distally from such sources, this problem is not prohibitive to using their morpholgy as an indicator of extraterrestrial provenance.

As noted previously, the survival of indigenous carbon within the spherical particles would appear unlikely, with only the more refractory phases (*i.e.* graphite, diamond and carbides) being possibly resistant to the pulse heating experienced. But a preliminary study of stable carbon isotopes within analogous deep-sea particles by Wright *et al.*, (1988) revealed that indigenous carbon components probably do survive to some extent, and additionally, recent petrographic work (Klock and Beckerling, 1991) has shown that *ca.* 25% of spherules collected from Greenland are only partially melted (this had been previously estimated at only *ca.*10% by Brownlee, 1981). Both of these observations suggest that carbonaceous species could either be retained in unmelted areas of the spherical particles, or do actually partially survive the ablation/melting process. The large size of the spherical particles (*i.e.* 50 to 1000μm)

means that even if their overall carbon concentration is low in comparison to the totally unmelted samples, their large masses will translate into yields of carbon sufficient for analysis by current static vacuum mass spectrometric techniques (*e.g.* a 200μm diameter spherule with only 0.2wt% carbon concentration will yield *ca.*17ng for analysis).

1.5.7. Conclusions.

For the reasons outlined in the previous section it was decided to schedule the spherical (partially of totally melted) micrometeorites for analysis, but in the final selection of the samples, a further important factor needed to be contemplated. In order to assess contamination levels from all the possible collection sites it was additionally decided to analyses a suite of spherules encompassing deep-sea deposits and both Greenland Cryoconite and Antarctic Ice samples.

1.6. Stable carbon isotopes and micrometeoroids.

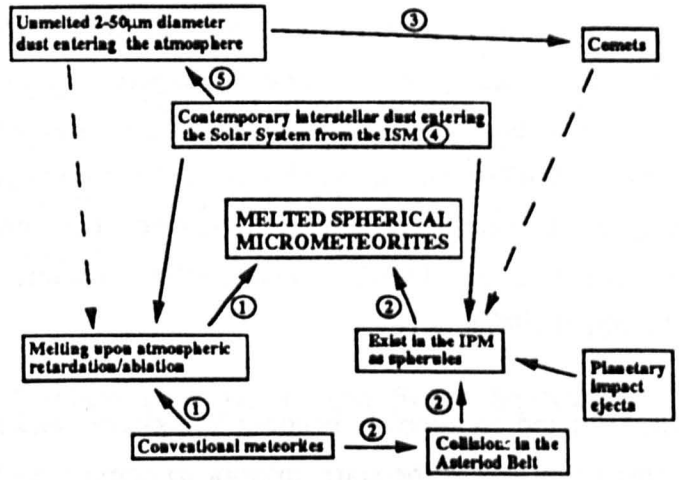

(1) Brownlee *et al.*,(1984).
(2) Parkin *et al.*, (1977).
(3) Bradley and Brownlee (1986).
(4) Brophy, (1991).
(5) Gustafson and Misconi, (1979).

Figure 1.6. A schematic diagram of the possible inter-relationships between the various probable reservoirs of extraterrestrial dust and associated processes as discussed in the first part of this chapter.

Carbon is the fourth most abundant element in the Solar System after hydrogen, helium and oxygen, and is one of the most abundant elements in the observable Universe (Cameron, 1982). Its ability to combine with itself to form long chain molecules gives it a chemistry more diverse than any other element. The aim of the following section is to attempt to summarise the stable carbon isotopic nature of the dust reservoirs within figure 1.6, and to facilitate any interpretations of the isotopic results presented within chapters 5 and 6.

1.6.1. Carbon isotopes in interstellar (pre-solar) dust.

Studies as to the nucleosynthetic origin of the stable isotopes of carbon indicate a history that is extremely complex (*e.g.* Trimble, 1975; Audouze, 1977), requiring varied astronomical sites for their production. In the simplest picture, ^{12}C is a 'primary' fusion product, forming in first generation stars by the stellar processing of ^{4}He (Penzias, 1980), whereas ^{13}C is 'secondary', formed by burning within the carbon-nitrogen-oxygen (CNO) cycle in later generation stars (Bethe, 1939). Such reactions lie at the center of a network of interrelated cycles, the relative rates of which are controlled by ambient stellar conditions, with the production of the stable carbon isotopes mainly within stellar interiors, novae, supernovae and red giant stars. The ensuing chemical evolution of the ISM in terms of stable isotopes is complicated due to the variety, spatial distribution and relative input from these sources, but only mass loss from red giants provides a continuous input, ejecta from novae and supernovae is more sporadic in nature (*e.g.* Dearborn *et al.*, 1978; Penzias, 1980; Wannier, 1980; Clayton, 1985; Pagel 1987).

Ageing stars expand and cool to become 'red giants', and it is this scenario that allows elements from within the stars' interior to convect to the surface, cool, and condense into solids (*e.g.* Iben and Renzini, 1983). Depending upon its life history, the surface of a red giant may be rich in either carbon or oxygen. In the latter case the oxygen atoms react with silicon and any metal atoms that are available to form silicates, and because of the relatively higher number of oxygen-rich red giants these silicate grains should constitute the major proportion of the ISM dust produced. In a carbon-rich example, condensation occurs in a variety of forms, including amorphous and graphitic carbon, carbides and possibly diamond (Pillinger *et al.*, 1989). After formation within the red giants in this way, the grains are expelled to the ISM by a

variety of pathways, and if by (super)novae, the associated shock experienced by the particles provides another possibility for diamond formation.

Theoretical calculations indicate that the isotopic nature of carbon within a star that has undergone the CNO cycle approaches a $^{12}C/^{13}C$ ratio of *ca.*4 (Dearborn, 1977). In practice, through incomplete CNO burning, this ratio does not reach its lowest level; spectral observations of red giants show $^{12}C/^{13}C$ ratios of between 5 and 51 (Dearborn, 1977). Once within the ISM, and particularily inside interstellar clouds, processing of these grains may take place, so further chemical fractionation must be considered. Within the cloud environment it appears that the dust fraction will be relatively enriched in ^{12}C, this being due to ion-molecule reactions of the type shown below that can proceed with very small activation energies (ΔE), a characteristic which is necessary because of the low temperatures (*ca.*10-100K) existing within the clouds (Watson *et al.*, 1976).

$$^{13}C^{+} + {}^{12}CO \rightleftharpoons {}^{12}C^{+} + {}^{13}CO + \Delta E$$

These reactions ultimately lead to an increase of ^{12}C in the dust, as the CO is less capable of further reaction than the radical C^{+} ion. Accurate determination of ratios within clouds has proved difficult, *e.g.* $^{12}C/^{13}C$ ratios ranging from *ca.*20 to 90 have been obtained by Matsakis *et al.*, (1976), although with corresponding large uncertainties (typically 1 sigma = ±10). Recently Hawkins and Jura (1987) presented a review of determinations of ISM $^{12}C/^{13}C$ ratios and concluded that the value for the local ISM is 43±4.

1.6.2. Carbon isotopes in the Solar System.

1.6.2.1. The Planets.

Measurements of carbon stable isotopes in the Solar System are dominated numerically by analyses of terrestrial samples. The combination of geological activity and a complex biosphere on the Earth contribute to a rich variation of isotopic compositions within organic, inorganic and elemental carbon species, but in spite of this, the range of $^{12}C/^{13}C$ ratios obtained range only between *ca.*87 to 93 (Murata *et al.*, 1967; Silverman and Oyama, 1968; Hoefs, 1987; Fisher *et al.*, 1990), and is small

in comparison to the galactic variations (see previous section). The average for the 'bulk' Earth, from studies of magmatic rocks and diamonds, is believed have a $^{12}C/^{13}C$ ratio of approximately 89 (*e.g.* Hoefs, 1987).

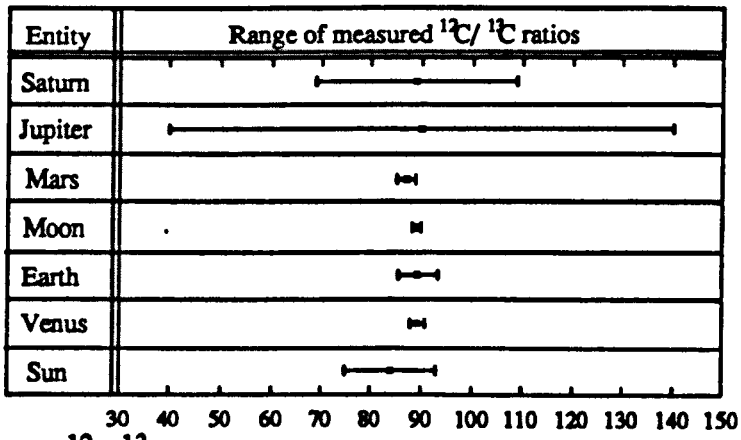

Figure 1.7. The $^{12}C/^{13}C$ ratios of some solar system objects (Epstein and Taylor, 1970; Hall,1973; Nier *et al.*, 1976; Combes *et al.*, 1977; Istomin *et al.*, 1980; Coutin *et al.*, 1983; Hoefs, 1987)

If the whole Solar System is examined then a somewhat wider range is encountered. Figure 1.7 illustrates the $^{12}C/^{13}C$ ratios measured for a variety of Solar System objects. Values for the inner planets lie within the terrestrial range, and although the outer gas giant planets have proven more difficult to determine and hence display a greater spread in values, they also lie within error of the inner Solar System value. It would appear that the overall Solar System exhibits a $^{12}C/^{13}C$ range between 84, that of the largest carbon reservoir - the Sun, and 89, the average for the remainder.

1.6.2.2. Meteorites.

Meteorites are defined here as extraterrestrial objects that arrive on Earth, having previously existed in the IPM as bodies larger than 1mm in diameter. Most such bodies are thought to represent fragments of asteroids that evolve into Earth crossing orbits by a combination of collision and subsequent gravitational perturbations (Wetherill, 1985).

Meteorites are traditionally classified according to their contents of metallic nickel-iron and silicates into three groups; the irons, stony-irons and stones. Figure 1.4

illustrates the corresponding observed type distribution of meteorites that have been observed to fall and have subsequently been collected and categorized. The system of Van Schmus and Wood (1967) forms the basis of the scheme in contemporary use, where meteorites are assigned to a chemical group on the basis of their major non-volatile elements and specific trace element abundances (see table 1.3). Examination of table 1.3 shows that the stony meteorites are split into two main groups, the achondrites and chondrites. The chondrites generally contain millimetre sized silicate spheres called 'chondrules', whereas the achondrites lack these chondrules and are also chemically dissimilar to the chondrites (*e.g.* Dodd, 1981). This being said, one group of chondrites (the CI1 carbonaceous chondrites) also lack chondrules, but this is a legacy of extensive hydrothermal alteration after their formation (Dufresne and Anders, 1962; Bunch and Chang, 1979), and their bulk chemical composition is similar to that of the other carbonnaceous chondrites. The achondrites, on the other hand, lack chondrules because they have undergone geological processing on their parent bodies to produce melted, chemically differentiated meteorites (Mason, 1962; Gast and Hubbard, 1970). In addition to the chemical classification, stony meteorites are assigned to a petrologic type on the basis of the degree of observed chondrule-matrix intergrowth, equilibration of constituent minerals and other textural and mineralogical criteria (Van Schmus and Wood, 1967).

STONES		STONY-IRONS	IRONS
Chondrites	Achondrites		
Carbonaceous: CI CM CO CV CR Ordinary: H L LL Enstatite: EH EL	HED group: Howardites Eucrites Diogenites SNC group: Shergottites Nakhlites Chassigny Aubrites Angrites Ureilites Lunar	Lodranites Mesosiderites Pallasites	IA, B, C IIAB, C, D, E IIIA, B, C, D, E, F IVA, B

Table 1.3. Meteorite chemical classification based on the scheme devised by Van Schmus and Wood, (1967), and modified by Wasson, (1974).

Carbon is present within meteorites in a variety of forms including organics (both solvent extractable (*e.g.* Briggs, 1963) and macromolecular (*e.g.* Kvenolden *et al.*, 1970)), amorphous elemental carbon (*e.g.* King *et al.*, 1969), graphite (*e.g.* King, 1936), diamonds (*e.g.* Lipschutz, 1962), carbides (*e.g.* Craig, 1953), carbonates (*e.g.* Dufresne and Anders, 1962) and in solid-solution within metals (*e.g.* Deines and Wickman, 1975). Isotopic studies (reviewed by Pillinger, 1984) show bulk values for the meteorites with $^{12}C/^{13}C$ ratios of 90±4, but the isolated phases are typically characteristic of individual meteorite groups and hence can be utilised to elucidate genetic links (see table 5.1).

1.6.2.3. Comets.

Determinations of the $^{12}C/^{13}C$ ratios in comets have, until recently, suffered from analytical problems that have limited their accuracy. Early measurements were made based upon the intensity of the C_2 emission band in observed comet spectra, but were plagued by low spectral resolution, low signal-to-noise ratios and overlapping NH_2 features (*e.g.* Vanysek and Rahe, 1978; Lambert and Danks, 1983). Studies using the C_2 band indicated a possible ^{12}C enrichment over Solar System values with $^{12}C/^{13}C$ ratios of 100±20 (Owen, 1973), 115(+20, -30) and 135(+65, -45) (Danks *et al.*, 1974) and 110 (+20, -30) (Vanysek, 1977) being obtained. It is apparent , however, that the correspondingly large errors associated with each measurement also make them consistent with Solar System values.

More recent data, obtained using the CN emission band that occurs within a more straightfoward part of the spectrum, would appear to indicate an enrichment in ^{13}C, with values for Comet P/West of 50-60±15 (Lambert and Danks, 1983) and Comet P/Halley of 65±9 (Wycoff *et al.*, 1989). In particular this latter measurement represents the highest resolution and probably most accurate determination to date.

Unfortunately, the data obtained by the *in situ* measurements of Comet P/Halley by the Giotto mass spectrometers showed a range of measured $^{12}C/^{13}C$ ratios between 1 and 5100, and due to possible machine interferences (especially with the low values due to the $^{12}CH^+$ ion) it is difficult to draw any firm conclusions to confirm the spectral observations (Grun and Jessberger, 1990).

1.7. Research objectives.

The overall aim of this study was to analyse and document the carbon components present within the micrometeorites. To achieve this aim, a dual approach was implemented. In the first instance, micrometeorite samples were sheduled for analysis as individual particles using stepped combustion, to assess their bulk carbon isotopic signatures, and to attempt to resolve any indigenous carbonaceous components (chapter 5). Secondly, acid-resistant residues of Greenland Cryoconite were analysed (chapter 6) in an attempt to determine whether any meteoritic, cometary or pre-solar components could be isolated which then could be attributed to the extraterrestrial dust fraction of the cryoconite.

A previous preliminary examination of stable carbon isotopes in micrometeorites by Wright *et al.*, (1988) highlighted two main problems with the respect to the successful analysis of individual samples. Firstly, terrestrial contamination was a limiting factor in the interpretation of the results, and secondly, this problem was exacerbated by the inability of their instrumentation to accurately resolve such contamination from any indigenous components. With respect to the these problems, a considerable amount of effort decribed herein was channelled into both reducing the overall experiment carbon contamination levels (chapter 4), and developent of analytical procedures for use with a new ultra-high sensitivity mass spectrometer (chapter 2).

It has been tacitly assummed that some indigenous carbon in micrometeorites survives atmospheric entry heating, but up to now there has ben no evidence on which to base such an assumption. Within chapter 7 the results of pulse heating experiments carried out on microgram-sized samples of whole-rock meteorites are presented and discussed, with a view to establishing the survival of carbon components during atmospheric entry. A further consideration concerns the question of weathering is dealt with in terms of major element chemistry in chapter 3, and again in chapter 5 with specific regard to the carbon isotopic effects of cryoconite algae.

If all the previous objectives could be successfully achieved, then it was envisaged that the results so obtained would enable the provenance of the micrometeorites to be determined with respect to either a Solar System or extra-solar origin, and then

hopefully to establish the role of the micrometeorites within the formation and evolution of the Solar System as a whole.

Chapter 2

The Analysis Protocol and Stable Carbon Isotope Mass Spectrometry.

2.1. Introduction.

To enable interpretation of the stable carbon isotopic results obtained from the micrometeorites, it was neccessary to also determine the major element chemistry of each sample. This requirement in turn dictated that a procedure was devised to split each sample into two portions, one of which would be used for isotopic work , and the other for major element chemistry. Such a procedure was needed because the combustion process used to liberate carbon dioxide gas for the isotopic determination (see 2.3) was destructive, and the techniques applied to determine the sample major element chemistry (see chapter 3) could not be applied prior to the isotopic analysis due to carbon contamination problems associated with each technique.

The latter, and major part, of this chapter is concerned with stable carbon isotope mass spectrometry, but the first section presents a description of the sample analysis protocol that was devised and evolved to split the samples into two portions.

2.1.1. The analysis protocol.

Several methods of dividing the particles into portions for separate analyses were investigated. It was anticipated from the outset that the criteria to be fufilled by the protocol were twofold;

(1) Because of the small size of each sample it was necessary to be able to split each one without incurring significant loss of material.

(2) The technique should not impart extraneous carbon contamination to the samples.

Bradley *et al.*, (1986) used an ultramicrotome to cut sections from <50μm diameter unmelted micrometeorites which had been embedded into epoxy resin. Obviously this sort of procedure was not possible for this study because any adhering resin remaining on the sample would make isolation of indigenous carbonaceous species extremely difficult. To circumvent this, the use of a cryo-ultramicrotome was investigated, where ice is used instead of the resin, and figure 2.1 illustrates a schematic of the procedure employed.

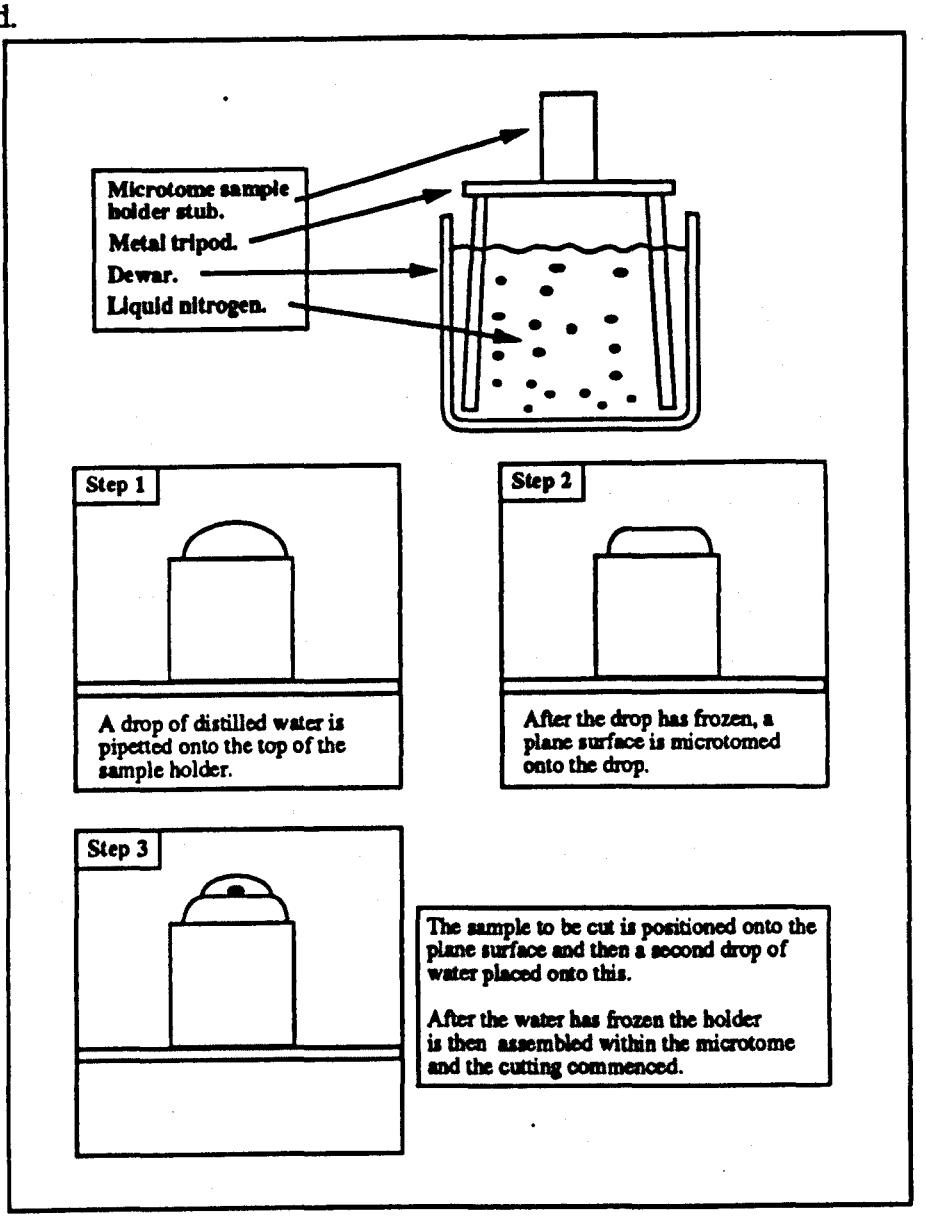

Figure 2.1. Schematic of the protocol used to prepare sample particles for cutting with a cryo-ultramicrotome.

In order to assess the efficacy of the cryo-ultramicrotome, 300 to 500μm diameter sized grains of olivine and pyroxene from a terrestrial igneous rock, and similar sized

pieces of deep-sea manganese nodule were used to establish the optimum speed of cut and cutting angle. Limited success was enjoyed in cutting sections of <5μm, but any attempt to cut materials thicker than this resulted in the sample being plucked from the ice, and since the particles of interest were >200μm in diameter, the technique of cryo-ultramicrotomy was abandoned.

A less elegant method of cleaving the samples is by crushing, being inferior for several reasons:

(1) It is impossible to choose where the particle is cleaved.

(2) Since it is crucial to obtain a representative piece of each sample for chemical analysis and clearly this control is lost by crushing.

(3) It may be envisaged that crushing produces a substantial size range of fragments. This poses the problem of how to retain these fragments for isotopic analysis after a suitably sized piece has been removed for the bulk chemical analysis.

(4) The degree of force used to crush needs to be controlled to avoid the possibility of totally destroying the particle.

The 'Leitz Miniload 2 Hardness Tester' (Urnst Leitz, Wetzlar GMBH, D6330, Wetzlar, Germany) is a device used for measuring the surface hardness of test materials, where a diamond-tipped tool is made to impinge upon the sample surface with a pre-determined force, with the hardness then being estimated from the dimensions of the resulting indentation. The use of this apparatus was investigated for cleaving the micrometeorite samples because in addressing point (4) above, the rate, force and depth of the crushing action could be adjusted so that any prospective particles should be cleaved in a controlled manner. Although proving successful in splitting the particles, there were considerable problems with retaining all the fragments, since during crushing some pieces were invariably ejected from the impact. Additionally, the use of the apparatus was ruled out because to minimise the risk of contamination, the cleaving procedure was scheduled to be executed in a clean-room environment, and the complexity of the apparatus did not allow it to be cleaned to the required levels to allow clean-room use. Notwithstanding this, and encouraged by the success of the crushing action in splitting the particles, the scheme outlined in 2.1.2 was devised.

2.1.2. The sample cleaving procedure.

The procedure can be divided into four main stages as follows;

(1) The size of the sample was estimated by utilising a calibrated graticule within the eyepiece of a binocular microscope. Also at this stage any optical properties of the sample were noted, including colour, lustre, shape and the presence of any distinguishing surface features such as striations and indentations.

(2) The sample was then placed onto the crushing substrate that had been constructed as shown in figure 2.2.

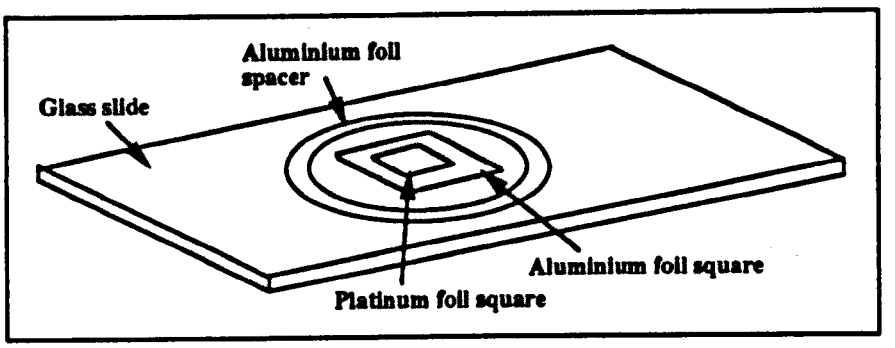

Figure 2.2. The crushing substrate as used within the sample cleaving procedure. See the text for detailed explanation of the workings of the procedure and the dimensions of the materials used to construct the substrate.

The base of the substrate was a pyrex glass microscope slide. Onto this was placed a *ca.*1 x 1cm aluminium foil (*ca.*25μm thickness) and *ca.*0.5 x 0.5cm platinum foil square. The thickness of the platinum foil (Goodfellows Metals, Cambridge Science Park, Cambridge, UK) used was initially 25μm, but as the protocol evolved (see chapter 4) this thickness was reduced to 4μm. The final part of the substrate was an aluminium foil ring (*ca.*2cm in diameter) that was placed to enclose the foil squares. (The action of this ring within the protocol and the thickness used is discussed in the last part of this section).

(3) The particle to be cleaved was placed onto the platinum foil and then another pyrex glass slide placed over this; a force was then applied by hand to the top slide whilst monitoring progress through the binocular microscope.

(4) After crushing the top slide was removed and a fragment removed and stored in a glass vial ready for the major element analysis. The platinum foil was then folded to make a packet which was then ready for introduction to the gas extraction system of the mass spectrometer for isotopic determination.

Although the principle of operation of the procedure outlined above was similar to that of the Vickers Hardness Apparatus, the new procedure had several distinct advantages. Because the crushing was carried out between the two microscope slides no material was lost as the particle fractured, and secondly, crushing directly onto platinum foil which then was folded to make the sample container, ensured that none of the smaller fragments were lost. This latter point is of major importance in view that the accuracy of the carbon isotope determination of the retrieved sample was related to the mass of material available for analysis. Early attempts showed that invariably there was a 'follow through' after the particle initially yielded which often resulted in over-crushing, but if an aluminium foil ring was chosen with a thickness slightly less than that estimated for the diameter of the particle it acted as a stop for the top slide. Experience showed that a ring with a thickness of approximately two thirds the diameter of the particle to be crushed was usually sufficient to prevent destruction of the sample. Most importantly, it was the simplicity of the protocol that is advantageous. There was very little scope for equipment malfunction the component parts could be kept scrupulously clean, which is of utmost importance when analysing carbon content and isotopic composition. The table below summarises the cleaning methods applied to each component of the protocol.

Material used within the protocol.	Method of cleaning employed.			
	A	B	C	D
Pyrex glass slides.	Yes	Yes	No	No
Aluminium foil.	No	Yes	Yes	No
Platinum foil.	No	No	No	Yes
Stainless steel sample handling implements.	No	Yes	Yes	No

A = Ten hours immersion in chromic acid, then rinsed in distilled water and air-dried overnight at *ca.*100°C.
B = Wrapped in aluminium foil and then combusted at *ca.*600°C for *ca.*1 hour.
C = Ultrasonication in a 50:50 solution of toluene and methanol (AnalaR grade, BDH Chemicals, Poole, UK) for *ca.*5 minutes and then air-dried overnight at *ca.*100°C.
D = Combusted in an evacuated quartz glass vial overnight in a partial pressure of oxygen at *ca.*1000°C (see figure 2.9) and then at 600°C until required.

Table 2.1. Summary of the cleaning methods applied to the constituent parts that make up the substrate used for the cleaving procedure and utensils used to handle samples and materials.

It is important to note that the table contains multiple cleaning methods for some components, the significance of which are discussed in Chapter 4, along with the actual levels of contamination imparted to the samples by the protocol.

2.2. Mass spectrometry.

In the early part of the 20th century much scientific effort was being applied to the careful study of radioactive isotopes. Amongst the findings of this work it was shown that these chemically identical elements in fact differed in their atomic weights. The discovery by Sir J.J. Thompson (*e.g.* Larsen, 1962) of isotopes within stable elements, and the fact that these isotopes could be separated as beams of ionized atoms by the action of electrical or magnetic fields, was the point of genesis for subsequent decades of stable isotope research.

Of equal importance for the study of carbon stable isotopes was the confirmation of the earlier postulated existence of ^{13}C by King and Birge, (1929) whilst observing the Sun utilising optical spectroscopic techniques. Specifically of interest to this thesis was the almost contemporaneous interpretation of Comet Halley's 1910 spectrum by Bobrovinikoff, (1930) as having a ^{13}C contribution. Studies by optical means continued, for example the first measurement of meteoritic carbon by King, (1936) and Jenkins and King, (1936) on a sample of the Canyon Diablo meteorite was using an optical spectroscope, until the method was superceded by the development of higher precision gas source stable isotope ratio mass spectrometers. The development of these machines was carried out by Nier and his co-workers during the late 1930s and throughout the 1940s (*e.g.* Nier, 1940, 1947; Nier and Gulbransen,1939; Murphey and Nier, 1941).

2.2.1. Constituent parts of the gas source stable isotope ratio mass spectrometer.

The gas source mass spectrometer originally described by Nier, (1947), and subsequently improved by McKinney *et al.*, (1950), has survived in the essence of its

design to the commercially available instruments of today. To determine the isotope ratios present, the mass spectrometer separates charged atoms, or molecules, on the basis of their masses as deduced by their movement in a magnetic, or electrical, field. The apparatus to achieve this can be separated into four basic components; the inlet, ion source, mass analyser and ion detectors. The function of these are described in the following paragraph.

The details of the actual inlets used will be discussed in more detail in section 2.3, but their main function is to convert the sample, in this case carbon, into a gaseous form (carbon dioxide). Within the ion source, ionization of this gas is effected by the impacting action of electrons produced from a heated filament. The ions produced are accelerated and focussed into a beam, which then passes to the mass analyser. Here the different isotopes are separated on the basis of their mass to charge ratio (m/z) by the action of a magnet; in the magnetic field produced the ions are deflected into circular paths, the radii of which are proportional to the square root of m/z. The separated ion beams are collected by the ion detectors and converted to electrical impulses by which their relative abundances can be measured. The ion detectors normally consist of a simple metal cup (Faraday cage) grounded through a high ohmic resistor; the potential drop in the resistor can be used to measure the impinging ion current as it passes to ground.

2.2.2. The delta notation.

With the initial results from his mass spectrometer Nier, (1940), (1947) quoted the true ratios of the (usually more common) light isotope to the heavy one. However, Urey, (1948) introduced the idea of a differential measurement between the sample and a reference material. This has practical value because absolute abundance measurements are not usually possible due to instrumental effects in the operation of individual mass spectrometers. By comparing the results to a standard material, data from different laboratories can be compared directly, any instumental effects being cancelled out. In addition, the difference between the sample and standard are expressed in parts per thousand (per mil ‰), thus allowing even very small isotopic differences to become apparent. Urey's ideas, which he christened the 'delta notation', were put into print two years later by McKinney *et al.*, (1950) and have survived to become the accepted format. The reference standard for carbon is a

Cretaceous fossil *Bellemnita Americana* from the Peedee formation in South Carolina, USA, this usually being abbreviated to PDB.

The derivation of the delta notation is as follows;

$$\delta^{13}C = \left(\frac{(^{13}C/^{12}C)\text{sample}}{(^{13}C/^{12}C)\text{reference}} - 1\right) \times 1000‰$$

It can be seen that an enrichment in the light isotope will produce a negative $\delta^{13}C$ value, conversely an enrichment in the heavy, a positive one. A perculiarity of the equation is that pure ^{12}C will have a $\delta^{13}C$ value of -1000‰, while pure ^{13}C +∞‰, but for small-scale enrichments the scale is approximately linear.

2.2.3. Mass spectrometer development; dynamic mass spectrometry.

The early designs of mass spectrometer of Nier and his co-workers neccessitated the differential analysis of sample and reference gases. The machine set up to achieve this is shown schematically in figure 2.3.

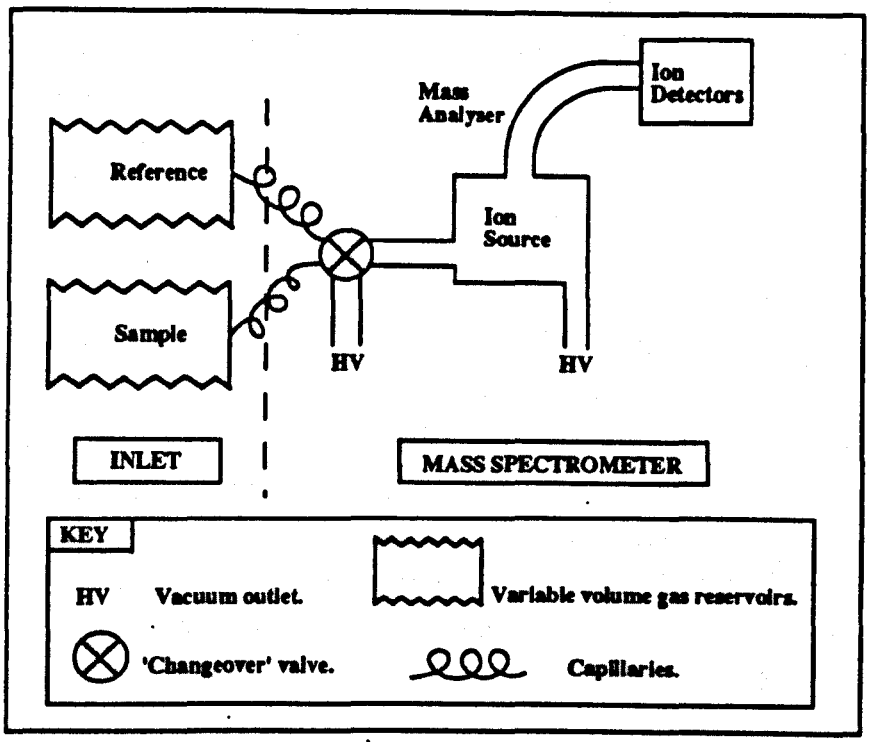

Figure 2.3. The constituent parts of the 'dynamic' operation mass spectrometer.

The mass spectrometer operates in a 'dynamic' mode; gas is leaked through capillaries at a constant rate to a change-over valve (Murphey, 1947), this valve allows one gas to be admitted to the ion source of the mass spectrometer whilst the other is bled to waste through a high-vacuum outlet. This system prevents differential isotopic fractionation because both sample and reference gas are depleted at the same rate, their initial starting pressures having been equalised by adjusting the reservoir volumes. The high vacuum outlet on the source ensures a constant source pressure which in turn produces a very stable ion beam.

Contemporary machines of this design (for example the SIRA 24; VG Isotech, Chesire, UK) can produce results with a precision of ±0.005‰, however to achieve this requires a relatively large amount of gas, typically 1.5μmol CO_2. This requirement for large samples is the product of several contributing factors, summarized as follows. (For details see Wright, 1984).

1) Half the gas is not admitted to the ion source, instead of which it is bled to waste due to the need to deplete the gases at the same rate.

2) Only a fraction of the gas that enters the ion source is analysed, the majority passes through the source to the pumps without being ionized.

3) Not all the gas in the sample reservoir is available for analysis as there is a finite volume to the reservoir and the capillaries.

4) A high pressure of gas is required in the inlet capillaries to maintain viscous flow and hence avoid fractionation (Halstead and Nier, 1950).

For most conventional terrestrial geochemical applications this limitation in sample size poses no great problem, the need for precision outweighing that of sensitivity. This is not the case for all geochemical work, and in particular the study of extraterrestrial materials where the preservation of valuable sample stocks is a necessity.

2.2.4. Improvements to dynamic mass spectrometry.

Several solutions have been investigated in an attempt to overcome the need for large samples of gas inherent in the dynamic mass spectrometer design:

(1) 'Gas mixing' where the sample gas is diluted with much larger quantities of a reference gas of known isotopic composition, and the isotopic nature of the sample is then calculated by a correction on the results (Wright, 1984).

(2) Halas and Krouse, (1983) investigated 'gas pushing' where an inert gas is utilised to force all the sample gas from the capillaries and sample reservoir through the mass spectrometer.

(3) Improved ion counting techniques by Schoeller and Hayes, (1975).

Although limited success was achieved in sensitivity gains, it became evident that for the analysis of submicromole amounts of gas an alternative method was required.

2.2.5. Ion microprobe mass spectrometry.

Determination of isotope ratios by ion microprobe would appear to provide a solution to the sample size requirement problem. In these machines an incident beam of ions (*e.g.* Cs^+) causes sputtering of the solid sample and the ejected ions are then extracted and analysed in a similar fashion to conventional mass spectrometry. A major advantage of this method is that because the sample ions are removed by the action of a beam of ions of only a few microns in diameter, then distinct areas of the sample can be analysed in turn by moving the analysis beam about the sample. This allows direct measurement of individual phases within each sample and allows investigation of the separate carbonaceous components that constitute the bulk. Ion microprobe studies of extraterrestrial stratospheric dust samples (IDPs) have shown that each analysis consumes $<10^{-10}$g of sample for a carbon isotopic measurement (McKeegan *et al* ., 1985; Zinner *et al.*, 1983, 1984), which corresponds to *ca.*8 pg of carbon at an average of 7.7wt% concentration (Blanford *et al* ., 1988). Initial results showed the carbon in the IDPs to be isotopically similar to terrestrial values, $\delta^{13}C$ values of -50 to +3 ‰ being obtained, but the errors of ± 24‰ did not allow separation from terrestrial contamination values (McKeegan *et al* ., 1985). For other isotopes, notably hydrogen, these errors do not pose a problem because large deuterium enrichments (*eg.* McKeegan *et al* ., 1985) are seen, and errors of ± 24‰ on values of +2790‰ become insignificant.

2.2.6. Static mass spectrometry.

Reynolds, (1956) developed a mass spectrometer to analyse small amounts of noble gases, and a schematic of its design is shown in figure 2.4.

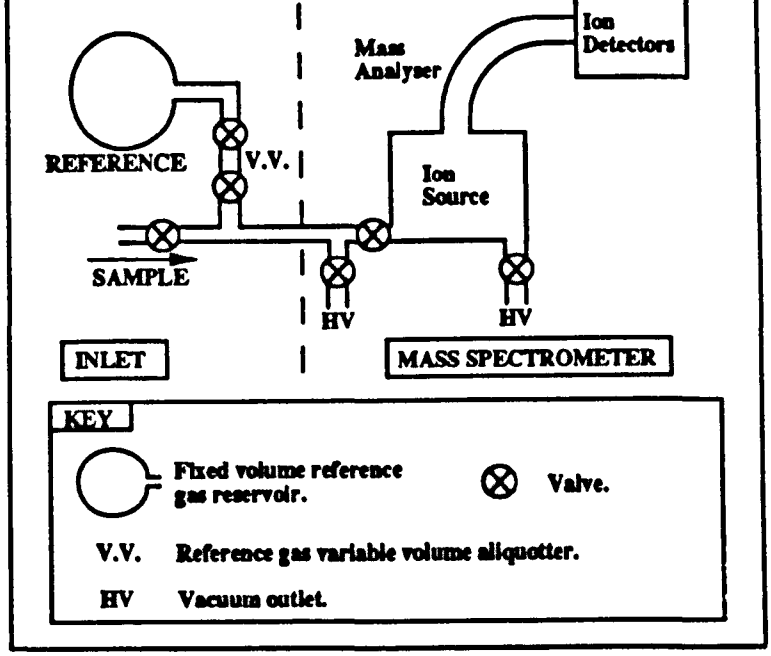

Figure 2.4. The constituent parts of the 'static' operation mass spectrometer.

The fundamental differences from the dynamic machine (described in section 2.2.3) are as follows:

1) The mass spectrometer is isolated from the pumps before any of the sample gas is admitted into an enclosed volume and, as a result, all the sample gas is potentially available for analysis.

2) There is no pumping of the gas during the analysis period; the mass spectrometer is operating in a 'static' mode.

3) The gas is not being pumped through the ion source, so the potential for its ionization and subsequent isotopic determination is greatly increased.

The combination of the above means that the static machine needs less gas to make an isotopic measurement than its dynamic counterpart.

Irako, (1975) investigated the use of active gases in static machines, looking at H_2, N_2, CH_4, CO_2, CO, O_2 and C_4H_{10} species. The problem encountered was that the lifetime of active gases within the mass spectrometer is much reduced compared to that of the inert noble gases, because of destruction or degradation on the hot filament, ionization processes, ion-molecule reactions and adsorption onto the clean walls of the instrument. The resulting short lifetime of the gas within the mass spectrometer dictates that any analysis of an active gas needs to be very rapid. Gardiner, (1978) and Gardiner and Pillinger, (1979) searched for a suitable carbon-bearing gaseous species that would enable measurements in a static machine. They found that deuterated methane (CD_4) was a likley candidate, having an increased mass spectrometer lifetime over CO_2, and that analysis could be made on CD_4 without any

appreciable detrimental isotope effects. Further development by Wright *et al*., (1983) culminated in a static mass spectrometer that could determine the carbon isotopic composition of nanomole amounts of CD_4 to precisions of ±0.25‰. This initially promising technique unfortunately ran into difficulties due to problems associated with quantitatively converting samples to CD_4 (McNaughton *et al*., 1983).

The resulting renewed interest in CO_2 led to the development of the mass spectrometer of Carr *et al*., (1986b); a machine capable of attaining precisions of ±0.8‰ on nanomole quantities of CO_2. The problem of the short lifetime of CO_2 within the machine (in this case its half life was found to be 35 seconds) was overcome by making very rapid data aquisition for a period of 35 seconds after an initial gas equilibration of 30 seconds. In order to collect enough data to make accurate measurements within this short time, it was neccessary to monitor all three ion beams (m/z = 44, 45 and 46) simultaneously and for this reason the mass spectrometer is colloquially known as the 'Triple Collector'. During the data collection period 625 measurements were made for each beam, this proving to be sufficient to allow determination of the isotopic nature of the gas to the precision quoted above. Table 2.2 shows exactly how these beams are constituted.

Mass	Species present	Ion beam collector
44	$^{12}C^{16}O^{16}O^{+}$	Major
45	$^{13}C^{16}O^{16}O^{+}$ $^{12}C^{16}O^{17}O^{+}$	Minor 1
46	$^{12}C^{16}O^{18}O^{+}$ $^{13}C^{16}O^{17}O^{+}$ $^{12}C^{17}O^{17}O^{+}$	Minor 2

Table 2.2. The molecular species of carbon dioxide in relation to the corresponding mass spectrometer collectors. Beam 46 is monitored so that a correction for the input of ^{17}O to beam 45 can be calculated (Craig, 1957).

2.2.7. A static mass spectrometer for the analysis of picomole quantities of CO_2.

The ability of the mass spectrometer developed by Carr *et al*., (1986) to analyse nanomole amounts of CO_2 to precisions of better than ±1‰ promoted a resurgence in

the study of carbon within extra-terrestrial samples (*e.g.* Carr *et al* ., 1985a, b; Wright *et al* ., 1988; Ash, 1990). However, a preliminary examination of carbon within deep-sea spherules using the Triple Collector indicated that the errors on the results acquired were too large to allow easy identification of any indigenous sample components (Wright *et al* ., 1988). With the solution of this and other problems in mind, a mass spectrometer was designed and built in an attempt to push the sample size requirement for carbon isotopic measurements down to the picomole level. The design, construction and early development of this machine, colloquially referred to as 'MS86', has been reported elsewhere (Prosser *et al* ., 1990), so only the salient features are discussed here.

The basic design is similar to the Triple Collector with the only major differences being the use of a closed ion source and semi-automation of the inlet. The Triple Collector utilised an open 'Nier Type' ion source. This type of source was required because it was found that admitting nanomole amounts of gas to a closed source produced transient high which in turn led to ion beam instability and enhanced abundance sensitivity problems, which were detrimental to the isotopic measurements (Wright, 1984). Abundance sensitivity results from tailing of the major ion beam onto the minor collectors. It was first noted by Craig, (1957) who discovered that the effect became worse with increasing source pressure. The cause of this tailing is peak broadening by collisional and coulombic ion scattering within the ion beams, and so the higher the gas pressure in the mass spectrometer, the more pronounced the effect. However, with the analysis of picomole aliquots of gas with accompanying lower source pressures the problem was largely overcome, and allowed a closed source to be used. The ability to use the closed source has two main advantages; firstly, the lifetime of the gas is much increased with the half-life of the gas being extended to 450 seconds - almost thirteen times longer than the Triple Collector. This effect was noted by Wright, (1984) but the detrimental effects of the high source pressure mentioned previously were deemed to outweigh the advantages of extended gas longevity. Secondly, the closed source was found to reduce the chance of the gas escaping without interaction with the filament, leading to an increased ionization efficiency. This in turn translates into an increase in sensitivity with a decrease in sample size, thereby minimizing the loss in precision associated with analysing smaller samples.

Prosser *et al* ., (1990) have quoted MS86 as being capable of analysing 10 picomoles of CO_2 standard gas with a $\delta^{13}C$ value of *ca.*-40‰ to a precision of

±3.0‰. When the machine was operated in a 'repeated-comparison' mode , making five consecutive sample/reference comparisons on individual 10 picomole CO_2 aliquots, this precision improved to ±1.3‰. This increase in precision was attributable in part to the ability of the semi-automated gas handling system of MS86 to mimic a dynamic machine. To do this it made repeated sample/standard comparisons , but at the same time retains the advantages of a static machine in that all of the gas was available for analysis. The figures quoted by Prosser *et al.*, (1990) were for 'zero enrichment' experiments; here individual aliquots of the same reference gas ($\delta^{13}C$ value of *ca.*-40‰) were compared as though they were sample and standard. If the mass spectrometer is functioning correctly then a value of zero is obtained from this comparison, because the mass spectrometer does not measure absolute $^{12}C/^{13}C$ ratios, but the value of the sample gas relative to a standard gas of known isotopic composition (see 2.2.2).

To assess the use of MS86 in analysing micrometeorite carbon, attempts were made to measure differential isotopic composition between picomole amounts of two different standard gases with $\delta^{13}C$ values of *ca.*0‰ and -40‰, but the resulting comparison yielded $\delta^{13}C$ values in error by 3 to 10‰ for different batches of gas. The variable inaccuracy of these experiments was attributed to the gas handling process, rather than in the mass spectrometer, since it was necessary to take gas samples at *ca.*760 torr (from the storage bulbs used routinely for conventional dynamic mass spectrometry) and reduce them to a pressure of *ca.*1x 10^{-5} torr for use on MS86. It was postulated that contaminants present in these storage bulbs (water vapour, nitrogen, *etc*) and diffusion pump oil derived hydrocarbons from the preparation line used to take aliquots from the bulbs, combined to cause the difficulties observed, by causing interferences within the mass spectrometer during analysis.

2.2.8. Development and evaluation of the performance of MS86.

In order to be able to use MS86 for the research herein, it was necessary to overcome the problems of standard gas analysis reported by Prosser *et al* ., (1990). This was achieved by preparing fresh standard gases on an alternative preparation line (described below), specifically for MS86 as and when they were required. A protocol was devised whereby individual fragments of diamond plates (taken from an industrial diamond powder) were combusted in sealed ampoules to give carbon dioxide. The diamonds were combusted overnight at *ca.*1000°C and the gas extracted on a new

preparation line that used a turbo-molecular pump instead of the diffusion pump used by Prosser *et al* ., (1990) in the preparation of their sample gases. The use of this turbo-molecular pump eliminated the possibility of diffusion pump oil contamination. It is noteworthy to mention that although the turbo pump was still backed by a rotary pump, the possibility of backstreaming[6] of oil contaminants from the rotary pump was prevented by fitting the rotary pump with alumina foreline traps. In this way the reference gas obtained was free of the contaminants associated with gases that have undergone prolonged storage, and the use of a preparation line without a diffusion pump eliminated the possibility of pump oil contamination. The gas was then split; the larger (*ca*.75%) portion being allocated for isotopic analysis by the conventional SIRA 24, and the remainder (typically 10 to 50 μg) to MS86 where it was transfered to an on-line reference storage bulb as described by Prosser *et al* ., (1990).

If the isotopic composition obtained from the analysis of the diamonds on the SIRA 24 could be closely replicated (to within the limits specified below) by analysis on MS86, then the gas was retained, as it was assumed that negligible fractionation or contamination of the gas had occured during transfer from the prepartion line to the MS86 storage bulbs. Table 2.3 shows the results for three individual diamond standards, prepared and analysed as described previously, that were loaded into MS86 over a six month period.

SIRA measured value			MS86 measured value		
$\delta^{13}C$(‰)	± 1 sigma	No.comp.	$\delta^{13}C$(‰)	± 1 sigma	No.comp.
-9.71	0.09	6	-10.2	0.2	5
-9.56	0.02	6	-10.1	0.2	5
-9.39	0.02	6	-9.8	0.2	5

Table 2.3. Results for the analysis of diamond standards prepared specifically for MS86. Isotopic values are in ‰, with one sigma standard deviation errors (also in ‰) presented on the mean of the individual analyses that constitute that final value.

[6] Backstreaming is the migration of vapours under molecular flow conditions against the apparent direction of pumping. (Molecular flow is the condition where collisions occur with the walls of the vacuum vessel rather than between molecules, and is typically prevalent at pressures below *ca*.10^{-4} torr).

There are two points for discussion that arise from the results in table 2.3; firstly, to obtain the $\delta^{13}C$ values for the diamonds presented in the table, the mass spectrometers must make a comparison to another reference gas. In the case of the SIRA 24 this is an internal laboratory standard (*i.e.* CO_2 gas in a 2 litre storage bulb), but for MS86 the reference gas is diamond-derived CO_2. In reality, MS86 measures the relative difference between the two gases and then calculates the isotopic value of one (normally the sample gas) by assuming the composition of the other (the reference). If this relative value is not correct, the two reference gases are renewed alternately, checking in each case against the SIRA 24, until it is achieved and then these two gases are retained for routine comparison to sample gas produced during stepped combustion experiments (see section 2.3). Daily checks of the relative $\delta^{13}C$ value allow the condition of the gases to be monitored; as soon as it lies outside of the correct relative value by more than the one sigma instrumental errors of the mass spectrometer, the gases are replaced. Note that the results quoted in table 2.3 give the calculated $\delta^{13}C_{PDB}$ value of the diamond, this is possible because all the SIRA 24 standard gases (against which MS86 gases are checked) are in turn measured against, and corrected accordingly, to international (National Bureau of Standards) standards on a six monthly basis. Secondly, MS86 is operated in the repeated-comparison mode making five reference/reference comparisons to produce the average value presented in the table. The one sigma standard deviation of the five individual results illustrates the reproducability of the measurements, and likewise, the SIRA 24 value is for six comparisons with an equivalent error presented on the average.

Initial examination of the diamond results confirmed that the problems experienced by Prosser *et al* ., (1990) were indeed of a handling nature rather than an instrumental effect as there was now a good agreement with the SIRA 24 results. There was however, some concern that the MS86 isotopic results were consistently light by *ca*.0.5‰. The reason for this was not completely clear, although suspicion fell upon minor isotopic fractionation occuring upon transfer of CO_2 from the preparation line to the inlet of MS86. However, this problem became less important upon consideration of the mass spectrometer instrumental errors that accompanied each individual measurement that constituted the five separate sample/reference comparisons within each diamond result in table 2.3. These instrumental errors vary with sample size, but for the diamonds analysed here ranged from 0.4 to 0.7‰, and when these were applied to the individual results that constitute the average value within table 2.3, the individuals all agreed with (or fell within 0.1‰) the SIRA 24 value.

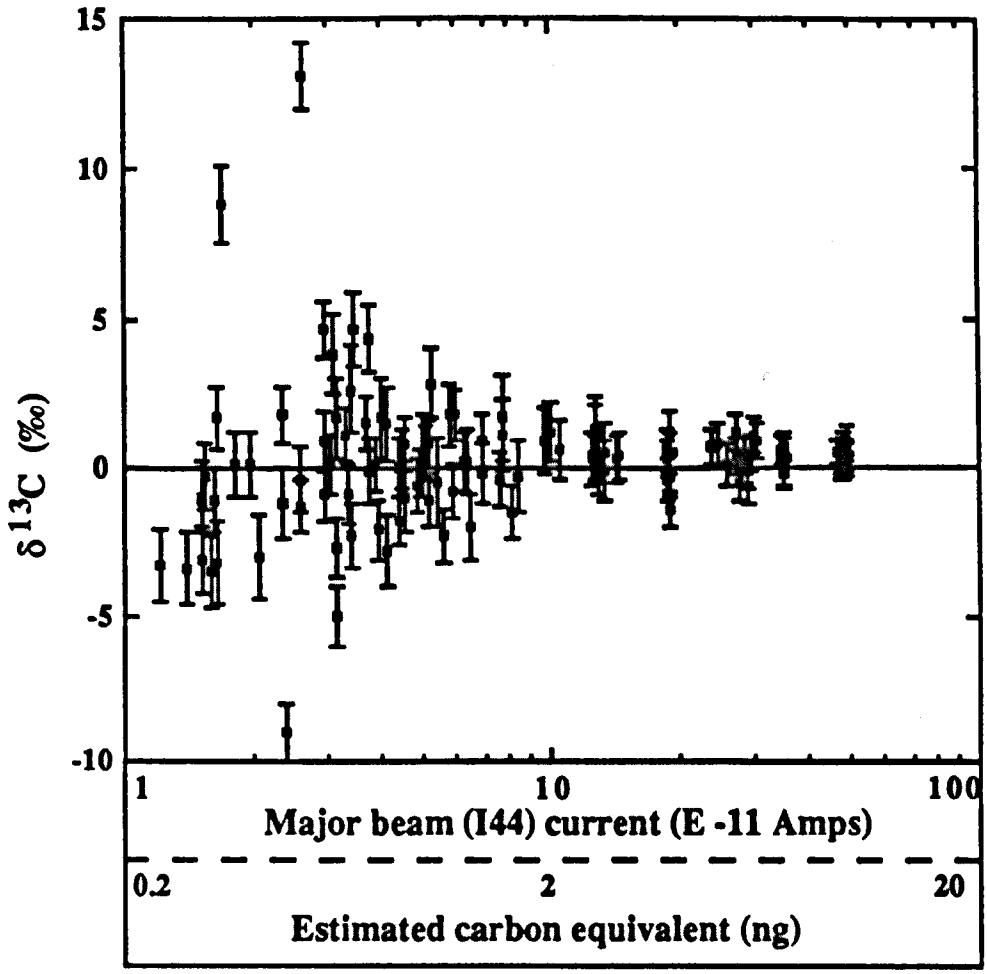

Figure 2.5. Measured $\delta^{13}C$ values for zero enrichments on aliquots of reference gas ranging in size from *ca.*0.2 to 6 ng of carbon. Error bars represent instrumental errors on the individual measurements (one sigma). (For discussion of I_{44} and ng carbon equivalents see text).

Figure 2.5 presents the results for zero enrichment experiments carried out during the everyday routine running of stepped combustion experiments to check the mass spectrometer was functioning as normal. The data plotted in figure 2.5 are for single reference/reference comparisons on aliquots of CO_2 ranging in size from *ca.*0.2 to 10 ng of carbon and were taken from experiments that span over a period of one year. To facilitate interpretation of the results in figure 2.5, table 2.4 shows averages of the measurements used to construct figure 2.5 and has been calculated by grouping samples of equivalent size together.

Major beam (I_{44}) (E - 10^{-11} A)	Aliquot size equivalent (ng of carbon)	Mean zero enrichment (±1 sigma ‰)
>40	>8.1	0.3±0.3 (n=13)
30 - 40	6.1 - 8.1	0.4±0.4 (n=6)
20 - 30	4.1 - 6.1	0.3±0.6 (n=12)
10 - 20	2.1 - 4.1	0.3±0.6 (n=23)
5 - 10	1.0 - 2.1	0.2±1.3 (n=21)
1 - 5	0.2 -1.0	0.0±3.4 (n=48)
Total cumulative zero enrichment		0.1±2.3 (n=126)

Table 2.4. Calculated averages of the data used to construct Figure 2.6 with a cumulative zero enrichment presented with decreasing sample size. Results are in ‰ with errors being equal to one sigma on the the standard deviation of the mean values.

In both figure 2.5 and table 2.4 the measured zero enrichment values are presented both in terms of ng of carbon and major beam current (I_{44}). Before discussing the implications of the results it is first necessary to briefly illustrate how these carbon equivalents were calculated. The data used for this task were extracted from the same experiments used for the zero enrichments; I_{44} values obtained in the analysis of measured aliquots of sample gas were taken and plot against each other to produce the graph presented in figure 2.6. The size of the sample aliquots had been determined in each case by the Baratron (capacitance manometer) within the MS86 inlet prior to introduction to the mass spectrometer.

From figure 2.6 it is evident that for the aliquots of CO_2 sample gas, whose Baratron measured size ranges from 0.2ng to 6ng, a straight line relationship exists with their corresponding I_{44} value. In other words, it is possible from the graph to calculate the absolute quantity of carbon represented by a given I_{44} value. It must be stressed that the value thus obtained can only be regarded as an approximation, because there are several sources of error inherent within the procedure employed:

a) It is probable that there are minor fluctuations of sensitivity (and hence in the I_{44} for a given aliquot of gas) on a daily basis, mainly as a result of the mains electrical power supply irregularities to the mass spectrometer hardware.

b) The baratron and I_{44} measurements both estimate the abundance of CO_2, but the measurements are effected by different contaminants. The baratron is a capacitance manometer and as such measures the total pressure of any gaseous species present, but

the I44 value is controlled only by the abundance of ions of mass 44 within the mass spectrometer and is only affected by specific contaminants of this same mass. Unless the reference gas used for the zero enrichment experiments and the sample gas for the calibration of the I_{44} value are equally contaminated (with the gases present in the same ratio) then there will be some descrepency.

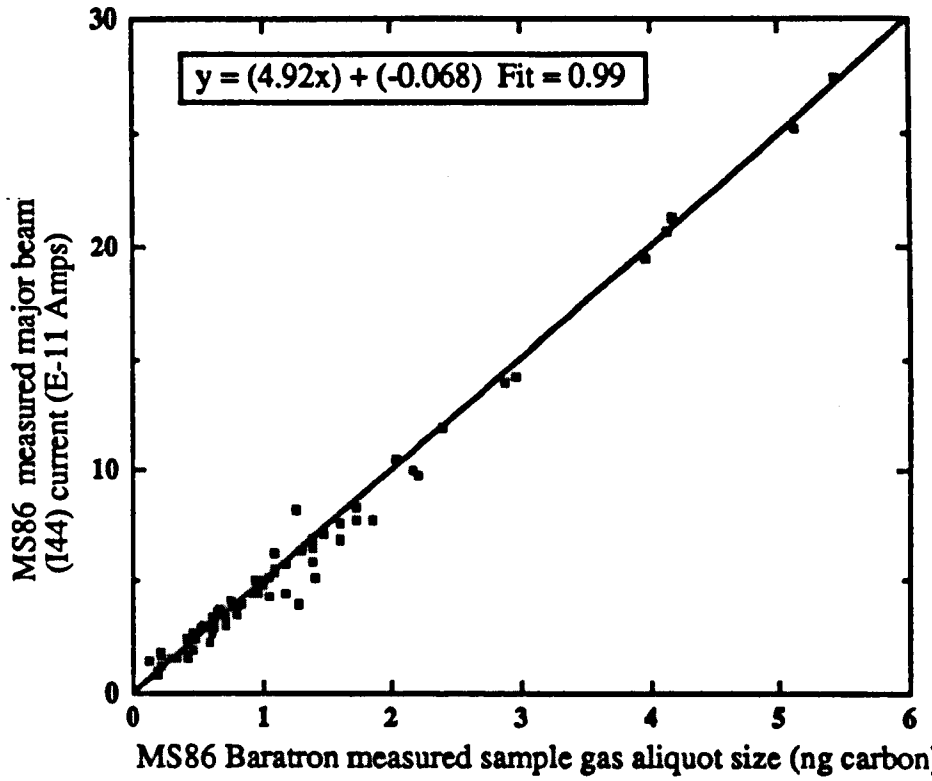

Figure 2.6. Plot of sample gas aliquots (*ca.*0.2 to 6 ng) against measured major beam current (I_{44} x 10^{-11} amps). The straight line relationship (y=mx+c) is used to calculate ng carbon equivalents for the reference gas aliquots in Figure 2.5. and Table 2.4.

The cumulative zero enrichment over the entire range examined (<8.1ng carbon equivalent) is 0.1± 2.3‰, but more can be learned about the performance of MS86 by examining the individual groups that constitute this result. From 8.1 to 2.1ng carbon the results are consistent, with the mean zero enrichments for the three groups in table 2.4 that span this range yielding zero enrichment results of 0.3 to 0.4 (±0.3 to 0.6‰) and examination of figure 2.5 shows the individual results that constitute these groups to be reproducable and accurate; *i.e.* within the instrumental errors the correct value of 0‰ is achieved. It is only as the sample size decreases that this confidence begins to degrade, this being illustrated by the increase of the errors (a measure of

reproducability) on the mean zero enrichments for the last two groups in table 2.4. Examination shows that although the means are in good agreement with the correct zero value (0.2 and 0.0), the corresponding errors on these is 1.3 and 3.4‰ respectively. Again this is illustrated by figure 2.5 where an increased spread of results occurs below 2.1 ng carbon with a corresponding higher proportion of individuals plotting outside of the zero value even when the instrumental errors are taken into account. It is extremely difficult to estimate where the inaccuracy of these results becomes unacceptable, but from examination of figure 2.6 and table 2.4 , it appears that below *ca.*1ng carbon the proportion of incorrect individuals increases. It therefore seems reasonable to assume that the 'working sensitivity' of MS86, *i.e.* the smallest aliquot of gas that can individually analysed and consistently yield the correct answer, is *ca.*1ng of carbon. When examining the results of stepped combustion experiments it is important to keep this figure in mind as it serves as an approximate cut-off point for confidence in the accuracy of the isotopic results.

2.3. Carbon dioxide extraction techniques and the stepped combustion method.

For the measurement of the stable isotopic composition of carbon within the micrometeorites using the Triple Collector or MS86 mass spectrometers, it was necessary in the first instance to convert any indigenous carbon to carbon dioxide (CO_2). Sakai *et al.*, (1976) showed that carbonaceous species could be converted to CO_2 without prohibitive isotopic fractionation of the original $\delta^{13}C$ value of the carbon by the simple process of combustion in an atmosphere of oxygen. In an attempt to refine this combustion technique for stable carbon isotopic studies, Des Marais (1978) performed sample combustions in two distinct temperature steps and when interpreting his results, largely ignored the results of the lower temperature step. The rationale behind this protocol was that any contamination would be combusted in the first temperature step, because such material is usually organic in nature and is relatively thermally unstable compared to other carbonaceous species (*i.e.* graphite, diamond, carbonates, carbides *etc.*). This ability to distinguish between different carbonaceous species based upon thermal stability forms the basis of the technique of 'stepped combustion' used within this study. In the first sections of this chapter the development of ultra-high sensitivity stable carbon mass spectrometry has been

discussed, but along side of this work has been the parallel development of the stepped combustion method (*e.g.* Grady, 1982; Swart *et al.*, 1983b; Wright and Pillinger, 1989), and recently, Russell *et al.*, (1991a, b) have reported results of experiments performed on meteorite acid residues utlilising 10 to 25°C combustion steps. Notwithstanding that such experimentation has revealed the full potential of the stepped combustion method in enabling the isolation of indigenous carbonaceous components in both terrestrial and extra-terrestrial samples, it has also highlighted the need for consideration of extraneous factors in the interpretation of stepped combustion results. Grady, (1982) reported the effect of 'promoted combustion'; if two different carbonaceous species that seperately have distinct combustion temperatures are mixed together in an intimate manner, the onset of combustion of one component may 'promote' the earlier combustion of the other. In particular, sample grainsize would appear to be an extremely important factor for consideration, because Ash, (1990) performed a set of experiments combusting diamonds ranging in size from <0.01 to *ca.*100μm, and found a difference in combustion temperature of *ca.*400°C. Such studies imply that care must be taken in attempting to make comparisons between stepped combustion data from samples that exhibit different grainsizes and carbon inventories, but for a potentially similar suite of samples, *e.g.* the micrometeorites, such problems can be assumed to be relatively insignificant.

Stepped combustion experiments within this work have been carried out from room temperature (*ca.*25°C) to 1200°C, this higher limit being dictated by the softening point of the quartz glass used in sample reaction vessel construction (see 2.3.2). The results of these experiments are presented as a stepped combustion plot, a hypothetical example of which is presented in figure 2.7. The histogram represents the yield of carbon in nanograms, as shown by the left hand ordinate axis, for the corresponding temperature increment shown on the abscissa axis. The isotopic composition of the carbon from each step is illustrated by the dotted line, its $\delta^{13}C$ value delineated by the right hand side ordinate axis.

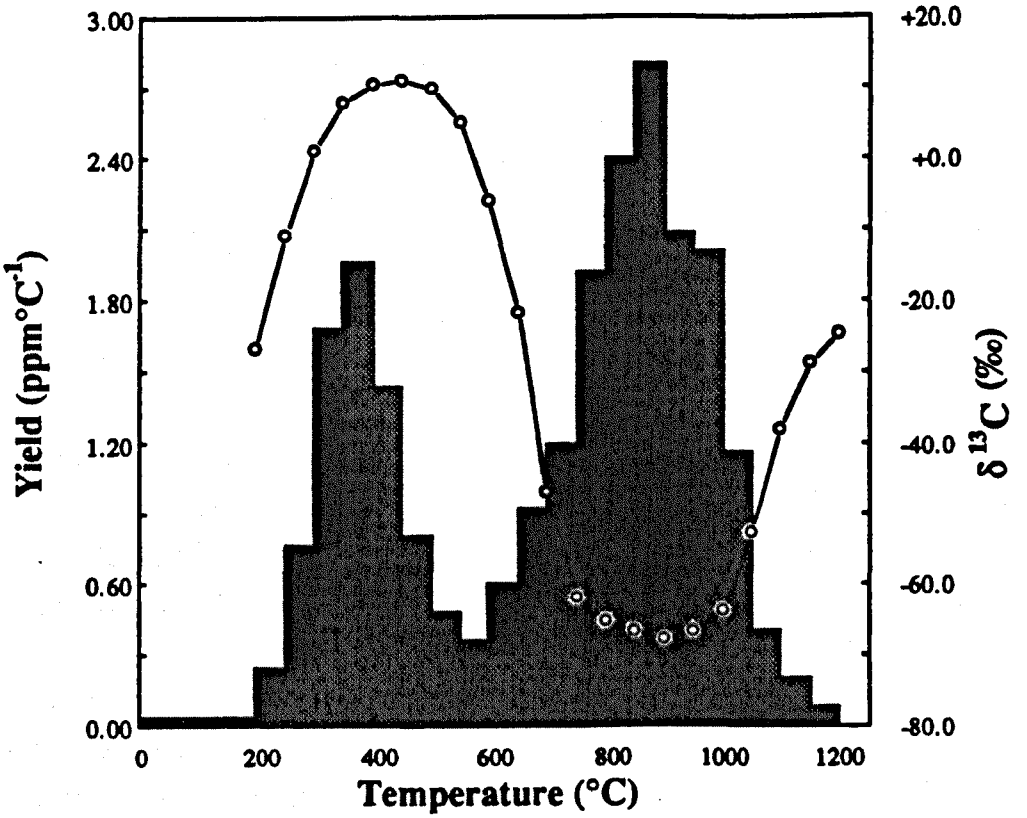

Figure 2.7. The stepped combustion plot; a format for presenting data acquired by stepped combustion experiments (for explanation see text). Sample weights, absolute carbon yields and details of the $\delta^{13}C$ measurements for each temperature step are presented in appendix A1 for each stepped combustion plot discussed within this thesis.

2.3.1. Carbon dioxide extraction lines.

The component parts of the CO_2 extraction line can be split into three intergrated sections:

(1) A reaction vessel where the sample can be heated in the presence of oxygen in controlled temperature increments.

(2) A gas purification section to separate CO_2 from the mixture of combustion products. This is achieved by using the differing volatilities of the gases, where the condensible gases (including CO_2) are frozen out of the reaction vessel using a liquid nitrogen trap, and then the CO_2 separated from the other condensibles by the use of a variable temperature cryogenic trap (Boyd, 1988).

(3) A facility to measure absolute quantities of gas. This is executed by the use of a capacitance manometer.

2.3.2. Gas extraction line design at the onset of the study.

The basic design of the CO_2 extraction lines used within this study was pioneered by Swart *et al.*, (1983), and a description of the initial improvements made to this design for use on the Triple Collector can be found within Carr *et al.*, (1986). Non-quantitative carbon yields obtained whilst analysing meteorite acid residues prompted Ash, (1990) to re-evaluate the operation of the Carr *et al.*, (1986) system, and led to the incorpation of improvements initially developed for nitrogen gas extraction (Boyd, 1988). A schematic of the resulting design of reaction vessel of Ash, (1990) is presented in figure 2.8, and this represents the design in use on the Triple Collector at the onset of this study. The construction of the reaction vessel is focussed upon because it is the part of the gas extraction system that supplies the majority of the experiment blank, and so was accordingly the section that has received the most development work in the course of this study.

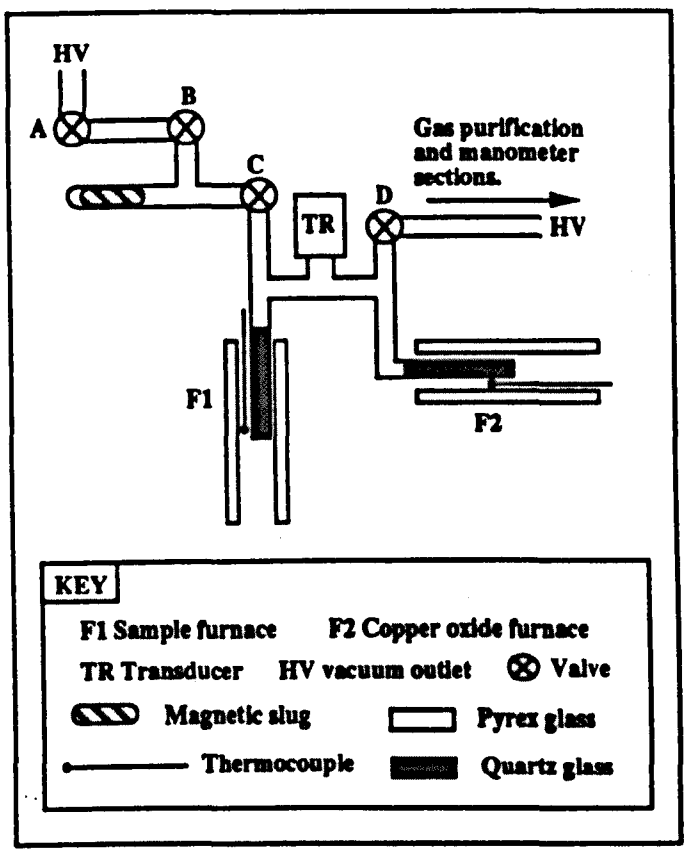

Figure 2.8. The design of reaction vessel as it stood at the beginning of this study. It was developed by Ash, (1990) for use on the Triple Collector in an attempt to redress the low-yield problems experienced when analysing acid residues of meteorites.

The reaction vessel in figure 2.8 was constructed of Pyrex glass tubing (8mm OD, 6mm ID) except for those parts which experienced heating to high temperatures, such as the sample furnace (F1) and copper oxide furnace (F2), which were fabricated from quartz glass (6mm OD, 4mm ID), the two glass types being connected by a quartz/Pyrex graded seal. The valves were all greaseless stopcocks constructed of Pyrex glass with teflon seals (Youngs Valves, Acton, London, UK) and were 'backed' to avoid the chance of accidental atmospheric ingression (Carr, 1985). The glassline was evacuated by the combination of an oil-diffusion pump backed by rotary pumps to a base pressure of better than 10^{-6} torr. The sample was heated using a thermally insulated resistance wire electrical furnace (F1), the temperature of which was controlled by a variable transformer and monitored by a thermocouple. This thermocouple was placed against the glass tube at the level of the sample, where its consistent and accurate placing was of crucial importance because high thermal gradients exist within the furnace. The large thermal inertia of the insulated furnace allowed precise control of its temperature to better than ±5°C. The oxygen for the combustion was generated by heating copper oxide ('wireform' CuO, BDH Chemicals, Poole, UK) using the resistance wire furnace (F2) to 850°C where it undergoes partial decomposition to copper and oxygen, the reaction being as follows;

$$Cu_xO_x \leftrightarrow Cu_xO_{x-y} + \frac{y}{2}O_2$$

The reaction is temperature dependent, at 850°C it is driven to the right hand side, and at 650°C the products recombine to force the reaction back to the left. Testing showed that the oxygen pressure supplied (4 to 12 torr as measured by the transducer - TR) was ample, mainly because this equilibrium pressure is constantly maintained by re-adjustment of the copper oxide breakdown reaction. This method of supplying oxygen was initially considered inappropiate by Carr, (1985) because of high carbon blank from the copper oxide. However, Ash, (1990) found that the blank contribution of the copper oxide could be reduced to >0.75ng of carbon for each 40minute combustion step by subjecting it to numerous (*ca.*20) repititions of the following cycle:

(1) Elevation of the temperature to *ca.*900°C for *ca.*2 minutes.

(2) Reduction to *ca.*650°C for *ca.*10minutes.

(3) Reduction to *ca.*450°C for *ca.*5 minutes.

During this *ca.*17minute period the combustion section and copper oxide were exposed to a liquid nitrogen trap to freeze out contaminant gases. Any cryogenic loss

of oxygen during the first two steps was found to be negligible compared to the benefits of removing the last vestiges of carbon during the 900°C period. Once this low-blank level had been achieved by this cycling, it required only sporadic recycling (*e.g.* after replacing the quartz glass combustion section) to maintain it.

The reaction vessel was kept at a temperature of *ca.*1200°C with valves C and D closed and the copper oxide at *ca.*850°C whilst not in use. In this way it was maintained as clean as possible, and prior to the onset of a stepped combustion experiment, the sample furnace was turned down to room temperature, and the copper oxide to *ca.*450°C to re-absorb unused oxygen, then any gaseous species in the reaction vessel could be pumped away be opening valve D. The samples were loaded into the reaction vessel by an air lock system devised by Ash , (1990) to allow the sample to be loaded without the necessity of exposing the reaction vessel to the atmosphere and so retain the cleanliness achieved before the beginning of the experiment. The samples were contained in a platinum foil envelope that had been pre-cleaned by preparation as shown within figure 2.9 and then combusted for *ca.*10 hours at *ca.*1000°C and then kept at *ca.*600°C until required.

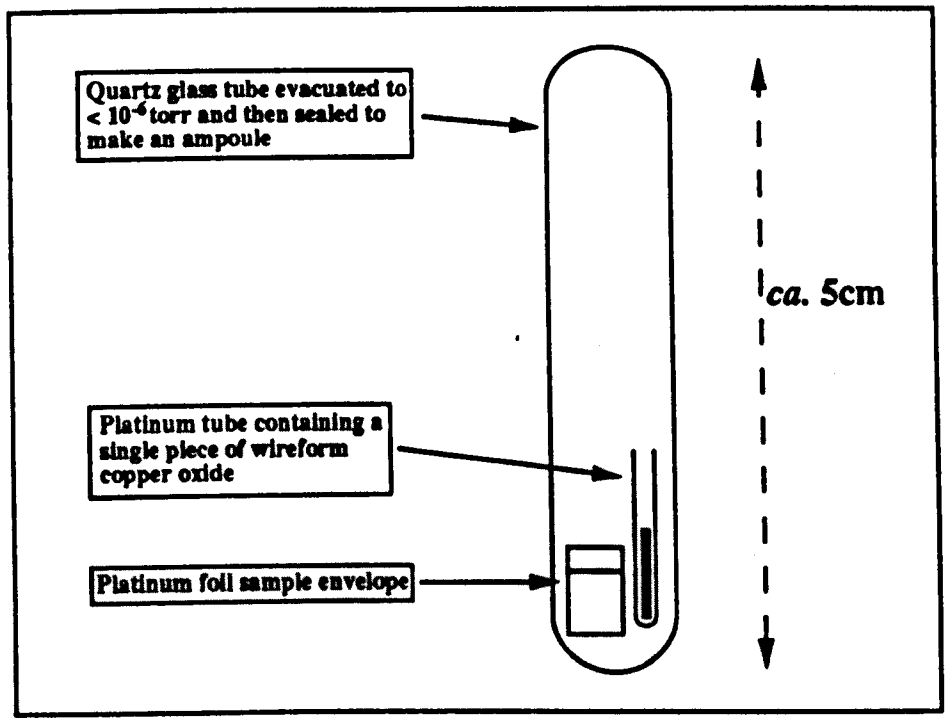

Figure 2.9. The method of preparing platinum sample packets for cleaning by combustion to *ca.*1000°C for *ca.*10 hours by Ash, 1990.

When the pre-cleaned platinum sample packet was required, the quartz glass ampoule (figure 2.9) was opened under clean-room conditions and any sample or platinum foil handling required was carried out by using solvent cleaned (protocol C in table 2.1) stainless steel implements. By then closing valves A and C and then removing B, the sample envelope was introduced to the extraction line using solvent cleaned tweezers and a clean length of quartz glass tubing. Valve B was then replaced and the loading section evacuated by opening valve A. When the pressure in the line had reached *ca.*1 x 10^{-6}torr the envelope was manouvered in to the reaction vessel by closing valve B (thereby minimising any blank input into the reaction vessel from the rest of the gas extraction line) and opening valve C, and then by external manipulation of the iron slug by a hand magnet, the envelope was pushed down into the reaction vessel. Figure 2.10 shows the results of a full procedural stepped combustion on an empty platinum foil sample envelope using the reaction vessel and platinum sample envelope preparation procedures of Ash, (1990).

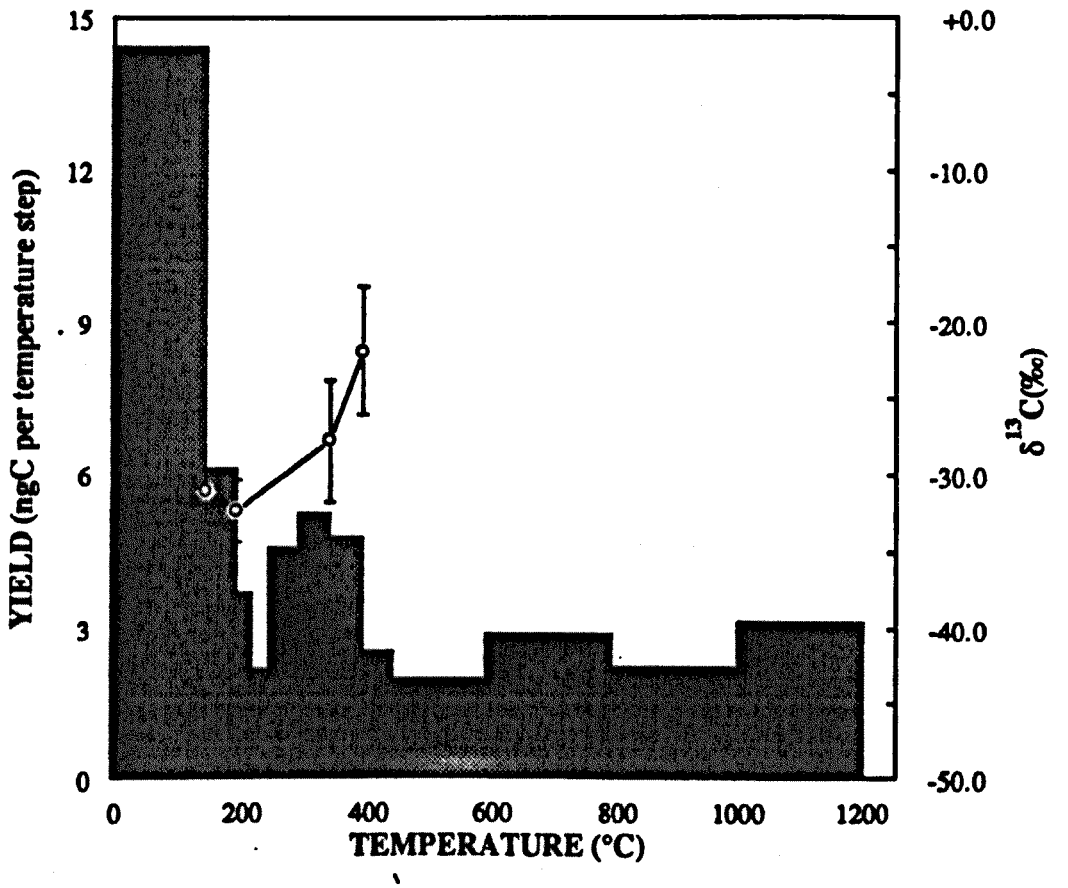

Figure 2.10. Full procedural stepped combustion profile for a platinum foil sample envelope prepared using the preparation protocol and reaction vessel of Ash, (1990).

From figure 2.10 it is evident that the total carbon blank from a stepped combustion experiment was approximately 40ng for the for the CO_2 extraction system in use at the beginning of this study. The combustion temperature and isotopic composition of the bulk of the carbon measured is indicative of organic contamination, and the carbon release profile indicated that the blank is possibly composed of three separate components but with the major release being between room temperature to 200°C.

2.3.3. Construction and testing of the MS86 reaction vessel.

With the development of MS86 a new reaction vessel was required. The basic design chosen was a doppleganger of that of Ash, (1990), but with the following modifications:

(1) The oxygen source was reduced to *ca.*20 pellets (50 to 100mg total mass) of wire-form copper oxide (CuO), this being at least a factor of ten less than previously.

(2) The surface area of the glass involved in the system and its overall volume was reduced by about an order of magnitude over that of the Ash, (1990) system.

(3) The practice of lubricating the valves in the extraction line with a low vapour pressure silicone oil (Abell *et al.*, 1979) was discontinued.

(4) Electical heater tapes (Electrothermal, c/o Jencons, Leighton Buzzard, UK) set at 130°C for continous running were wound around all pyrex sections of the system.

(5) The transducer for measuring oxygen pressure was removed.

These changes were made in an attempt to further reduce the carbon blank from the extraction line, the rationale behind the changes are explained as follows; in addressing (1) and (2), the copper oxide and glass are both suspected of contributing to the carbon blank (see Chapter 4), whereas in (3) the oil serves as a source of hydrocarbons. It is believed that cold glass serves as a potential surface to trap down contaminants which can be remobilised later during combustions. To avoid this possibility the glass is kept hot by the action of the heater tapes (4), and although it initially causes increased degassing and so takes longer to reach the same apparent level of low-blank as unheated glass, their action theoretically arrests this behavior. The transducer was removed (5) essentially because, intuitively, any extraneous component within the combustion section provides a blank input.

In addition to the reaction vessel changes in MS86, the single diffusion pump of the Triple Collector was replaced by two turbo-molecular pumps thereby removing the possibility of pump oil contamination. Likewise the rotary pumps that back the turbos were fitted with alumina foreline traps to prevent backstreaming of contaminants to the system.

It was anticipated that a possible consequence of reducing the amount of CuO within the combustion section was that the combustion process could be impaired. Taking the mass of CuO present (*ca.*50 to 100 mg), and assuming 100% disproportionation upon heating to copper and oxygen, the absolute amount of oxygen available for combustion is 10 to 20 mg of O_2, or in other words approximately 5mg of carbon could be converted to CO_2. Notwithstanding the fact that the disproportionation reaction is unlikely to be 100%, it is still evident that there is more than enough oxygen potentially available to combust the yields of carbon anticipated (ideally 10 to 20 ng from each temperature step). To check that the changes to the MS86 reaction vessel and gas extraction line had not impaired its performance in relation to that of the Triple Collector, two meteorite acid residues experiments that had previously analysed on the Triple Collector by Ash, (1990) were replicated on MS86. Table 2.5 shows the results of these experiments.

Sample	Triple Collector*		MS86	
	Weight (mg)	[C] (wt%)	Weight (mg)	[C] (wt%)
Cold Bokkeveld (CB2-C-Spinel)*	0.268	4.4	0.109	5.7
Allende (CIII)*	0.231	38.2	0.030	44.4

* Acid resistant residues, see Ash, (1990) for details of their preparation.

Table 2.5. Comparison of carbon concentrations derived by indentical stepped combustion experiments carried out on the Triple Collector and MS86 to investigate the performance of the MS86 extraction line.

From table 2.5 it is evident that there was a good agreement between the carbon yields obtained from the two sets of experiments, so indicating that any doubts about the changes made to the MS86 gas extraction system were unfounded.

The carbon blank of the MS86 reaction vessel is dealt with in detail within chapter 4 and so is not addressed here.

Chapter 3

Major Element Chemistry and Mineralogic Studies.

3.1. Objectives.

The primary objective for this section of the research was to determine the major element chemistry of selected micrometeorites so that in turn it could be possible to decide to which mineralogic type each sample belonged. The ability to perform this task was imperative for the interpretation of the micrometeorite stable carbon isotopic results because it was considered likely that similar mineralogic groups could share similar isotopic signatures.

After using the major element chemistry to allocate the micrometeorites to mineralogic types, it was envisaged that the data could then be further used to provide evidence of extraterrestrial origin, and to monitor the effects of algal contamination in the Greenland cryoconite samples.

3.2. The choice of analytical technique.

During the execution of the analysis protocol (2.1.1) a fragment of each individual micrometeorite had been selected for the purpose of major element analysis. Since only microgram quantities of material were available for this analysis it was necessary to explore the suitabilities of various analytical techniques with regard to the objectives set out in 3.1.

3.2.1. Ion microprobe.

Notwithstanding the fact that the use of an ion microprobe would have been difficult because of instrument availability, its use was further discounted due to analysis problems. The majority (*ca.*75%) of the micrometeorite samples scheduled for analysis were selected from Greenland cryoconite (1.5.5) and a previous mineralogic study by Maurette *et al.*, (1986) had revealed that *ca.*84% of the spherical micrometeorites within cryoconite were of a silicate composition. Ion microprobe analyses of silicates are complicated by problems of molecular interference and surface chemistry, and subsequently require very detailed calibration to achieve reliable results (Ray and Hart, 1982), and so would be of little use in the analysis of the silicate micrometeorites.

3.2.2. Proton microprobe (PIXE).

Although again the lack of instrument availability would have been problematic, the sample size requirements for analysis by PIXE made it inexpedient for use in determining the major element chemistry of the micrometeorite fragments. These fragments were typically <50μm in diameter and to obtain a reasonable analysis by PIXE requires a proton beam excitation volume of *ca.*20 to 30μm^3 (*e.g.* Griffen *et al.*, 1988). Even though the samples would provide enough material for bulk analysis, the micrometeorites are known to be composed of individual crystals that are typically only a few microns in size (*e.g.* Brownlee, 1985), and if the compositions of these individual crystals were to be determined, which is desirable in addressing the objectives of the work, then a much reduced excitation volume was required.

3.2.3. Synchrotron X-ray fluorescence (SXRF).

A single particle was analysed by Dr.P.Potts at the experimental synchrotron X-ray fluorescence (SXRF) facility at Daresbury (Cheshire, UK) as a part of a study to explore the system's potential for micro-analysis. An advantage of SXRF is that sample preparation is minimal. For this initial investigation a single 200μm diameter deep-sea spherule was mounted directly (without cutting or polishing) onto an acetate sheet. The data obtained were unfortunately only qualitative, but it was still apparent

from the results that the technique in its present form was not capable of fufilling the analytical requirements. The SXRF technique was found to be most efficient at detecting a relatively narrow band of trace elements (^{34}Se to ^{28}Ni for K-lines and ^{72}Hf to ^{82}Pb for L), with the detection characteristics for major elements below Ca (K-line) ineffective due to poor X-ray excitation. Although detection limits were good (*ca.*60ppm), this restricted band of element detection means that the system is only really of use for trace element measurement.

3.2.4. X-ray diffraction techniques (XRD).

The use of XRD techniques were investigated in order to assess their efficacy for sample identification. XRD does not provide major element chemistry results but facilitates identification of the constituent minerals of each analysed samples based upon their crystal structure. An incident beam of X-ray radiation is diffracted by the crystal structure in each sample and then the pattern of diffraction lines so produced is used to calculate the dimensions of the crystal lattices present, and then these characteristic values are used to determine which minerals are present (*e.g.* Lipson and Steeple, 1970).

Conventional XRD analysis is by powder diffraction methods, where the sample is ground into a fine powder so that all orientations of the stuctural cells are obtained during analysis. This is necessary to give strong and complete X-ray diffraction lines and so facilitate easy identification of the mineral phases present. Such destructive powdering of the samples was not applicable herein, but could be avoided by the use of the Gandolfi X-ray diffraction camera (Officina Electtrotecnica di Tenno, Tenno, Italy); here the sample, usually a single crystal for conventional work, is held in the radiation beam and rotated in a manner so that almost all orientations of the sample are exposed, thereby mimicking the effects of powdering. The experimental set-up to achieve this is shown in figure 3.1.

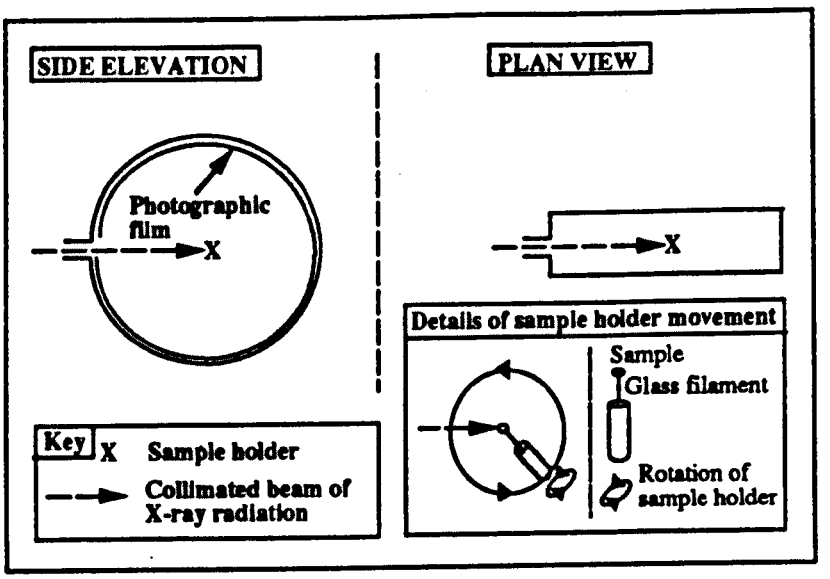

Figure 3.1. Schematic of the operation of the Gandolfi X-ray Diffraction Camera. Use of this apparatus allows structural information to be obtained from samples without the destructive powdering associated with conventional techniques.

The sample holder is positioned within the camera so that the sample is held in the incident beam of radiation, and the illustrated double rotation of the holder ensures that all orientations of the particle are exposed to the radiation. The size of the sample used in the Gandolfi camera is crucial in obtaining good XRD results. The sample needs to be small enough to allow the X-ray beam to penetrate the whole particle and so yield a representative diffraction line pattern, but not so large so that the beam is absorbed or too small so that no pattern is recorded at all. Experimentation has shown that the ideal sample size diameter is between 200-500μm (*e.g.* Lipson and Steeple, 1970), and this requirement dictated that the samples were analysed as whole-particles. Sample mounting is usually by adhesive onto a glass filament, as both are amorphous and so do not produce any diffraction lines. The residual carbon contamination of this adhesive would obviously be catastrophic for any carbon isotopic work and so an alternative system was devised where a *ca.*5mm length of cobalt wire of *ca.*0.5mm diameter was substituted for the glass filament. The cobalt wire was magnetised with a hand magnet prior to use and so allowed the magnetic nature of the samples to be utilised in holding them in position without the prohibitive contamination of adhesives. The wire was sharpened with the tapered end being used to hold the sample. The reasoning behind this was that the cobalt produces a potentially obscuring diffraction line pattern and so sharpening the wire minimised its exposure to the X-ray beam. This procedure was chosen instead of simply using a thinner wire because the non-sharpened end of the thicker wire, which was kept out of the radiation beam, allowed

Sample	Diameter	Phases identified by X-ray diffraction							AEM analysis^
	(μm)	Maghemite	Wuestite	Magnetite	Goethite	Taenite	Calcite	Olivine*	
2.18	180	Yes			Yes		Yes		$
2.17	200	Yes	Yes						$
1.1	160	Yes							Iron oxide
2.6	200	Yes							Iron oxide
C5	160	Yes							Iron oxide
4.1	180	Yes	Yes	Yes		Yes			Iron oxide
?13	220	Yes						Yes	Fe-rich olivine

$ = Sample lost after XRD analysis.

* = Fayalite (Fe-rich olivine).

^ = Differentiation between different iron oxide minerals was not possible because the AEM gave results expressed in FeO only. (See appendix for full details of major element compositions).

Table 3.1. Results of the Gandolfi XRD analyses of seven deep-sea micrometeorites. After XRD analysis the samples were then analysed for their major element chemistry using an analytical electron microscope (AEM).

good retention of the applied magnetism which was necessary to hold the samples. Cobalt was chosen out of the magnetic materials available because intuitively it was the least likely element to be present within the samples.

Seven samples were analysed using the Gandolfi X-ray diffraction camera and sample mounting procedure described in the previous section. To check the results obtained, these samples were then analysed by an analytical electron microscope (AEM) for major element chemistry. The results of this are shown in table 3.1, where the minerals identified by XRD are presented along with the corresponding results of the AEM analysis. From table 3.1 it is evident that in all the cases where the major element chemistry of each sample was subsequently determined after the XRD analysis (5 out of 7) the same mineralogy was deduced from both methods. However, the XRD method was abandoned for the following reasons:

(1) Sample loss rates were judged to be unacceptably high. Losses ocurred both during the analysis period within the Gandolfi camera and also when attempting to retrieve the samples from the magnetised cobalt needle. The problem was that either the samples were not sufficiently strongly held and so were lost as the Gandolfi sample holder rotated within the camera, or too strongly held so that they could not easily be removed from the cobalt needle. The strength of the magnetic bond with the needle was seeemingly controlled by the sample composition with respect to ferro-magnesium minerals and so was out of the control of the procedure.

(2) Experimentation revealed that to obtain a diffraction pattern strong enough to allow indentification of the constituent minerals of the samples, they needed to be exposed to the X-ray beam for between 16-24 hours. Unfortunately the time avalailable for using the Gandolfi camera was limited. However, this did not infact become a problem because development of the AEM technique (3.2.5) rendered the XRD technique largely obsolete.

Ablation of particles during atmospheric entry (*e.g.* figure 1.5) normally produces iron oxide predominately in the form of magnetite, which has a formula of $Fe^{3+}Fe^{2+}{}_2O_4$. Evidence for this comes from studies of meteorite fusion crusts (*e.g.* Blanchard and Davis, 1978), artificially produced fusion crusts (*e.g.* Blanchard, 1972; Blanchard and Cunningham, 1974) and petrographic studies of deep-sea spherules (*e.g.* Caistaing and Fredriksson, 1958; Brownlee *et al.*, 1975). In despite of this, magnetite was only positively identified in one sample, with the diffraction line spacings for the samples always showing a closer match to those of maghemite.

Maghemite is an iron oxide of the spinel group with a chemical formula of $Fe^{(3+)}_2O_3$. Ablation also can produce a minor amount of wuestite (Marvin, 1963). Wuestite ($Fe^{2+}O$) is of particular interest as it is almost unknown in the terrestrial environment, but is almost ubiquitous as a minor component in meteorite fusion crusts. This is because it has a metastable nature and so is only able to form at high temperatures coupled with a low oxygen partial pressure (*e.g.* Brownlee,1981). Wuestite does not share the spinel structure with maghemite and magnetite and so possesses a diffraction line pattern that is readily recognisable. This meant that even if wuestite was only present as a relatively minor component, and so only produced a feint diffraction line pattern, it could be identified with confidence. The presence of wuestite is confirmation of an extraterrestrial origin (Castaing and Fredriksson, 1958), and with two of the particles analysed here showing its presence, their origins are likewise confirmed. However, of equal importance to the relationship between the different iron oxides was that the two samples that contained wuestite also contained maghemite.

To summarise the observations from the XRD results;

(1) Maghemite was present in all the samples. This was unexpected because if the iron oxide was produced as a result of ablation/oxidation during atmospheric entry, then primarily magnetite should have been formed.

(2) Two samples contained wuestite which could be used as evidence of their extraterrestrial provenance.

(3) The association of maghemite with the samples that contained wuestite suggested that either the maghemite was also formed by ablation/oxidation, or was an alteration product of the original magnetite/wuestite assemblage.

3.2.4.1. A proposed alteration cycle for ablation/oxidation produced iron oxide as a result of oceanic weathering.

It is proposed that the primary ablation/oxidation produced iron oxides (magnetite and wuestite) within the deep-sea micrometeorites have undergone alteration to maghemite and then goethite as a result of oceanic weathering during their sojourn in the oceanic environment. It is already known that wuestite, being metastable in nature, reverts to magnetite in the terrestrial environment (*e.g.* Brownlee, 1981), and that goethite is a common marine weathering product of maghemite (*e.g.* Deer *et al.*,

1983), so the only remaining problems to reconcile are the alteration of magnetite to maghemite, and how to explain these alteration pathways with regard to the oceanic environment. Upon residing in the oceanic sediment, the following pattern of diagenesis is proposed.

	A		B		C	
Wuestite	→	Magnetite	→	Maghemite	→	Goethite
($Fe^{2+}O$)		($Fe_2^{3+}Fe^{2+}O_4$)		($Fe^{3+}{}_2O_3$)		($Fe^{3+}O.(OH)$)

To explain this scheme it is necessary to closely examine the conditions that prevail in the deep-oceanic sediment and relate these to possible reaction pathways.

Ablation/oxidation produces magnetite and wuestite, but any wuestite thus formed will revert to magnetite (reaction A) due to its metastable nature (*e.g.* Brownlee, 1981). Under certain conditions magnetite will undergo transition to maghemite by 'supergene' alteration (*e.g.* Krauskopf, 1982); this type of reaction occurs where regions of differing oxidation state are in close enough proximity to allow percolation of fluids between the two regions. These fluids enable the movement of ionic species and in the scenario proposed here, it is the movement of Fe^{2+} and Fe^{3+} which controls the reactions. Although the water at the sediment-ocean interface is oxidising, *ca.*20cm into the sediment column the conditions rapidly become reducing (*e.g.* Bearman *et al.*, 1989) with the concentration of oxygen declining, and Fe^{2+} increasing, with depth. This situation is ideal for the supergene alteration of magnetite to maghemite with oxidising and reducing environments existing only *ca.*20cm apart and the potential for fluid movement between the two. The percolating reducing fluids allow leaching of the Fe^{2+} from the magnetite and then a return to oxidising conditions coverts the magnetite to maghemite. With continuing exposure to the oxidising environment the maghemite will alter to goethite (reaction C), this being a common marine weathering product (Deer *et al.*, 1983).

When considering the feasibility of these reactions it is also prudent to keep in mind the time scales involved. Sedimentation rates in the deep-ocean environment are extremely slow, being in the order of (<5) millimeters per million years (*e.g.* Bearman *et al* ., 1989), so it is apparent that there is little problem in allowing ample time for these reactions to proceed, because the micrometeorites will remain in the oxidising zone for up to *ca.*50 million years. It is also important to remember that the Challenger sediments from which all the samples were extracted (Murray and Renard, 1891), had

all been collected by dredging and not coring, and so originate from the upper oxidising layer.

In relation to the XRD results of the micrometeorites within table 3.1, the alteration scheme proposed would suggest that sample 4.1 has the youngest, and 2.18 the oldest terrestrial age. Sample 4.1 contained both magnetite and wuestite which are both primary ablation/oxidation products, but also maghemite, which presumably represents the onset of the supergene alteration of the indigenous magnetite. The presence of taenite, an iron-nickel alloy common in meteorites, in sample 4.1 substantiates these arguments, because intuitively a metallic alloy would be ephemeral in the oceanic environment. On the other hand, sample 2.18 contained goethite, and it is proposed that this represents the alteration product of maghemite that had in turn been formed from the alteration of either indigenous magnetite or that produced by the revertion of wuestite. Sample 2.18 was also the only particle to exhibit calcite, but this was not considered to be related to the age of the sample but had presumably either been precipitated onto the sample or become adhered to it from calcite within the sediment. The latter explanation would appear to offer the most feasible solution in light of the evidence that the sediment from which the sample was extracted was found to contain *ca.*25% calcite so any further precipitation would probably take place upon the existing calcite crystals.

Examination of previous studies of deep-sea oceanic spheres provides further evidence as to the validity of the proposed alteration scheme. Firstly, Finkleman (1970), in a XRD study of spheres extracted from manganese nodules, identified spherules composed purely of goethite or maghemite, and also ones where wuestite and maghemite co-existed. Manganese nodules are perculiar in that they remain at the sediment/water interface and do not become submerged by sedimentation processes. Although the reasons behind this are not clear (*e.g.* Bearman *et al.*, 1989), it is apparent that a micrometeorite that becomes incorporated into a nodule will thus remain in the oxidising environment for timespans larger than those that fall directly into the sediment and are eventually submerged. In view of this, it is not surprising that spheres composed entirely of goethite were discovered, these representing the samples that have been allowed to reach the extreme of of the cycle due to the prolonged exposure to oxidising conditions. Secondly, Chevallier *et al.*, (1987) noted that the iron oxide ablation rims in oceanic spheres were thicker than those in Greenland samples, and inferred that some sort of secondary oxidation was occuring.

Although the proposed scheme has little implication for the bulk of the Greenland Cryoconite and Antarctic Ice collected samples analysed in this study, it maybe of considerable use for alternative studies. The ability to judge the relative age from the degree of alteration experienced by a micrometeorite using this simple non-destructive XRD technique maybe of use to studies of oceanic sedimentation rates through core analysis, or to investigators examining spheres for purposes such as oxygen isotopes (*e.g.* Clayton *et al.*, 1986) or radiogenic isotopes (*e.g.* Nishiizumi, 1983).

3.2.5. Electron probe microanalysis (EPMA).

The EPMA system works by monitoring the X-ray radiation emitted by the sample as it interacts with an impinging electron beam (≤1μm diameter and *ca.*20KV). The presence of a particular chemical element is inferred by the wavelength of this radiation, and its abundance by in the sample by its intensity. The system can detect elements that are present within samples at >*ca.*0.1wt%. The advantages of the EPMA system over PIXE, where a proton beam is used and much better detection limits are available (3.2.2) were as follows;

(1) The electron excitation volume during an analysis is typically only a few μm^3 (*e.g.* Griffen *et al.*, 1988), and so would present no problems in determining the composition of individual crystals within the micrometeorite samples scheduled for analysis.

(2) EPMA instruments were readily available for use.

Sample preparation is of fundemental importance to the quality of results obtained by EPMA analysis, with optimum analysis conditions upon a flat, highly polished, electrically conducting surface. This is because the intensity of the X-ray radiation emmitted by the sample is affected to differing extents by absorption within the sample material surrounding the analysis spot. These effects are normally compensated for by applying various mathematical corrections to the acquired data; these are calculated for interaction of the beam on a flat surface held in a specific orientation relative to the radiation collectors. Analyses carried out on an unpolished, non-orientated samples may lead to incorrect element abundances, because although the correct elemental composition will be obtained from the wavelengths of radiation present (unless the radiation is absorbed completely), the relative intensities of these elements may be

erroneous. During analysis of unpolished samples care must be taken to analyse spots situated on flat surfaces that appear to be orientated parallel to the surface of the microscope stage; this being the same as a flat, polished thin-section would define.

Since the fragments of micrometeorite available for analysis were produced by a crushing action, the exposed fractures tended to follow lines of weakness, and although some were found to approximate flatness, they were not smooth or polished. In order to polish these fracture surfaces, several samples were individually mounted in epoxy resin and polished using grinding wheels and diamond paste (4 to 0.5μm grade). This technique proved relatively successful, with only a few (*ca.*10%) of the samples being plucked out of the epoxy and lost during grinding. Such losses were probably the result of two contributing factors; the samples may be weathered and therefore liable to break-up on polishing, or the bond formed between the resin and the particle may not be strong enough to hold the particle during the polishing process. Experience with thin-section cutting from <50μm unmelted micrometeorites (Bradley, 1988) has shown such sample cleanliness to be imperative, and where applicable pre-cleaning by oxygen plasma ashing is carried out (J.P.Bradley, *pers.comm.*). The addition of a cleaning step to the protocol, with the concomittant risk of sample loss, was judged as unacceptable, and although the total loss rate through polishing was low, taking into account the effort applied during the processing, collection and splitting of the samples, an alternative solution was sought for the sample mounting procedure.

For conventional scanning electron microscope (SEM) work using the Hitachi S-2500, the samples are either mounted onto aluminium stubs (*ca.*0.5cm in diameter), or if samples larger than this are scheduled for analysis, directly onto the *ca.*15cm diameter aluminium microscope stage. To obtain scanning electron images using this system the samples are usually pre-coated by carbon or gold to avoid sample charging during analysis. The Hitachi S-2500 offers the additional feature in that it contains an EPMA system (Link AN-10-55-S), and so can used to obtain major element chemistry from samples, and for this reason such instruments are called analytical electron microscopes (AEM). The same limitations apply to the quality of the EPMA chemical data acquired by AEM systems, *i.e.* quantitative or qualitative depending upon the whether the sample has been polished, but their use offers the additional ability of obtaining conventional scanning electron images of the samples.

The use of the AEM system was investigated for determining the major element chemistry of the micrometeorite fragments. Because the analyses would be carried out on fracture surfaces, as explained previously, it was anticipated that the data acquired would be qualitative or semi-quantitive at best. It was, however, the capability of the AEM to analyse unprepared samples that was of importance to this work, but if the technique was to be usefully applied, then a mounting procedure for analysis of the sample fragments had to be devised that involved a reduced risk of loss over that for the polishing procedures. Subsequent experimentation led to the sample mounting method as shown in figure 3.2.

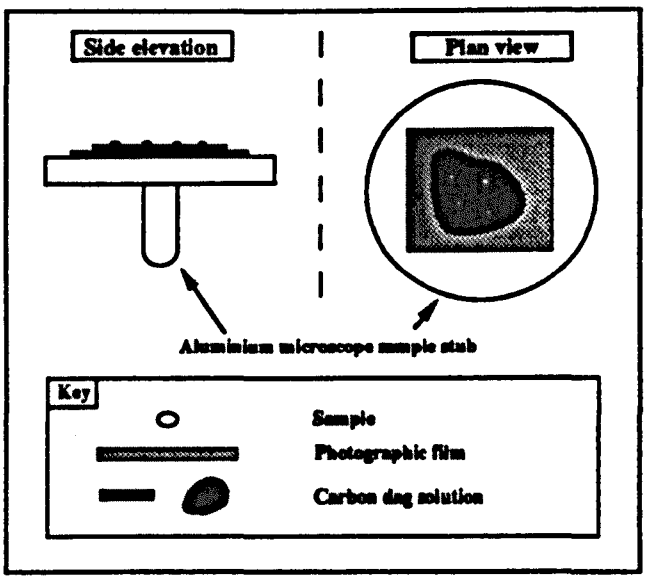

Figure 3.2. Particle mounting procedure developed for the analysis of micrometeorite fragments by analytical electron microscope.

To avoid particle loss during analysis by specimen charging, it was imperative that good electrical conduction was maintained from the sample to the specimen stage of the microscope, and it was for this reason that a conventional aluminium microscope stub was chosen. Photographic film was used as the sample substrate because it provided an excellent surface for the carbon dag due to its adhesive qualities when moist, and so facilitated a good bond between the two. Carbon dag is a colloidal suspension of graphite particles in distilled water and has excellent conducting qualities and so provided a conduction pathway between the micrometeorite fragments and the aluminium stub. It was found that if the dag was applied and then left for a couple of minutes to allow it to become partially solid, then the particles could easily be transferred to the dag from the point of a magnetic needle. After drying, the whole

stub was then coated with a *ca.*1μm film of carbon (by a conventional carbon coating machine) ready for introduction to the AEM for analysis.

This mounting protocol proved to be extremely successful. The analysis protocol using the AEM had additional advantages that compensated for the loss of precision in the data acquired compared to the samples that had been polished. Morphological information was available in the form of conventional SEM photographs, and this provided another possible means to classify particle types. The mounting technique also enabled easy subsequent removal of the fragments as the dag was found to form only a relatively weak physical bond with the samples. This ability to retrieve the sample fragments after analysis in the AEM was envisaged as being potentially useful if further analytical work was to be carried out on the samples. For instance, the retrieved fragment could be mounted in epoxy resin and then polished in an attempt to gain more quantitative results by EPMA analysis, but the accompanying risk of loss during polishing would be less important because the AEM would have already provided qualitative data. It was likewise anticipated that the sample fragment could be analysed by different analytical techniques (*i.e.* PIXE, SXRF, XRD *etc.*) where additional chemical and mineralogical data over the major element results from the AEM analysis could be acquired.

3.3. Success of the analytical techniques.

The final adopted scheme for the determination of major element chemical data, and subsequent mineralogic identification of the micrometeorite fragments, involved analysis by AEM alone. The reasons for not pursuing the initially promising results of the Gandolfi XRD work were as follows: At the onset, it was expected that the AEM data from unpolished samples would be of poor quality. However, examination of initial AEM results showed that these fears were largely unfounded, the relative ratio of the detected elements allowed easy identification of mineral species, in agreement with the Gandolfi XRD results. The fact that this secondary confirmation of the mineralogy deduced from the major element AEM derived chemistry appeared unnecessary, coupled to the increased risk of particle loss in the additional XRD analysis step, led to the decision to concentrate efforts solely upon the AEM. Subsequent analyses, presented in the remainder of this chapter, have shown that the AEM technique, applied in the manner described, is sufficient in all cases encountered

to fufill the primary objective of mineral identification and similar-particle grouping defined at the beginning of the study. In addition, the quality of the data has indeed proved good enough to address the secondary criteria outlined in 3.1; that of confirmation of extraterrestrial origin and of algal contamination of Greenland samples.

3.4. Results.

3.4.1. A summary of the petrologic study of spherical micrometeorites.

Murray and Renard (1891) classified the microscopic magnetic 'cosmic spherules' that they had collected during the voyage of H.M.S. Challenger into one of two petrographic groups. One type (type I) which was shiny and black, was found to be composed predominately of iron oxide. The second type (type S) was brown and had a silicate composition. The collection efforts of the 1950s (*e.g.* Brunn *et al.*, 1955; Laevastu and Mellis, 1955; Castaing and Fredriksson, 1958; Pettersson and Fredriksson, 1958; Smales *et al.*, 1958), allowed more detailed chemical analyses to be applied to the collected samples. Brunn *et al.*, (1955) executed a very detailed study of polished sections of spheres, and amongst their findings were Fe-Ni carbides and phosphides within type I particles and zoned silicates and small magnetite crystals in type S examples. With the application of improved analytical techniques, such as the electron microprobe (Castaing and Fredriksson, 1958) and neutron activation (Smales *et al.*, 1958), more detailed characterisation was possible, and the types isolated from oceanic sediments can be summarized as follows;

(1) Type I - Composed of magnetite and wuestite that commonly enclose either a small metallic Fe-Ni core or a smaller nugget of platinum group elements (*e.g.* Brownlee *et al.*, 1984)

(2) Type S - Composed almost exclusively of olivine, magnetite and glass. They commonly exhibit barred, and less frequently, porphyritic textures. Rarely they also contain a Ni-Fe metal bead, and troilite spheroids or relict grains of forsterite, enstatite and chromite (*e.g.* Blanchard *et al.*, 1980).

(3) Type G - These are a rare type of spherule composed essentially of type I material plus a small amount of glass. They differ from type S spheres in that they do not contain crystalline silicate material and usually possess a volume ratio of magnetite to glass greater than unity. Occasionally they also exhibit metal cores. For a detailed discussion see Millard and Finkleman (1970) and Finkleman (1970;1972).

With recent collection efforts moving away from the oceans to the ice fields of Greenland and Antarctica (see 1.5), collection of more pristine spherules and unmelted particles has been possible, but the spherules that have been collected so far fall largely into the groups presented above. However there are exceptions; Greenland cryoconite contains glassy spherules of chondritic compostion and metallic Fe-Ni spherules (Maurette *et al.*, 1987). The chondritic glassy samples are either 'homogenous', in which case they show no structure at all, or 'barred', exhibiting an ultra-fine texture of amorphous material with orientated deposits of small magnetite inclusions. Of the spherules collected in Antarctica, no new types outside of the oceanic and Greenland examples have been found (Koerberl and Hagen, 1989; Maurette *et al.*, 1991).

3.4.2. Allocation of micrometeorite fragments to petrographic types.

Table 3.2 presents a summary of the chemical and morphological characteristics of the micrometeorite fragments analysed by AEM. Individual samples are denoted by a unique identification number along with a corresponding carbon isotope analysis extraction number. Major element chemical abundances obtained during AEM analysis are listed in the Appendix, only the interpretation of these data are presented in this section.

In order to classify samples into either type I or S groups broad beam AEM analyses were performed, *i.e.* an area on each particle up to *ca.*50μm^2 was analysed. Examination of the results shown in table 3.2 illustrates that only 2 out of 20 samples were allocated type I, with the remainder being type S. Of the 5 particles extracted from the deep-sea sediment, 2 were of type I which is in keeping with the work of Blanchard *et al.*, (1980), who found *ca.* 50% of oceanic particles were type I. For the Greenland samples, no type I samples were identified and this again is in agreement with Maurette *et al.*, (1986), who reported that only *ca.* 2% of Greenland samples were type I in composition.

Sample	Run number*	Type(I/S)	Locality@	Matrix mineral composition	Textural type$
KKF	T597	S	DSS	Olivine£ (Fo 47)	CG
KKB	T598	S	DSS	Olivine (Fo 64)	B
KKE	T600	S	DSS	Olivine (Fo 81)	B
Csp1	T621	I	DSS		G
Csp2	T630	I	DSS		G
SS89M07	T687	S	CRY		B
SS89M08	T688	S	CRY		B
SS89M05	MS14	S	CRY		B
SS89M12	MS15	S	CRY		B
SS89M09	MS22	S	CRY	Pyx^ (Wol 18/ En 29/ Fs 53)	B
SS89M10	MS23	S	CRY		B
SS89M17	MS27	S	CRY		B
SS89M14	MS29	S	CRY	Olivine (Fo 71)	B
SS89M16	MS30	S	CRY		B
SS89M18	MS31	S	CRY		B
MA1	MS33	S	ANT		B
MA2	MS34	S	ANT		CG
MA3	MS35	S	ANT	Pyx (Wol 7/ En 15/ Fs 78)	CG
MA4	MS92	S	ANT	Olivine (Fo 83)	CG
MA5	MS93	S	ANT		B

* = (T = Triple Collector and MS = MS86 mass spectrometers).
@ = (DSS= deep-sea sediment, CRY = Greenland cryoconite and ANT = Antarctic ice).
$ = (CG = coarse grained, B = barred and G = glassy).
£ = (Fo = weight % (wt%) forsterite).
^ = (Pyx = pyroxene, Wol = wt% wollastonite, En = wt% enstatite and Fs = wt% ferrosilite).

Table 3.2. A summary of the petrographic and textural types and matrix mineral compositions after AEM analysis of the micrometeorite fragments. (For full details of major element chemistry see the appendix).

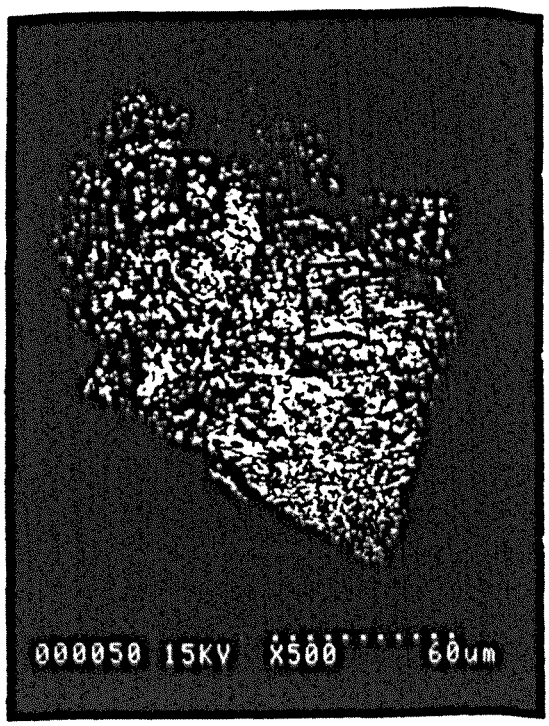

Plate 3.1. AEM electron image of a fragment of a type S micrometeorite. This example exhibits the 'barred' texture, where lamellae of olivine, or occasionally pyroxene, occur with smaller crystals of iron oxide. (The annotated boxes on the plates indicate positions of AEM measurement).

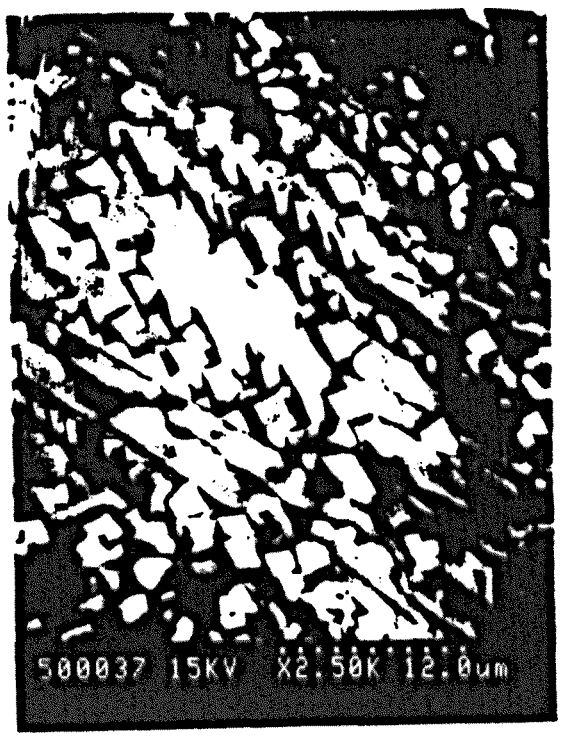

Plate 3.2. Close-up of the 'barred' texture as shown in plate 3.1. The use of the back-scatterred electron detector of the AEM highlights differences in elemental composition within the sample. The relative brightness of the sample reflects the mean atomic weight of the constituent elements, with heavier minerals showing brighter shading.

Plate 3.3. A back-scattered electron AEM photomicrograph illustrating an example of a 'coarse grained' type S micrometeorite. Olivine crystals up to *ca.*10μm in size occur with smaller (and brighter) iron oxide crystals.
(The dark patch in the lower right hand corner of the sample is a layer of carbon dag used to fix the sample to the microscope stub).

Plate 3.4. A back-scattered electron AEM photomicrograph illustrates an example of a 'glassy' type I micrometeorite. In comparison to plates 3.1 and 3.3 there is an absence of crystal structure, and the uniform shading suggests an equally uniform chemical composition, which in this case is iron oxide.

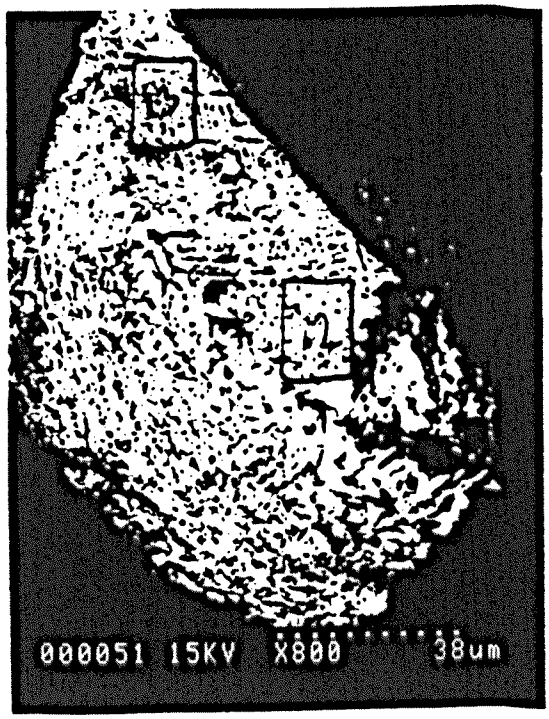

Plates 3.5, 3.6 and 3.7. Secondary electron AEM photomicrographs of Greenland cryoconite micrometeorites SS89M05, SS89M16 and SS89M17. The porous nature of these samples (which maybe the result of biogenic etching by algae within the cryoconite) is a diagnostic feature of some cryoconite micrometeorites.

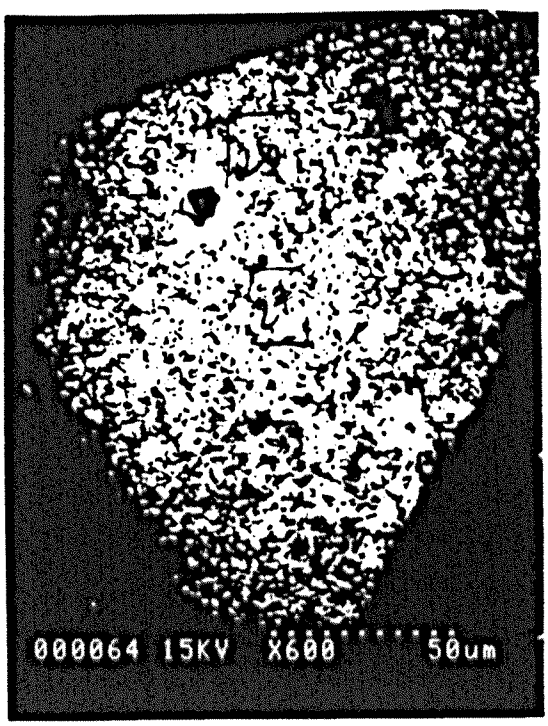

Plate 3.8. A back-scattered electron AEM photomicrograph of Antarctic micrometeorite sample MA2. The high sulphur and phosphorus content of the adhereing filament obtained during AEM analysis indicated that it represented Greenland cryoconite algae, and the sample had been contaminated in the laboratory prior to cleaving within the analysis protocol.

(The apparently sinuous nature of the filament was caused by movement due to charging).

The morphology and texture of each sample fragment was determined by using the SEM facility within the AEM. Examination of these results for the type S particles indicated the presence of two different textural groups; out of a total of 18 particles, 14 were of 'barred' morphology while 4 were 'coarse grained'. Plates 3.1 and 3.2 illustrate a typical barred example. These SEM photomicrographs were taken using the back-scattered electron detector of the AEM, so the relative degree of brightness of the sample reflects its elemental composition; the higher the average atomic weight of the constituent chemical elements, the brighter the mineral appears in the image. Plate 3.2 shows a close-up of the texture, illustrating a matrix of thin lamellae (*ca.* 2-3 μm thickness) with less abundant smaller (*ca.* 2μm), more euhedral crystals of a higher average atomic number. Plate 3.3 represents an example of the coarse grained textural type; here a mixture of crystals of differing brightnesses (and composition) occur in what appears to be a darker matrix. Care must be taken here, as any changes in the surface morpholgy of the sample also effects the degree of brightness, with depressed areas showing darker, *i.e.* shaded, and elevated brighter, *i.e.* highlighted. The grain size of the coarse grained samples is more varied than in the barred types, with individual crystals approaching *ca.* 10μm in size. The final type of micrometeorite, classified as 'glassy', is seen only in the type I samples, and is shown in plate 3.4. Essentially no crystal structure can be seen, and the uniform shading of the samples indicates that there is little compositional variation across the grains. All of the textural types identified here are again in common with previous studies, inparticular the predominance of the barred type is in accordance with other recent petrographic work of Greenland and Antarctic spherules, where both Maurette *et al.*, (1986) and Koeberl and Hagen (1989) found >50% of their samples to be of this type.

In an attempt to further investigate the different morphological types deduced from the SEM photomicrographs, the ability of the AEM to analyse the major element chemistry of individual spots (*ca.*2μm^2) was utilised. The back-scattered electron photomicrographs indicated that minerals of different mean atomic weight were present in the barred and coarse grained type S micrometeorites, and so the AEM spot analysis system was used to determine the chemical difference between the minerals with the aim of their identification. The mineralogy of the type S samples was found to be dominated by Fe-Mg silicates and minor quantities of iron oxides. The lamellae of the barred samples were found to consist mainly of Mg-rich olivine (Fo $_{64\text{-}81}$) or occasionally Mg-rich, low-Ca pyroxene. The smaller euhedral crystals were found to be of Fe oxide composition, although determining whether as magnetite, wuestite or

maghemite was not possible. The coarse grained samples were found to share a similar mineralogy to the barred particles, with olivines (Fo $_{47-83}$), pyroxenes and Fe oxides being identified. In each case with the coarse grained samples, the silicates were still the major phase and constituted the larger crystals, with the Fe oxides being present as smaller crystals similar in type to the barred samples. Thus, the only major difference between the two type S textural groups was in their respective grain sizes, which could simply be a result of different cooling histories. Spot analyses taken across the glassy samples revealed that their compositions , as indicated by the back scattered electron images, were indeed uniform in composition. The glassy particles were all type I in composition but from their major element chemistry it was again not possible to differentiate whether this iron oxide was present as wuestite, magnetite, maghemite or goethite (see 3.2.4).

3.4.3. Major element chemistry.

Notwithstanding the fact that the spherules have experienced a strong heating (and melting) event at some period in their evolution, the relative concentration of refractory elements such as Mg, Ca, Cr, Al, Ni, Ti, Mn, Si and Fe *etc.* should represent their chemical composition prior to atmospheric entry. It could be anticipated that the elemental data will be primitive in nature having similarities with the composition of the carbonaceous chondrites (Brownlee *et al.*, 1975). To explore this possibility, the AEM data for each spherule was normalised to average CI chondrite composition, the meteorite data being taken from Anders and Grevesse (1989). The atomic abundance of the refractory elements in each micrometeorite were calculated and normalised to 10^6 silicon atoms. In order to compare this information with carbonaceous chondrite data, the atomic abundances were then divided by the corresponding CI chondrite abundance. A summary of the results are shown in figure 3.3. The range of values obtained for the refractory elements analysed (shown on the abscissa axis from left to right in order of increasing relative volatility) are plotted for samples from the deep-sea, Greenland cryoconite and Antarctic ice collections. For comparison purposes the results of a similar study carried out by Blanchard *et al.*, (1980) are included, where 19 polished sections of type S deep-sea spherules were analysed for major element chemistry using an EPMA system. In the study of Blanchard *et al.*, (1980) only those samples that did not show any evidence of seawater weathering were selected for

analysis - the resulting agreement with chondritic values was interpreted as providing good evidence as to their extraterrestrial origin.

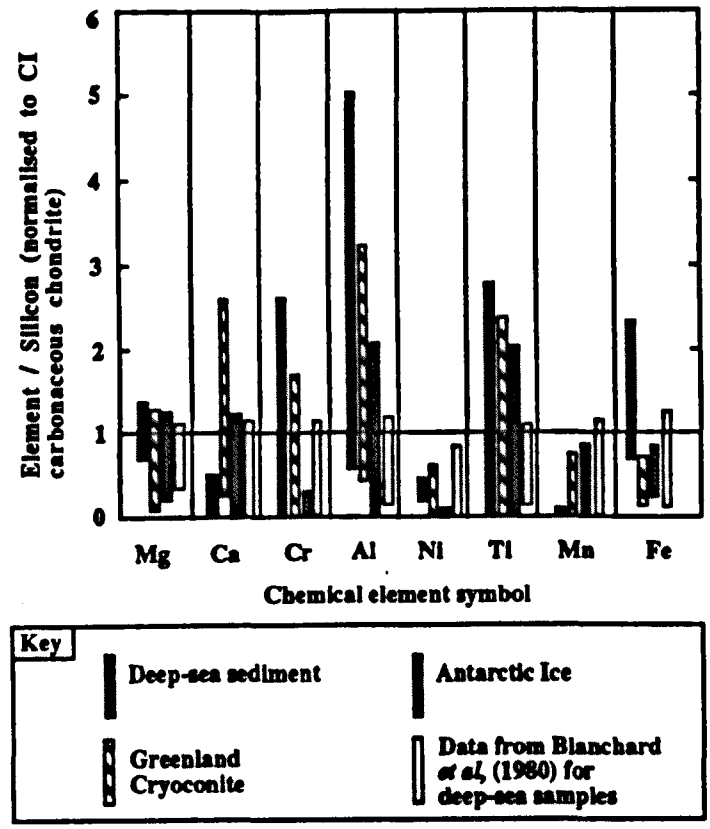

Figure 3.3. The range of values obtained by normalising the AEM micrometeorite data to CI carbonaceous chondrite data taken from Anders and Grevesse (1989). Results are presented for refractory elements only and have been divided into deep-sea, Greenland cryoconite and Antarctic ice groups. For comparison purposes the results of a previous study by Blanchard *et al.*, (1980) are included.

It can be seen from figure 3.3 that the results for the samples analysed here show a reasonable correlation with chondritic values. The major exceptions are;

(1) For a number of samples some of the elements were below the level of detection.

(2) In some samples certian elements (*e.g.* Cr, Al and Ti) show quite considerable enrichments.

The elements that were below the detection limit were those that are present in chondrites typically below the weight % level, and considering the limitations of analysing unpolished samples, it is not surprising that problems were encountered in their detection. For those refractory elements that are relatively abundant in CI chondrites, *i.e.* Mg, Ca, Al and Fe, there was a good correlation.

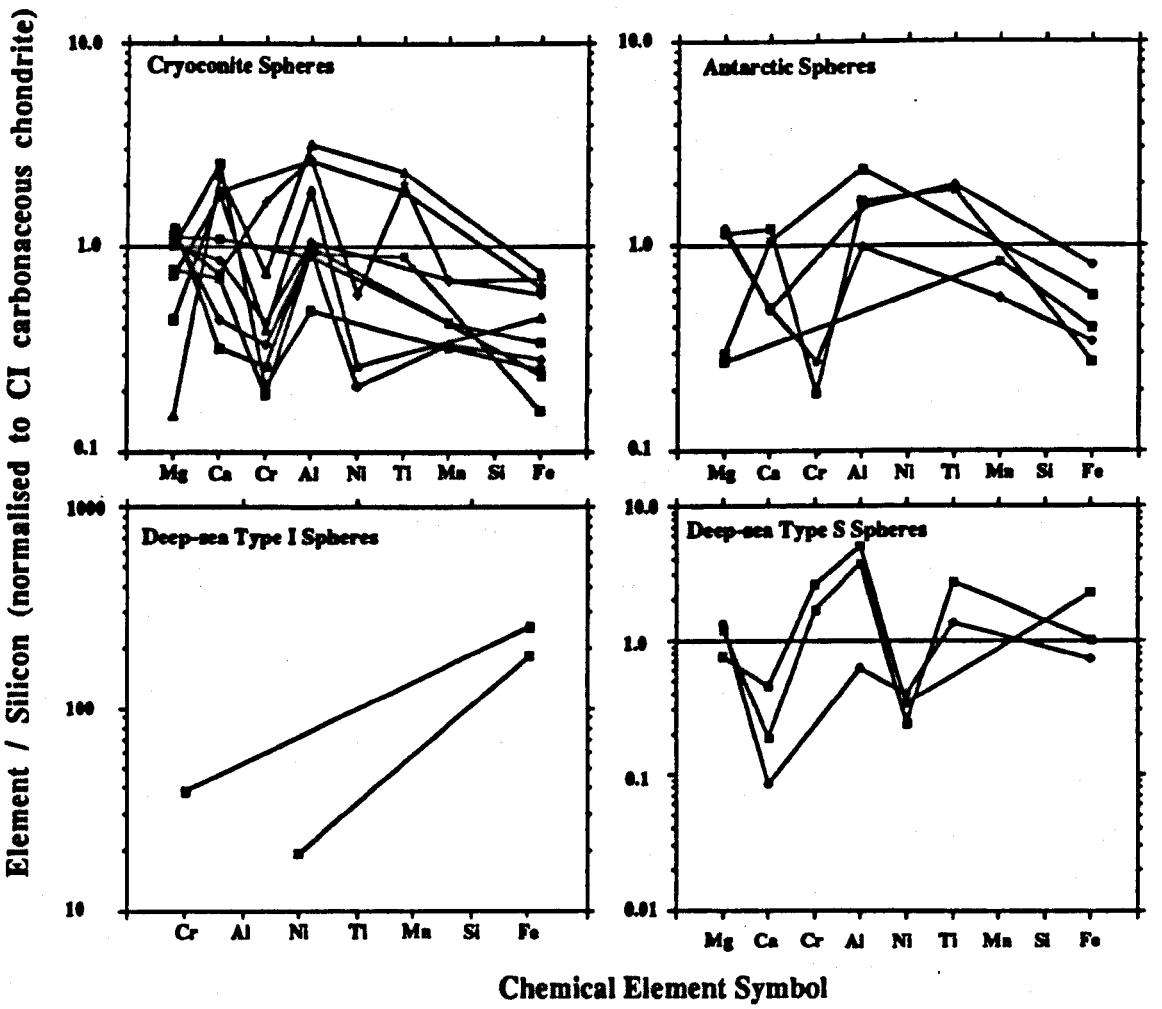

Figure 3.4. Chondrite normalised major refractory element plots for AEM area analyses. (Note that silicon, the element that the others have been normalised to, is not plotted).

Figure 3.4 shows a more detailed breakdown of the results for each group of samples analysed, presenting the individual element abundance patterns that constitute the range of values shown in figure 3.3. This diagram has been constructed solely to illustrate the general refractory element trends between micrometeorites from different localities and for this reason the individual sample identities have been omitted. The results for the two type I deep-sea samples are also included. Analysis of the results indicates that there were no obvious differences in the chemical composition of the different textural types, again providing evidence that perhaps all samples share the same parent material. In general, the patterns displayed are similar between the different families of collections, and in particular the Antarctic and Greenland groups share common signatures, with the deep-sea samples exhibiting slight variations from these two.

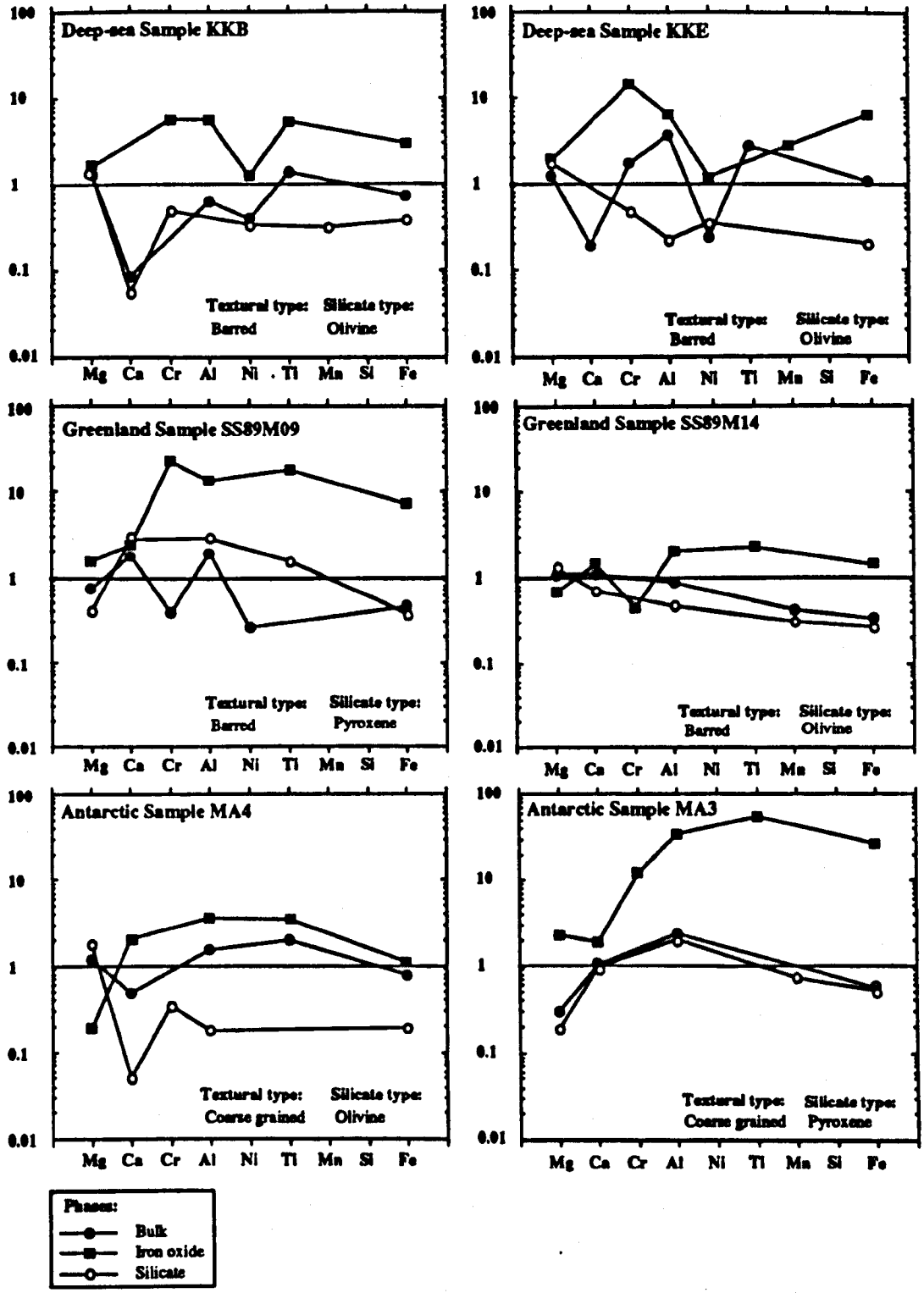

Figure 3.5. Chondrite normalised plots for individual micrometeorites. Each plot contains the AEM broad beam area analysis used to allocate the petrographic type of the sample and for the construction of figures 3.3 and 3.4, but additionally the AEM spot analyses of the silicate and iron oxide minerals that constitute the samples.

Although efforts were made to analyse representative areas of the sample fragments to gain an accurate idea of their chemistry, with the samples being typically multi-mineralogic it was possible that bias still exists in the analyses. Figure 3.5 shows the chondrite normalised plots for those samples where spot analyses of the constituent mineralogical phases was possible and the quality of these analyses was sufficiently high to enable mineral identifications to be carried out. These results indicate that the silicate phase is generally depleted in refractory elements with respect to chondrite values, and the iron oxides are correspondingly enriched. Encouragingly, the broad beam analyses of all the samples shown in figure 3.5 define the closest match to chondritic values. The silicate and Fe oxide phases appear to represent the end members of a two component system, that when analysed together within the broad beam analyses, demonstrate chondrite abundance. In sample MA3, the silicate phase appears to exhibit the same element abundances as the sample average as depicted by the area analysis pattern, although the Fe oxide phase still shows enrichments similar to other samples. In sample M09 the silicate phase is actually enriched in elements compared to the area analysis, even though again, the area analysis plots close to chondrite values, showing a depletion of elements to both phases. Whilst highlighting the problem of how the phases are related, it is more likely that these results are caused by an input of Fe oxide to the silicate spot analysis, due to the small grain size of the samples. Correspondingly, the enrichments in Cr, Al and Ti seen in some of the other sample areas analyses in figures 3.3, 3.4 and 3.5 are probably the result of the area being chosen for analysis possessing a high abundance of Fe oxides. Notwithstanding this, it would seem that in the majority of the samples, the area analysis does appear to give a representative idea of the bulk chemistry, and the associated correlations with CI chondrite values to confirm extraterrestrial origin, and provide evidence for a possible meteoritic origin for the samples.

Of interest here is how the silicate and iron oxide observed in the type S samples are genetically related. It would appear that during the heating experienced by the samples as a result of atmospheric entry, the Fe oxide forms from the silicate. The textural evidence demonstrates that the Fe oxide is always the minor constituent, the silicate forming the matrix or the larger crystals. During the heating episode when Fe oxide is formed, the more volatile refractory elements become preferentially incorporated into the oxide phase - the same elements become consequently depleted in the silicate. Furthermore, Ti, Cr and Al are all able to substitute for the relatively volatile Fe in the oxide phase (*e.g.* Blanchard *et al.*, 1980). Brownlee *et al.*, (1984)

suggested that initially, the type I and S spherules form by complete melting of a precursor material, with subsequent inertial seperation of the melt droplet into silicate and Fe-Ni metal phases. This model explains the observed low nickel abundances of both the Blanchard *et al.*, (1980) and this study, because in meteorites the silicates contain essentially no nickel, it being a siderophile element and residing in the Fe metal, so upon separation the nickle remains within the metallic fraction. The results for the type I samples, presumably the cooled separated Fe-Ni metal fraction, confirm this by showing enrichments in Ni and Cr (Cr is also depleted in many of the area analyses in figure 3.5). It must be remembered that the type I samples analysed here were composed of Fe oxide, the original Fe-Ni (-Cr) metal seemingly has suffered secondary ablation and oxidation after separation, with a concomitant loss of nickel, so explaining why only one sample shows a nickel enrichment and why it is not as large as might be anticipated. Analysis of type I samples that still retain the original metal (*e.g.* Caistaing and Fredriksson, 1958), confirm this loss by commonly exhibiting nickel concentrations in the metal as high as *ca.* 30 weight %. It is proposed here that the partitioning seen between the silicate and Fe oxide has also taken place after the initial separation of the metal and silicate phases, also as a result of secondary ablation.

A further observation apparent from figure 3.3 is depletion in Ca, and enrichment in Cr and Fe for the deep-sea samples relative to the Greenland and Antarctic samples. Blanchard *et al.*, (1980) noticed in the type S spherules that Ca is concentrated in a minor glass which was susceptible to weathering Thus the depletion of Ca found herein is probably a result of oceanic weathering. The enrichment of Cr and Fe may also be related to such processes, although Maurette *et al.*, (1986) has noted that a large proportion of Greenland spheres are depleted in Fe, and suggested that this is a primary feature. Possible explanations are that the Greenland spheres are younger than those collected from the deep-sea sediments and so may sample a different parent material, or that the samples actually have lost some Fe during the melting/ablation by evaporation, and the deep-sea samples for some reason, possibly weathering related, do not show this. This Fe depletion is real from evidence in this study, as all 15 Greenland and Antarctic samples are Fe poor, whereas 2 deep-sea samples are enriched. Davis *et al.*, (1991) in a study of Fe isotopes, calculated that *ca.*87% of the mass of a type I particle is lost by evaporation during melting/ablation, but could find no evidence for mass loss in type S samples. This evidence suggests the Fe depletion is real, with the parent material of the Greenland/Antarctic samples being Fe poor in relation to CI chondrite. Another explanation is that Fe is removed as a result of

weathering in the Greenland/Antarctic environment, but the only common factor here is initial incorporation into ice, so would have to take place within this environment where intuitively the potential for weathering is small.

3.4.4. Assessment of micrometeorite origin using the Ca/Al ratio.

The Ca/Al ratio within stony meteorites ranges from 1.00 to 1.25 with an average of 1.10 (Deuser, 1968; Ahrens and Von Michaelis, 1969). A comparison of the AEM measured Ca and Al contents within the micrometeorites analysed in this study with mean chondrite meteorite values taken from Ahrens and Von Michaelis, (1969) is presented in figure 3.6. For comparison purposes the mean Ca and Al results from the study of unweathered deep-sea micrometeorites executed by Blanchard *et al.*, (1980) is also included in the figure.

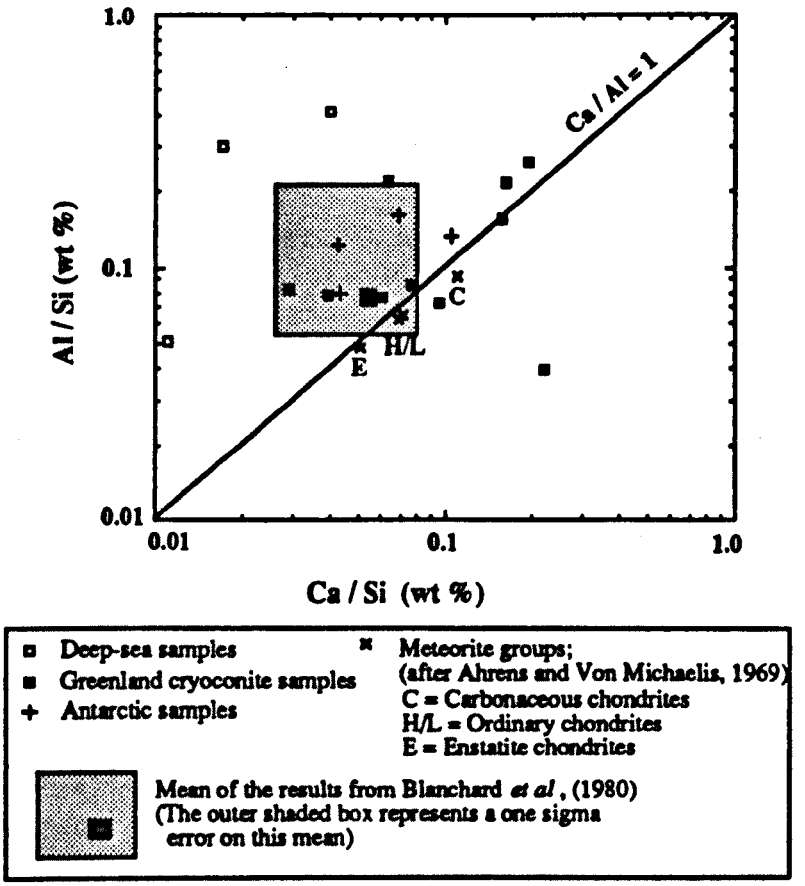

Figure 3.6. A comparison of the Ca and Al contents of the AEM analysed micrometeorites with mean meteoritic values and a previous study of unweathered deep-sea micrometeorites.

The three deep-sea samples analysed in this study all exhibit a strong Ca depletion, which is a result of weathering. The mean result for the Blanchard *et al.*, (1980) deep-sea micrometeorites show the same Ca depletion, but not to such a great extent. This is presumably because the individual samples in the Blanchard *et al.*, (1980) study were carefully selected to avoid badly weathered examples. The Ca and Al results for the individual Greenland and Antarctic micrometeorites show a closer correlation to the Ca/Al unity line, although again being slightly depleted in Ca relative to Al. The abundances of Ca and Al within the Greenland and Antarctic samples exhibit a range that encompasses that shown by the meteorite groups. The conclusions from these observations are:

(1) The deep-sea micrometeorites have lost Ca through oceanic weathering.

(2) The Greenland and Antarctic micrometeorites show a good correlation to meteoritic values, with abundances that can be reconciled with either an enstatite, ordinary or carbonaceous chondrite provenance.

(3) Notwithstanding (1), Ca is generally also depleted in the Greenland and Antarctic samples. It is proposed that either this is a real depletion and so indicates that the source of the micrometeorites is depleted in Ca relative to that of the macrometeorites, or the low Ca values are a artifact of the AEM analysis, or evidence of minor weathering similar to that occuring in the oceans.

Blanchard *et al.*, (1980) noted that if bulk major element analyses of unweathered and undepleted micrometeorites could be obtained, then these may be useful for deducing possible parent meteoroids. A comprehensive study of the major element composition of stony meteorites (Ahrens and Von Michaelis ,1969; Von Michaelis *et al.*, 1969) indicated that if the measured Ca/Al ratio falls between 1.0 and 1.25, then the other elements will not have been depleted. Blanchard *et al.*, (1980) assumed that if micrometeorite samples could be isolated that showed similar Ca/Al ratios, then possible correlations between their bulk chemistry and that of meteorite groups could reveal genetic connections. Subsequent analysis of the Blanchard *et al.*, (1980) data revealed two samples that possessed a Ca/Al ratio between 1.0 and 1.25 and by comparing abundances of Fe, Mg, Ca, Al and Si within these sample to meteoritic values they could be connected to H-group ordinary and enstatite chondrite parents. Inspection of the Ca/Al ratios of samples analysed in this study yielded 4 within the designated range, and table 3.3 shows their corresponding major element abundances.

The table also contains the mean elemental abundances of the chondritic meteorites taken from Von Michaelis *et al.*, (1969).

Sample	Elemental abundances (wt %)				
	Iron	Magnesium	Calcium	Aluminium	Silicon
MA2	17.9	16.8	2.7	2.4	18.6
SS89M05	34.3	5.5	3.6	3.2	15.2
SS89M16	38.4	1.8	4.0	3.6	14.4
SS89M18	14.6	11.2	2.4	2.2	25.9
Chondrite group					
Carbonaceous	29.5	11.5	0.9	0.8	16.8
Ordinary (H)	27.0	13.9	1.2	1.1	16.7
Ordinary (L)	21.5	15.0	1.3	1.2	18.6
Enstatite	29.5	11.5	0.9	0.8	16.8

Table 3.3. Elemental abundances for undepleted micrometeorite samples compared to the equivalent elemental abundances of chondritic meteorite groups taken from Von Michaelis *et al.*, (1969)

Even though similarities are evident between sample MA2 and the L-group ordinary, and SS89M05 and the enstatite chondrites, the correlation is not convincing, with Ca and Al abundances within the samples being a little high. A more rigourous study using more quantitative data is necessary before it can be determined whether this method provides a meaningful way to elucidate parent meteoroids, although the results obtained here on only semi-quantitative AEM data are encouraging.

3.4.5. Algal contamination.

Samples collected from the annual cryoconite melt water pools of the Greenland ice sheet have suffered extensive exposure to algae (see 1.5.5). An isolated sample of such algae from unprocessed cryoconite, was identified by Dr D.John of the British Museum (Natural History) as a 'blue-green' variety, and can be categorised as follows;

Class - Cyanophyta

Order - Nostocales

Family - Oscillatoriaccae

Genus - Lyngbya

It was anticipated that algal contamination could severely limit investigations of the carbon chemistry of cryoconite micrometeorites, thus attempts were made to assess the levels of algal contamination by utilising the major element chemistry of the cryoconite micrometeorites.

It is known that differences in major elemental compositions of algae are influenced more by ambient environmental conditions, *i.e.* water temperature and available nutrients, than by class or species (*e.g.* Tissot and Welte, 1984). Accurate determination of the composition of algae is difficult and laborious, involving drying, incineration and analysis of the resulting oxides within the ash produced (*e.g.* Gunsalus and Stanier, 1960). Notwithstanding these problems, the average composition of blue-green algae can be estimated as follows (*e.g.* Stewart, 1974);

Carbon - 50wt% (dry weight)

Oxygen - 20wt%

Nitrogen - 8-15wt%

Hydrogen - 10wt%

Phosphorus - 3-6wt%

Sulphur - 1wt%

It was anticipated that if micrometeorites within the cryoconite were contaminated by algae that possessed an elemental composition similar to that presented above, then the AEM major element chemistry of the micrometeorite fragments would exhibit excesses of these elements. Phosphorus (P) and sulphur (S) are both routinely detectable within the Hitachi S-2500 AEM, but to analyse elements with an atomic mass lighter than fluorine demands an instrument equipped with a thin window X-ray radiation detector. Sulphur can be present in chondritic meteorites in concentrations approaching *ca.*6wt%, whereas this value is only *ca.*0.3wt% for P (*e.g.* Dodd, 1981). Even though both S and P are volatile and presumably largely volatilised during atmospheric entry, the low potential indigenous P content, coupled to its high corresponding algal concentrations, make it an ideal signature of contamination.

Examination of the AEM cryoconite micrometeorite results indicated that only two samples contained P above the limit of detection, with SS89M05 and SS89M16 both at *ca.*0.3wt% concentration. In addition to the P, these two samples were the only micrometeorites to contain measurable S, with SS89M05 at *ca.* 1wt% and SS89M16 at

ca. 0.3 wt%. Further evidence is provided by the carbon abundance data (chapters 5/6) in that SS89M16 yielded the largest carbon concentration of all the samples analysed. Plates 3.5 and 3.6 show the fragments of samples SS89M05 and SS89M16, and although they possess the barred morphology discussed previously, their suface textures appear very porous in comparison to others of the same type (*cf.* plates 3.1 and 3.2), with only SS89M17 (plate 3.7) showing a similar degree of porosity. (Plates 3.5, 3.6 and 3.7 were taken using the 'secondary electron' facility of the AEM, and so do not reflect the compositional differences highlighted by back-scattered electron images). The connection between porosity and the algal contamination is strengthened with the observation that SS89M17, although not exhibiting measurable P or S, has the third richest carbon content of the Greenland samples. It is not clear whether this porosity is a result of algal etching, and is secondary, or if it is a primary feature and facilitates algal permeation of the sample.

Callot *et al.,* (1987) studied etching rates of amorphous (glass) and crystalline (olivine) silicates using a variety of sterilised hot solutions and algae similar to that extracted from the Greenland cryoconite. Their results indicated that biogenic etching by the algae was very potent, and in particular the process was enhanced by algal excretion of acids and deposition of spores. This dual action had the effect of opening fractures, so from this evidence it would appear that the porous nature of the contaminated samples is a secondary phenomenon. Additionally, the Callot *et al,* (1987) study revealed that the algae preferentially attacked the olivines, especially if they were Mn-bearing. Out of all the Greenland samples analysed, only SS89M05 and SS89M16 did not contain Mn, providing further evidence as to the action of the algae. The olivines in the samples are generally Mg-rich, and the observed depletion of Mg also evident in these two samples is also in agreement with the removal of olivine by etching.

It should be noted that sample MA2, which was extracted from the Antarctic Ice, and thus has not been exposed to the Greenland algae, contained *ca.*3wt% P and has the highest carbon content of the Antarctic samples, similar to that of the contaminated Greenland particles. This problem can be addressed by the AEM photomicrograph of the MA2 sample fragment as shown in plate 3.8. Of particular relevance here is the presence of an adhering filament-like body. The filament is not intimately associated with the sample, it is only loosely attached to the broken surface of the fragment, and the remainder of the sample is non-porous, which is in direct contrast to the Greenland

examples. The filament appears sinuous in the AEM image, but this is caused by the movement of the protruding body as a result of specimen charging. If the filament has moved across the field of view of the analysing electron beam, then the observed high P content of the sample can be explained, and the sample does not actually contain indigenous P. This appears a likely explanation because the measured sample P concentration of *ca.* 3wt% matches exactly that predicted as the bulk composition of the algae, whereas in the contaminated Greenland samples, where the algae pervades the body of the sample, this signature has been diluted by an order of magnitude. The observation that no S was detected in MA2 implies only that the S fraction of the algae is not present within the filaments, probably constituting a separate component. It is unlikely that this contamination could be the result of the handling procedures outlined in section 2.1.2, as the equipment used is scrupulously cleaned, and processing was carried out on individual samples in a clean room environment. MA2, along with the other Antarctic samples were supplied as individual particles by Dr M.Maurette (University of Paris, Orsay, France). It appears likely that contamination occurred during the selection stage, especially in view that Dr Maurette, at the time of allocation, was working on both Greenland and Antarctic collections, and because of his research interests of sample petrography only, did not execute the selection in a clean room environment (M.Maurette, *pers.comm.*).

3.5. Conclusions.

Attempts to deduce the mineralogy of deep-sea micrometeorites using a custom developed Gandolfi camera XRD technique proved to be extremely informative in revealing the effects of oceanic weathering on the indigenous iron oxides within the samples. The use of this promising technique, which was initially envisaged as only augmenting the AEM major element data, had to be curtailed because of time constraints and an unacceptable risk of sample loss during analysis.

The AEM derived major element chemistry of the micrometeorite fragments was used to demonstrate the extraterrestrial nature of the samples, to investigate atmospheric entry heating processes, and to evaluate the extent of algal contamination within the Greenland cryoconite samples. With specific regard to this latter point, the results indicated that only 2 Greenland micrometeorite samples had been contaminated, which is encouraging for the carbon isotopic work in chapters 5 and 6.

In summary, the major element chemistry of the micrometeorite fragments determined by the use of the AEM were of such a high quality that all of the objectives outlined in the introduction of this chapter (3.1) have been fufilled.

Chapter 4

Evaluation of the Sample Handling Protocol and Attempts to Elucidate the Carbon Isotopic Composition of the Stepped Combustion Experiment Blank

4.1. Introduction.

Prior to the onset of this work, a preliminary investigation into the stable carbon isotope chemistry of deep-sea particles was undertaken by Wright *et al.*, (1988), where six samples were analysed using the Triple Collector mass spectrometer and sample handling/gas extraction system (as described previously in chapter 2) of Carr *et al.*, (1986). The samples had been pre-selected by Prof. D.E.Brownlee (University of Washington, Seattle, USA) to span different particle types (*i.e.* type S, type I and melted and unmelted samples *etc.*), as the emphasis of the study was to survey carbon in different sorts of samples rather than in analysing large numbers. A summary of the results taken from Wright *et al.*, (1988) are shown in figure 4.1, and from them the following four components were suggested;

(i) Low-temperature carbon (<600°C/LTC), $\delta^{13}C$ values *ca.* -25 to -35‰.

(ii) LTC, $\delta^{13}C$ values *ca.* -18 to -20‰.

(iii) High-temperature carbon (>600°C/HTC), $\delta^{13}C$ values *ca.* -30 to -34‰.

(iv) HTC, $\delta^{13}C$ values *ca.* -16 to -21‰.

Components (i) and (iii), due to their isotopic similarity to terrestrial contamination, were believed to have been supplied from the sample handling procedures, and it was postulated that only (ii) and (iv) were indigenous to the samples. An additional observation from the results was that the unmelted particles defined a separate group, containing about five times more carbon than the melted particles, but without exhibiting different $\delta^{13}C$ values. In light of the similar isotopic nature of this excess carbon it was simply interpreted that the increased porosity of the unmelted samples had led to a higher degree of terrestrial contamination. Taking into account the limited

data set, interpretations of the two indigenous components were only tentatively attempted, but genetic connections to meteoritic macromolecular/amorphous carbon and a small input from isotopically anomalous high temperature silicon carbide (SiC) were inferred.

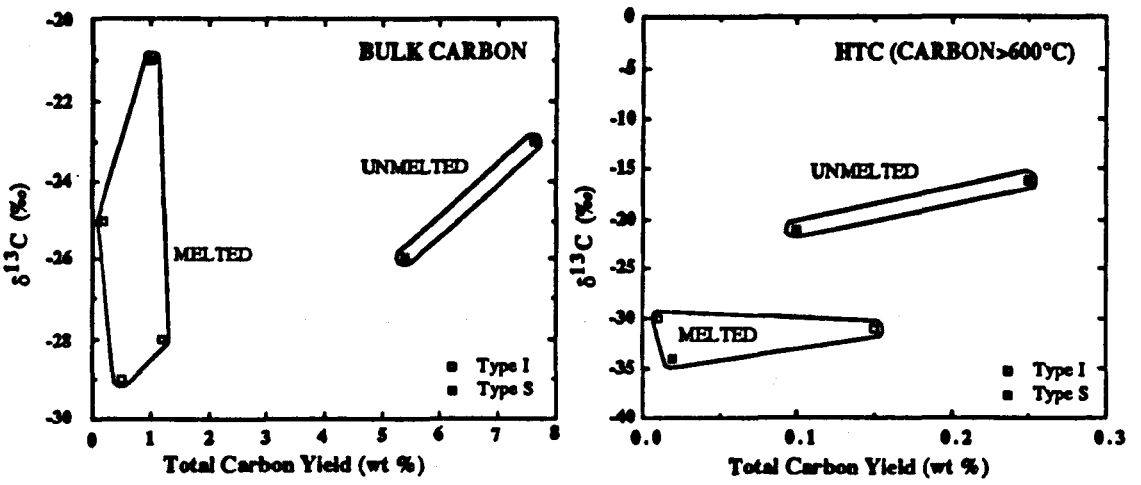

Figure 4.1. Results of a preliminary examination of carbon within deep-sea micrometeorites after Wright *et al.*, (1988). Individual samples were petrographically characterised prior to carbon isotopic analysis, as to their degree of melting, and into type S or I mineralogic groups. The isotopic results are divided into the total (bulk) carbon release and that solely obtained >600°C (HTC).

The samples analysed by Wright *et al.*, (1988) had been pre-selected and petrographically characterised in Seattle before being transported, in platinum foil packets or loose in screw topped glass vials, to Cambridge University (Cambridge, Cambridgeshire, UK) for isotopic analysis. Such a procedure undoubtedly involved a certain degree of carbon contamination, and was probably responsible for the majority of the carbon seen within the samples. To investigate this hypothesis further, and also to continue evaluating the capability of the Carr *et al.*, (1986) system, a second suite of deep-sea particles were scheduled for analysis. In addition, the new sample handling protocol (as outlined in 2.1.2) was assessed.

4.2. Evaluation of the sample handling protocol by analysis of individual deep-sea micrometeorites.

Three deep-sea spherical micrometeorites were selected from an ocean floor sediment separate (for details of collection see Brownlee *et al.*, 1979) and processed through the new analysis protocol. Although the sediment separate had been transported from Seattle within a glass vial similar to the samples analysed by Wright *et al.*, (1988), the micrometeorite samples had been spared the excess handling (and probable concommitant contamination) involved with petrographic determination. As part of the new protocol, petrographic work was carried out on a separate fragment of each sample removed after crushing. This procedure minimised handling of the remaining portion allocated for stable carbon isotopic analysis. To evaluate the effects of this change in handling procedure the results were initially compared directly to those of Wright *et al.*, (1988), as illustrated within figures 4.2 and 4.3.

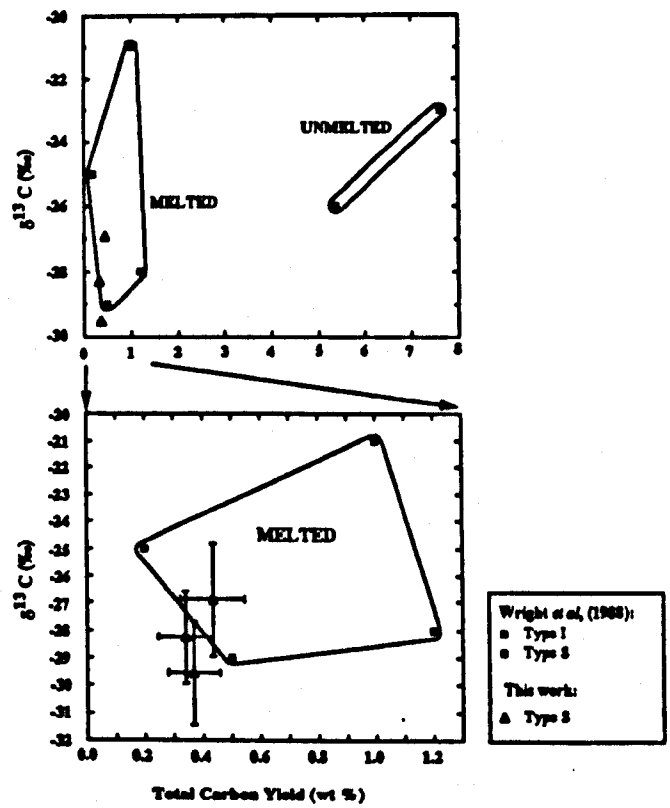

Figure 4.2. Bulk carbon isotopic results of the three deep-sea micrometeorites analysed to evaluate the sample handling protocol. The results of Wright *et al.*, (1988) have been included for comparison purposes.

The results for the three deep-sea micrometeorites analysed here include an attempt to evaluate the uncertainty in the bulk and HTC carbon isotopic and abundance signatures. Whenever stepped combustion data has been summed to produce an average result from a number of individual temperature steps in this thesis, the corresponding uncertainty has been evaluated. (The method for the derivation of this uncertainity is reproduced in appendix A2). Examination of figure 4.2 revealed that the samples exhibited total carbon concentrations and isotopic compositions similar to the melted type I samples analysed by Wright *et al.*, (1988), but in spite of this, the petrographic work subsequently executed on the sample fragments showed them to be of type S composition. Even assuming that the samples were all totally melted, the one analogous melted type S particle analysed by Wright *et al.*, (1988) still contained about twice the carbon concentration with a slightly heavier isotopic composition.

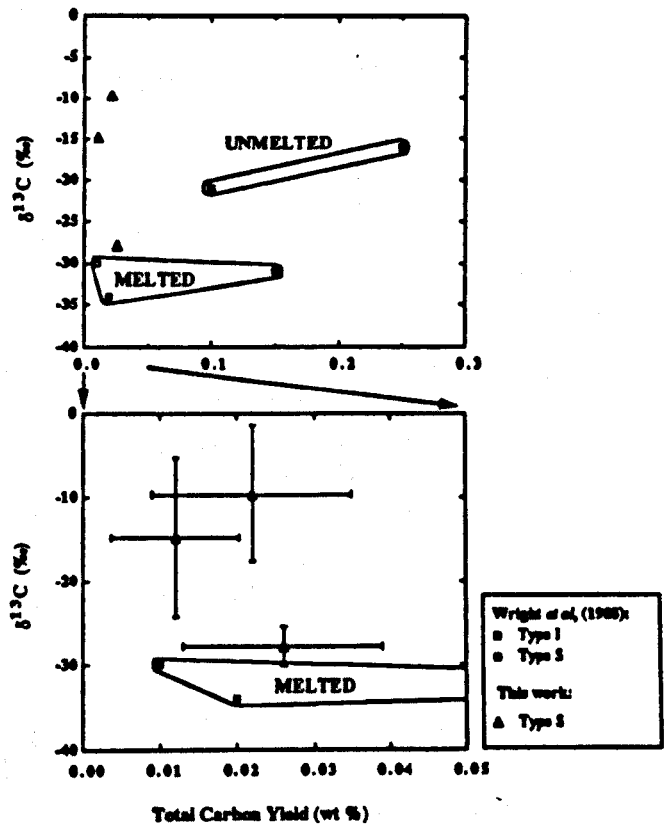

Figure 4.3. HTC carbon isotopic results of the three deep-sea micrometeorites analysed to evaluate the sample handling protocol. The results of Wright *et al.*, (1988) have been included for comparison purposes.

Figure 4.3 suggested the samples contained HTC carbon concentrations equivalent to the Wright *et al.*, (1988) melted type S/I particles, but in two samples this carbon was isotopically heavier in composition, with signatures similar to those previously isolated within the unmelted type S samples. It was apparent that even after this brief comparison to the previous results, that the situation was more complex than concluded by Wright *et al.*, (1988). However, the samples analysed herein were found to contain lower carbon concentrations than the study of Wright *et al.*, (1988), which suggests that handling contamination may have contributed to the results of the previous study.

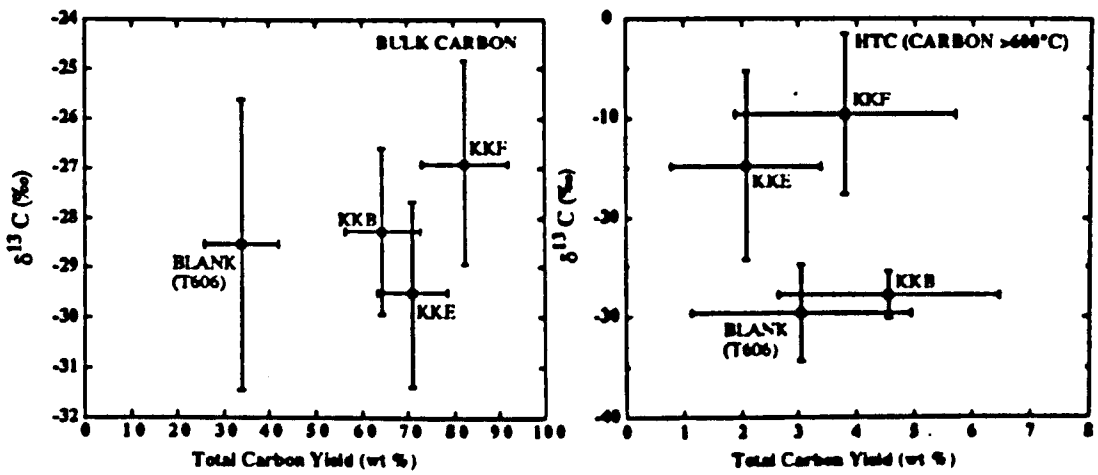

Figure 4.4. A comparison of the bulk and HTC yields and isotopic composition of carbon released from deep-sea micrometeorites KKE,KKF and KKB with the corresponding experiment blank.

To evaluate the levels of contamination inherent within the new sample handling protocol, and hopefully to further aid interpretation of the results, a blank experiment was performed (*i.e.* where the protocol was executed without a sample). The resulting platinum foil was then subjected to a full stepped combustion. Figure 4.4 shows the results of this experiment (T606) compared to those of the three deep-sea micrometoerites that had been undertaken using the same experiment protocol. The figure has been split into two; being presented as the bulk carbon release between room temperature and 1200°C, and that released >600°C only (HTC). The bulk results showed all three samples contained more carbon than the blank, but again the similar

isotopic nature of this carbon to the blank suggested that the samples were merely exhibiting excess terrestrial contamination. The HTC releases confirmed that even though the the carbon obtained was apparently at blank levels, in two samples a slightly ^{13}C-enriched component was present.

In agreement with the Wright *et al.*, (1988) conclusions, it is apparent that the total carbon yield in the deep-sea particles was still controlled by contamination levels, the three samples analysed here being relatively less contaminated than those analysed in the Wright *et al.*, (1988) study. This conclusion was strengthened by examining the absolute amounts of carbon obtained for each sample relative to that from the blank as shown in figure 4.4. It is evident that the blank supplies *ca.*50% of the bulk carbon release from the deep-sea samples, and within errors it was impossible to distinguish between the blank and indigenous HTC. Notwithstanding this, the isotopic results for the HTC releases of samples KKE and KKF revealed that the component (iv) isolated in the Wright *et al.*, (1988) study possessed an isotopically heavier signature than originally defined by Wright *et al.*, (1988). Of additional importance was that, as shown in figure 4.5, in both KKE and KKF the individual temperature steps that constituted the HTC release showed a trend to increasingly heavy values as the combustion temperature was elevated.

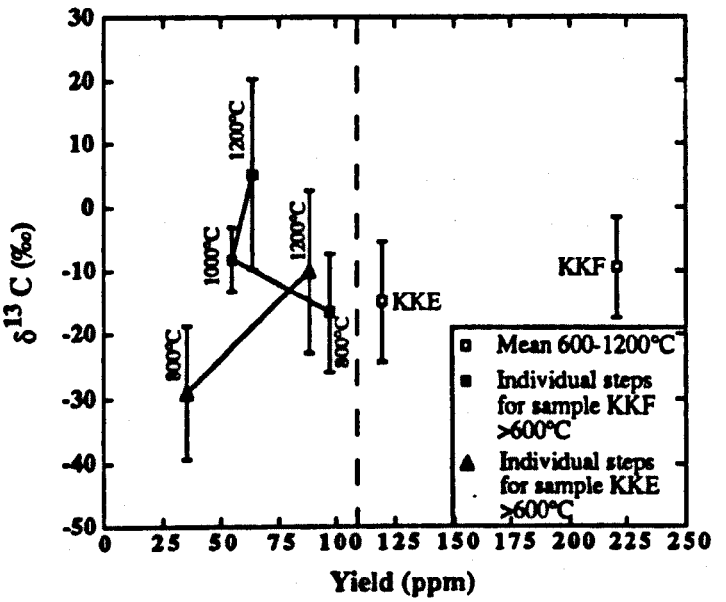

Figure 4.5. A trend to isotopically heavier values with increasing temperature of combustion is shown by the individual temperature steps that constitute the HTC carbon release of deep-sea micrometeorite samples KKE and KKF.

Within the Wright *et al.*, (1988) study, the sample containing the ^{13}C-enriched HTC component had been combusted in a single step from 600 to 1200°C and so allowed only one isotopic measurement of the component of interest. However, the trends of two and three consecutive temperature steps exhibiting consistently isotopically heavy carbon observed within the samples analysed here, are good evidence that the component was not simply an erroneous single measurement. This pattern, as shown in figure 4.5, was also consistent with the meteoritic SiC interpretation for the component. Stepped combustion profiles of bulk samples of meteorites that are known to contain such SiC characteristically show the pattern observed here (*e.g.* Swart *et al.*, 1982), which is interpreted as being the product of the peak of SiC combustion occuring between 1000 and 1200°C. Individual SiC grains exhibit extremely heavy $\delta^{13}C$ values (*i.e.* Alexander *et al.*, (1991) measured individual grains at *ca.* +33,000‰), but are commonly present within meteorites only at the ppm level so their signature is diluted by more isotopically normal carbon, leading to bulk $\delta^{13}C$ values only as heavy as *ca.*+10‰ (*e.g.* Grady *et al.*, 1991). This dilution effect can be used to explain why the $\delta^{13}C$ values of the HTC release in samples KKE and KKF were isotopically heavier than that of the samples analysed in the Wright *et al.*, (1988) study. The sample analysed by Wright *et al.*, (1988) that yielded a HTC $\delta^{13}C$ value of -16‰, and from which the presence of the SiC component was inferred, released 8ng of carbon (which corresponded to a concentration of 2500ppm within the sample) between 600 and 1200°C. In contrast, samples KKE and KKF yielded only 4.6±1.9ng (*ca.*220ppm) and 2.1±1.3ng (*ca.*120ppm) for the same temperature range but with HTC $\delta^{13}C$ values of -9.6±8.1‰ and -14.1±9.5‰. If the three samples all contained a similar amount of SiC (*i.e.* 0.001 to 14ppm if concentrations are similar to those in the primitive chondritic meteorites - Huss, 1990), then the trend to heavier $\delta^{13}C$ values with a decrease in HTC carbon yield can be explained by smaller dilution effects by isotopically lighter carbon in samples KKE and KKF.

4.2.1. Conclusions from the individual deep-sea micrometeorite experiments.

The only major problem with the execution of the new analysis protocol was in the determination of the sample mass, where the measured mass of the platinum foil

sample envelope was subtracted from that of the same foil after addition of the sample; the difference was then equal to the mass of the sample. In reality it was found that the relative mass of the foil (*ca.* 20mg) to that of the sample (*ca.* 10-40μg[7]) was too great for the balance used to distinguish between the two weighing steps, and so gave the same value both before and after the sample had been introduced. Correspondingly, for the three experiments here, an estimated sample mass of 20μg was used, but for future experiments it was proposed to either reduce the mass of foil used, or increase the precision of measurement to enable an accurate mass determination to be carried out.

Even though the three deep-sea micrometeorites were not examined petrographically prior to the carbon analyses, it was apparent that handling contamination was still at an unacceptably high level. The shrouding effects of this carbon was particularly well shown in the HTC results, where a reduction in contamination facilitated a better insight into the hypothetical indigenous ^{13}C-enriched SiC component. To address the problem of this carbon contamination, either the absolute levels of blank within the stepped combustion experiment needed to be reduced, or a suitable correction applied to the sample data. To enable a meaningful correction to be applied, the blank carbon contamination needs to be tightly constrained both in absolute carbon yield and carbon isotopic composition. Examination of the experiment blank results within figure 4.4 revealed that the bulk yield of the blank was only constrained to *ca.*±35%, with a $\delta^{13}C$ value of -28.5±3‰, and in the important HTC range to *ca.*±100% and -29.7±5‰ respectively. It was apparent, as illustrated by these large errors, that the Triple Collector mass spectrometer/gas extraction system was operating at the limits of its capabilities, and as such was not ideally suitable to implement the scheme of work proposed within this study. In order that the components already tentatively identified could be further studied, and with the possibility of discovering new indigenous components, it was decided that attempts would be made to both reduce the absolute blank input, whilst at the same time enhance the accuracy of the isotopic determination of the blank carbon. If this could be achieved it was postulated that new, previously shrouded, components would be revealed, and accurate blank corrections could be applied to these to elucidate their true isotopic compositions.

---

[7] For a 200-300μm diameter sphere with a density between 2 and 3 gcm^{-3}.

The mass spectrometer developments to fufil these aims have been previously dealt with in chapter 2, whereas the remainder of this chapter will be concerned with the attempts to refine the sample handling protocol, largely in terms of absolute levels of carbon contamination imparted to the samples, but in the first instance, to address the problem of sample mass determination already highlighted. A summary of much of chapter 2 and the evolution of blank technology towards the application of ultra-high sensitivity stable carbon isotope techniques has additionally been composed and presented within Yates *et al.*, (1992).

4.3. Evolution of the sample handling protocol.

To combat the inability of the sample handling protocol to yield an accurate sample mass for each processed particle, experiments were carried out using a thinner grade of Pt foil in an attempt to reduce the problematic mass disparity between the sample and the foil sample envelope. In the experiments executed on the three deep-sea micrometeorites to evaluate the efficacy of the sample handling protocol (KKE, KKF and KKB), platinum foil of 25μm thickness was used; this being the same as that used within the Ash, (1990) protocol. However, it was anticipated that a reduction in this foil thickness may be detrimental to the sample loading characteristics of the envelope, *i.e.* thinner foil would be more likely to tear during handling, and due to decreased rigidity, potentially more difficult to fashion into an envelope. In addition, examination of the initial blank experiments (4.3.1) indicated that the platinum foil was responsible for a proportion of the experiment carbon blank. From consideration of these observations and arguments it was apparent that experimentation was required to find out what thickness the foil could be reduced to, and hence enable an accurate sample mass determination to be executed and minimise its potential blank input, without impairing its function as a sample envelope.

Subsequent experimentation revealed that if the mass of the platinum foil could be reduced to *ca.*<5mg then the balance problems in the analysis protocol could be overcome. The dual criteria of an envelope with a mass of <5mg whilst maintaining a similar envelope size (*ca.*5mm^2), dictated that the thickness of the foil was reduced to <10μm. The size of the envelope could not be

Sample	Diameter (μm)	Type (S/I)	Platinum foil*		Calculated mass$ (μg)			Measured mass (μg)
			Thickness	Mass	2 gcm^{-3}	3 gcm^{-3}	6 gcm^{-3}	
Csp2	200	I	7.5	2.98			25.1	19
SS89M01	180	S	5.0	5.36	6	9		6
SS89M05	240	S	5.0	5.33	15	21		13
SS89M10	300	S	4.0	3.62	28	42		32
SS89M17	320	S	4.0	3.24	34	52		31
SS89M13	360	S	4.0	2.73	49	73		41
SS89M14	280	S	4.0	3.02	23	35		31
SS89M16	400	S	4.0	2.68	67	101		66
SS89M18	360	S	4.0	3.43	49	73		52
MA1	250	S	4.0	2.64	16	25		23
MA2	380	S	4.0	2.35	58	86		60
MA3	500@	S	4.0	2.38	65@	98@		84

* = Foil thickness in μm and mass in mg.
$ = Calculated for spheres with a diameter as shown.
@ = Sample MA3 was a broken half sphere, so the estimated masses have been halved also.

Table 4.1. A comparison of the sample masses measured within the analysis protocols with estimated equivalents calculated based upon the measured sample diameters and estimated densities as shown. The measured masses are for the samples after they have been crushed and a fragment removed for petrographic work. Notwithstanding this, a good correlation exists between the measured and estimated masses, indicating that the problems in determining the samples masses using the heavier (*ca.*20mg) 25μm thickness platinum foil sample envelopes had been overcome by using thinner (and lighter) foil. (Only those samples where an accurate (*ca.*±10μm) determination of diameter was obtained are included).

further reduced without increasing the risk of sample loss. With regard to the efficacy of such thinner foil as an effective sample envelope, it was discovered that the lower limit of foil thickness that could be used was 1.25μm. Sample envelopes fashioned using 1.25μm platinum foil were liable to tear, but more importantly, problems were encountered with their loading into the mass spectrometer gas extraction system. The small mass (*ca.*<1mg) coupled with a relatively large surface area of the 1.25μm sample envelopes made them susceptible to any static electric charge in the laboratory or within the gas extraction system. To facilitate a compromise between these two limits, foil of between 7.5 and 4.0μm was used for the sample envelopes used herein. Table 4.1 shows a summary of the sample masses measured within the sample protocols using the thinner foil. In an attempt to confirm whether the figures obtained were reasonable and not obviously erroneous, these measured mass results were compared to estimated values that had been calculated by using the measured sample diameters to estimate volume, and then by assuming an appropiate density, to estimate the mass. Table 4.1 shows the results of this work, giving the measured sample masses and diameters along with the thickness and mass of foil used, and then the estimated sample mass using different densities (either 2 or 3 gcm^{-3} for type S, and $6gcm^{-3}$ for type I (*e.g.* Hunter and Parkin, 1960)), according to the subsequently allocated sample petrologic type. It must be remembered that the estimated and measured masses were not strictly comparable, because the estimated values are for whole-particles, whereas the measured values are for the samples after crushing and removal of a fragment for petrologic work. Allowing for the fact that the measured sample masses would be lower than that of the whole particle, examination of the results in table 4.1 reveals that a good correlation existed between the estimated and measured sample masses. This indicated that by implementing the use of thinner, and therefore lighter, platinum foil within the analysis protocol the sample mass determination problems had been solved.

It was considered that the majority of the sample contamination was from handling operations and thus organic in nature, and as such, most of this material would be soluble in various solvents. Mattey *et al.*, (1989) tried a solvent cleaning procedure with some success to remove organic contamination from ocean basalt glasses; the solvent used was dichloromethane (CH_2Cl_2), and was selected because of its exceptional volativity. It was decided to implement a similar solvent treatment step within the sample handling protocol devised herein. Firstly, all samples (not the Pt

foil) were thoroughly washed in *ca.*50ml of CH_2Cl_2 (AnalaR grade, BDH Chemicals, Poole, UK) prior to being processed, and secondly, fresh solvent was used within the protocol to facilitate transfer of the sample to the Pt foil for crushing. Early experience with the protocol had revealed that the greatest chance of sample loss occurred at this latter stage, because the sample was not easily coaxed from the point of the magnetic needle used for the transfer. Experiments with an electromagnetic needle and using a second magnet below the Pt foil substrate proved unsuccessful, but it was found that the surface tension within a drop of liquid placed onto the Pt foil was sufficient to safely remove the sample from the needle point when it was pulled out of a droplet (<5ml) of CH_2Cl_2.

4.3.1. Results with the Triple Collector.

The effects of reducing the platinum foil sample envelope thickness and implementing a solvent cleaning step within the analysis protocol, (corresponding to protocols A to D as explained below), can be seen within figure 4.6, where the total yield and isotopic composition of carbon released from blank experiments performed on the Triple Collector are shown; (Each protocol progresses from the previous one with only the new steps within each being explained)

(i) Protocol A - Procedure as explained in section 2.1.2. Pt foil of thickness 25μm was used.

(ii) Protocol B - Pt foil reduced to 7.5μm in thickness.

(iii) Protocol C - As for protocol B but to mimic the sample transfer step within the blank, a drop of CH_2Cl_2 was placed onto the Pt foil square after weighing.

(iv) Protocol D - After execution of protocol C, the sample packet was transported from the clean room to the gas extraction line submerged in a petri dish of CH_2Cl_2.

It was apparent from figure 4.6 that the protocol alterations had also precipitated a *ca.* 75% reduction in the total blank input. Examination of these results, when also considered in light of the individual stepped combustion plots as shown in figure 4.7, additionally revealed some interesting points about both the composition of the blank and the performance of the Triple Collector, and these will be discussed in the remainder of this section.

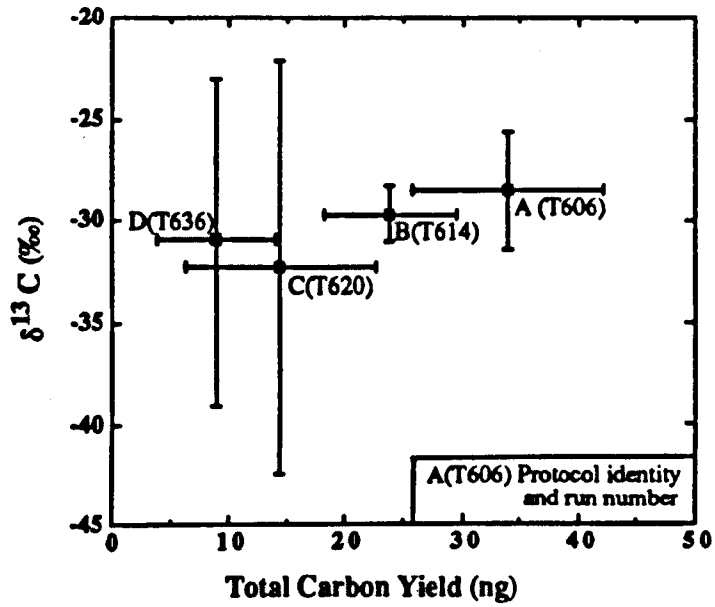

Figure 4.6. Bulk carbon yields and isotopic signatures of stepped combustion blank experiments executed on the Triple Collector mass spectrometer in an attempt reduce absolute levels of carbon contamination within the sample handling protocol. (For explanation of the individual protocols see the text).

In reducing the thickness of Pt foil from 25 to 7.5 μm (protocols A to B) the blank for the sample handling protocol was also reduced, but the reason for this was at first unclear. Notwithstanding the observation that within errors the overall yields for A and B (as shown within figure 4.6) were essentially the same, the individual stepwise plots in figure 4.7 reveal that a reduction in blank had taken place in the <600°C regime, with in particular the <200°C step showing a *ca.*50% reduction from A (13.9±1.3ng) to B (5.5±1.3ng). It was assumed that carbonaceous species released at such low temperatures would be dominated by surficially absorbed gases and other volatiles such as C_xH_y compounds and airbourne organics *etc.*, and that the surface area of the foil would therefore dictate contamination levels. If absorbed atmospheric CO_2 was the source of this release then it appeared that the foil thickness, and porosity thereof, was the controlling criterion because aside from thickness, the foil squares used were all of equal dimensions. A problem with this hypothesis was that the $\delta^{13}C$ value of the carbon release from both A and B was *ca.*-30‰, and it is known that the $\delta^{13}C$ value of the lower atmosphere is heavier at *ca.*-7‰ (*e.g.* Keeling, 1961). In

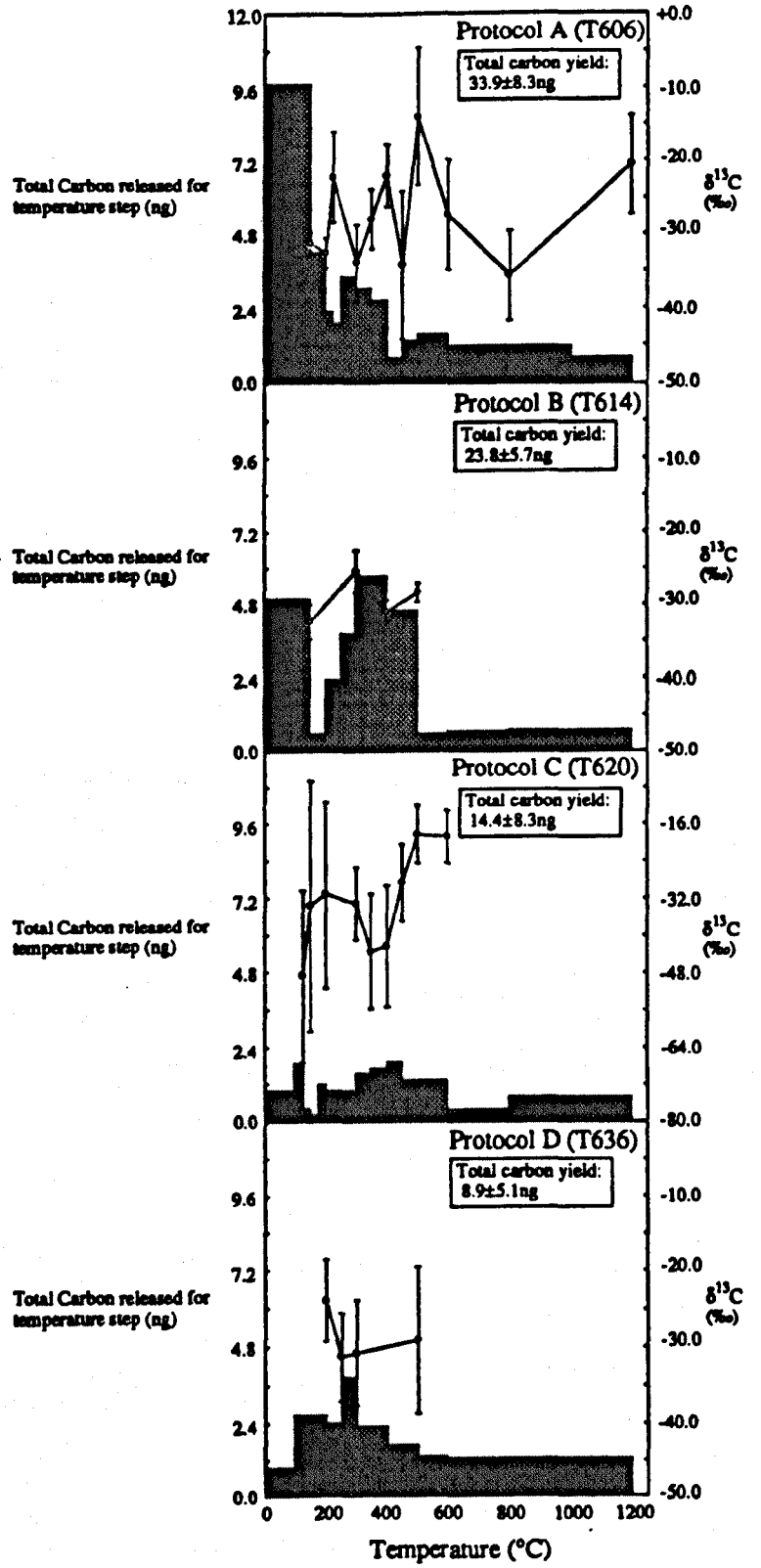

Figure 4.7. Individual stepped combustion plots for experiments executed on the Triple Collector implementing the changes to the analysis protocol.

view of this, an alternative explanation was sought, and two further possibilities were considered. Firstly, contamination during handling by an extremely thermally unstable non-gaseous carbonaceous species, the level of which is somehow related to the thickness of the foil, or secondly, a similar species had not been completely eliminated during cleaning of the foils, with the thicker foil retaining comparatively more. Both foils were of the same grade as specified by the manufacturer (Goodfellow Advanced Materials, Cambridge, UK) and had been cleaned by combustion in a muffle furnace to 1000°C, and so should not in theory have carried any residual carbon, so the first option appeared to offer the most reasonable explanation.

Within the temperature range 200 to 400°C, where organic contamination usually combusts (*e.g.* Wright and Pillinger, 1989), the protocols yielded 13.3±3.2 and 11.8±1.9 ng of carbon for A and B respectively. The similiarity of these amounts, independent of the foil differences, was interpreted as indicating that this carbon was the result of handling contamination within each protocol, reflecting the identical procedures applied to both foils. This was further substantiated by the $\delta^{13}C$ value of the carbon being measured between *ca.*-20 to -30‰, values commonly associated with laboratory organic contamination (*e.g.* Des Marais, 1983; Wright and Pillinger, 1989). The remaining steps from 400 to 1200°C all yielded between *ca.*1 and 2ng (within errors) irrespective of the magnitude of the temperature spanned by the individual step. This observation suggested that the carbon so released was controlled solely by the duration of combustion, as each step was carried out over 40 minutes independent of temperature. Unfortunately, the Triple Collector was not capable of determining the $\delta^{13}C$ value of this carbon to any degree of accuracy, so the hypothesis of whether it was derived from a single source could not be addressed further. Stepped combustion experiments carried out on the combustion section/gas extraction system alone (a 'system blank') to explore this hypothesis were inconclusive due to the inability of the Triple Collector manometer to measure the yields of gas released to better than ±0.95 ng of carbon. The additional time dependent blank input for each temperature step becomes important considering that the protocol A experiment was carried out over 13 temperature steps whilst protocol B over only 9. Accordingly, of the apparent *ca.*10ng disparity between the two bulk yields, perhaps as much as 8ng could be accounted for as a product of the extra steps inherent within the protocol A experiment, leaving the remainder easily supplied by already observed difference in the <200°C region. These

additional steps also explain the larger errors on the bulk results for A compared to B, as each step incurs a finite error in yield and isotopic measurement (appendix A3).

The implementation of the solvent-cleaning step did, as predicted, result in the lowering of the absolute blank levels. The protocol where the foil remained submerged in CH_2Cl_2 until a few moments before loading into the gas extraction system (D) appeared to yield the lowest contamination level, with figure 4.6 showing the total to be roughly half of that obtained using the 7.5μm foil but without a solvent step (B), and distinct from it in yield even when the estimated range of its value as represented by the error bars were taken into account. Protocol C showed a similar reduction but with a slightly higher total yield and greater error bars so that it was not possible to distinguish between C and B with complete confidence. A note of caution is necessary here, as again, an alternative explanation for the higher blank levels and larger errors of C compared to D is available in that the blank experiment for C was executed over 12 steps, whereas for D over 7 only. Using arguments discussed previously, the extra 5 steps within blank C could explain the apparent disparity between the overall yields where C gave *ca.*15ng and D *ca.*10ng, and also explain the larger errors inherent in C over D shown in figure 4.6. As a result it was not possible to differentiate between C and D in terms of absolute contamination levels, but was reasonable to conclude that a real reduction had taken place by applying the solvent step, because the balance of *ca.*15ng difference between B and C or D cannot be explained by an excess of combustion steps in B. Examination of the individual stepwise plots in figure 4.7 shows the experiment for B to have been executed over 9 steps, which when compared to the two solvent treated blanks is 4 less than C, and only 2 more than D, and B would infact need 10 to 15 more steps to explain the disparity. Accepting that a reduction has taken place, further comparison of the plots can be used to elucidate where this has taken place. The <200°C release has remained unchanged by the application of a solvent, with B yielding 5.5±1.3ng compared to 4.6±3.2ng for C and 4.0±1.3ng for D, indicating that whatever species are liberated below 200°C, and assuming that the carbon contamination was not a soluble species added after the sample was removed from the solvent, they are not CH_2Cl_2 soluble. Likewise, the steps above 400°C all again yield between *ca.*0.5 and 1 ng carbon, irrespective of the temperature range of the individual step and the solvent treatment, providing more evidence for an input from an unknown source dependent only upon the step duration time. As expected, the reduction in contamination has taken place in

the carbon released between 200 and 400°C, from 11.8±1.9ng for B, to 4.2±1.9ng and 3.4±1.9ng for C and D respectively, the combustion having taken place over 3 steps in each case. This would imply that of the organic contamination within the protocols, approximately two thirds of the total was solvent extractable with presumably the remainder present as an insoluble macromolecular form.

4.3.2. Conclusions from the Triple Collector analysis protocol experiments.

By a combination of reducing the thickness of the Pt foil used for the sample packet and implementing a solvent cleaning step, a *ca.*75% reduction in blank was achieved over that obtained for the initial analysis protocol. Use of a thinner foil not only enabled accurate sample masses to be obtained but also led to a reduction in the blank, predominately in the low-temperature (<200°C) region. The nature of this low-temperature component was unclear, but it appeared to be associated with either the total mass, or thickness, of the foil used. The application of a CH_2Cl_2 cleaning step resulted in a further *ca.*66% reduction in the component (presumably organic) that was released between 200 and 400°C. Examination of the carbon yields for the temperature steps above 400°C revealed that a finite input of *ca.*1 to 2 ng of carbon occurred in each step irrespective of the temperature range spanned by the individual step, or the protocol technique used. The Triple Collector was unable to measure accurately the isotopic composition of this carbon so its provenance remained undetermined, although its ubiquitous presence strongly suggested a connection to a component part of the gas extraction system, with either the CuO or the glass of the extraction line being suspected.

The interpretation of the results highlighted the need for care in attempting comparison between individual blank experiments, where unless identical experiment procedures were followed in terms of the number of constituent temperature steps, then the additional yields and increase in error associated with excess steps could cause confusion.

4.4. The performance of the new protocols when applied to MS86.

The dual capability of MS86 to analyse sub-nanogram amounts of carbon to isotopic precisions of better than ±1‰ (see 2.2.8) and to determine yields of carbon liberated during stepped combustions to ±0.13ng (appendix A3), allowed a detailed investigation of both the absolute amounts and isotopic composition of the carbon blank from the sample analysis protocols, and that from the MS86 gas extraction line. Figures 4.8 and 4.9 show a summary of such blank experiments executed on MS86 over a period of eight months. Following on the Triple Collector experiments, the results have been divided according to which protocol they correspond as listed below;

(i) Protocol C - Foil of 7.5μm thickness but to mimic the sample transfer step within the blank, a drop of CH_2Cl_2 was placed onto the Pt foil square after weighing.

(ii) Protocol D - After execution of protocol C, the sample packet was transported from the clean room to the gas extraction line submerged in a petri dish of CH_2Cl_2.

(iii) Protocol E - No solvents used, but with a further reduction of the Pt foil thickness to 4μm.

(iv) Protocol F - Identical to protocol D, but using methanol (CH_3OH - AnalaR grade, BDH Chemicals, Poole, UK) in place of CH_2Cl_2.

(v) Protocol G - Identical to E, but the Pt foil packet was pulse heated for *ca.*10seconds to 1500°C prior to loading into the combustion section.

(vi) Protocol H - System blank results for the MS86 gas extraction system.

Changes were also introduced into the procedures used to clean the implements used to manipulate the Pt foil. Whereas formerly the tweezers, aluminium foil and any glassware were solvent/acid cleaned (see table 2.1), they were subsequently combusted at *ca.*600°C in the muffle furnace for a period of approximately one hour prior to use. These changes were introduced because it was anticipated that the previous methods could still leave residues on the implements that were potential contaminants, as indicated by the large organic component seen within the Triple Collector experiments where no solvent was used.

The results from the new series of experiments have again, in the first instance, been presented as the total carbon yield and isotopic composition for each individual

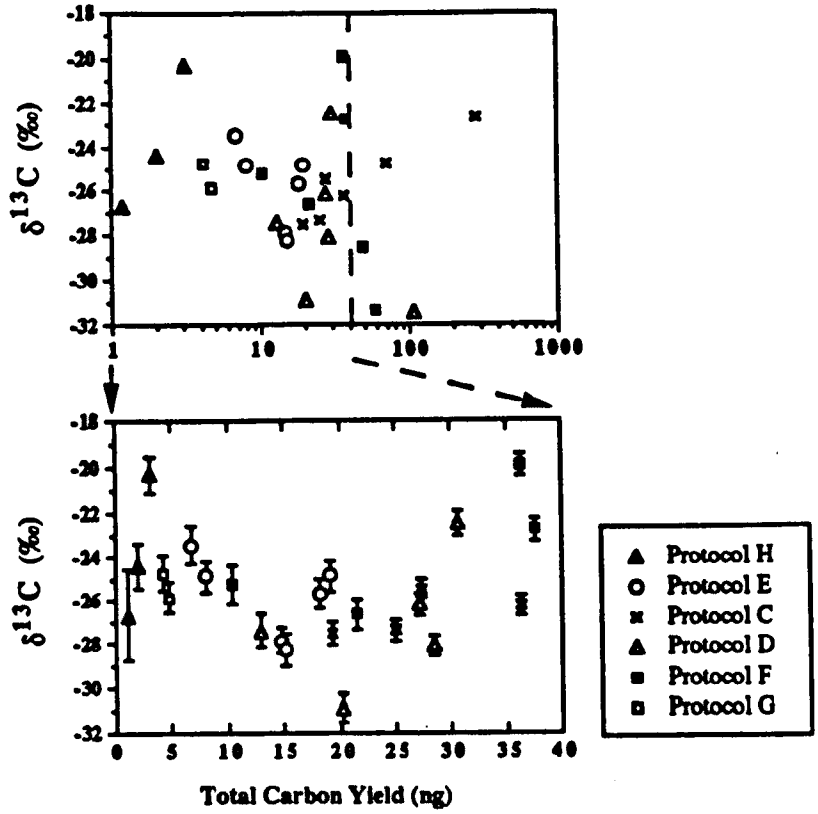

Figure 4.8. A summary of stepped combustion blank experiments executed on the MS86 mass spectrometer to evaluate different analysis protocols. Data is presented as the bulk carbon yields for each experiment plotted against the corresponding bulk carbon isotopic composition. (Yield error bars in the lower plot are smaller than the size of the symbols).

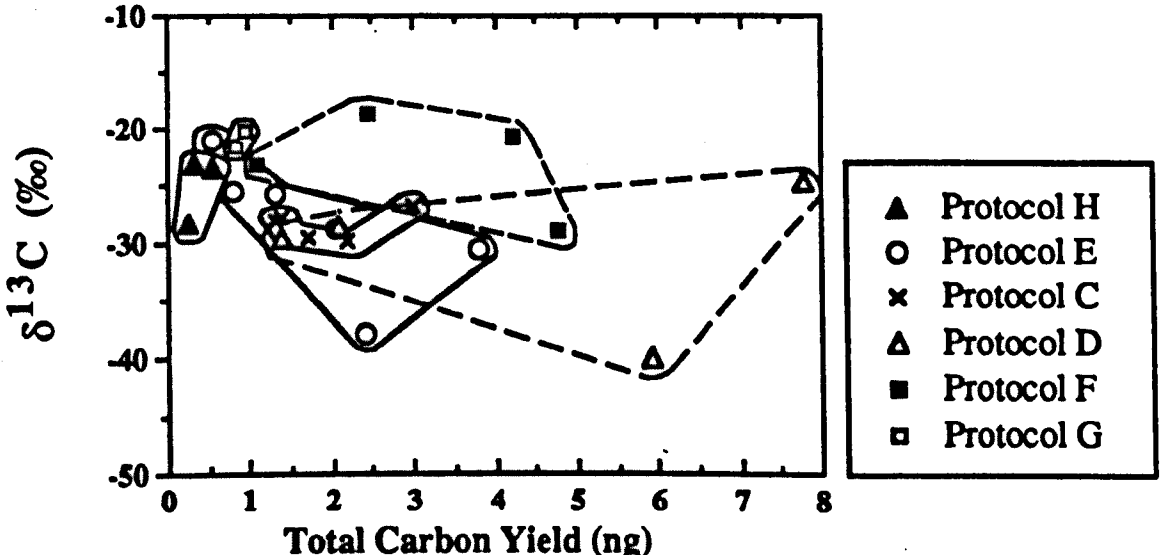

Figure 4.9. A summary of stepped combustion blank experiments executed on the MS86 mass spectrometer. Data is presented as the carbon yields >600°C for each experiment plotted against the corresponding bulk carbon isotopic composition. (Error bars have been omitted and similar results grouped together for clarity).

experiment (figure 4.8), and also as the analogous average for that released above 600°C alone (figure 4.9). Each individual group of experiments will be examined in more detail but these two figures serve as an important means of comparing the absolute blank input from each protocol, particularily in evaluating their relative performances. A brief examination of the results (without isolating different groups), reveals that in comparison to the blank experiments carried out on the Triple Collector (see figure 4.6) the higher precision to which MS86 could measure both the yield and isotopic composition of the carbon release has considerably reduced the errors on the data acquired, so that individual experiment results can now be easily resolved from each other.

4.4.1. The system blank (protocol H).

With the increased sensitivity and precision of MS86 it became possible to obtain meaningful abundances and $\delta^{13}C$ measurements on the carbon blank input from the gas extraction line itself (the system blank). This was important both in terms of the ability of isolating and identifying system blank components for possible blank correction purposes, but also if the sources of the system blank could be elucidated then improvements could be made to the system.

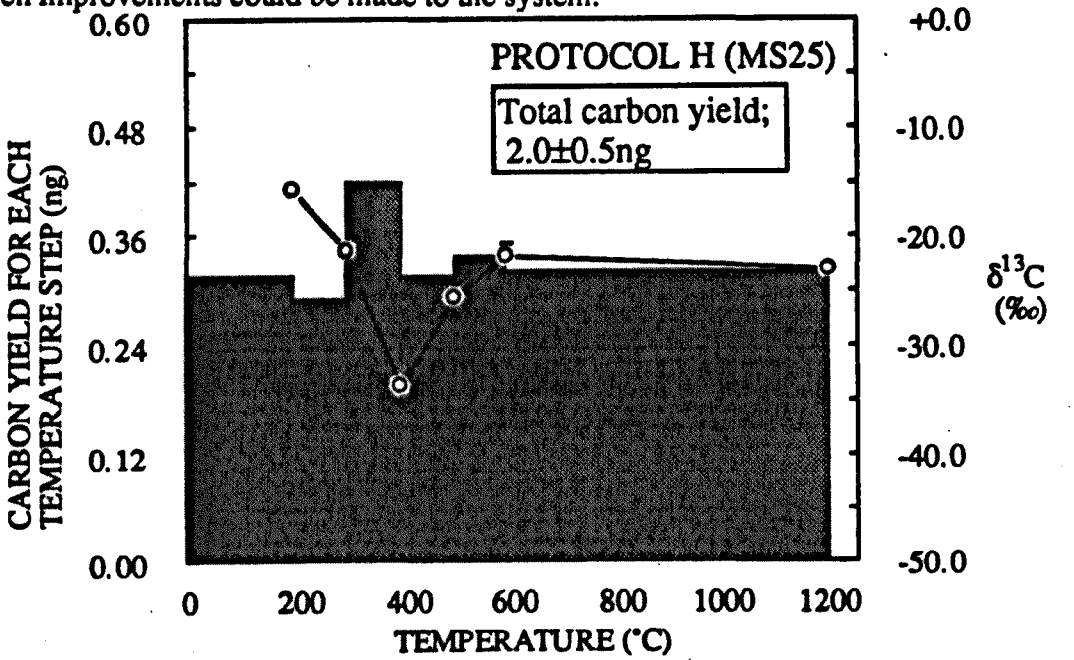

Figure 4.10 A typical stepped combustion profile of the system blank of the MS86 gas extraction system (protocol H).

Figure 4.8 shows that the three system blank experiments produced similar bulk results, yielding between *ca.*1 and 3ng of carbon with corresponding $\delta^{13}C$ values between *ca.*-20 and -27‰. Above 600°C (figure 4.9) the results were still tightly grouped, yielding *ca.*0.3ng with $\delta^{13}C$ values between *ca.*-23 to -28‰. A stepwise plot for a typical system blank is shown in figure 4.10. The most important observation is that, particularly after taking into account the errors on the carbon yield measurements (*ca.*±0.13ng), the release profile is essentially flat. This profile was repeated in the other two system blanks indicating again that, independent of the temperature of combustion or step size, a constant yield of carbon was obtained for each step, in this case *ca.*0.3ng, which within the yield errors was in agreement with the corresponding values for the other two system blank experiments. Interestingly, the isotopic profile suggested the presence of two components, one relatively ^{13}C-rich at 200°C and another ^{12}C-rich component at 400°C, both of which were superimposed over the background release with a $\delta^{13}C$ between -21 to -23‰, this background being illustrated by the remaining steps. The flat yield release meant that the 200/400°C components could not be corrected for the background input, so the only conclusions that can be made was that the 200°C component possessed a $\delta^{13}C$ value of > -15.8±1.2‰, and the 400°C < -34.0±1.3‰. Notwithstanding this, the same isotopic pattern was observed in the other two stepwises, indicating that these components were real and not anomalies perculiar to this particular experiment.

The basic design of the MS86 gas extraction line was essentially the same as that of the Triple Collector (for details see chapter 2), but with the results of the Triple Collector blank experiments in mind, *i.e.* where a solely time-dependent input of carbon between *ca.*1 and 2ng appeared to occur within each temperature step, the design had been modified as outlined in 2.3.5. Of specific relevance to the conclusions of the previous sections, the MS86 gas extraction system had been miniaturised with respect to both the overall amount of glass used in its construction, and also in the quantity of copper oxide used as the oxygen source. It was difficult, in the absence of detailed data for the Triple Collector system blank, to evaluate whether these changes had produced an actual blank reduction, as the value of *ca.*1 and 2ng per step quoted previously for the Triple Collector was for experiments when a Pt foil sample packet was also present. Irrespective of this, the release profile of the MS86 system blank had been accurately determined both in terms of yield and isotopic composition, so allowing blank corrections to be estimated if desired.

A further reduction in the MS86 system blank would require additional experimentation. Intuitively, more attention to miniaturisation may lower the absolute system blank input. As the isotopic profile indicated that at least two separate components were present within the system blank, the identity and provenance of these needs to be addressed inorder to facilitate substantial improvements. Such experiments, involving reconstruction of the gas extraction system using different materials and alternative oxygen sources *etc.*, were perceived as a later generation problem outside the initial aims of the current study, but are discussed further in chapter 7.

4.4.2. Evaluation of the blank input from the MS86 sample loading section (protocol G).

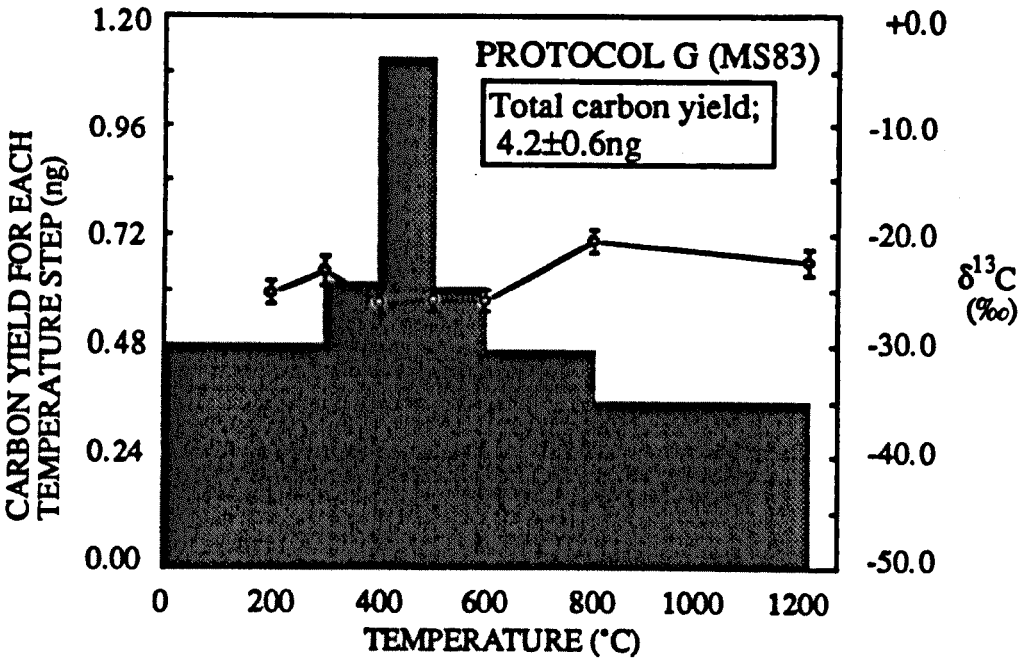

Figure 4.11. A stepped combustion plot for a platinum foil envelope that has been pulse-heated for *ca.*10 seconds at *ca.*1500°C prior to loading into the MS86 mass spectrometer gas extraction system (protocol G).

Protocol G experiments produced the smallest carbon yields for the stepped combustion of a Pt foil packet. Protocol G is however not strictly very useful because it could not be implemented with samples without affecting the specimens from which are hoped to acquire data. Protocol G was investigated to obtain information on the sample loading aspect of preparation as opposed to the sample weighing and

manipulation stage. The foil packets within the protocol were pulse-heated to *ca.*1500°C just before loading into the MS86 gas extraction system to remove carbon contamination from manipulation and weighing of the foil. The experiments were also relevant to the meteorite heating experiments (see chapter 7). Figure 4.8 shows that the combustion of foils handled using protocol G yielded between *ca.*4 and 5ng of carbon in total, which is marginally above that obtained for the system blanks.

The stepped combustion plot for a protocol G experiment is reproduced in figure 4.11 and reveals that the excess *ca.*2ng over the system blank carbon was predominately the product of a component that burned between 300 and 600°C with an isotopic value of *ca.*-26‰, whilst the remaining steps all yield carbon within errors of the system blank. In view of this observation it is interesting to note that the two components observed in the system blank stepped combustion plot (figure 4.9) were apparently not present; the reason for this is not obvious. Correcting for the time-related system blank carbon component input to the protocol G 300-600 °C component (*i.e* three steps at 0.30±0.13ng), produces a possible yield of between 0.69 and 2.25ng, but an isotopic correction was not necessary because the $\delta^{13}C$ value obtained for the 400-500°C step in MS83 (the peak of combustion of the component) was identical to the system blank 400-500°C step, with both being equal to -25.9‰. From these arguments it was apparent that the Pt foil sample packet accrued between 0.69 and 2.25ng of carbon contamination as a result of loading into the gas extraction system, which in turn manifested itself between 300 and 600°C with an isotopic value of -26‰. The exact nature of this component is dealt with further in 4.4.7.

4.4.3. Isolation of severely contaminated blank experiments.

The remaining results within figures 4.8 and 4.9 are for experiments that involved execution of the full sample analysis procedure, but using slightly different protocols in order to investigate specific carbon blank inputs. Figure 4.8 reveals that these experiments produced bulk carbon yields between *ca.*6 and 300 ng, but with *ca.*85% plotting <40ng. It was considered that if an unexpectedly large blank occured, such carbon could be erroneously identified as being indigenous to any potential sample. In view of this, the release profile and isotopic composition of such contamination was of considerable interest. Subsequent examination of the individual stepped combustion

plots of the high blank (>40ng) experiments revealed that the excess contamination was present in two forms;

(1) Either being present simply in the same form as that liberated from analogous protocols that yielded lower totals, but at a higher concentration.

(2) As a 'catastrophic' contamination event that bore no resemblance to the carbon obtained in the other blank experiments.

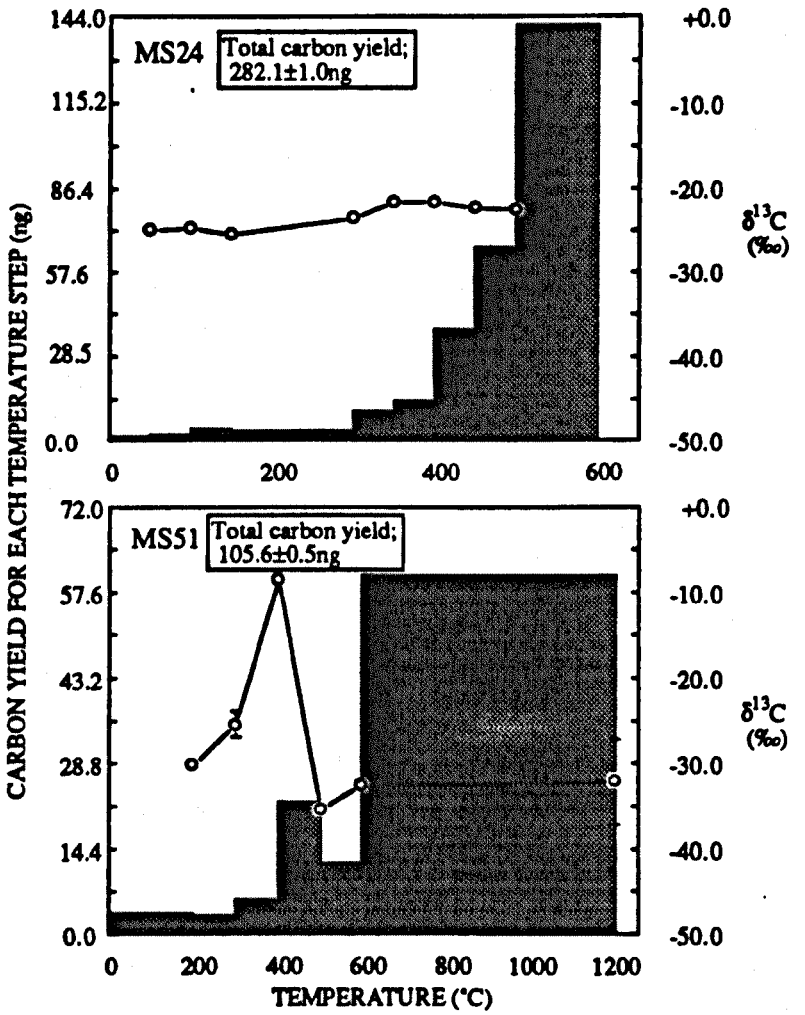

Figure 4.12. Stepped combustion combustion plots of blank experiments that had suffered 'catastrophic' carbon contamination during execution of the sample analysis protocols.

The situation as defined in (1) above was not completely prohibitive to interpretation of any sample results, because as the excess carbon manifested itself as identical components to lower blank examples, misinterpretation of this excess carbon

as being indigenous to the sample should not occur. The only perceivable problem in this situation would be in the under-estimation of the absolute amount of blank that should be used in any attempted blank corrections. Following on from these arguments the second situation (2) was potentially more serious, but for the following reasons the problem actually became relatively negligible. Firstly, the release profiles of the catastrophic blanks were characteristic, this being illustrated by figure 4.12 where the individual stepwise plots for the two blank experiments (one protocol C and one D) that yielded bulk carbon abundances in excess of 100ng are reproduced. In both cases the amount of carbon obtained increased as the temperature of combustion was elevated, producing a profile that would easily be resolved from any sample experiments, because, secondly, such large carbon yields would translate into unrealistic >600°C sample carbon concentrations. (Note that in experiment MS24 the combustion was terminated at 600°C because the amounts of gas released >600°C would have been harmful to the gas extraction system, but it was assumed that a similar profile to the other example in figure 4.12 would have been obtained).

Identifying the contaminants responsible for the catastrophic blanks proved problematical, as they did not exhibit release profiles similar to any other known laboratory contaminant. The observation that the experiments carried out on days either side of the catastrophic blanks showed no similar contamination appears to exonerate the gas extraction line as the source, and the high combustion temperature of the bulk of the carbon likewise indicated that the contamination was probably non-organic, and so equally not the result of sample handling procedures. For these reasons it was assumed that the contaminant was some kind of refractory airborne particulate, that had ingressed either into the sample packet during the handling and weighing procedures, or through the airlock during loading into the combustion section. One final observation was that the isotopic profile of one of the examples (MS51) exhibited a particularily anomalous $\delta^{13}C$ signature between 200 and 500°C. The combustion temperature of this component suggests an organic nature, but the peak $\delta^{13}C$ value of *ca.*-8‰ is not consistent with this interpretation, being more characteristic of either terrestrial carbonate (*e.g.* Hoefs, 1987), or atmospheric CO_2 (*e.g.* Keeling, 1961). However, carbonate usually decrepitates between 600 and 700°C, and surficially bound gases should be released <200°C (*e.g.* Wright and Pillinger, 1989), so unless the component represents CO_2 that had been trapped until release at a higher temperature, its origin remained undetermined.

4.4.4. The dry foil blank experiments (protocol E).

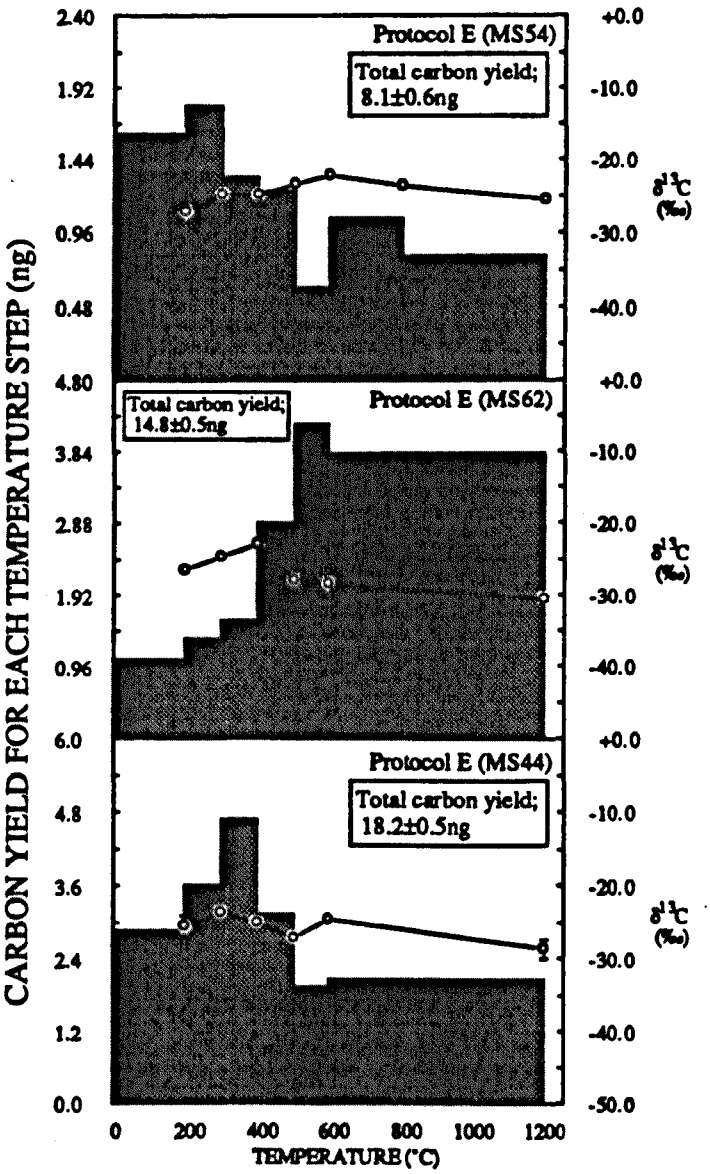

Figure 4.13. Stepped combustion plots showing the range of carbon release profiles encountered during blank experiments executed on MS86 using the dry foil sample analysis procedure (protocol E).

Examination of figures 4.8 and 4.9 shows that the dry foil (protocol E) experiments yielded between *ca.*6 and 20ng of carbon in total with accompanying bulk $\delta^{13}C$ values between *ca.*-23 and -28‰, whilst in the >600°C regime beween *ca.*0.5 and 4ng was released with a $\delta^{13}C$ value of *ca.*-21 to -37‰. Considering the results as a whole, the most surprising observation was that in contradiction to the Triple Collector blank

experiments, the MS86 dry foil experiments consistently yielded less blank than the MS86 CH_2Cl_2 treated protocols (C and D). Typical stepped combustion plots of the protocol E experiments are reproduced in figure 4.13.

The three plots within figure 4.13 cover the range of release patterns observed from the experiments, the remaining three exhibited various permutations of the components seen within these examples. This initial observation highlights perhaps the most important conclusion from the blank experiments, in that although individual components could be attributed to the blank, their presence was variable, and this must be taken into account when considering the results of any attempted blank corrections. The plot of experiment MS54 shown in figure 4.13 shows the profile a low-carbon yield example for protocol E, yielding a total of 8.1±0.6ng of carbon, *i.e.* only *ca.*5ng over the system blank. Unlike the protocol G examples, this carbon excess was not concentrated in a single release, but the predominately flat carbon yield profile seen here indicates it was more evenly distributed. Each step yielded *ca.*1ng of carbon, irrespective of step size or combustion temperature, indicating that in this case at least, the Pt foil seemingly generates a time related blank component of carbon. When the equivalent system blank yield is taken into account (*ca.*0.3ng $step^{-1}$), it would seem that there is an input of *ca.*0.7ng $step^{-1}$ of carbon from the platinum. Comparison to the protocol G experiments, which were carried out under similar conditions to the experiments discussed here with the exception that the foil packet was pulse heated immediately prior to loading, shows this excess 0.7ng carbon $step^{-1}$ to be absent in the pulse heated samples (see 4.4.2). This observation can be explained as;

(1) The pulse heating to *ca.*1500°C for *ca.*10 seconds in atmosphere was a more efficient Pt cleaning method than combustion to *ca.*1000°C in oxygen as described in 2.3.4.

(2) After cleaning by combustion, the absolute amount of time-related carbon blank component from the platinum foil was dependent on the length of time before the foil was used, or the length of time it was exposed to atmosphere before loading into the mass spectrometer gas extraction system. The pulse heated samples were loaded within *ca.*5 minutes of combustion to 1500°C, whereas the 1000°C combusted envelopes were kept at *ca.*600°C in oxygen for 1-5 hours before processing, and then exposed to atmosphere for *ca.*15minutes after opening the ampoule (figure 2.9) before loading into the gas extraction system.

As already noted in 4.3, the dry foil experiments executed on the Triple Collector showed that at temperatures above 600°C 1 to 2 ng of carbon were released per step, indicating either that the system carbon blank associated with the Triple Collector was higher than MS86, or the carbon contamination from the Pt foil had been reduced as a result of the thinner foil used in the case of experiment MS54. It can be seen that in MS54 there was additionally a slight excess over this 1ng in the first steps, with a peak in the release at 300°C of 1.8ng, but this was probably caused by the addition of a small amount of handling organic contamination. The carbon yield of *ca.*0.9ng released at 500°C in experiment MS54 can be explained by the *ca.*0.3ng $step^{-1}$ system blank and *ca.*0.7ng $step^{-1}$ Pt foil time-related carbon components. It was therefore evident that the component isolated from experiment MS83 that had been attributed to an origin in the loading section of the gas extraction system was absent. Isotopically the carbon release profile from room temperature to 1200°C of MS54 is flat, ranging from -22.4±1‰ to -27.2±1‰. Below 600°C the organic contamination introduced from handling and the Pt foil input have diluted the previously isolated system blank components, and above 600°C, even with the time-related Pt foil contribution, the isotopes were within errors of the system blank values. This latter observation suggests that the Pt foil component shares a similar carbon isotopic composition to the system blank >600°C, *i.e.* between *ca.*-22 to -26‰.

The other two stepwises in figure 4.13 represent relatively more contaminated examples of protocol E blank experiments. MS62 exhibits a similar profile to the 'catastrophic' contaminated blanks discussed in 4.4.3, but with a much lower bulk yield of only 14.8±0.52ng and a peak release of *ca.*5ng for each of the two last steps. Below 400°C the carbon release profile of MS62 was almost identical to that of MS54 both in carbon yield and $\delta^{13}C$ composition, but above this temperature there was an excess of *ca.*7ng over MS54 with a $\delta^{13}C$ value of *ca.*-30‰, this isotopically being the same value obtained within the 'catastrophic' examples. It would appear that the high temperature carbon in MS62 represents contamination by the same species isolated within MS51 in figure 4.12, and that the problem may have been more prevalent than originally anticipated. It is noteworthy that in the absence of an unreasonable yield excess, it would extremely difficult to recognise such a input of carbon similar to that seen in MS62 to a sample experiment, especially in view of the observation that the $\delta^{13}C$ value of -30‰ is not in any way anomalous.

The final plot in figure 4.13, MS44, illustrates the Protocol E experiment that produced the highest bulk blank value, yielding 18.2±0.5ng of carbon. This excess carbon is liberated at every step between room temperature and 1200°C, but with the majority in the 200-500°C range. The $\delta^{13}C$ values of -23.6±0.7 to -27.3±1‰ suggests an organic handling contamination provenance for the excess. Additionally, there was a >600°C excess of *ca.*1.7ng over the system blank exhibiting a $\delta^{13}C$ value of *ca.*-30‰, indicating that perhaps again there is evidence for an input from the refractory airborne component.

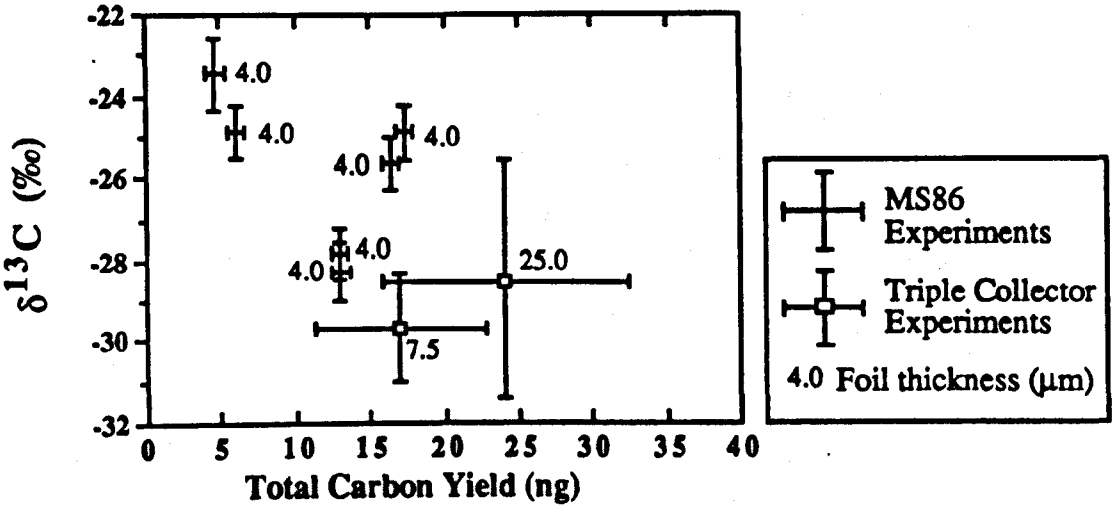

Figure 4.14. System blank corrected bulk carbon yields for dry platinum foil blank experiments executed on MS86 (protocol E) and the Triple Collector (protocols A and B) mass spectrometers.

A brief comparison of the MS86 dry foil experiments (protocol E) to the Triple Collector dry foil experiments (protocols A and B) proved rather inconclusive. A qualitative attempt to estimate the bulk carbon yields after adjusting for the system blanks (0.3ng step^{-1} for MS86, and 0.75ng step^{-1} for the Triple Collector) is shown in figure 4.14. The large errors on the Triple Collector data made it difficult to resolve the individual experiments with any confidence, but it appeared that the MS86 results spanned the range of yields encompassed by the thicker foil results from the Triple Collector. In the two MS86 experiments where the yield was distinctly lower, the stepped combustion plots indicate that the reduction has occurred not only in the <200°C step, where a *ca.*50% reduction was previously observed in the Triple Collector experiments in moving from Pt foil of thickness 25 to 7.5μm, but also in the

200-400°C region. With the MS86 evidence that the dry foil blank is highly variable and strongly dependent upon several components that are seemingly unrelated to foil thickness, it is difficult to draw any conclusions other than the foil thickness exerts little control over the total blank yield.

4.4.5. Solvent treated blank experiments (protocols C and D).

Figures 4.15 and 4.16 contain stepped combustion data for MS86 blank experiments where CH_2Cl_2 was used to mimic the sample transfer procedure (protocol C) and additionally kept submerged under the solvent during transportation to the gas extraction system (protocol D). Looking first at figure 4.15, the plot for experiment MS26 shows a total release of 27.4±0.8ng of carbon, with *ca.*32% of this combusting between 400 and 500°C. The temperature of release and measured $\delta^{13}C$ value of -24.7±0.5‰ suggested that the component was probably related to the loading section contaminant isolated from the protocol G experiments, so did not reflect the performance of the solvent treatment step. Notwithstanding this, it was also evident that the steps between 200 and 400°C yielded *ca.*10ng of carbon, *i.e.* a factor of 2 to 3 greater than the analogous steps for the dry foil (protocol E) experiments. It was considered that this contamination was unlikely to be solely a part of the 400-500°C loading section component because the combustion profile for the protocol G experiments (figure 4.11) showed a relatively sharp combustion peak, so the excess here probably represented an additional organic component. If this interpretation was correct, then either the contamination was accrued after the solvent treatment step, or it represented a non-soluble component or was supplied from the solvent itself. The Triple Collector protocol C and D experiments only yielded *ca.*1.5 to 2.5ng of carbon between 200 and 400°C (after allowing for the system blank input), an observation that implied that the non-soluble organic component could probably not supply the balance of the disparity. With the evidence presented below that contaminated CH_2Cl_2 was characterised by an excess of carbon largely released below 200°C, then it was probable that the component seen in

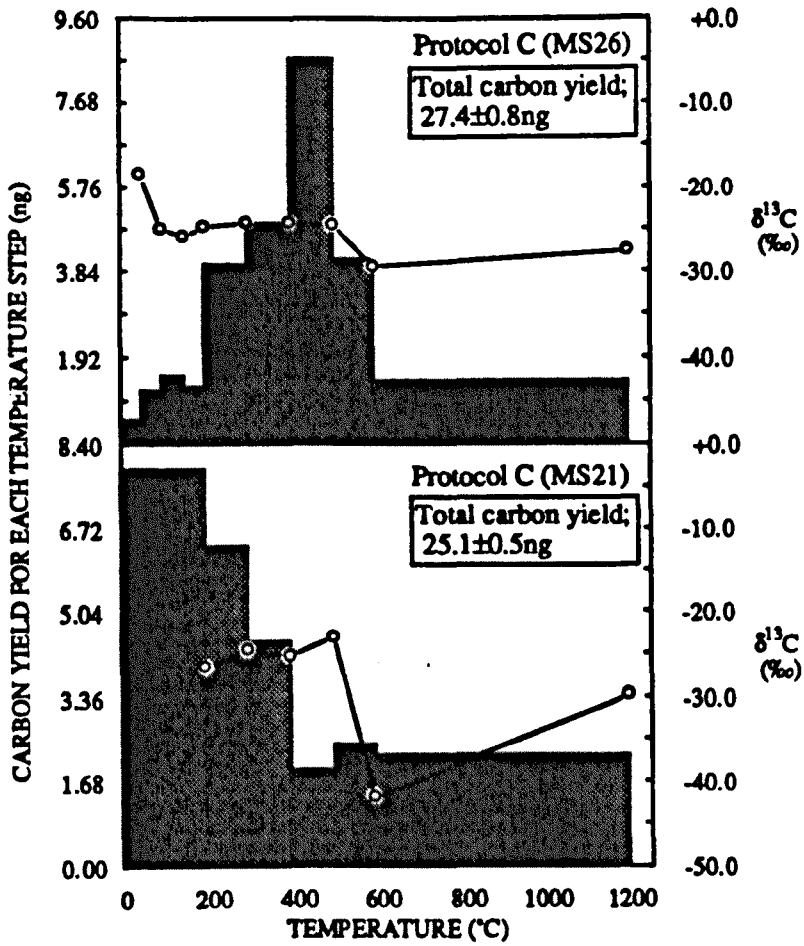

Figure 4.15. Typical stepped combustion plots for MS86 blank experiments executed according to protocol C.

MS26 between 400 and 600°C was an organic handling contaminant accrued after the solvent treatment step, probably from the stainless steel implements used to manipulate the Pt sample packet into the MS86 gas extraction system. The <200°C steps showed only a small excess (*ca.*2ng) over the dry foil results, but the 50°C combustion steps within it illustrated the previously only postulated effect of the release of surficially absorbed CO_2, this being indicated by the $\delta^{13}C$ value of -18.6±0.9‰ for the first step. The isotopic departure to -29.7±0.5‰ within the release profile of MS26 at 600°C can be explained as an input of relatively ^{12}C-enriched carbon superimposed on the already noted sample handling organic and loading section components. The carbon yield for the 600 to 1200°C step in MS26 could be accounted for by the sum of the Pt foil and system blank time-related inputs, but the $\delta^{13}C$ value showed a departure to -29.7±0.5‰, which is lighter than the

combined system blank/Pt foil time-related component, which was estimated at *ca.*-22 to -26‰ in 4.4.4, and more indicative of the postulated airborne contaminant (4.4.3).

The release pattern of MS21 in figure 4.15 was generally different to MS26, with the exception that the istopically light carbon component at 600°C seen in MS26 was present in MS21 also, but being considerably more ^{12}C-enriched; yielding a $\delta^{13}C$ value of -42.0±0.9‰. With the effects of this component being seen within all the remaining protocol C experiments, and its absence dry foil experiments, it was apparent that it was related to the CH_2Cl_2. The exact provenance of the component was not known, but it may have been related to interference effects of a chlorine containing species within the mass spectrometer. Aside from the 600°C component, the carbon release profiles for MS21 and MS26 were otherwise dissimilar, in MS26 the major carbon release ocurred between 200 to 600°C, whereas in MS21 between room temperature and 400°C. In terms of bulk carbon yields, MS26 yielded *ca.*27ng and MS21 *ca.*25ng. It has already been determined in this section that the carbon released between 200 to 600°C in MS26 was most likely the product of the loading section contamination component and an organic handling contaminant. In contrast, the <400°C carbon release that dominates MS21 was the product of contaminated CH_2Cl_2. Evidence to support this conclusion comes from the observation that three contemporaneous blank experiments using the same batch of solvent all yielded similar release profiles dominated by <400°C carbon. When this solvent was replaced by a fresh batch, the first blank experiment executed using the new solvent (MS26) did not show the <400°C component. The mechanism of contamination was undetermined; the solvent was stored under clean room conditions and was used solely for this study, but its presence underlines the importance of executing frequent blank experiments to check on its condition, and to use small batches of solvent that were frequently replaced. Finally, the 600 to 1200° step in MS21 within figure 4.15 contained an excess of *ca.*1ng carbon over the postulated *ca.*1ng yield for the combined Pt foil/system blank input, and the corresponding $\delta^{13}C$ value of -29.9±1.0‰ again points to possible contamination by airborne particulates.

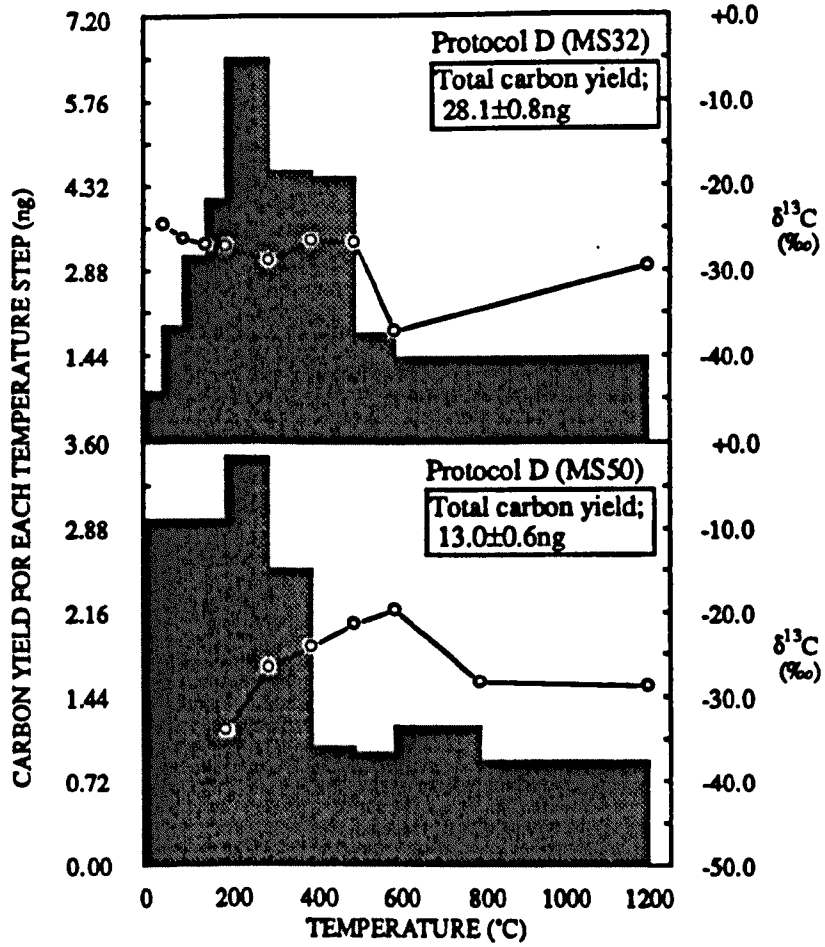

Figure 4.16. Typical stepped combustion plots for MS86 blank experiments executed according to protocol D.

The plot for MS50 in figure 4.16 shows the stepped combustion of the only solvent-treated experiment that yielded <20ng of carbon in total, being an example of a protocol D experiment. The total yield (*ca.*13ng) was comparable to that obtained in the dry foil experiments (protocol E), showing no signs of the contamination prevalent with the protocol C experiments, and with a release pattern similar to that seen in the low-blank protocol E experiments (*cf.* MS54 within figure 4.13). Unfortunately the corresponding isotopic profile was not equally correlative, and exhibited two characteristics not previously observed. Firstly, the <200°C step was isotopically light at -34.2±1.1‰, whilst secondly, the 600°C step was accompanied by relatively ^{13}C enriched value of -19.9±1.2‰. The plot of MS32 in figure 4.16 illustrates a protocol D experiment that yielded *ca.*28ng of carbon, a more typical total and with a more representative release pattern. The majority of the carbon combusted between 200 and 500°C with a $\delta^{13}C$ value of *ca.*-27‰, and this was interpreted as a similar organic

component to those isolated within the protocol C experiments, coupled to a smaller input from the gas extraction loading section. Aside from this, the <200°C steps isotopic measurements again indicate an input from atmospheric CO_2, whilst similarily the 600°C step exhibits the effect of the hypothetical CH_2Cl_2 chlorine containing species. The 600-1200°C step yielded only *ca.*0.4ng of carbon in excess of the Pt foil/system blank input and was isotopically similar to previous experiments.

4.4.6. The use of methanol as an alternative to dichloromethane within protocol D (protocol F).

Dichloromethane was originally chosen for its exceptional volatility, but the protocol C and D experiments carried out on MS86 showed it to display two detrimental properties as listed below;

(i) Release of a contaminant at 600°C that then interferred with the mass spectrometer to produce isotopically light $\delta^{13}C$ values.

(ii) A variable yield release pattern, possibly due to solvent contamination problems.

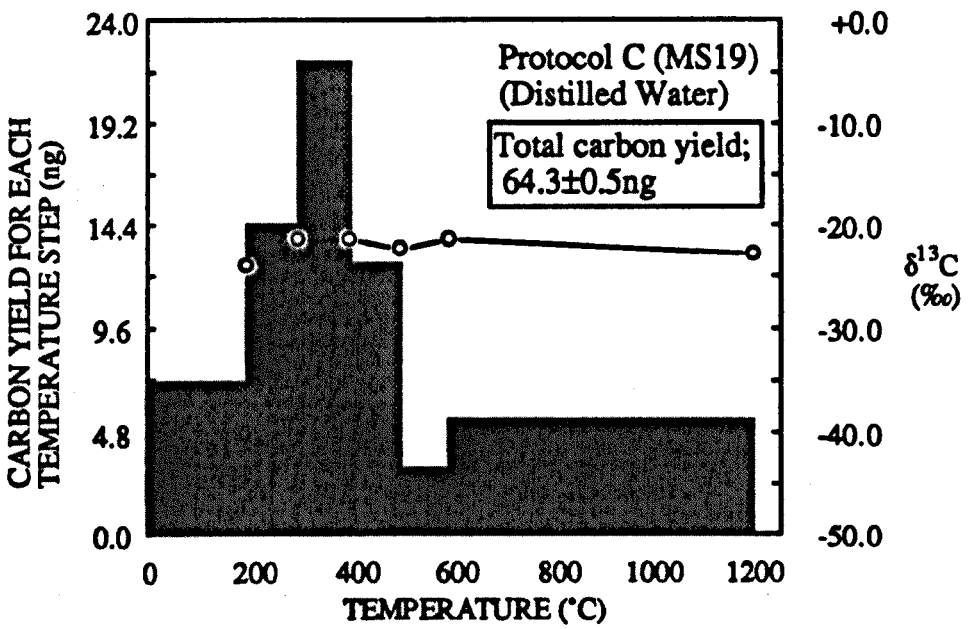

Figure 4.17. A stepped combustion plot to illustrate the results of a protocol C blank experiment where the solvent had been replaced with distilled water.

Both of these were considered as essentially prohibitive to the analysis protocol, because the variability of the interference effect and yield profile would considerably lower the confidence by which any blank corrections could be applied, so an alternative solvent was sought. A tentative look at the potential of distilled water (figure 4.17) as a transfer medium was quickly abandoned without ever testing its solvent characteristics, because it yielded *ca.*65ng of carbon for a protocol C experiment. More importantly, it was found that the water was extremely difficult to evaporate, prolonging the analysis protocol for in excess of one hour.

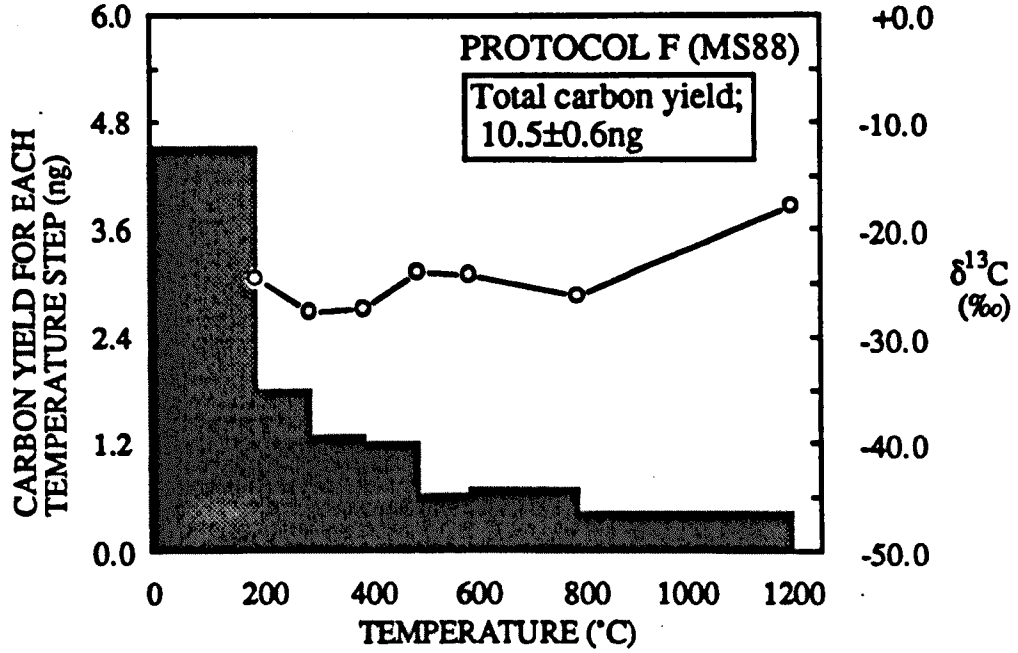

Figure 4.18. A typical stepped combustion plot for a protocol D experiment executed using methanol in place of dichloromethane (protocol F).

Figure 4.18 presents a typical stepwise plot for a protocol D experiment executed on MS86 using 'AnalaR grade' (BDH Chemicals, Poole, UK) methanol (CH_3OH) in place of CH_2Cl_2. Examination of the bulk carbon yields within figure 4.8 for protocol F experiments revealed a spread of bulk yields from *ca.*10 to 60ng of carbon, which was similar to that of CH_2Cl_2 treated blank experiments (protocols C and D), but for several reasons the use of CH_3OH was preferred over CH_2Cl_2. Firstly, the interfering CH_2Cl_2 species observed at 600°C dissappeared, and secondly, and of more importance, the carbon yield and $\delta^{13}C$ profiles of the protocol F experiments proved to be exceptionally reproducable in terms of the individual carbon components that constituted the bulk release. Of specific importance here was that in all the CH_3OH

experiments (as illustrated in figure 4.18), the peak of the carbon release occurred <200°C, and experimentation with 50°C steps up to 200°C revealed that this peak was always within the first temperature step. Whilst indicating that the component probably represented surficially bound CH_3OH, this effect additionally meant that after execution of the first temperature step, the remainder of the stepwise consistently only suffered from between 1 and 2ng of blank input for each step, and with a predictable isotopic composition. The problem of relative volatility also proved to to be of negligible importance, as although the use of CH_3OH typically prolonged the execution of the analysis protocol by a few minutes, its positive attributes were deemed to outweigh this delay.

The carbon release profile of experiment MS88 in figure 4.18 shows that after the <200°C release of surficially bound methanol, then between 200 and 400°C only a further *ca.*3.5ng of carbon was obtained. This low yield between 200-400°C is typical of the protocol F experiments; the remaining five examples gave yields spanning between 3 and 5ng. This observation is important because carbon combusting in the 200-400°C range is assumed to represent organic sample handling contamination, and in contrast to the similar amounts obtained here for the protocol F blanks, in both the dry foil (protocol E) and CH_2Cl_2 blanks (protocols C and D) the yield across this temperature range was extremely variable. This observation would indicate that either the methanol is a more efficient solvent than the CH_2Cl_2, or that it is less susceptible to contamination. The remaining temperature steps in MS88 beween 400 and 1200°C all gave carbon yields below *ca.*1ng, a pattern that was likewise mirrored in the other protocol F experiments. Of specific relevance here was that in none of the protocol F experiments was there any evidence for the gas extraction loading section contaminant, which again had been isolated from within both the dry foil and CH_2Cl_2 blanks, but the reason for its absence was not clear. It is also noteworthy to mention that in only one protocol F stepped combustion plot was the effect of the airbourne particulate contamination seen; where 4.8±0.13ng of carbon was obtained for the last temperature step with the characteristic $\delta^{13}C$ value of -29.1±0.5‰. This was of importance because intuitively, if the interpretation of the contaminant was correct, then the additional exposure time within the analysis protocol waiting for the methanol to evaporate would be reflected by an increase in the occurrence of the contamination. Unless the interpretation of the contaminant as airborne particulates was erroneous, this observation implied that the contamination event occurred outside of the clean-

room environment, *i.e.* during transfer of the sample to the mass spectrometer gas extraction system, because the excess exposure time took place within the clean room. The only negative property associated with the use of the CH_3OH was that the isotopic value for the final temperature step was typically ^{13}C-enriched, this being shown within MS88 in figure 4.18 where the 800-1200°C step gave a $\delta^{13}C$ value of -17.9±1.2‰. In the remaining 5 protocol F experiments this ^{13}C-enrichment produced a range of $\delta^{13}C$ values between -10.2±1.1‰ and -19.2±1.0‰.

4.4.7. An evaluation of possible sources of contaminants during the routine operation of the sample analysis protocols.

In an attempt to isolate the sources of the various carbon blank components revealed during the MS86 blank experiments detailed in sections 4.4.1 to 4.4.6, a further series of experiments was devised to investigate possible genetic connections to the routine operation of the sample analysis protocols. From within the protocols four such likely contamination sources were identified; (see 2.1.2 for details of the general execution of the protocol)

(1) Pyrex glass fragments adhering to the sample as a result of the crushing step.

(2) Aluminium (Al) foil used both as a general substrate for the crushing /weighing procedures, and also to wrap the implements used within protocols C, D, E, F, and G for combustion in the muffle furnace.

(3) The lining of the muffle furnace itself, which was in the form of heat resistant tiles and was extremely friable. As a result of abrasion accompanying movement of objects within it, a fine powder was ubiquitously present within the furnace which conceivably could adhere to the implements during the combustion cleaning, and thence to the sample or Pt foil.

(4) As part of the loading procedure, the Pt sample packet was passed through an airlock in the gas extraction system (see figure 2.11). Although this airlock was theoretically kept clean by the action of electrical heater tapes set at *ca.*130°C and continuosly kept at vacuum in between experiments, it was envisaged that a potential for contamination existed during the loading procedure. The sample packet entered the airlock by means of removing the teflon body of a valve and then dropping it down through the outer glass sleeve. This glass sleeve was in constant contact with the teflon of the valve

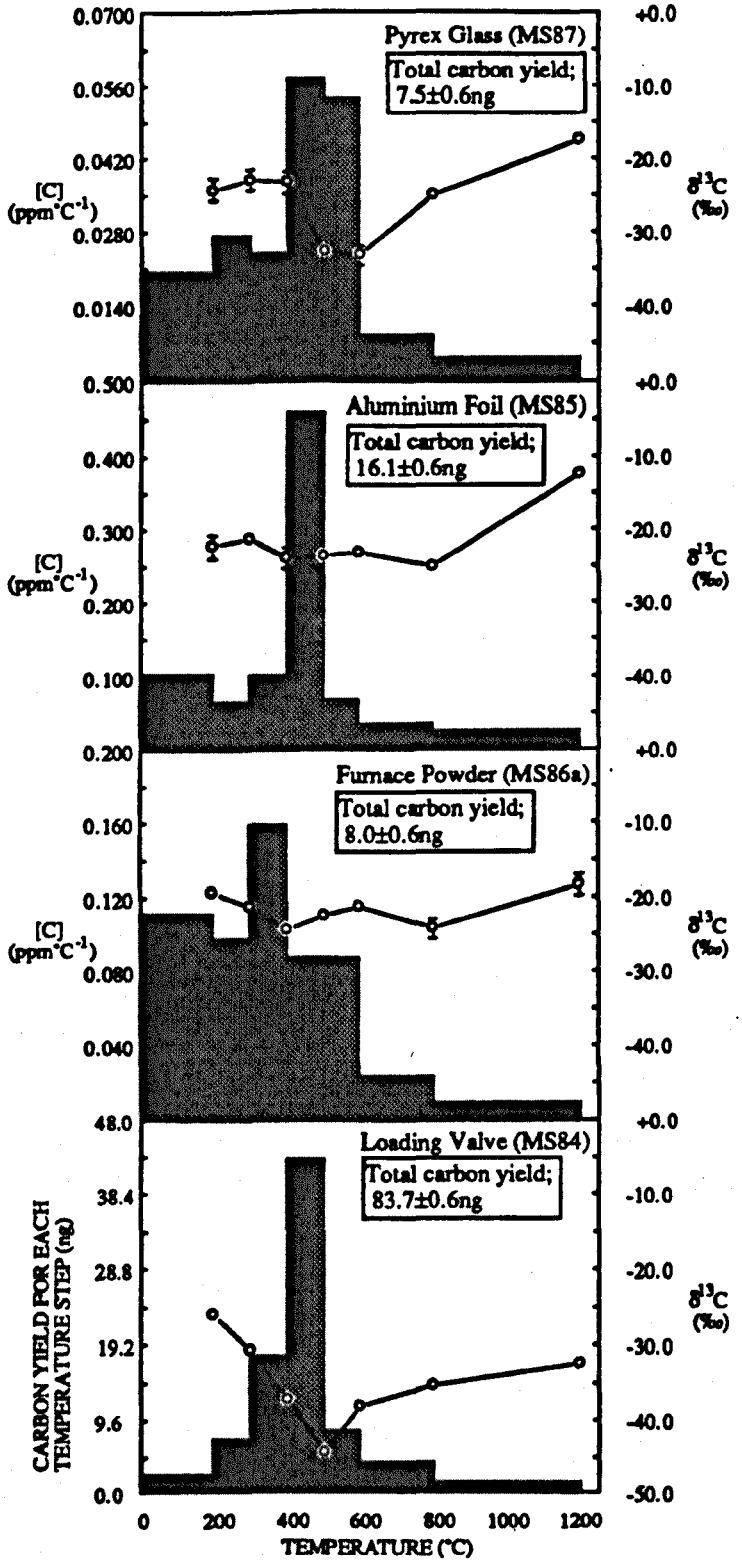

Figure 4.19. Stepped combustion plots of experiments performed on MS86 designed to elucidate possible sources of carbon contamination from within the sample analysis protocols.

sealing rings and so even though efforts were made to avoid the packet coming into contact with the glass, it was a possible source of contamination. Of greater importance was that the sample packet was manipulated into the combustion section from the airlock by a path that crossed the seat of one of the combustion section valves, so again coming into contact with an area of glass that was otherwise in constant contact with a teflon sealing ring.

The results of the experiments carried out on MS86 to investigate these four postulated sources are shown in figure 4.19. The plot for experiment MS87 illustrates the stepped combustion of a *ca.*0.3mg fragment of Pyrex glass taken from the microscope slide used for crushing the samples. It can be seen that the glass combusted predominately between 400 and 600°C, yielding carbon with a $\delta^{13}C$ value of *ca.*-33‰. Notwithstanding that the only similar carbon to this had been isolated within the protocol C and D experiments where it had been interpreted as the product of the interference of a chlorine containing species (4.4.3.), the possibility of the glass being responsible for carbon components within the blank experiments could be discounted on the basis of the concentration of the 400-600°C component in the glass. For experiment MS87 a fragment of Pyrex glass of *ca.*0.3mg mass was combusted and yet this only yielded a total of *ca.*2ng of carbon across the peak of combustion (400-600°C) of the glass. In order to account for the components observed within the blank experiments, a similar yield of carbon would be required, necessitating an excess mass of glass of *ca.*0.3mg to be incorporated with the sample packet and this was a completely unfeasible situation. The sample crushing was monitored during operation by a binocular microscope and the addition of such a large fragment of glass to the sample envelope would not have been overlooked.

The results of a combustion of a *ca.*0.15mg piece of Al foil is shown in figure 4.19 by the plot of MS85. In this case the only carbon that was released over time-related carbon components from the system blank and Pt foil used as a sample envelope was seen between 400 and 500°C with a $\delta^{13}C$ value of -23.6±1.3‰. It would appear likely that this component at 400-500°C represents the gas extraction system loading section contaminant referred to in 4.4.2. However, even if the component was indigenous to the Al foil, the low carbon concentration of the 400-500°C release within the Al foil (*ca.*100ppm) would dictate that an equivalent mass of foil become incorporated into the Pt sample envelope as used in the MS85 experiment, and for the

same reasons that precluded incorporation of a 0.3mg glass fragment, this was extremely unlikely. The muffel furnace powder experiment (MS86a[8] in figure 4.19) yielded the least carbon of the four experiments, which translated to a bulk carbon concentration of *ca.*70ppm when the time-related carbon inputs from the system blank and Pt foil had been taken into account. Again, this low carbon concentration meant that the muffle furnace powder was not a plausible candidate for a source of contamination within the analysis protocols.

In contrast to the others, the results for the experiment where a sample packet that had been processed through protocol E (no solvent) and then subjected to wiping around the inner glass sleeve of the airlock loading valve (MS84 in figure 4.19), appeared to provide one explanation for a blank component. The foil released a total of 83.7±0.6ng of carbon, *ca.*50% of which combusted between 400 and 500°C with a $\delta^{13}C$ value of -44.4±0.4‰. It was not surprising that on comparison to the blank experiments a match was obtained to the component previously attributed to the loading section from the protocol G experiments. From the protocol G experiments, the $\delta^{13}C$ value of the loading section contaminant had been estimated at *ca.*-26‰, but the disparity between the $\delta^{13}C$ value of *ca.*-44‰ determined from experiment MS84 could be explained as the product of mixing the 'pure' loading valve (teflon) component at -44‰ with the time-related system blank/Pt foil carbon components at *ca.*-22 to -26‰. Presumably during routine operation of the loading section, the sample packet would accrue a fraction of the contamination seen in the MS84 stepwise plot, but enough for its ^{12}C enriched carbon to accordingly lower the average $\delta^{13}C$ value of the 400-500°C step.

A final observation from the experiments was that in two examples (MS85 and MS87) the temperature steps >600°C exhibited a trend to heavier isotopic values, even though their corresponding yields were at blank levels. Whilst the reasons for these trends are not clear, the isotopic pattern and heaviest values obtained (-12.5±1.1 and -17.4±1.1‰ respectively) were equivalent to the results obtained for the Triple Collector deep-sea spherule experiments (see 4.2), so possibly provide an alternative explanation to the indigenous SiC interpretation. However, the problem was

---

[8] To avoid confusion the muffle furnace powder blank experiment has been given the experiment number MS86a.

compounded further in that the Wright *et al.*, (1988) study also revealed the presence of the component, and their samples did not undergo crushing with a glass slide or their cleaning materials/implements suffer such extensive exposure to Al foil, so on balance the component would still appear to be indigenous.

4.5. Summary and conclusions.

The initial experiments to evaluate the sample analysis protocol using the Triple Collector mass spectrometer using a suite of three deep-sea spherules proved to be of considerable use. The sample results themselves facilitated a better insight into the carbon inventory of the spherules, and confirmed the presence of a high temperature (>600°C) component which had been observed in a previous analogous study by Wright *et al.*, (1988). At the same time they served to to illustrate that carbon contamination, especially that associated with the analysis protocol (the 'blank'), essentially controlled the results. It was also evident that the Triple Collector mass spectrometer and gas extraction system were operating at the limits of their capabilities, so that the precision of the determination of yield and isotope measurements were poor. This was particularily problematical considering that if the controlling influence of the blank was to be corrected for, then its carbon yield and $\delta^{13}C$ composition would need to be accurately known. The analysis protocol itself was successful in allowing samples to be split into two portions for isotopic/petrographic work, but not in determining sample masses. Subsequent experimentation was executed on the protocol using the Triple Collector and involved the implementation of a thinner grade of Pt foil and a solvent treatment step. These refinements enabled the mass of the micrometeorites to be adequately measured and also resulted in an apparent *ca.*75% reduction in the bulk carbon blank.

With the advent of the ultra-sensitive MS86 mass spectrometer, a detailed examination of the blank associated with the analysis protocol was undertaken. The increased precision in both isotopic and absolute yield measurement available, allowed both the blank input from the gas extraction system alone (the 'system blank') to be evaluated, and also those obtained from the different protocols originally implemented on the Triple Collector to be differentiated from each other. The most important conclusion from the MS86 results was that the total carbon blank was extremely

variable in $\delta^{13}C$ composition and absolute carbon abundance, was not solely controlled by the analysis protocol used, but equally by random contamination events largely beyond the control of each protocol. Table 4.2 presents an attempt to summarise the MS86 blank experiments and shows a list of blank components that were isolated from each protocol. On examination of this table the following must be stressed;

(1) The components within the protocols are cumulative, *i.e.* all experiments could show effects of the system blank components and all experiments where Pt foil was used could exhibit components recognised from protocol E *etc.*

(2) Notwithstanding (1), each component was not neccessarily restricted to a particular protocol; each individual experiment contained a unique mixture to compose its observed final composition.

Protocol	Temperature* (°C)	Isotopic signature $\delta^{13}C$ (‰)	Maximum yield (ng)
H	All$	*ca.*-21 to -28	*ca.*0.3
H	200	-15.8±1.2	ND@ (<0.3)
H	400	-34.0±1.3	ND (<0.3)
G	500	-44.4±0.4^	7.0±0.13
E	All	*ca.*-22 to -26	*ca.*0.7
E	300	*ca.*-27 to -25	1.5±0.1
E	400	*ca.*-24 to -27	3.6±0.1
C/D&	200	*ca.*-25 to -27	<32
C/D	200	-34.2±1.1	2.0±0.1
C/D	300	-28.9±0.9	5.5±0.1
C/D	400	-24.3±0.4	3.9±0.1
C/D	600	-19.9±1.2	ND (<1.0)
C/D	600	-42.0±0.9	1.4±0.1
E	200	*ca.*-20 to -28	22.7±0.1
E	1200	-10.2±1.1	ND (<1.2)
All	1200	*ca.*-30	<60

* = Peak combustion temperature.

$ = Dependent upon time duration, and not combustion temperature, of each step.

@ = Value *not determined* (ND)because the yield was indistinguishable from the system blank, but at least as great as the value quoted in the brackets.

^ = Value as determined in experiment number MS86a (4.4.7).

& = This component is characteristic of contaminated dichloromethane.

Table 4.2. Summary of the carbon blank components isolated as a result of the MS86 blank experiments.

The variability of the stepped combustion experiment carbon blank on a day-to-day basis underlined a further conclusion; if blank corrections were to be applied, the results thereof must be considered as speculative only. A series of experiments were devised to attempt to trace the origins of these components to materials or procedures employed within the routine operation of the protocols. Whilst exonerating the glass, aluminium foil and muffle furnace insulating tiles, the results revealed the gas extraction line loading section valves to be responsible for a previously isolated component, thereby indicating a possible area where improvements could be made.

On a more specific basis, the MS86 results prompted a re-evaluation of the conclusions from the Triple Collector experiments where an apparent reduction in blank levels had accompanied the implementation of thinner Pt foil and a solvent cleaning step. The MS86 results showed the lowest blank levels were obtained for the protocols where no solvent was used, and additionally it was discovered that with a better understanding of the time-related blank input associated with each temperature step, that the thickness of the foil used had little effect on the total levels of blank. In actual fact, it was considered that the improvement in blank associated with the 'dry foil' protocols was probably a result of the changes made to the methods used to clean the sample handling materials/instruments. It was also considered equally likely that the relatively higher blank level experiments performed on the Triple Collector were not representative, and if they had been replicated then lower blank examples would have been obtained. Even though the MS86 dry foil protocols suffered on average less carbon contamination than their solvent cleaned equivalents, the use of a liquid was still beneficial to the successful operation of the analysis protocol. Dichloromethane and distilled water were both found to be unsuitable either in terms of volatility or yield/isotopic interferences, but methanol appeared to offer a viable solution. Methanol treated blanks were found to display reproducable carbon release patterns, where the majority of the carbon combusted <200°C and so would hopefully not interfere with any sample components. The variation in the $\delta^{13}C$ pattern was also predominately flat, but the high temperature steps showed a slight ^{13}C-enrichment in their measured $\delta^{13}C$ values. To overcome the possible problems of this latter characteristic obscuring or being mistaken for the similar hypothetical deep-sea spherule SiC component, it was proposed to to analyse samples using both

dichloromethane, which did not exhibit the deleterious effect, and methanol, where a better insight into the low-temperature carbon could be obtained.

Although the absolute carbon blank reduction was not deducible, the changes in the design of the MS86 gas extraction system appeared to have precipitated a reduction in the system blank. Even though it was anticipated that a concomittant effect would accompany further miniaturisation of the system, it was evident that for any considerable improvements a totally new approach would be required. The experiments also revealed that a considerable proportion of the blank was being supplied by the platinum foil sample packets, experimentation having shown them to produce a purely time related input in excess of twice that of the system blank. Of specific interest here was that Pt foil that had been pulse heated *ca.*1500°C before loading did not display this excess, thereby suggesting that a change in the protocol used to pre-clean the Pt foil would be beneficial to the blank levels, especially in the >600°C regime where the system/Pt foil time related input is often the only contamination.

It is difficult to generalise about the absolute levels of blank performance achieved, but it was apparent that bulk blank carbon yields of less than one nanomole could be obtained for the sample analysis protocols. In particular, in the protocols where no solvent was used, the controlling factor on the bulk MS86 carbon yield was the combined Pt foil/system blank input of *ca.*1ng step^{-1}. With this in mind it is evident that if the blank levels are to be pushed substantially below this level, then a completely different approach would be need to be implemented to both the sample manipulation/loading methods and also to the gas extraction system, and some tentative ideas for such changes are presented in chapter 8.

Chapter 5

Carbon Stable Isotopic Analyses of Multiple Aliquots of Deep-Sea and Individual Greenland and Antarctic Micrometeorites.

5.1. Introduction.

In an attempt to identify individual carbonaceous components and determine the stable carbon isotopic nature of carbon within the micrometeorites the following experiments were scheduled:

(1) To consolidate the initial carbon isotopic results obtained in the analysis of three individual deep-sea micrometeorites (4.2), two multiple-particle experiments were planned, because it was anticipated that the higher carbon yields would enable the Triple Collector mass spectrometer to determine the isotopic nature of the carbon to a higher degree of accuracy.

(2) After the successful development and testing of the ultra-high sensitivity MS86 mass spectrometer (chapter 2), and modification of the analysis protocols (chapter 4), an extensive study of the carbon within individual Greenland and Antarctic micrometeorites was to be carried out utilising MS86 and the new protocols.

5.2 Analyses of multiple-sample deep-sea micrometeorites.

Three deep-sea spherules analysed as individual samples on the Triple Collector primarily to evaluate the working of the sample analysis protocol (see 4.2), seemed to confirm the existence of an indigenous ^{13}C-rich sample component previously isolated by Wright *et al.*, (1988). However, a similar component was also observed in experiments devised to locate potential sources of contamination from within materials used in the sample analysis protocol (see 4.4.7), so raising the possibility that the ^{13}C-

rich material had an alternative, non-indigenous provenance. Since the carbon yield across the temperature range where the ^{13}C-rich component was released (600-1200°C), was of a similar magnitude to the experiment blank, it was additionally considered possible that the apparent ^{13}C-rich signals could be an artifact associated with the mass spectrometer detection system. In an attempt to elucidate the true nature of the ^{13}C-rich component, and to gain a better insight into the overall carbon inventory of the deep-sea samples, two multiple-particle experiments were executed on the Triple Collector. For these experiments to be practical only one sample packet could be used, and this requirement in turn dictated that the samples were analysed as whole-particles. It was not possible to crush *ca.*20 samples onto a single platinum foil substrate (2.1.2.) and then remove a fragment of each for petrographic work, but it was important to determine what proportion of micrometeorite mineralogic types were included in each experiment. To overcome this problem, the samples were allocated to either type S or I groups based solely upon their optical characteristics by using criteria as defined by Brownlee, (1985). Thus by employing hand-picking, 20 spherules of type S and 17 of type I were grouped together and analysed on the Triple Collector using sample analysis protocol D (4.3.1.). After completion of the analysis, the Pt packets were retrieved from the combustion section and the spherules extracted. These were then analysed for their major element chemistry in the usual way (see chapter 3) to ascertain their actual petrographic type as a check of the efficacy of the optical segregation.

The petrographic examination of the retrieved spherules revealed that;

(i) Type S experiment - Out of 20 spheres analysed, 11 were type S and 9 of type I composition.

(ii) Type I experiment - Out of 17 spheres analysed, 16 were of type I and only 1 of type S composition.

These results illustrate that it was easier to optically identify type I than type S samples; despite the S group containing almost even numbers of type I and S samples this experiment is referred to as the type S experiment.

The individual stepwise results for the type S and I multiple particle experiments are presented within figure 5.1, along with a contemporaneous blank experiment (T664) that was executed on a Pt foil packet equivalent in size (*ca.*1cm by 1cm) to that used

for the samples. The Pt sample packets used were of a larger size than those utilised during the single particle experiments to accomodate the greater sample volume.

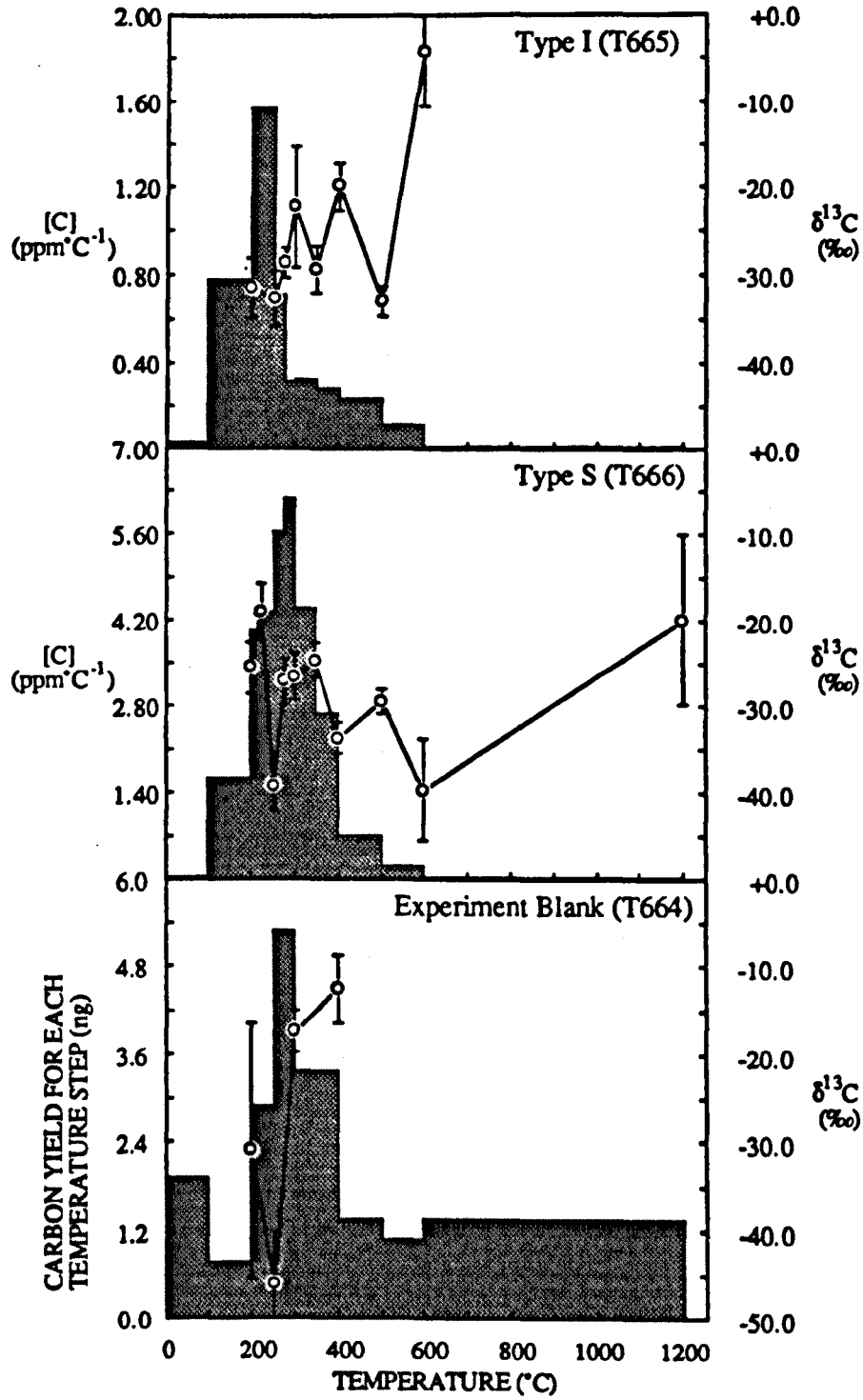

Figure 5.1. Individual stepped combustion plots for the two multiple-particle deep-sea sample experiments with the corresponding experiment blank.

With regard to substantiating whether the postulated meteoritic SiC component was indigenous to the type S samples, the 600-1200°C temperature step for the type S experiment yielded *ca.*0.7ng of carbon with a $\delta^{13}C$ value of -20.0±9.9‰. It is difficult to interpret whether this >600°C release confirms or precludes the existence of SiC within the samples, because although with the reduced dilution effect of the blank carbon to the 11 type S micrometeorite samples one would expect to obtain a heavier $\delta^{13}C$ value, it cannot be assumed that all the samples contained SiC.

The blank experiment (T664) yielded 20.1±5.1ng of carbon with a bulk $\delta^{13}C$ value of -28.4±5.4‰, whereas the type S and I experiments yielded 138.0±7.0ng carbon with a $\delta^{13}C$ value of -28.1±1.7‰ and 86.5±7.0ng carbon with a $\delta^{13}C$ value of -29.5±2.3‰ respectively. After correcting for the blank input of 20.1±5.1ng of carbon to the experiment yields, and taking into account the total sample mass of 0.124mg for the type S experiment and 0.343mg for type I, bulk carbon concentrations of 0.098±0.005 weight % (wt%) and 0.020±0.002wt% for types S and I were calculated. Likewise the bulk $\delta^{13}C$ values were blank corrected using the following formula;

$$\delta^{13}C_c = \frac{(Y_m \times \delta^{13}C_m)}{(Y_m - Y_b)} - \frac{(Y_b \times \delta^{13}C_b)}{(Y_m - Y_b)}$$

Where;

$\delta^{13}C_c$ = Corrected isotopic value.
$\delta^{13}C_m$= Measured isotopic value.
$\delta^{13}C_b$ = Measured isotopic value of the blank.
Y_m = Measured yield.
Y_b = Measured blank yield.

After applying this correction to the results of the multiple sample experiments, and having considered the errors on the bulk $\delta^{13}C$ measurements, the following corrected $\delta^{13}C$ signatures of -26.9±2.3‰ for type S and -30.0±3.9‰ for I were obtained. Examination of the blank corrected carbon concentrations and $\delta^{13}C$ values for the type S and I micrometeorites revealed that although it was impossible to differentiate between the different petrologic types in terms of their bulk carbon isotopic composition, the type S samples contained a factor of *ca.*5 higher concentration of carbon compared to the type I. Of greater importance was that the bulk $\delta^{13}C$ values of

both the type S and I experiments were indistinguishable from the bulk $\delta^{13}C$ of the experiment blank, so suggesting they shared the same provenance. Before attempting to interpret the results of the micrometeorite experiments it was therefore necessary to examine the individual stepped combustion plots to determine if the carbon obtained did indeed simply represent excess experiment blank.

Initial examination of figure 5.1 reveals that for both the type S and I experiments the carbon release occurs almost exclusively between 100 and 400°C, which is in agreement with the experiment blank stepwise. However, on closer examination of the combustion profiles it is evident that differences exist between the three experiments that suggest that the carbon obtained below 600°C in the type S and I experiments was indeed indigenous to the micrometeorites.

The low temperature (<600°C) release for the type I experiment was dominated by carbon that combusted between 100 and 250°C, where *ca.*65% of the total was released with a $\delta^{13}C$ value of *ca.*-32±3‰. In contrast, the major release of the blank experiment was seen between 250 and 400°C, and although the $\delta^{13}C$ release pattern was variable, the peak of the combustion (between 200-300°C) gave a $\delta^{13}C$ value of -17.5±2.4‰. Notwithstanding the observation that other protocol D blank experiments showed a component isotopically similar to the type I 100-250°C component (chapter 4), its maximum yield within the blank experiments was always less than *ca.*2ng in total, whereas the yield obtained in the type I experiment was an order of magnitude greater. This large difference in size suggests it unlikely that the 100-250°C type I component could have been provided solely by the blank. If the 100-250°C release was not supplied by the experiment blank, then it probably represented either sample carbon present as terrestrial organic contamination accrued in the deep-sea sediment, or an indigenous extra-terrestrial component. The remaider of the low-temperature release of the type I experiment showed no evidence of any further indigenous components, with the yield pattern and isotopic values between *ca.*-20 to -30‰ indicating that the carbon released was constituted of a mixture of experiment blank components and the tail of the 100-250°C component. Just one step from 500-600°C yielded an anomalous $\delta^{13}C$ value of -4.5±6.1‰, but taking into account the irregular pattern of isotope measurement seen in the immediately preceding steps and the small yield (*ca.*3ng), the measurement can probably be interpreted as an instrumental effect.

It has already been noted that with respect to bulk carbon concentrations the type S samples contained *ca.*5 times more carbon than the type I samples, but a comparison of their stepped combustion profiles in figure 5.1 reveals that this excess type S carbon was present in a different form than that seen in the type I stepwise. The peak of carbon combustion in the type S experiment was between 200-400°C, and if the $\delta^{13}C$ values for the 200 and 250°C temperature steps are assumed to be erroneous, then the average $\delta^{13}C$ value of the 200-400°C carbon is *ca.*-25‰. In contrast, the peak of combustion in the type I experiment was 100-250°C with $\delta^{13}C$ value of *ca.*-32‰. Although the 200-400°C type S release shares the same combustion temperature as the peak of the blank experiment <600°C release, and the departure in $\delta^{13}C$ at 250°C to -39.9±2.6‰ in the type S experiment was mirrored in the blank stepwise, it was considered that the total of 127ng carbon obtained between 200-400°C in the type S stepwise could not have been supplied by the experiment blank alone. Assuming that any oceanic carbon contamination would manifest itself as identical material in both the type I and S samples, it was initially proposed that the <600°C carbon could be explained by one of the following scenarios:

(1) The 100-250°C component in the type I experiment represents oceanic contamination. The <600°C release obtained for the type S experiment represents a combination of the 100-250°C oceanic contamination component and terrestrial sample handling contamination accrued whilst the samples were being curated and selected for the experiments. The lower concentration of this second component in the type I results can be explained by the relative porosities (and thence surface area) of the type I and S samples; the higher degree of porosity of the type S samples has led to increased handling contamination.

(2) The <600°C releases of both the type I and S experiments represent indigenous extra-terrestrial carbon that has survived from the micrometeorite pre-cursor material.

Of these two options the latter is preferred because; (i) notwithstanding the increased handling contamination potential inherent as a result of the relative porosities, invoking such a large excess of handling contamination to the type S samples is a tenuous argument because the essentially non-porous type I samples would still suffer contamination on their outside surfaces. (ii) Basaltic glasses dredged from the ocean floor show evidence of carbon contamination at *ca.*-18‰ (Mattey *et al.*, 1984; Exley *et al.*, 1986) which does not agree with the *ca.*-32‰ carbon seen in

the type I sample between 100-250°C, or the 200-400°C component in the type S samples with a $\delta^{13}C$ of *ca.*-25‰. It was therefore considered that the <600°C carbon obtained from both the type S and I experiments probably represented indigenous extra-terrestrial carbon and could, after being corrected for the experiment blank, be used to elucidate the provenance of the micrometeorites.

5.2.1. The origin of the type I deep-sea micrometeorites.

In view of the largely successful separation of an aliquot of type I micrometeorites, the blank-corrected bulk carbon concentration and $\delta^{13}C$ value of 0.020±0.002 wt% and -30.0±3.9‰ obtained from the type I experiment represented a good approximation of the true nature of the average type I spherule carbon inventory, and so could be utilised further to facilitate interpretation of their origin.

Iron meteorites exhibit bulk carbon concentrations between 0.002 and 0.185wt% (Moore *et al.*, 1969) and bulk $\delta^{13}C$ values between -30.3 to -4.0‰ (Deines and Wickman, 1973). The bulk carbon signature for the type I micrometeorites are within this wide range. Iron meteorites are not solely composed of iron-nickel metal, but contain many other minor mineral phases, the most common of which are shown in table 5.1.

Mineral	Composition
Graphite	C
Cohenite	$(Fe,Ni)_3C$
Haxonite	$(Fe,Ni)_{23}C_6$
Schreibersite	$(Fe,Ni)_3P$
Carlsbergite	CrN
Roaldite	$(Fe,Ni)_4N$
Troilite	FeS
Sphalerite	ZnS
Daubreelite	$FeCr_2S_3$
Chromite	$FeCr_2O_3$
Chloropatite	$Ca_5(PO_4)_3Cl$
Whitlockite	$Ca_3(PO_4)_2$
Olivine	$(Mg,Fe)_2SiO_4$
Orthopyroxene	$(Mg,Fe)SiO_3$
Clinopyroxene	$(Mg,Fe,Ca)SiO_3$
Plagioclase	$NaAlSi_3O_8$ - $CaAl_2Si_2O_8$

Table 5.1. The most common non-metallic minerals found in iron meteorites. (After Buchwald, 1977 and Nielsen and Buchwald, 1981)

Examination of table 5.1 shows the carbon within non-metallic minerals in iron meteorites is present either as graphite or the two carbides, cohenite and haxonite. Graphite is commonly present as nodules, although in common with the carbides, it may also be present as crystals dispersed throughout the metal (*e.g.* Craig, 1953). However, carbon also occurs dissolved in solid-solution within the Fe-Ni metal, and also as graphite and carbides within silicate nodules (the silicates are listed in table 5.1). With respect to the bulk $\delta^{13}C$ signatures of the iron meteorites, analyses of individual carbon-bearing minerals show variable $\delta^{13}C$ values, with the range of $\delta^{13}C$ of minerals from individual meteorites often spanning 50% of the total bulk $\delta^{13}C$ signatures observed from the iron meteorites as a whole (Deines and Wickman, 1973). Table 5.2 shows the $\delta^{13}C$ of different iron meteorite minerals.

Mineral	$\delta^{13}C$ range (‰)	Key
Fe-Ni metal*	-19.7 to -22.1	1
Cohenite	-18.1 to -19.2	1
	-17.4 to -20.6	2
Graphite	-5.0 to -6.4	1
	-5.6 to -8.2	3
Silicate	-3.9 to -8.8	3

* = Carbon within the metallic phase is largely present as dissolved carbon in solid-solution and finely dispersed carbides.

(1) Deines and Wickman, (1975).

(2) Hoefs, (1973).

(3) Deines and Wickman, (1973).

Table 5.2. The measured range in $\delta^{13}C$ of some iron meteorite carbon-bearing minerals.

If it is assumed that the type I micrometeorites are produced by either atmospheric ablation of iron meteorites, or by collision and fragmentation of iron meteorite parent bodies within the asteroid belt, it is important to consider which of the carbon-bearing minerals within the iron meteorites are most likely to become incorporated into the micrometeorites, because these minerals would control their isotopic composition. The greatest volume (*ca.*>85%, *e.g.* Dodd, 1981) of most iron meteorites is composed

of metallic Fe-Ni, so it is logical to assume that if a genetic connection exists between the two, that the bulk type I micrometeorite $\delta^{13}C$ signature would most likely mirror the $\delta^{13}C$ value of the metallic (carbide) phase. Of equal importance is the observation that if the micrometeorites have been melted or strongly heated as a result of asteroidal collision or atmospheric heating, then any graphite present will be preferentially lost due to its volatile nature. Table 5.2. shows that the bulk type I micrometeorite signature of -30.0±3.9‰ does not agree with the $\delta^{13}C$ values of either the Fe-Ni metal or the (cohenite) carbide. It is also apparent from table 5.2. that no correlation can be made between the type I micrometeorites and either the iron meteorite graphite or silicate inclusions.

The major carbon release from the type I stepped combustion experiment, which therefore controls the bulk $\delta^{13}C$ value, occurs between 100 and 250°C. Carbon from Fe-Ni metal or the combustion of carbides is released >600°C. It is therefore apparent that the 100-250°C release is probably not related to an iron meteorite carbonaceous component, and so either has a terrestrial provenance or has been supplied from an alternative extraterrestrial source. Unfortunately, no carbon was released above blank levels in the >600°C regime and so the generic connection to iron meteorite components cannot be further addressed. Although it was previously argued that the 500-600°C $\delta^{13}C$ value of -4.5±6.1‰ was probably an instrumental effect, it is interesting to note that this $\delta^{13}C$ value, and combustion temperature, is in agreement with iron meteorite graphite. However, graphite is the most volatile of the carbon-bearing iron meteorite minerals, and so it could be argued that if the graphite has survived, then evidence of carbon from the other more refractory minerals should be seen. This argument cannot be used to rule out the iron meteorite graphite generic connection because the relative abundance of graphite with regard to the other components is highly variable, and so it is possible that lower concentrations of Fe-Ni metal carbon and carbides have not been detected in the stepped combustion experiment.

An alternative meteoritic origin for the type I samples is that they represent metallic iron that forms a minor component of the stony meteorites, and upon atmospheric entry melting of the stony meteorite-like type S micrometeorite pre-cursor material, the metal and silicate melts have separated (figure 1.5.). Unfortunately, the carbon

isotopic composition of iron metal within the stony meteorites has not been determined and so this hypothesis cannot be further addressed.

In summary:

(1) The 100-250°C carbon release cannot be reconciled with an iron meteorite provenance and so it either represents terrestrial contamination or extraterrestrial carbon of an undetermined origin.

(2) The low yields of carbon in the 600-1200°C regime, where iron meteorite carbon components should combust, do not allow $\delta^{13}C$ measurement and so the iron meteorite provenance cannot be addressed further. There is some evidence for the combustion of iron meteorite graphite, but large $\delta^{13}C$ errors and an irregular $\delta^{13}C$ profile erode the confidence of this measurement.

5.2.2. The origin of the type S deep-sea micrometeorites.

Since the collection of micrometeorites thought to be type S in composition actually contained a mixture of petrologic types, the values obtained for bulk carbon concentration and $\delta^{13}C$ of 0.098±0.005wt% and -26.9±2.3‰ from the multiple-sample experiment cannot be considered as representative of the true nature of the type S micrometeorite carbon inventory. To address this problem an attempt was made to correct for the input of type I sample material to the experiment. The measured total mass of spherules analysed within the type S experiment was 0.124mg, but assuming that half of the sample volume was actually constituted of type I material (as indicated by the subsequent petrographic work), and considering the relative densities are *ca.*3gcm^{-3} for type S and *ca.*6gcm^{-3} for I (see section 4.3.1), then of this total, probably only *ca.*0.04mg was of type S material, with the remaining *ca.*0.08mg being type I in composition. From the multiple-sample type I experiment it is known that the carbon concentration within type I material is *ca.*0.02wt%, so the 0.08mg of type I material within the type S experiment would yield *ca.*16ng of the total yield of *ca.*138ng obtained. After also subtracting the experiment blank input of a further *ca.*20ng from the total, the remainder (*ca.*102ng) must have been provided by the type S component, and by using the previously estimated type S material mass of 0.04mg, this translated into a new type S carbon concentration of *ca.*0.22wt%, *i.e.* a factor of two higher than that estimated previously. Because the $\delta^{13}C$ values initially measured

for type S and I multiple-particle experiments were essentially the same, correcting the measured data from the type S experiment would not effect the measured $\delta^{13}C$ value. In summary, after allowing for the type I input to the results of the type S multiple-sample experiment, the bulk carbon signature of the type S material was estimated to *ca.*0.22wt% carbon with a $\delta^{13}C$ value of -26.9±2.3‰.

Table 5.3 has been constructed to determine whether the type S multiple-sample bulk carbon signature is in agreement with equivalent signatures of the major stony meteorite groups. Comparison of the bulk type S signature and the range of bulk carbon concentrations and $\delta^{13}C$ values in table 5.1 reveals that only the H, L and LL ordinary chondrites and enstatite chondrites share a similar signature. Figure 1.4 shows that the ordinary chondrites dominate the contemporary meteorite falls, and so if it is proposed that the type S micrometeorites represent material that has been ablated from macrometeorites during atmospheric entry, then they would share the same bulk $\delta^{13}C$ values. The enstatite chondrites constitute only *ca.*2% of meteorite falls and with their parent bodies forming <5% of the asteroid belt (figure 1.4), it was considered the generic connection to the ordinary chondrites was more feasible.

Carbonaceous chondrites			
Sub-group	[C] (wt %)	$\delta^{13}C$ (‰)	Reference
CI	2.70 to 4.46	-6.6 to -15.6	1, 2, 3
CM	0.94 to 5.21	+9.8 to -22.0	1, 2, 3, 4
CR	1.42 to 2.38	-9.1 to -13.3	1
CV	0.27 to 1.10	-12.8 to -23.7	1, 3
CO	0.12 to 0.64	-8.0 to -19.3	1, 3
Ordinary Chondrites			
H	0.03 to 1.77	-11.1 to -30.2	1, 5, 6
L	0.02 to 0.95	-11.0 to -28.4	1, 5, 6
LL	0.02 to 0.58	-15.1 to -26.7	1, 5
Enstatite Chondrites			
EH/EL	0.15 to 0.70	-4.1 to -28.5	7
Achondrites			
Ureilites	0.22 to 6.16	-0.7 to -13.2	1, 8
HED/SNC*	*ca.*0.01 to 0.1	*ca.*-12 to -28	4

* = HED = Howardite, Eucrite and Diogenite association.
SNC = Shergotty, Nakhla and Chassignite association.

(1) Grady, (1982).
(2) Smith and Kaplan, (1970).
(3) Kerridge, (1985).
(4) Grady *et al.*, (1991).
(5) Otting and Zahringer, (1967)
(6) Belsky and Kaplan, (1970).
(7) Grady *et al.*, (1986).
(8) Grady *et al.*, (1982a).

Table 5.3. Bulk carbon concentrations and $\delta^{13}C$ signatures for the major stony meteorite groups.

Figure 5.2 shows a comparison of the bulk carbon concentrations and $\delta^{13}C$ signatures of the H, L and LL-group ordinary chondrites with the type S micrometeorite signature. The data used to construct both figures 5.2 and 5.3 is composed of non-Antarctic samples only, because the formation of carbonate weathering products on Antarctic samples translates into potentially misleading bulk carbon concentrations and $\delta^{13}C$ signatures (*e.g.* Grady *et al.*, 1991).

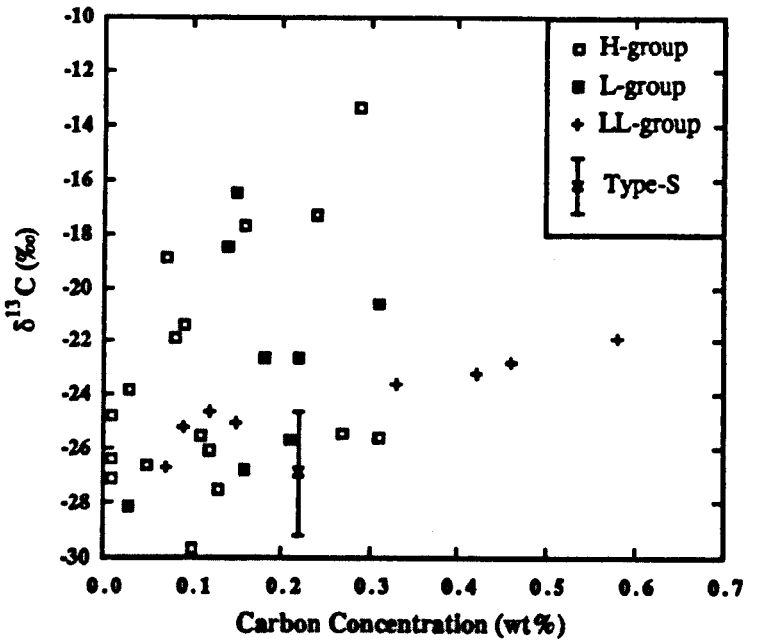

Figure 5.2. A comparison of bulk $\delta^{13}C$ and carbon concentration signatures of the H, L, and LL group ordinary chondrites with the equivalent value calculated for the type S deep-sea micrometeorites. Note that the result for the Sharps H-group ordinary chondrite (1.77 wt% carbon and -24.17‰) has been ommitted. The data has been taken from Grady, (1982) and does not include Antarctic samples which give misleading carbon values due to Antarctic weathering effects. (Errors for the meteorite data and the carbon concentration of the micrometeorites are smaller than the symbols).

It is apparent from figure 5.2 that although the type S micrometeorite bulk carbon concentration and $\delta^{13}C$ value compares favourably with the ordinary chondrites as a whole, there is no evidence for a generic connection to any specific chemical group. In figure 5.3 the same ordinary chondrite data is plotted in relation to the petrologic grade of each meteorite (1.6.2.2.). Figure 5.3 shows that as the ordinary chondrite petrologic grade decreases from 5 through to 3, there is a concomittant increase in bulk carbon concentration and $\delta^{13}C$ value. Note that due to a paucity of isotopic determinations that no data for ordinary chondrites of grade 6 has been included in figure 5.3, but they typically possess carbon concentrations <0.01wt% (*e.g.* Otting and Zahringer, 1967). The position of the type S micrometeorite bulk value on figure 5.3 suggests that although the $\delta^{13}C$ value shows a closer correlation to the higher petrologic grades, the carbon concentration is more in agreement with the type 3 ordinary chondrites.

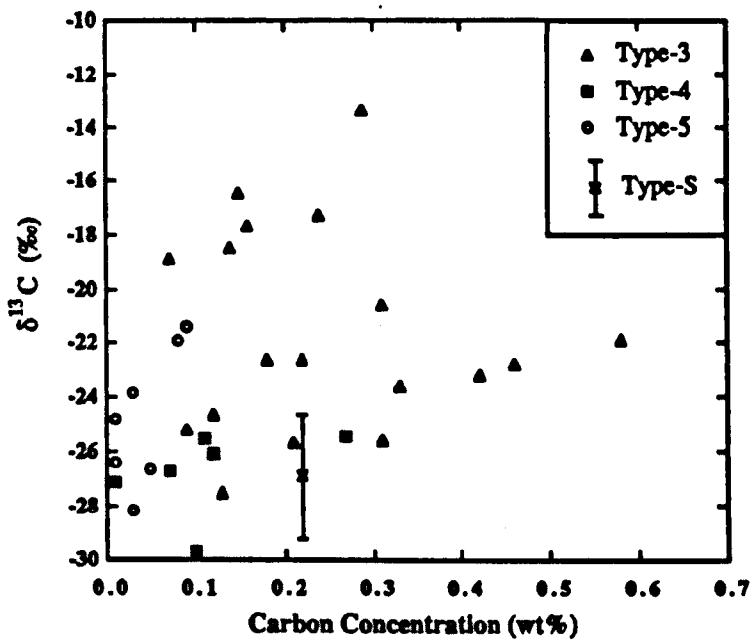

Figure 5.3. A comparison of bulk $\delta^{13}C$ and carbon concentration signatures of the ordinary chondrites with the equivalent value calculated for the type S deep-sea micrometeorites. In this figure the ordinary chondrite data has been divided according to the petrologic type of each meteorite. Note that the result for the Sharps type 3 ordinary chondrite (1.77 wt% carbon and -24.17‰) has been ommitted. The data has been taken from Grady, (1982) and does not include Antarctic samples which give misleading carbon values due to Antarctic weathering effects. (Errors for the meteorite data and the carbon concentration of the micrometeorites are smaller than the symbols).

Figure 1.4 shows that the ordinary chondrites constitute *ca.*80% of contemporary meteorite falls, but more specifically, the data compiled in table 5.4. reveals that of this 80% there is a strong bias to ordinary chondrites of the higher petrologic types.

Group	Total	Petrologic types (% of total)*			
		3	4	5	6
L	319	2.5	6.6	16.6	66.8
LL	66	15.2	10.6	22.7	48.5
H	276	2.9	18.1	42.3	27.2

* = Totals do not sum to 100% because petrologically unclassified samples have been ommitted.

Table 5.4. A breakdown of the ordinary chondrite falls into petrologic types. The data (taken from Graham *et al.*, 1985) has been split into L, LL and H chemical groups and the % of falls of petrologic types 3 to 6 within each group has been calculated.

From the data in table 5.4 it is apparent that if the type S micrometeorites represent quenched melt droplets from ablating ordinary chondrite parent bodies during atmospheric entry, then they should mirror the bulk carbon concentration and $\delta^{13}C$ values of the higher petrologic types. The results of the small-sample meteorite whole-rock stepped combustion experiments (6.2) show that the measured $\delta^{13}C$ values of the micrometeorites are probably more representative of their parent body composition than their measured carbon concentrations. The $\delta^{13}C$ of the type S micrometeorites in figure 5.3. shows a closer correlation to the higher ordinary chondrite petrologic types, and coupled with the uncertainty in the estimated type S carbon concentration due to the mixture of sample types in the type S multiple-sample experiment, it is believed that the generic connection to the higher petrologic types suggested by the $\delta^{13}C$ value is more feasible.

The stepped combustion plot of the type S multiple-sample micrometeorite experiment was dominated by carbon that combusted between 200 and 400°C with a $\delta^{13}C$ of *ca.*-25‰. Similar components have been isolated from the ordinary chondrites but have been interpreted as terrestrial contamination (*e.g.* Grady *et al.*, 1989). From this observation it is apparent that the generic connection to the ordinary

chondrites maybe largely based upon the similar amounts of terrestrial contamination they have suffered.

5.2.3. Conclusions from the multiple deep-sea spherule experiments.

The bulk concentration of carbon within the type I deep-sea micrometeorites was found to be 0.020±0.002wt% with a $\delta^{13}C$ value of -30.0±3.9‰. After allowing for the mixture of particle types analysed within the type S multiple-sample experiment, the concentration of carbon within the type S deep-sea micrometeorites was estimated to be *ca.*0.22wt% with a $\delta^{13}C$ value of -26.9±2.3‰. The bulk type I carbon signature could be reconciled with an iron meteorite provenance, whereas the type S was in agreement with the ordinary and enstatite chondrites.

A closer examination of the stepped combustion data from the type I experiment and comparison to carbon-bearing components within the iron meteorites showed the generic connection between the two to be tenuous. Notwithstanding that the type I stepped combustion isotopic profile showed some evidence for an iron meteorite graphite component, the results of the experiment did not allow the provenance of the type I micrometeorites to be accurately constrained. The stepped combustion profile for the type S micrometeorites was difficult to interpret due to the mixture of petrologic types analysed. On the evidence of similarities between the type S <400°C carbon and material from stepped combustion experiments of ordinary chondrites, it was only possible to conclude that both had suffered similar levels of terrestrial contamination. There was no evidence to substantiate the presence of meteoritic SiC within the type S samples which had been previously inferred from the single-sample deep-sea micrometeorites (4.2.).

5.3. Analysis of individual micrometeorites from Greenland and Antarctic samples using MS86.

A suite of 9 Greenland cryoconite and 5 Antarctic micrometeorites were analysed as individual particles using MS86 and analysis protocols E and F (4.4).

5.3.1. Evaluation of micrometeorite sources using bulk $\delta^{13}C$ signatures.

The individual stepped combustion profiles are examined in detail later in this chapter, but in the first instance, and for comparison purposes to the bulk deep-sea micrometeorite and major meteorite group $\delta^{13}C$ signatures, their bulk $\delta^{13}C$ values and carbon concentrations have been calculated from the stepped combustion data, blank corrected, and presented within table 5.5 and figure 5.4. All 14 samples were found to be type S in composition (table 3.2).

Greenland cryoconite samples			
Sample	Weight (μg)$	Yield (wt %)	$\delta^{13}C$ (‰)
SS89M18	52	0.115±0.007	-20.8±0.6
SS89M14	31	0.046±0.007	-16.2±2.4
SS89M01	6	1.516±0.508	-25.4±0.5
SS89M12	21	0.151±0.019	-26.8±1.0
SS89M17	31	0.183±0.014	-21.5±0.6
SS89M09	34	0.078±0.007	-23.6±0.8
SS89M10	32	0.086±0.008	-25.0±0.8
Antarctic samples			
MA1	23	0.081±0.011	-23.7±1.3
MA3	84	0.027±0.002	-23.6±1.1
MA4	28	0.050±0.007	-25.4±2.0
MA5	57	0.135±0.006	-31.3±0.6
Algal contaminated samples*			
SS89M05	13	0.500±0.085	-22.7±0.5
SS89M16	66	0.254±0.009	-21.7±0.4
MA2@	60	0.139±0.006	-22.4±0.4

* = Based upon evidence of high sulphur or phosphorus contents (3.4.5.).
$ = ±3μg (see appendix A3).
@ = This Antarctic sample was contaminated during laboratory manipulation (plate 3.8).

Table 5.5. A summary of blank-corrected bulk carbon concentration and $\delta^{13}C$ compositions of individual Greenland and Antarctic micrometeorites analysed using the MS86 mass spectrometer.

From the results in table 5.5 it could be seen that the following ranges in carbon concentration and isotopic composition were encountered;

(i) Greenland Cryoconite samples.
0.046±0.007 to 1.516±0.508 wt%.
-26.8±1.0 to -16.2±2.4‰.

(ii) Antarctic samples.
0.050±0.007 to 0.135±0.006 wt%.
-31.3±0.6 to -23.7±1.3‰.

(iii) Algal contaminated samples.
0.139±0.006 to 0.500±0.085 wt%.
-22.7±0.5 to -21.7±0.4‰.

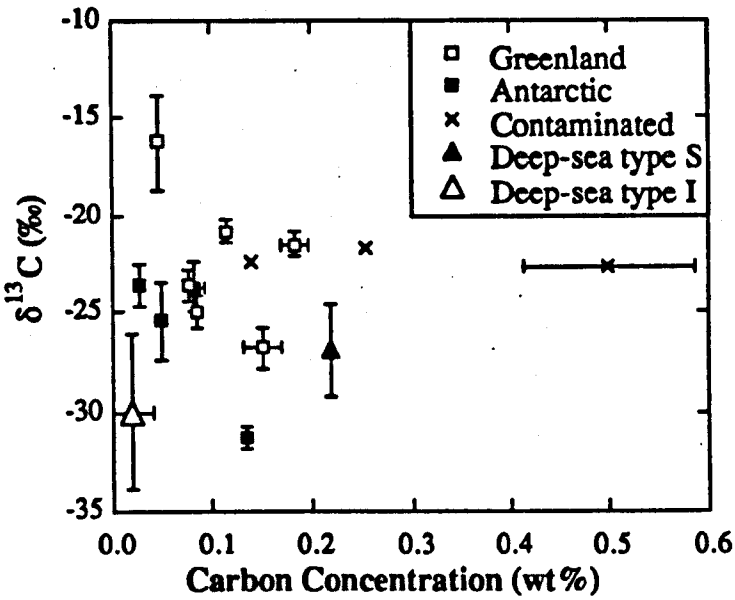

Figure 5.4. Bulk blank-corrected $\delta^{13}C$ and carbon concentrations for Greenland and Antarctic micrometeorites analysed as individual samples on MS86. Greenland sample SS89M01 has been ommitted but plots at 1.516±0.508 wt% carbon and -25.4±0.5‰. The bulk carbon values derived from the multiple-sample deep-sea micrometeorite experiments are also included.

Figure 5.4 shows that, aside from Greenland sample SS89M01 and two samples that were believed to have been contaminated by algae, the samples all exhibit lower carbon concentrations than the estimated type S deep-sea micrometeorite signature. Only one Antarctic sample shows a ^{13}C depleted $\delta^{13}C$ value with respect to the type S deep-sea micrometeorites, the remainder showing a trend to higher $\delta^{13}C$ values. The

two algally contaminated Greenland samples, despite showing an increased carbon yield, possess similar $\delta^{13}C$ values to the remaining samples. The Antarctic contaminated sample MA2 yields both a carbon concentration and $\delta^{13}C$ value similar to the non-contaminated samples, so suggesting that the portion of the sample analysed after a fragment had been removed for petrographic work was probably not contaminated.

A cursory comparison of the ranges of $\delta^{13}C$ and carbon concentration deduced from table 5.5 with the meteorite carbon signatures in table 5.3 shows that, in addition to the previous generic connection to the ordinary and enstatite chondrites inferred from the results of the multiple-sample type S experiment, similar connections can be made to the CM, CV and CO carbonaceous chondrites and the achondrites. The achondrites can be largely discounted as a major source of the micrometeorites on arguments of their observed falls and parent body abundance (1.1.2.). Although the carbonaceous chondrites only constitute *ca.*4% of meteorite falls, their parent bodies compose *ca.*60% of the asteroid belt (1.4.2.), and so potentially are a major source of the micrometeorites through collisional debris. Figure 5.5 shows a comparison of the bulk blank-corrected carbon concentrations and $\delta^{13}C$ values of the Greenland and Antarctic micrometeorites with the ordinary chondrites.

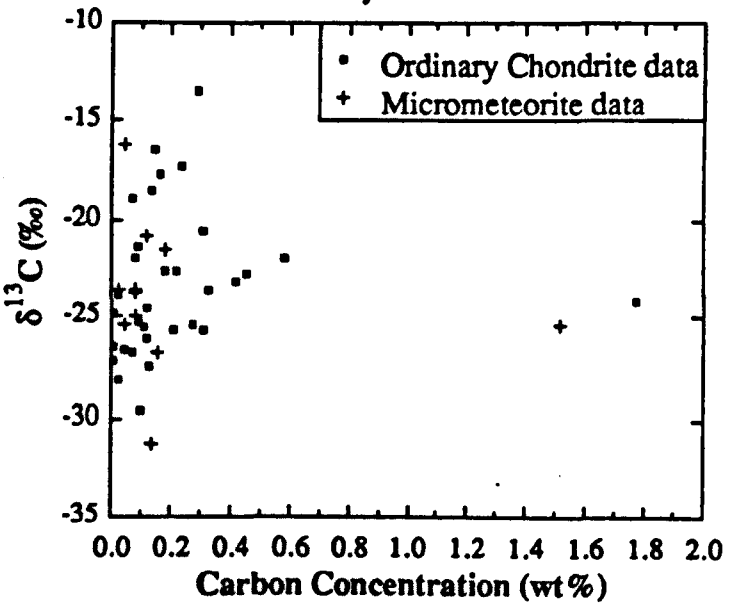

Figure 5.5. A comparison of the bulk blank-corrected carbon concentration and $\delta^{13}C$ values of the Greenland and Antarctic micrometeorites with the ordinary chondrites (data taken from Grady, 1982). For clarity the data has not been divided into either chemical or petrologic groups, and error bars have been ommitted.

Examination of figure 5.5 reveals a good correlation between the micrometeorites and the ordinary chondrites, even suggesting that Greenland sample SS89M01, which exhibited an apparently anomalous carbon yield of *ca.*1.5wt%, can be matched with the Sharps H3 ordinary chondrite. Figure 5.6 has been constructed using the same data as within figure 5.5, but with an enhanced yield scale to enable a closer inspection of the correlation suggested by figure 5.5. To further investigate the hypothesis suggested when interpreting the type S deep-sea micrometeorite results (5.2.2) that the micrometeorites could be connected to a specific ordinary chondrite petrologic grade, the meteorite data in figure 5.6 has been divided into petrologic grades 3 to 5.

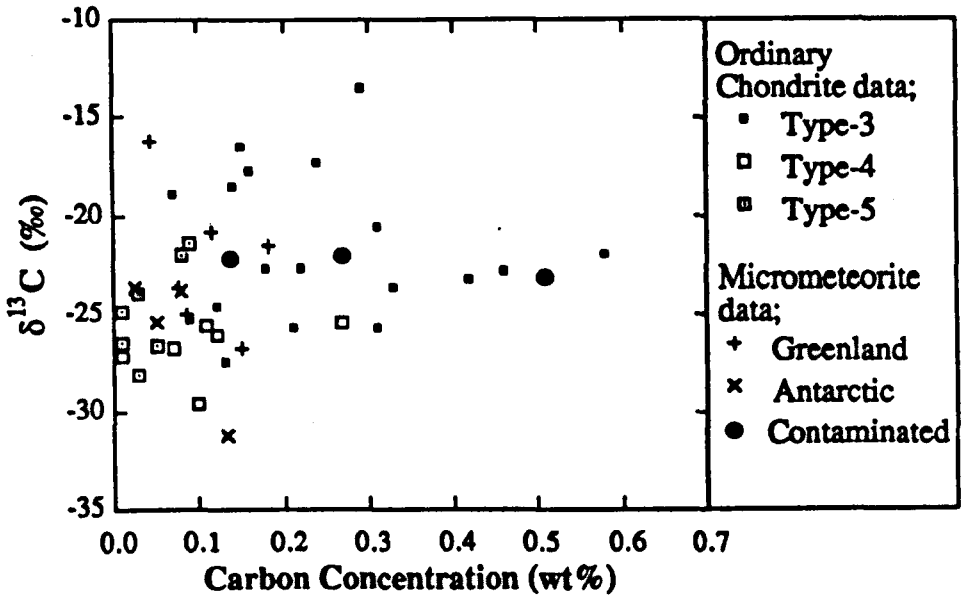

Figure 5.6. A comparison of the bulk blank-corrected carbon concentrations and $\delta^{13}C$ values of the Greenland and Antarctic micrometeorites with the ordinary chondrites (data taken from Grady, 1982). The ordinary chondrite data has been divided according to respective petrologic types. (Error bars have been ommitted for clarity).

Figure 5.6 shows that the micrometeorite data can be correlated with ordinary chondrite petrologic types 3, 4 and 5, but with an apparent bias to the lower types. If the micrometeorites are derived directly from ablation of the ordinary chondrites during atmospheric entry, then the opposite should be observed, *i.e.* a bias to the higher petrologic types that are seen to dominate ordinary chondrite falls (table 5.4).

The parent bodies of the ordinary chondrites are believed to make up a proportion of the Apollo asteroids (*e.g.* McFadden *et al.*, 1989). This population of asteroids

have orbits that take them outside the asteroid belt and cross that of the Earth. Interpretation of ordinary chondrite petrologic types with respect to their parent bodies has been a subject of much debate. Of the more plausible models, Wood (1967) and Dodd (1969) suggested that the petrologic grade was related to metamorphism within the parent bodies after their initial accretion from the solar nebula. The corresponding increase of temperature with depth led to a concomittant increase of petrologic type with depth. Larimer and Anders (1967) and Hutchison *et al.*, (1980) related petrologic type to the temperature of the gas from which the ordinary chondritic material accreted, with the earlier material, that formed the core of the bodies, possessing a lower concentration of volatiles than the later material that would form the surface. These latter models also produce parent bodies with increasing petrologic type with depth. The observed bias of micrometeorites to lower petrologic types could be explained by the following model;

(1) The ordinary chondritic meteorites, which are dominated by material of higher petrologic grade, are largely derived from (completely) disrupted Earth-crossing asteroids. The collisional break-up of an asteroidal body would produce a wide range of debris size (*e.g.* Piotrowski, 1953) and so would act as a source for both the micrometeorites and meteorites. Although this model can excavate material of higher petrologic grade, it does not fully explain why such material preferentially survives over the lower petrologic grade material.

(2) The micrometeorites represent material ejected from the surfaces of the Earth-crossing asteroids by smaller impacts. Surface material would presumably be petrologic type 3 in composition, and the smaller impacts would eject a higher proportion of micrometeoriite-sized grains than the impact in (1).

A final observation from figure 5.6 is that the samples that had been postulated have suffered algal contamination also yield bulk carbon signatures that can be reconciled with an ordinary chondrite provenance. Figures 5.7 and 5.8 investigate the similarities between the carbonaceous chondrites and the Greenland and Antarctic micrometeorites.

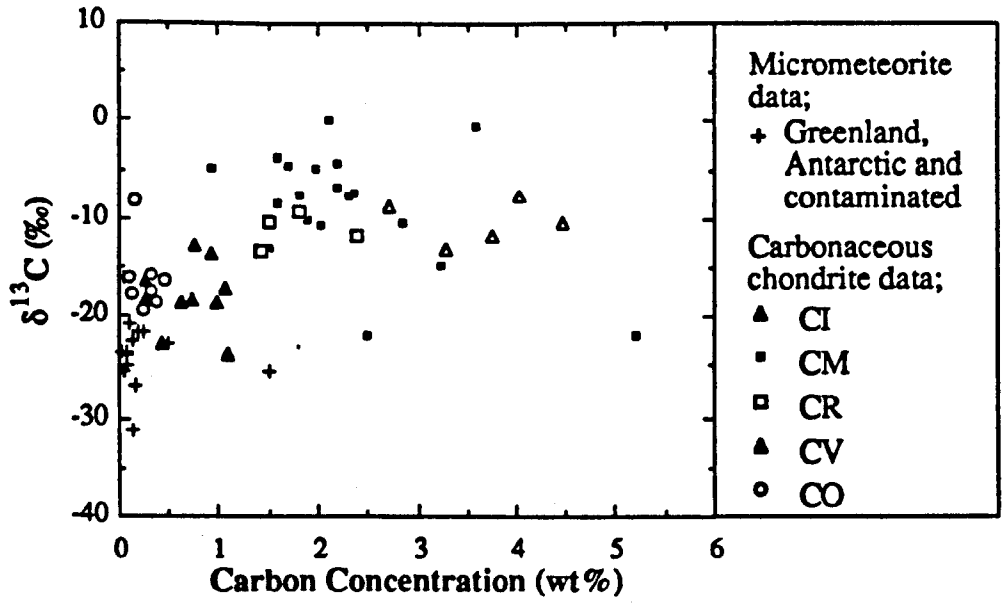

Figure 5.7. A comparison of the bulk blank-corrected Greenland and Antarctic micrometeorite $\delta^{13}C$ and carbon concentration data with the major carbonaceous chondrite groups (data taken from Grady, 1982 and Kerridge, 1985). Error bars for the micrometeorite data have been ommitted for clarity.

Within figure 5.7 the Greenland and Antarctic micrometeorites are compared to the major carbonaceous chondrite groups. In contrast to the correlation observed with the ordinary chondrites in figures 5.5 to 5.6, it is apparent that only a tenuous generic connection can be made between the micrometeorites and the CV and CO carbonaceous chondrites. Figure 5.8 has been constructed to compare only those CV and CO chondrites that exhibit <0.7wt% carbon with the micrometeorite data after it has been divided into Greenland, Antractic and contaminated samples, and furnished with error bars. Examination of figure 5.8 confirms the initial conclusion from figure 5.7 in that none of the uncontaminated samples can be directly connected with a carbonaceous chondrite bulk carbon signature. With the additional observation from 6.2 that the bulk $\delta^{13}C$ value is a more reliable tool than carbon concentration in determining meteoritic parent material, the correlation becomes worse.

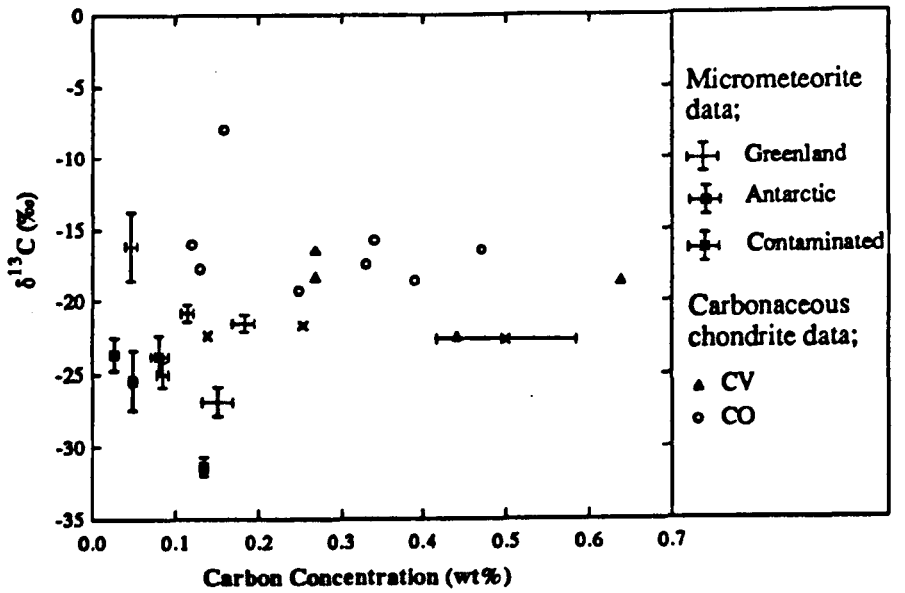

Figure 5.8. A comparison of the bulk blank-corrected carbon concentrations and $\delta^{13}C$ of the Greenland and Anarctic micrometeorites with the CV and CO carbonaceous chondrites that exhibit <0.7wt% carbon (data taken from Grady, 1982 and Kerridge, 1985). Greenland sample SS89M01 is not included but plots at 1.516±0.508wt% carbon and -25.4±0.5‰.

5.3.2. Stepped combustion profiles, the experiment blank and algal contamination.

In order to investigate further the generic relationships of the Greenland cryoconite, Antarctic and contaminated micrometeorites, figures 5.9 to 5.11 have been constructed. Each figure contains the bulk (blank-corrected) sample $\delta^{13}C$ and carbon concentration for one of the three groups, but also for interpretation purposes, the bulk $\delta^{13}C$ of the relevant blank experiment, and for the Greenland samples, a bulk $\delta^{13}C$ value for the cryoconite algae that had been obtained from two stepped combustions that were executed on a separated sample of cryoconite algae. The results for Greenland cryoconite spherules are presented in figure 5.9 and have been separated into two groups. These groups reflect to which blank experiment they correspond to.

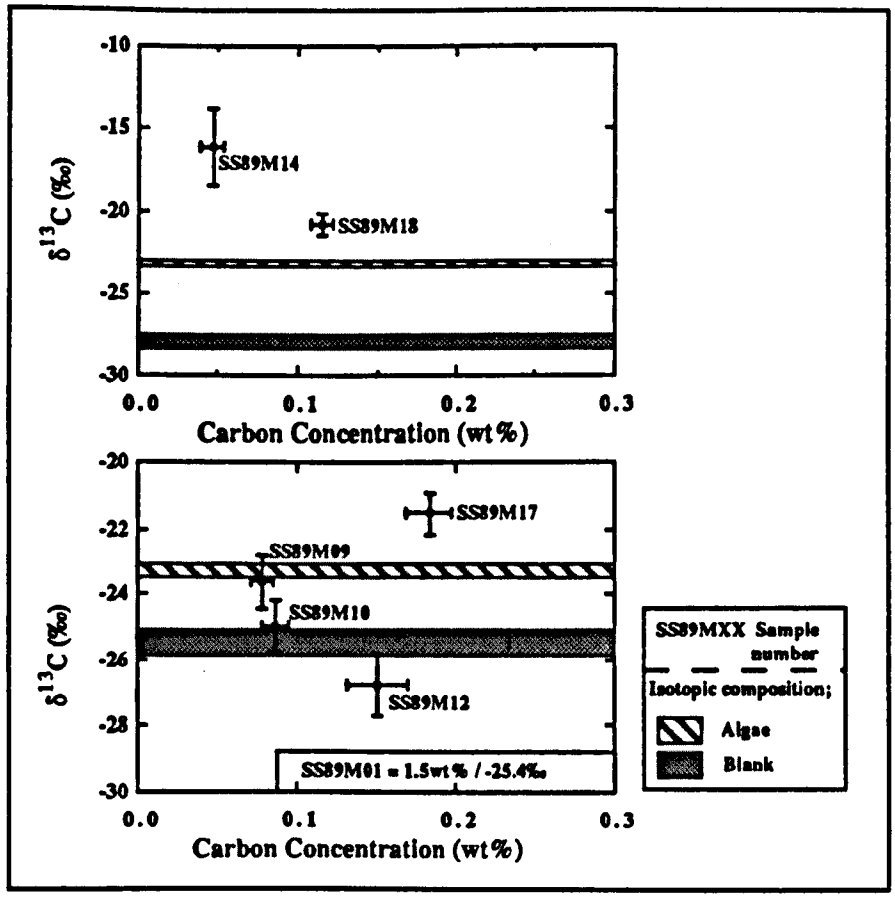

Figure 5.9. Blank-corrected bulk carbon concentrations and $\delta^{13}C$ values for the Greenland cryoconite micrometeorites.

Figure 5.9 shows that 4 of the 7 samples were distinct from the blank in terms of $\delta^{13}C$; all showing a relative ^{13}C enrichment. If this increase in the $\delta^{13}C$ value was a product of algal contamination, then some correspondance with the $\delta^{13}C$ of the algae would be expected. The algae were found to exhibit a ^{13}C enrichment over the blank, with bulk $\delta^{13}C$ (blank-corrected) of -23.3±0.2‰. However, from figure 5.9 it can be seen that 3 of the samples possessed higher $\delta^{13}C$ values than that of the algae which mitigates against this source as contamination. Caution needs to be expressed since the results in figure 5.9 had been blank corrected; it is already known that due to the variability in both the absolute level and isotopic composition of the blank that such corrections provide semi-quantitative results only. This effect can possibly be used to explain the observation that within figure 5.9 samples SS89M14 and SS89M18 plot at higher values than the other samples, this perhaps being the product of over blank correction , *i.e.* by using a $\delta^{13}C$ of *ca.*-28‰ as opposed to *ca.*-25‰. Adopting this philosophy for samples SS89M09, SS89M10 and SS89M17 and by applying a -28‰

blank moves the samples towards higher $\delta^{13}C$. There are two other noteworthy observations from figure 5.9: firstly, the sample that yielded an anomalously high carbon concentration of *ca.*1.5 wt% (SS89M01) also possessed a $\delta^{13}C$ value the same as the blank, indicating that the excess carbon was probably simply supplied by relatively higher levels of blank. Secondly, one analysis (SS89M12) gave a result that indicated a slight degree of ^{12}C enrichment relative to the blank, indicating the presence of yet a further carbonaceous component.

The results for Antarctic samples are given in figure 5.10, and have also been split in accordance to their most relevant blank. Figure 5.10 shows that 2 out of the 4 samples showed a ^{13}C enrichment over the blank, and of the remaining 2, one yielded a ^{12}C enriched value (MA5), whilst the other (MA4) was indistinguishable from the blank. The Antarctic samples had been collected by direct melting of ice and so theoretically had not been exposed to algae, and so the prescence of the two samples which showed similar $\delta^{13}C$ values to the Greenland samples was evidence that the ^{13}C enriched component was indeed indigenous, and it was apparently only a coincidence that the algae shared a similar signature.

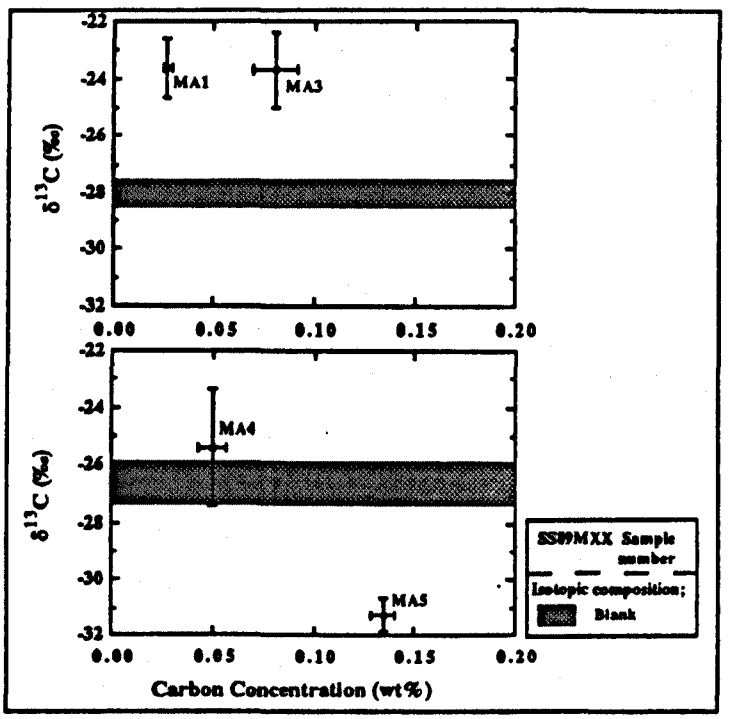

Figure 5.10. Blank-corrected bulk carbon concentrations and $\delta^{13}C$ values for the Antarctic micrometeorites.

Figure 5.11 shows the results for the three samples that were believed to be contaminated by algae, based upon the detection of sulphur (S) or phosphorus (P) during analysis of fragments of each sample for major element chemistry. As already noted from table 5.5 and figures 5.4 to 5.8, they did not possess enhanced carbon concentrations, but showed similar values to both the Greeenland and Antarctic samples. Based on this evidence it would appear that if these three samples did represent specimens that had suffered algal contamination, then the other Greenland and Antarctic samples has suffered a similar fate. However, it was interesting to note that there also appeared to be a slight ^{13}C enrichment in relation to the algae, and although again the effect of the blank correction was suspected, this observation provided potential evidence for the component being indigenous.

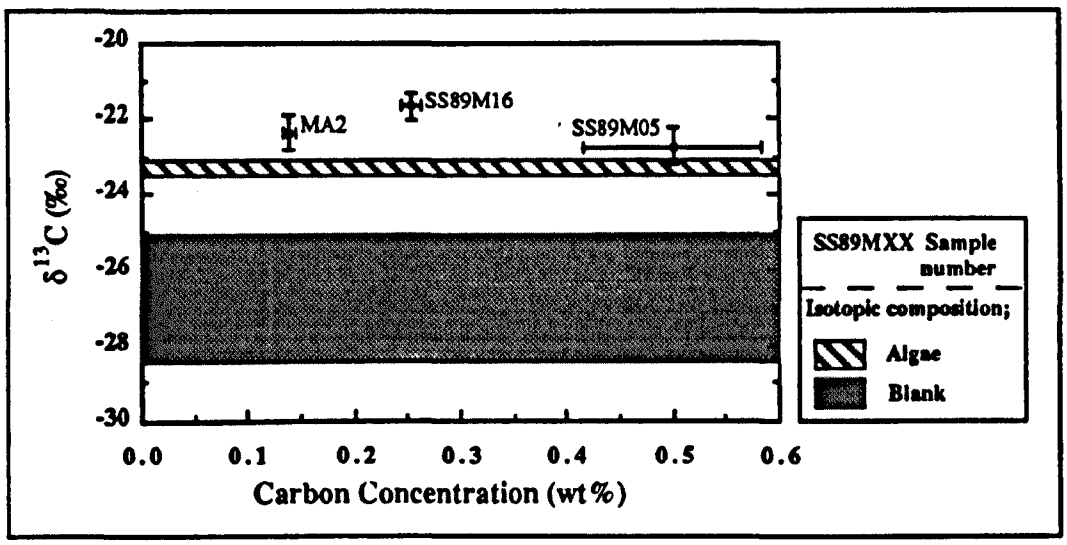

Figure 5.11. Blank corrected bulk carbon concentrations and $\delta^{13}C$ values for the micrometeorites samples that had suffered from algal contamination.

Individual stepped combustion plots for Greenland Cryoconite samples are shown in figure 5.12. Examination of the plots reveals a similarity between all the extractions both in carbon release patterns and isotopic profiles. In particular it is evident that the release in each case is dominated by carbon that combusts between *ca.*200 and 500°C. The $\delta^{13}C$ values for this material approach *ca.*-20‰, and plot in a similar trend for all samples suggesting that the carbon is responsible for the elevation of the bulk $\delta^{13}C$ over the blanks values. The high temperature releases are also equally similar for each experiment, and in every instance close to the blank in both yield and $\delta^{13}C$ and showing no evidence for any ^{13}C enriched component. The exceptions to this overall

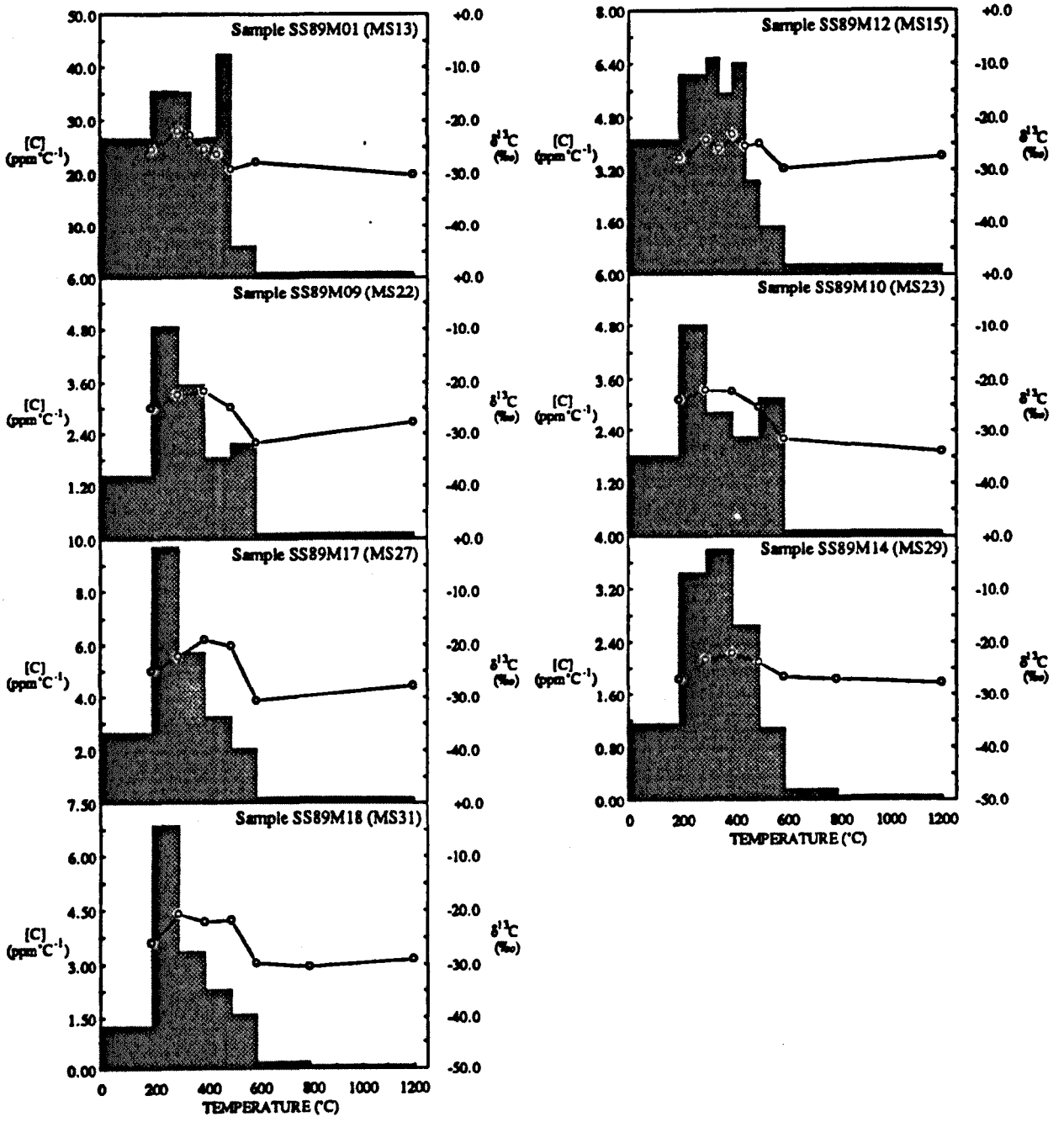

Figure 5.12. Stepped combustion plots for the Greenland cryoconite micrometeorites. This data has not been blank corrected.

pattern were samples SS89M01, SS89M09 and SS89M10, where a second low-temperature component was apparent, burning at 500-600°C with a $\delta^{13}C$ of *ca.*-30‰. It should be noted that all three samples had been treated with dichloromethane and this was known to produce an interference effect at 600°C (sample SS89M17 in figure 5.12 illustrates this), but the component could also have been related to the gas extraction line loading section contamination component previously isolated from the blank experimentation (see 4.4.2).

Having already noted the similarity between the bulk $\delta^{13}C$ value of the cryoconite algae and the Greenland and Antarctic samples, two stepwise plots for the experiments carried out on algae separated from unprocessed cryoconite are presented in figure 5.13. It should be noted that these algae samples were treated in an identical way to the spherules themselves, *i.e.* they were solvent-treated during the analysis protocol. It is obvious that the stepped combustion profiles were again extremely similar between the algae and the cryoconite micrometeorites, the combustion profile of the algae being likewise dominated by a component combusting between 200 and 500°C with peak $\delta^{13}C$ values of *ca.*-21 to -23‰.

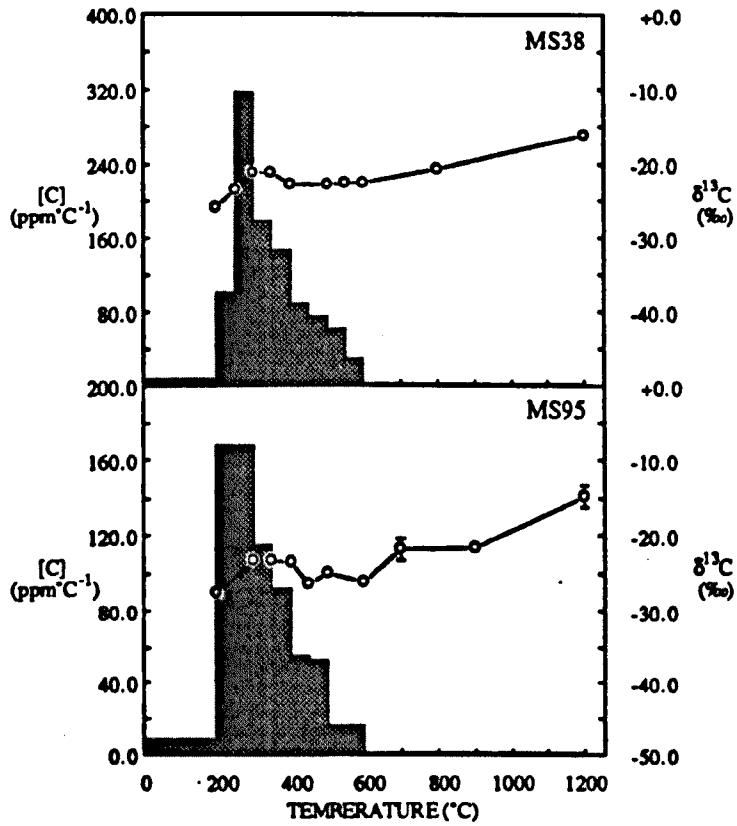

Figure 5.13. Stepped combustion plots of aliquots of cryoconite algae.

Table 5.6 has been constructed to more closely compare the algal and sample 200-500°C carbon in terms of the isotopically heaviest $\delta^{13}C$ values achieved with the corresponding combustion temperature observed during the stepped combustion. Based on these results there appeared to be little difference between the components in as much as they shared the same peak temperatures of combustion and only sample (SS89M17) yielded a $\delta^{13}C$ value that was marginally distinct from the algal components, being *ca.*2‰ heavier. The data within table 5.6 have been composed without taking into consideration any blank contribution so the next stage was to subtract the blank so that a more representative comparison of the true nature of the sample component could be made. When such an allowance is accounted for, the comparison yielded a different conclusion.

Cryoconite algae		
Run number	$\delta^{13}C$ (‰)	Combustion temperature (°C)
MS38	-21.2±0.5	350
MS95	-23.4±0.4	300
Sample	Greenland cryoconite samples	
SS89M01	-22.2±0.5	300
SS89M12	-23.4±1.0	400
SS89M10	-22.2±0.5	300
SS89M09	-21.8±0.6	400
SS89M17	-19.2±0.5	400
SS89M14	-22.3±0.5	400
SS89M18	-20.9±0.5	300

Table 5.6. A comparison of the 200-500°C component of the cryoconite algae and micrometeorites extracted from the cryoconite. The results are presented in terms of the heaviest $\delta^{13}C$ value obtained across the release with the corresponding combustion temperature.

Figure 5.14 shows the same results as within table 5.6, but after suitable blank corrections have been applied to all the data, including the algae. It can be seen that the majority of the samples are distinct in $\delta^{13}C$ from the algae and the experiment blanks, with 5 out the 7 samples showing a ^{13}C enriched component, characterised by a corrected $\delta^{13}C$ value between *ca.*-21 and -18‰ at concentrations of *ca.*0.05 to

0.15wt%. In the two remaining samples, SS89M12 had a $\delta^{13}C$ the same as the blank, and SS89M01 possessed an anomalously high concentration (*ca.*0.7wt%) of carbon, which was similar isotopically to the blank-corrected algal component. Although not providing conclusive evidence, the results of these blank corrections appeared to indicate that the ^{13}C-rich component was probably not due to algae. With specific regard to algal contamination, it is believed that the ultra-high carbon yield shown by sample SS89M01 in figure 5.14 represents a more diagnostic test that such contamination had occurred, *i.e.* an approximate sevenfold increase in carbon concentration relative to the other samples, and a corresponding $\delta^{13}C$ value indistinguishable from the equivalent algae component.

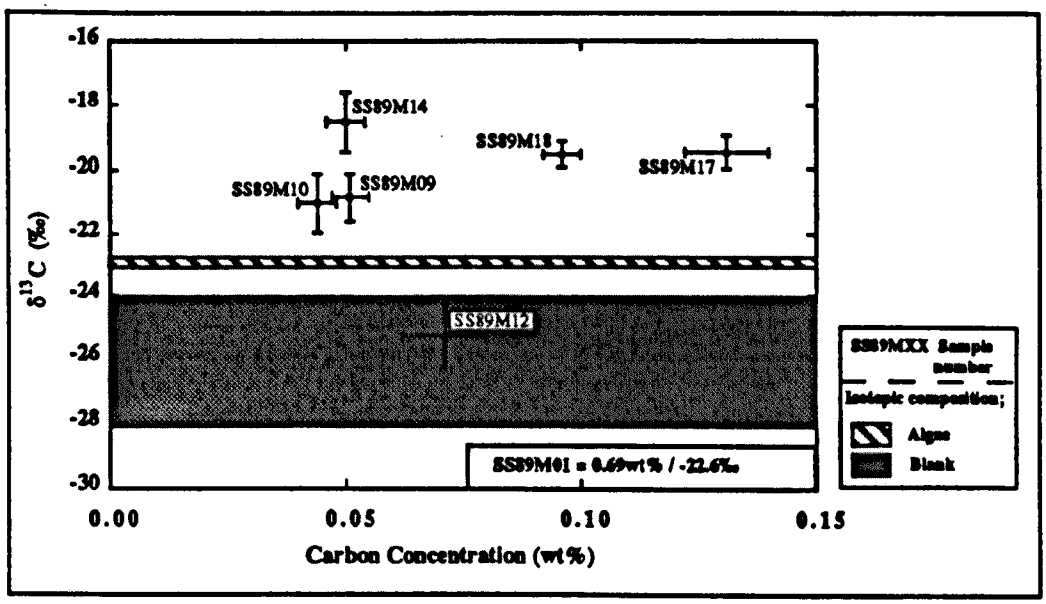

Figure 5.14. Bulk carbon concentration and $\delta^{13}C$ of the blank corrected 200-500°C component within the Greenland cryoconite micrometeorites.

Comparing individual stepped combustion plots (figure 5.15) and blank-corrected 200-500°C bulk data (figure 5.16) from the three samples that were believed to have suffered algal contamination with the Greenland samples (figures 5.12 and 5.14), it can be seen that the results are remarkably similar. None of the three contaminated samples exhibited high carbon concentrations similar to SS89M01. This observation suggested that the high S/P criterium used as an indicator that contamination had occurred was not reliable, but this question will be returned to in 5.3.3.

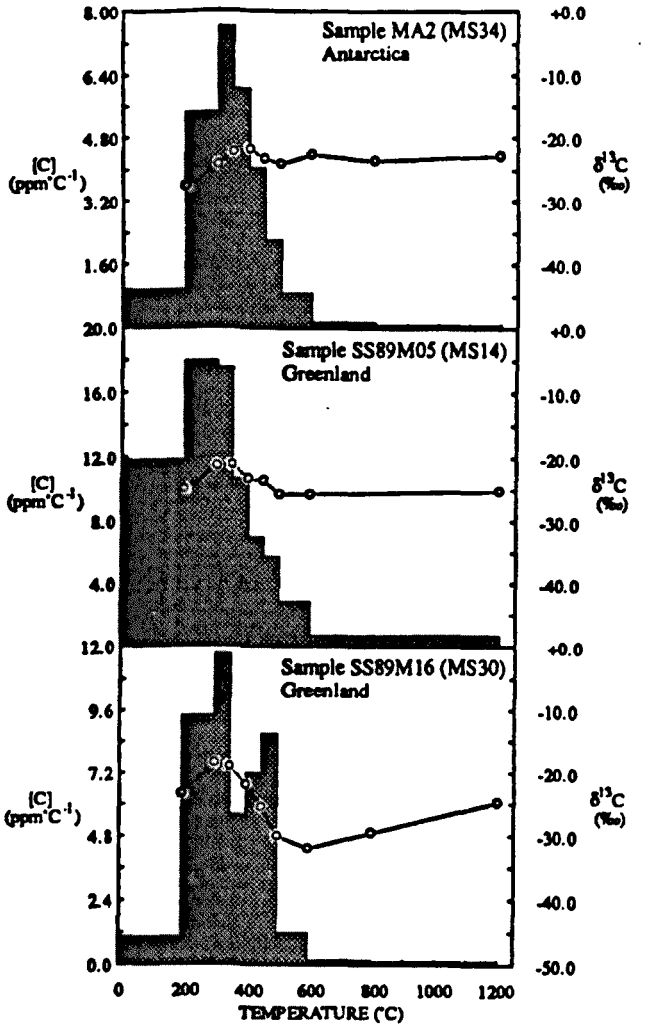

Figure 5.15. Stepped combustion plots for the three micrometeorites contaminated by cryoconite algae.

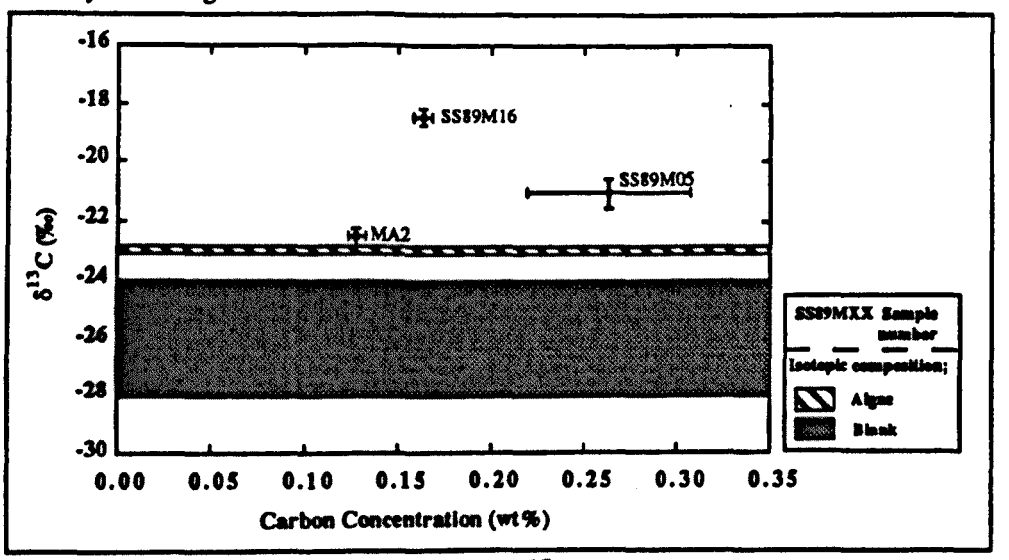

Figure 5.16. Bulk carbon concentration and $\delta^{13}C$ of the blank corrected 200-500°C component within the algally contaminated micrometeorites.

The final evidence for the indigenous nature of the component was provided by a similar examination of the individual stepped combustion plots and blank-corrected 200-500°C components within the Antarctic samples. The blank-corrected bulk carbon results (figure 5.10) had already indicated the ^{13}C enriched carbon was indigenous, and it was anticipated that a similar conclusion would be precipitated on closer scrutiny of their blank-corrected 200-500°C components (figure 5.18) and individual stepped combustion plots (figure 5.17).

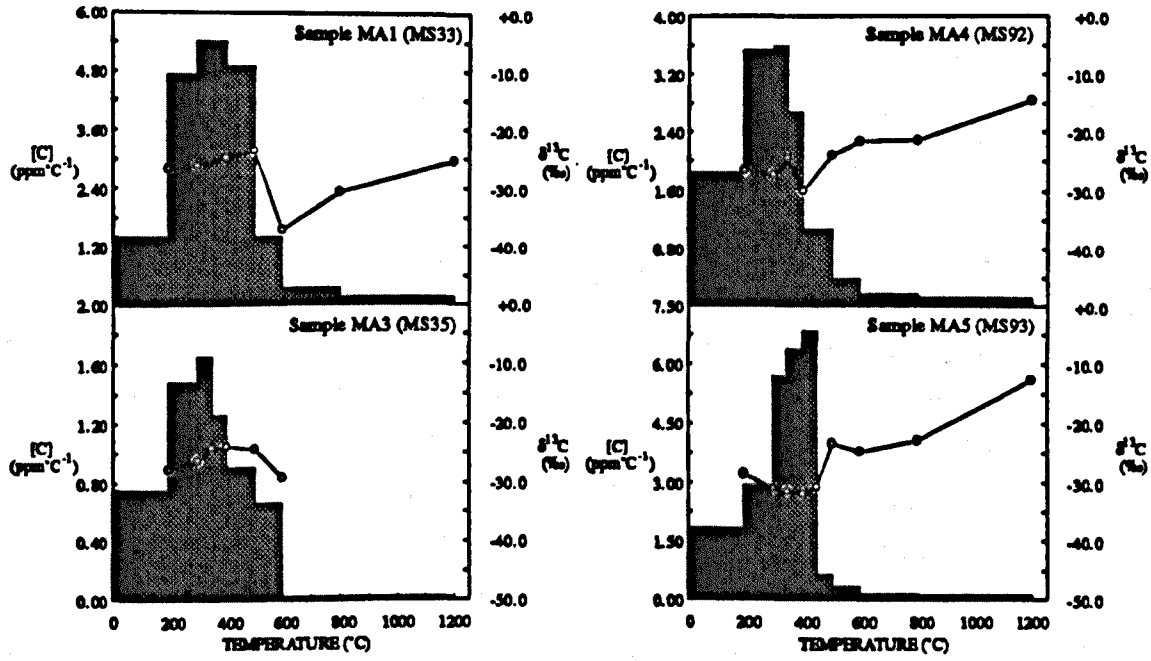

Figure 5.17. Stepped combustion plots for the Antarctic micrometeorites.

Examination of the individual stepped combustion plots presented in figure 5.17, shows the Antarctic samples to exhibit slightly different isotopic release profiles to the Greenland samples. Notwithstanding this, in all 4 samples the carbon yield release was still dominated by carbon combusting between 200-500°C, and when this had been isolated and blank-corrected (figure 5.18), it was apparent that the ^{13}C-enriched component was present in 3 of the samples at concentrations of *ca.*0.02 to 0.10 wt%, but with slightly less ^{13}C enriched signatures of between *ca.*-25 to -22‰.

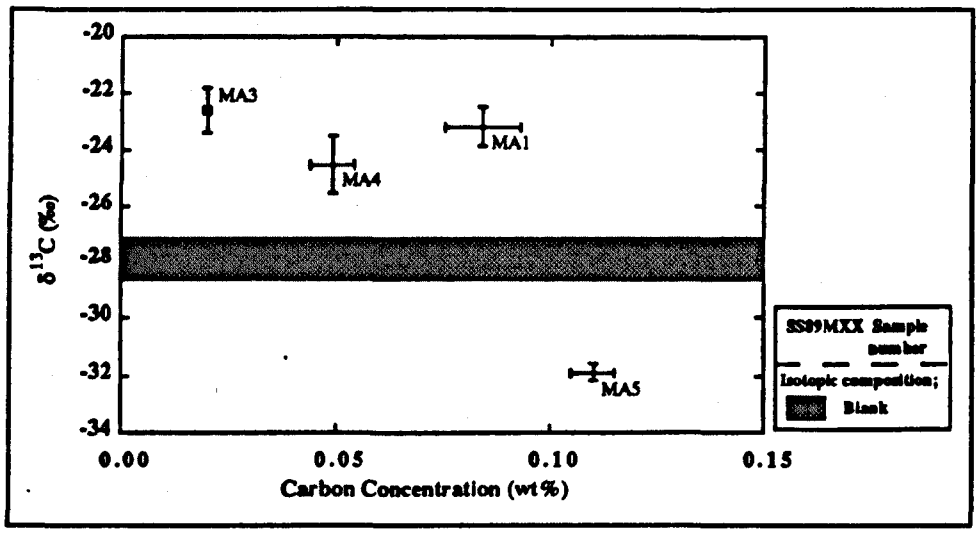

Figure 5.18. Bulk carbon concentration and $\delta^{13}C$ of the blank-corrected 200-500°C component within the Antarctic micrometeorites.

Explaining the isotopic profiles in figure 5.17 is relatively simple. The elevation in $\delta^{13}C$ values in the high temperature regimes of samples MA4 and MA5 is attributable to the use of methanol in the corresponding analysis protocols (4.4.6.), and the isotopically light (*ca.*-37‰) value obtained in MA1 at 600°C was probably the product of the interfering effect of dichloromethane (4.4.5.). The $\delta^{13}C$ value of *ca.*-30‰ at 400°C within sample MA4 remains problematic as there was no immediately obvious blank equivalent. Moreover, its observed similarity to the 200-500°C component in MA5 suggested that possibly a relationship existed between the two, and mixing with a ^{13}C enriched component combustable between 200-500°C had occurred to produce observed profile in MA4. This mixing hypothesis is compatible with the results shown in figure 5.18, here the $\delta^{13}C$ value for MA4 plots at intermediate values between MA1 and MA3 and the ^{12}C enriched component that dominated the results for MA5. The release profile for MA5, as seen in figure 5.17, has 4 consecutive steps which yielded *ca.*16 to 20 ng of carbon at $\delta^{13}C$ values between *ca.*-30 to -32‰, so strongly suggesting that this component is indigenous. The absence of an equivalent component in the blank experiments, or any of the samples that had been treated with dichloromethane, prompted the conclusion that the component was perhaps soluble in dichloromethane but not in methanol, and so otherwise could have represented a more common constituent of the carbon inventory of the samples.

5.3.3. Conclusions from the Greenland and Antarctic individual micrometeorite stepped combustion experiments.

The stepped combustion release profiles of the Greenland and Antarctic micrometeorites facilitated the isolation of two probably indigenous components; both combusting at low temperatures between *ca.*200-500°C, but characterised by $\delta^{13}C$ values of *ca.*-25 to -18‰ and *ca.*-30 to -32‰ respectively. The first component was not solvent extractable, whilst the second was removed by dichloromethane. The first component was found to be common to most samples and so provided a signature that could be potentially utilised to elucidate generic connections. Examination of stepped combustion experiments performed on ordinary chondrites by Grady, (1982) and Grady *et al.*, (1989) revealed the presence of a carbonaceous component similar to the ^{13}C-enriched low-temperature micrometeorite component. Table 5.7 shows a summary of the combustion temperature, $\delta^{13}C$ and concentration of the ordinary chondrite component.

Meteorite*	Combustion Temp.(°C)	Concentration (wt%)	$\delta^{13}C$ (‰)
Brownfield (H3.6)	300-400	0.124	-14.00
Tieschitz (L3.6)	400-500	0.083	-12.74
Assam (L5)	400-500	0.014	-14.20

* = The information in brackets gives the chemical group and petrologic type of each meteorite.

Table 5.7. A summary of $\delta^{13}C$, combustion temperature and concentration of a carbonaceous component isolated from stepped combustion data of ordinary chondrites (data taken from Grady, 1982; Grady *et al.*, 1989). This component is similar to the ^{13}C-enriched low-temperature micrometeorite carbon seen within the Greenland and Antarctic samples.

The micrometeorite carbon combusted between 200-500°C with $\delta^{13}C$ values of *ca.*-25 to -18‰ and was present in concentrations between *ca.*0.02 to 0.15wt%, which , apart from slightly ^{13}C-depleted values, is in agreement with the data in table 5.7. The identity of the ordinary chondrite component in table 5.7 has not been determined, although Grady, (1982) suggested that it may represent elemental carbon. However, there are several problems associated with attempting to make a generic connection between the two components;

(1) The provenance of carbon that combusts <500°C in the ordinary chondrites is poorly understood. Grady *et al.*, (1989) suggested that any carbon released <500°C in both Antarctic and non-Antarctic ordinary chondrites was a mixture of 'organics' (both terrestrial and indigenous but with a $\delta^{13}C$ of *ca.*-28‰) and 'weathering products' of predominately carbonate. (Carbonates are the major source of contamination in Antarctic meteorites, but the effects of carbonate contamination are normally seen at combustion temperatures >600°C, *e.g.* Grady *et al.*, 1991). With regard to these 'weathering products', Grady *et al.*, (1988) isolated carbonates from non-antarctic ordinary chondrites with $\delta^{13}C$ values ranging from -25.9 to -2.3‰, and of the meteorites in table 5.7, Brownfield was found to contain 0.057wt% carbonate with a $\delta^{13}C$ of -10.1‰, Assam was not studied, and Tieschitz was found to not contain any detectable carbonates.

(2) The most common form of carbon which is known to be indigenous to the ordinary chondrites is poorly-graphitised carbon (*e.g.* Grady *et al.*, 1982b; Scott *et al.*, 1988). Such material combusts at temperatures >700°C with $\delta^{13}C$ values as high as *ca.*-10‰, and concentrations typically between *ca.*0.01 to 0.02 wt%. Poorly-graphitised carbon has been observed in samples that span all the ordinary chondrite chemical groups and petrologic types (*e.g.* Grady *et al.*, 1989).

With the ensuing possibility that the ordinary chondrite component represents a secondary carbonate weathering product, and the absence of ordinary chondrite graphitic material in the micrometeorites, it is difficult to provide further evidence from the stepped combustion plots to corroborate the generic connection to the ordinary chondrites implied by the micrometeorite bulk carbon signatures.

Another candidate for the source of ^{13}C-enriched low-temperature micrometeorite component is macromolecular material found in the carbonaceous chondrites. Table 5.8 contains a summary of the measured $\delta^{13}C$ values of macromolecular carbon extracted from CI and CM chondrites. Examination of table 5.8 shows that the macromolecular carbon can be correlated to the ca.-18 to -25‰ range of $\delta^{13}C$ ehibited by the micrometeorite component. In common with the micrometeorite component, the macromolecular material combusts <500°C (*e.g.* Kerridge, 1983; Kerridge *et al.*, 1987). The hypothesis is also consistent with the fact that such macromolecular material is not solvent-extractable and so would have survived the solvent cleaning steps implemented during the sample handling protocols.

Meteorite	Type	$\delta^{13}C$ (‰)	Reference
Orgueil	CI1	-16.9	1
		-19.4	2
		-16.7	3
Cold Bokkeveld	CM2	-16.4	1
		-14.6	2
		-17.8	4
Murchison	CM2	-13.0	2
		-17.5	5
Murray	CM2	-14.8	1
		-13.0	2
		-17.0	3

(1) Smith and Kaplan, (1970).
(2) Robert and Epstein, (1982).
(3) Kerridge, (1983).
(4) Grady *et al.*, (1991).
(5) Kerridge *et al.*, (1987).

Table 5.8. Isotopic compositions of macromolecular material in CI1 and CM2 carbonaceous chondrites.

Between 70 and 95% of carbon in the carbonaceous chondrites is present as macromolecular material (Hayes, 1967; Anders *et al.*, 1973; Hayatsu and Anders, 1981). Using the carbon concentrations for the carbonaceous chondrite groups in table 5.3, this translates into a possible range of macromolecular material concentration of *ca.*0.084 to 4.7wt%. The concentration of the micrometeorite component was *ca.*0.02 to 0.15wt% which limits the possible carbonaceous chondrite parents to either the CV or CO chondrites. Spectroscopic observations of the Earth-crossing asteroids shows that 22 of the total 42 asteroids which have been successfully imaged are of a spectral type which is possibly related to the CV and CO chondrites (*e.g.* McFadden *et al.*, 1989). The main asteroid belt is also believed to be dominated by carbonaceous chondrite parent bodies (1.4.2.), but of predominately spectral types that more closely match CI and CM chondrites (*e.g.* Lipschutz *et al.*, 1989). The Earth-crossing asteroids are believed to provide the source of the ordinary chondrites which account for *ca.*80% of contemporary meteorite falls, and so it is perhaps feasible that these

same asteroids provide the majority of the micrometeorites. The results of the small-sample meteorite stepped combustion experiments (chapter 7) suggested that $\delta^{13}C$ is a more reliable criterium than carbon concentration for determining generic relations. The arguments a micrometeorite provenance from the Earth-crossing asteroids is largely based upon the low concentration of the macromolecular component, but with the results of the small-sample experiments in mind, it is not possible to rule out a generic connection to the more carbon-rich carbonaceous chondrites which would favour an origin from the main asteroid belt.

Providing a meteoritic provenance for the second (solvent-extractable) component is more problematic. Studies of solvent-extractable organics from meteorites have been limited, mainly due to problems of seperating indigenous species from terrestrial contamination. Notwithstanding this, such material has been isolated from the CM and CI carbonaceous chondrites and found to have $\delta^{13}C$ values between -27 and -4‰ (Briggs, (1963); Smith and Kaplan, (1970)), *i.e.* not in agreement with the $\delta^{13}C$ value of *ca.*-30 to -32‰ obtained for the micrometeorite solvent-extractable carbon. This observation indicates that either the micrometeorite solvent-extractable component was in a form of contamination not previously isolated or represented an indigenous solvent extractable component different to the already characterised meteoritic material. In view of the extensive testing of the stepped combustion experiment blanks in chapter 4, the latter conclusion is believed to be correct.

5.3.4. Algal assimulation of micrometeorite carbon.

A caveat to any interpretations of the origin of carbon in the cryoconite micrometeorites is the continuing problem of the possibility of algal contamination, especially since the carbonaceous fraction of the algae was found to possess a similar $\delta^{13}C$ to the postulated sample (meteoritic) carbonaceous component. A hypothesis that the algae was assimilating the micrometeorite carbonaceous material during growth and was thereby mirroring the $\delta^{13}C$ value of the micrometeorites can be discounted. Biological carbon fixation is by the blue-green algae is by assimilation of CO_2 (*e.g.* Schidlowski *et al.*, 1983). The concentration of dissolved CO_2 in surface waters is dependent upon the temperture (Rogers *et al.*, 1972), with an increase of dissolved gas with a lowering of temperature. The Greenland melt pools are only a fraction of a

degree above 0°C, so it is likely that dissolved atmospheric CO_2 is utilised by the algae. Even if the micrometeorite carbon species were dissolved and converted to CO_2 in the pool water, then CO_2 fixation by algae is associated with a ^{13}C depletion of the CO_2, resulting in a shift of up 35‰ to lighter $\delta^{13}C$ values (Wong *et al.*, 1979). Lower atmospheric CO_2 has a $\delta^{13}C$ of *ca.*-7‰ (Keeling, 1961) and so this isotopic shift during CO_2 fixation can be used to explain the measured bulk $\delta^{13}C$ of the cryoconite algae of *ca.*-23‰.

Whatever the correct explanation, it was evident from the results of the stepped combustion experiments that a complex relationship exists between the samples and the algae. Perhaps the most perplexing problem was that the three samples that had been found to contain high S or P contents, and so had been interpreted as being contaminated by algae, showed identical carbon isotopic results to the other Greenland samples, but more importantly, also to the Antarctic samples that had not been exposed to the algae. Only one sample (SS89M01) showed what was considered as good evidence of algal contamination, *i.e.* a considerable increase in carbon concentration over the other samples and $\delta^{13}C$ values identical to the algae even when blank corrections had been taken into account, but this sample did not show high S or P contents. From these observations it was concluded that in reality the Greenland samples had all suffered from minor contamination by algae, but to a sufficiently small degree so that their carbon inventory remained dominated by meteoritic carbonaceous material. This hypothesis would also explain why the Antarctic samples as a group exhibited on average a slightly lower carbon concentration with respect to the Greenland samples, and allow explanation of the high S and P contents in two of the Greenland samples that did not then exhibit characteristics like SS89M01. It is proposed that all the Greenland samples would probably have yielded a similar result for S and P if the whole surface area of each particle had been examined in the analytical electron microscope, but with only a fragment being analysed, and then only upon a few selected areas, the contamination could have been missed.

5.4. Summary and conclusions.

The most likely provenance for micrometeorites is the asteroid belt or comets, and an aim of this study was to elucidate the origins of the analysed samples with respect to these. With a view to identifying the isotopic signatures associated with each source, it was anticipated that cometary material may be characterised by anomalous stable carbon isotope signatures (1.3.2. and 1.6.2.3.), exhibiting large excesses in either ^{12}C or ^{13}C over known solar system values, whereas an asteroidal origin would be indicated by the samples possessing meteoritic components (1.6.2.2.). Subsequent examination of the results obtained showed no evidence for isotopically anomalous carbon, so suggesting that the samples were of an non-cometary origin, or if cometary material had been sampled, then it shared a similar bulk carbonaceous signature to the remainder of the solar system.

The bulk $\delta^{13}C$ and carbon concentration signatures of the type I deep-sea micrometeorites derived from the multiple-sample Triple Collector experiment was within the range shown by the iron meteorites. However, the stepped combustion profile of the type I experiment revealed the carbon released to be dominated by a component that combusted >250°C, and this could not be related to analogous iron meteorite components. The bulk carbon signature derived from the type S Triple Collector deep-sea micrometeorite experiment was in agreement with an ordinary chondrite provenance. The stepped combustion plot showed no evidence of the meteoritic SiC component inferred from the single-particle deep-sea micrometeorite experiments, and suggested that the micrometeorites and ordinary chondrites could be linked on the basis of their bulk carbon signatures solely because they had suffered similar amounts of organic terrestrial contamination.

The bulk $\delta^{13}C$ and carbon concentration signatures of the individual Greenland and Antarctic micrometeorites analysed on MS86 could be correlated most closely with the ordinary chondrites, but also to the CV and CO carbonaceous and enstatite chondrites and the achondrites. It was considered unlikely that the enstatite chondrites or the achondrites would constitute a major source of micrometeorites because they compose only a fraction of contemporary meteorite falls, and have low parent body abundances within the asteroid belt (1.4.2.). Although the bulk carbon signatures of the Antarctic

and Greenland micrometeorites exhibited a closer correlation to the ordinary than the CV or CO chondrites, their stepped combustion profiles were more readily explained by the presence of carbonaceous chondrite macromolecular carbon, and in concentrations similar to the CV and CO chondrites.

Notwithstanding that the main asteroid belt is dominated by carbonaceous chondrite parent bodies, if the majority of the micrometeorites were indeed supplied by the CV and CO chondrites, then it is proposed that they may have originated from the Earth-crossing asteroids. Spectral observations of the Earth-crossing asteroids can be matched to the ordinary chondrites, which are believed to be absent in the main asteroid belt, but also to the CV and CO chondrites (*e.g.* McFadden *et al.*, 1989). It is of particular importance to note that *ca.*50% of the Earth-crossing asteroids that have been studied are of the latter type. If the interpretation of these spectral observations is correct, then the domination of CV and CO parent bodies in the Earth-crossing asteroids can be correlated with the dominance of CV/CO-like carbon components in the micrometeorites analysed in this study.

Chapter 6

The Preparation and Analysis of Cryoconite Acid-Resistant Residues.

6.1. Collection of cryoconite.

Cryoconite is a black extra-terrestrial dust-rich sediment that collects in the melt water pools and streams on the Greenland Icesheet (1.5.5.). The cryoconite deposits from which the micrometeorites analysed in chapter 5 were isolated, and the acid-resistant residues described within this chapter prepared, were collected between the 18th to 29th June 1989. The ice sheet inland at the latitude of Sondre Stromfjord on the west coast of Greenland was chosen because earlier collection expeditions (*e.g.* Maurette *et al.*, 1986) had shown the area to be rich in cryoconite deposits.

6.1.1. The collection technique.

The cryoconite pools and streams were located from the air. To reduce the amount of wind-blown terrestrial dust within the cryoconite, the collections were made at a distance of >20km from edge of the Greenland Icesheet. Maurette *et al.*, (1988) found the concentration of extraterrestrial dust dependent upon the rate of water flow; with an increase in dust concentration accompanying a decrease in water flow speed. Accordingly, collection efforts were focussed upon either isolated cryoconite 'holes' (plate 6.1) or small steams (plate 6.2). Partial or total ice covering of the streams was found to be indicative of low water flow rates (*ca.*<1cm s^{-1}), and was subsequently used as a selection criterium. The cryoconite was removed from the pools and streams by using a water pump, and then the cryoconite separated from the water by directing the sediment laden flow through a 90μm stainless steel sieve. To avoid contamination by the exhaust fumes associated with a motorised pump, a problem experienced by Dr

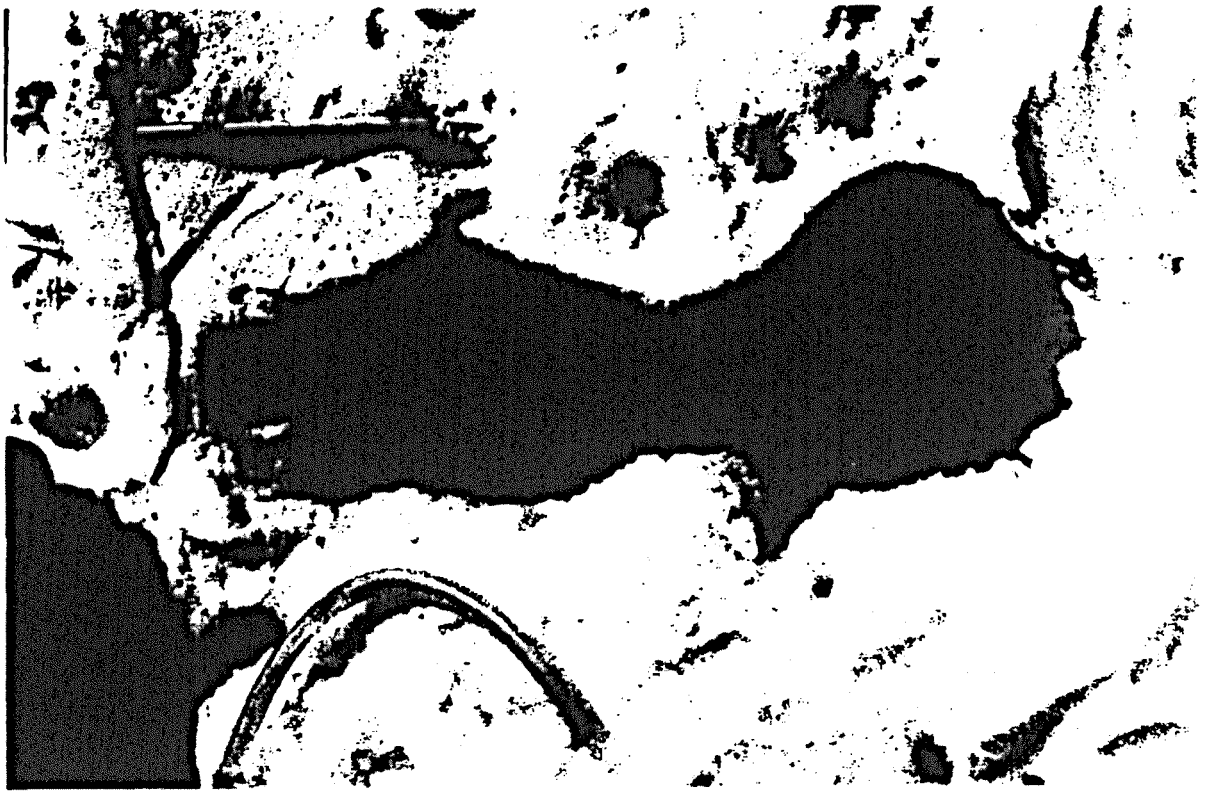

Plate 6.1. An example of a cryoconite 'hole' (approximate width of view is 2m). These deposits contain the highest concentration of extraterrestrial dust (Maurette *et al.*, 1988). (This photograph corresponds to locality 3 in table 6.1).

Plate 6.2. A cryoconite stream deposit (stream width is approximately 2m). The degree of ice cover of icesheet streams was found to be related to the water flow, and could be used as a selection criterium due to the observed increase in extraterrestrial dust concentration with a decrease in water flow (Maurette *et al.*, 1988). (This photograph corresponds to locality 2 in table 6.1).

Maurette (pers.comm), a hand operated pump was used (Patay Hand Pump Number 44). The pump was connected to braided plastic suction and delivery hoses (one inch internal diameter), and was capable of processing *ca.*1m^3 of water per minute. The cryoconite collected in the sieve was stored in plastic containers, frozen within *ca.*2 hours of collection and kept frozen until required.

6.1.2. Details of the collected cryoconite samples.

Two flights were made onto the Greenland Icesheet, during which *ca.*10.5kg of cryconite was collected. Table 6.1 shows a summary of the details of the collection localities.

Locality	Type*	Ice margin distance (km)	Flow rate (cm s^{-1})	Amount collected (kg)
1	S	30	1-2	1.0
2	S	23	<1	5.0
3	H	23	0	4.5

* S = Stream deposit (plate 6.1) / H = Cryconoite 'hole' (plate 6.2)

Table 6.1. A summary of localities from which cryoconite deposits were collected.

Cryoconite collected from locality 3 has been used for the work described within this thesis, *i.e.* individual micrometeorite were isolated from it for the work described in chapter 5, and it has been used for the acid-resistant residue work described in the remainder of this chapter.

For acid residue work the cryconite was used unprocessed, but for removal of individual micrometeorites, the majority of the algae must be removed. Processing of the cryoconite to produce algae-free concentrates from which micrometeorites could be hand-picked was carried out according to the procedure of Maurette *et al.*, (1986), *i.e.* the cryoconite was gently abraded under running water. Maurette *et al.*, (1986) carried out this processing in the field using nylon brushes and a pressurised jet of ice-meltwater, but to minimise contamination, processing was executed in a clean-room environment with distilled water (that had been passed through a *ca.*4μm sieve) from washbottles. Additionally, the nylon brush was replaced by a pyrex glass rod

(*ca.*2mm diameter) which had been pre-cleaned by combustion to *ca.*600°C for *ca.*30 minutes.

6.2. Acid-resistant residues.

The analysis of multiple samples of deep-sea and individual Greenland and Antarctic micrometeorites had not revealed evidence of any isotopically anomalous carbon that could be attributed to interstellar grains. The presence of such interstellar dust within primitive meteorites has been a subject of much debate and study (*e.g.* Cameron, 1977; Clayton and Ramadurai, 1977; Clayton *et al.*, 1977; Swart *et al.*, 1983a; Yang and Epstein, 1984; Fahey *et al.*, 1987; Zinner and Epstein, 1987; Ash *et al.*, 1988; 1990; Alexander *et al.*, 1990; Russell *et al.*, 1991) and it has been determined that such components are invariably present in only very low concentrations, for example, nanometric diamond has been found to be most common species, but it is still present in concentrations <500ppm. It has also been recognised that many interstellar grains are present as (or within) extremely resistant mineral phases, and that these have facilitated their survival through the rigours of the solar nebula formation and then subsequent incorporation into their parent bodies. For example, silicon carbide (SiC) is known to be the carrier of a multitude of isotopically anomalous species in addition to carbon, including nitrogen, neon, xenon, calcium, titanium, chromium, iron, and silicon (Alaerts *et al.*, (1980); Tang *et al.*, (1988); Zinner *et al.*, (1991). The detailed study of such components in meteorites has only been made possible by removing components of a solar system origin, and by relying on the chemical inertness and physical strength of the carriers of the interstellar material. This task has most commonly been achieved by using harsh chemical and physical processes such as crushing followed by treatment by strong acids.

Although the stepped combustion profiles of both the Triple Collector multiple-sample and MS86 individual sample experiments contained no evidence for SiC, this observation was not considered as prohibitative to its presence. Many meteorites have been shown to contain SiC in only small amounts (*ca.*1ppm). For these same meteorites anomalous $\delta^{13}C$ values were not encountered during analysis of the whole-rock but observed only after the preparation of acid-resistant residues. It was therefore decided to subject samples of whole-rock micrometeorites to acid dissolution treatment

in an attempt to ascertain whether interstellar could be concentrated. The logic behind this effort must be two fold; firstly, the removal of isotopically normal components makes it easier to see isotopic anomalous phases, and secondly, Brownlee and Schramm (1990) suggested that a distinction existed between the sources of small (<10μm diameter) and large spherical micrometeorites in that the smaller ones were more likely to possess a cometary rather than asteroidal origin. For reasons dictated by the amounts of sample material required for acurate carbon isotopic determination (1.5.6.), the samples analysed within this study were all generally in excess of 200μm in diameter, suggesting that the cometary particles may not have been sampled. Coupled with the fact that the unmelted extra-terrestrial dust fraction likewise probably included a considerable proportion of cometary derived material (*e.g.* Bradley and Brownlee, 1986), it was postulated that if a sample of either deep-sea sediment or Greenland cryoconite was subjected to acid dissolution treatment, then subsequent isotopic and mineralogic characterisation of the resulting residue would enable determination of whether any interstellar material was present, and at approximately what concentration with respect to the expected extratrrestrial dust content of the sample. In a previous study Prombo *et al.*, (1991) isolated six SiC grains (of 0.2 to 3.0μm diameter) from Greenland cryoconite by acid-dissolution; ion probe analysis determined their $\delta^{13}C$ values to be -14 to -36‰, suggesting a terrestrial in origin. Whilst terrestrial SiC contamination would dilute any interstellar SiC, a grain-by-grain study would only by chance be successful in locating interstellar SiC. Stepped combustion experiments on the other hand could overcome this problem, as the extremely ^{13}C-enriched interstellar SiC would give some shift in the $\delta^{13}C$ of a residue, indicating the presence of only a minor amount of interstellar material.

The choice of whether to use deep-sea sediment or Greenland cryoconite as the starting material was controlled by the probable concentration levels of micrometeorites within each. It is noteworthy here to remember that with respect to the isolation of interstellar material, the preservation state of the samples was theoretically insignificant, because upon the breaking down of the dust by either weathering or algal action, the resistant interstellar grains would theoretically not be affected. With this in mind it was difficult to estimate the probable relative concentrations of dust, but a comparison was attempted based on upon an examination of the numbers, sizes (hence mass) and petrographic types of the spherules that could be extracted from sediments or cryoconite. Two deep-sea sediments (kindly supplied by Dr.D.W.Parkin) were evaluated in this way and were found to contain *ca.*1ppm and *ca.*0.005ppm of type S

sample material. The large difference between the two presumably highlighted how relative sediment accumulation rates had diluted the input of the dust, as the samples were both red clays but had been collected from differing localities; the first from the Pacific Ocean and the second from the Atlantic. In contrast to these sediments, the sample of cryoconite that was examined yielded *ca.*10ppm of equivalent type S sample. Cryoconite was thus favoured over deep-sea sediment for preparing the acid-resistant residues..

6.2.1. Preparation of the cryoconite residues.

The processing of the cryoconite sample was undertaken by Dr.J.W.Arden at the University of Oxford following procedures used on bulk meteorite samples for the isolation of interstellar dust components (see Alexander *et al.*, (1990) for details of the experimental methods). Figure 6.1 shows the details of the preparation of the cryoconite residues, but for completeness a summary of the effects of each stage is given below;

(i) The hydrofluoric (HF)/ hydrochloric (HCl) acid mixture removes any silicates present in the sample. The HF reacts with silicates to produce gaseous silicon tetrafluoride whereas the HCl acts to inhibit the formation of aluminous fluorides which cause problems when using stepped combustion.

(ii) Chromic acid ($Cr_2O_7^{2-}$ in H_2SO_4) is used for the removal of organic carbon by relatively gentle oxidation.

(iii) Perchloric acid ($HClO_4$) is also an oxidative acid used for the removal of elemental carbon. (Chromic acid treatment must precede the perchloric acid as the reaction of the latter with organics is extremely vigorous and potentially explosive).

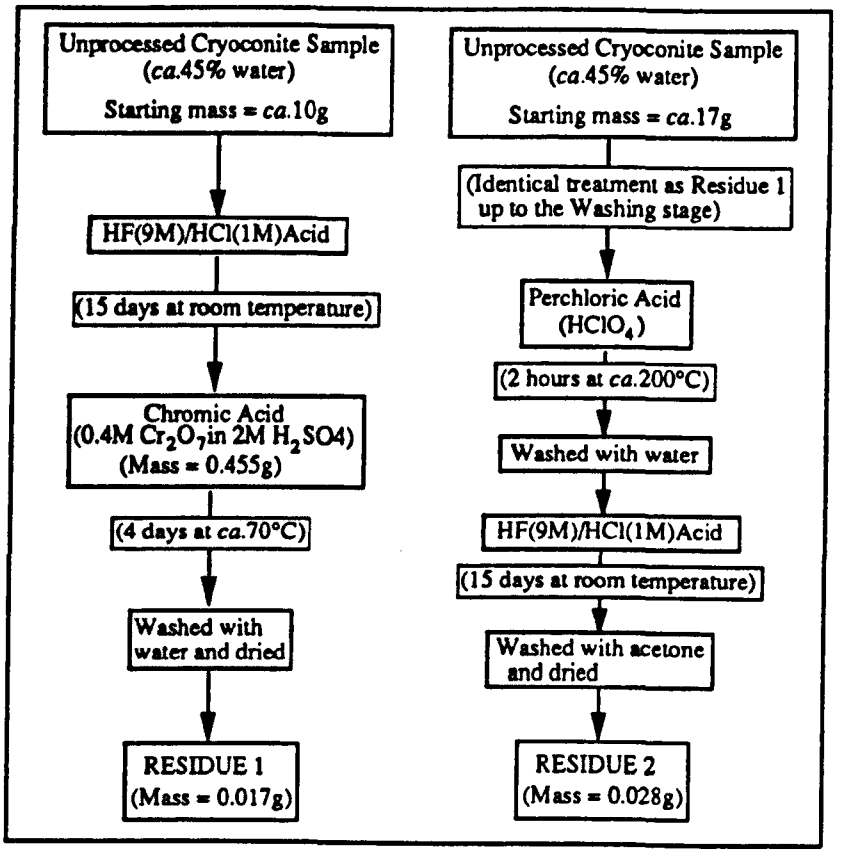

Figure 6.1. The preparation of acid-resistant residues for the analysis of interstellar material from Greenland cryoconite..

6.2.2. Examination of the mineralogy of the residues.

In an attempt to identify the major components in the cryoconite acid resistant residues, aliquots of residue 2 were analysed by electron probe micro-analysis system (EPMA-3.2.5.) for major element chemistry and by X-ray diffraction (XRD-3.2.4.) to elucidate the structure of any constituent mineral phases.

The EPMA results showed the residue to be composed mainly of a mixture of micron sized metallic alloy grains composed of aluminium, titanium, or a chromium-titanium-iron composite, which were found to be embedded in larger (up to *ca.*400μm) grains rich in silicon (Si) and zirconium (Zr). The XRD results, which were obtained by conventional powder diffractometry, revealed a plethora of diffraction lines but from which, only the mineral zircon ($ZrSiO_4$) could be positively identified. The presence of zircon explained the Si and Zr from the EPMA results, but it was somewhat surprising that no lines characteristic of the metallic alloys were identified.

With respect to the interstellar components, conventional meteorite residues prepared by analogous techniques contained diamond in amounts varying from a few % to 60% (Ash, 1990); discrete SiC grains of interstellar origin can also be seen. No evidence of either diamond or silicon carbide was found during the EPMA analysis of residue 2.

It is well established that aerospace activities have produced a debris belt about the Earth composed largely of metals, refractory oxides and silicate grains (*e.g.* Kessler and Cour-Palais, 1978). Decay of the orbits of such particles allows them to enter the Earth's atmosphere, where they are subject to the same collection mechanisms as extraterrestrial dust. Zolensky *et al.*, (1988) in a search for refractory micrometeorites in Antarctic Ice found metallic aluminium, silicate, steel and rutile (TiO_2) particles which they attributed to a spacecraft origin. It is therefore perhaps not surprising that such debris has become concentrated along with the micrometeorites in the cryoconite samples. Given their possible source it is feasible to explain why the alloys in the residues could not be identified by XRD, as intuitively the ablation processes that formed them are not replicated in the formation of terrestrial alloys.

6.2.3. Carbon isotopic analyses of the residues.

The results of three stepped combustions carried out on the residues using MS86 are presented in figure 6.2. The original mass of the bulk cryoconite had been reduced by *ca.*99.83% in the preparation of residue 1. The carbon release profile for residue 1, as illustrated figure 6.2.A, revealed it to be composed of *ca.*25wt% carbon, with four components constituting the bulk of the release pattern. The overwhelming majority of the carbon (*ca.*95%) was represented by a component that combusted between *ca.*300 and 600°C with a $\delta^{13}C$ value of *ca.*-25‰. The relatively high temperature of combustion and the survival of the material through the chromic acid suggested that it was most likely a macromolecular species. For the purpose of argument we can assume that the carbon in residue 1 represents a mixture of macromolecular carbon supplied from the algae and the micrometeorites. The micrometeorite macromolecular carbon had a measured $\delta^{13}C$ value of -18 to -25‰ (5.3.2.), whereas the analogous

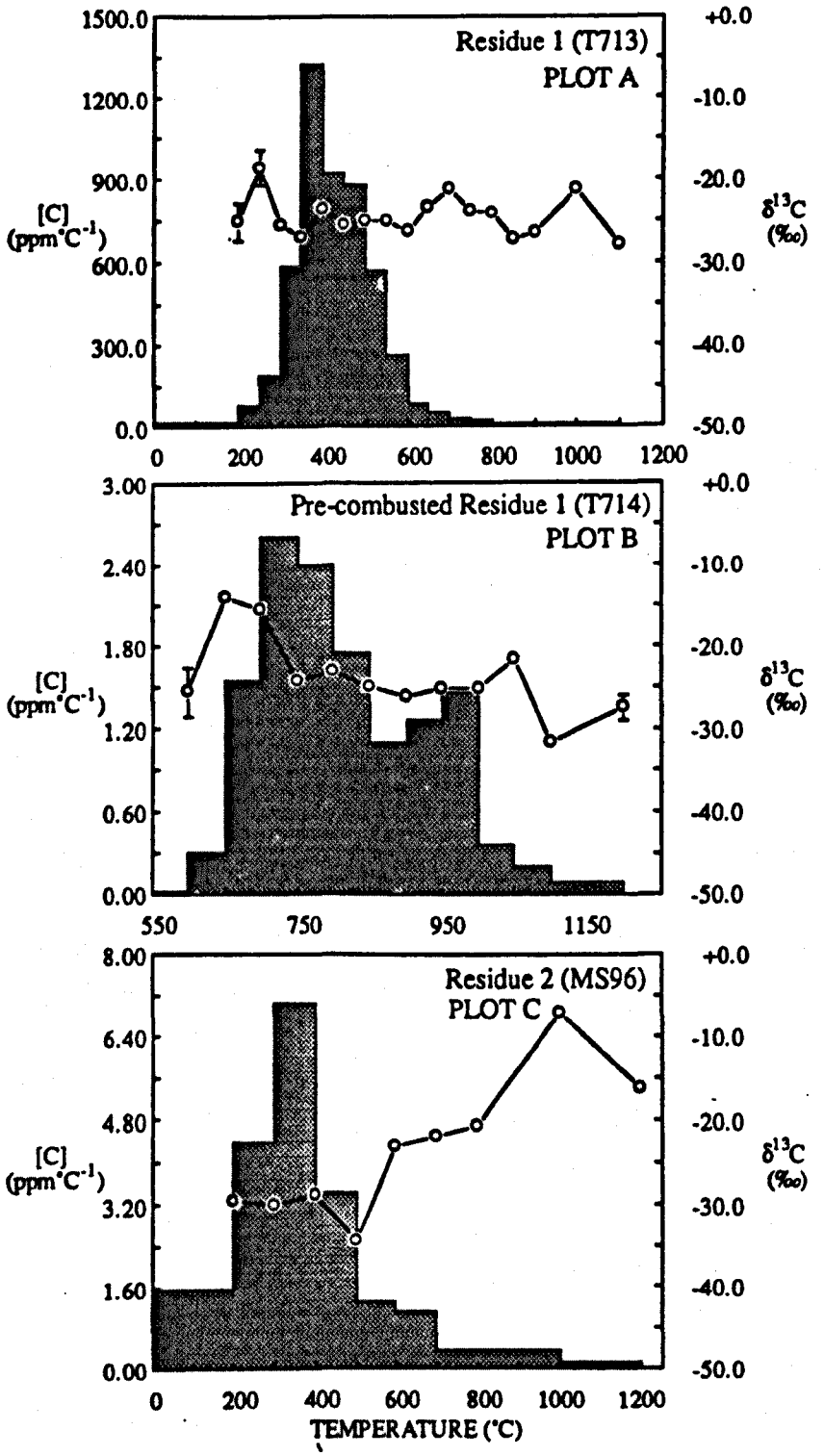

Figure 6.2. Stepped combustion profiles analyses carried out on the Greenland cryoconite acid-resistant residues

algae component showed $\delta^{13}C$ values between -21 to -23‰ (5.3.2.). Attempting to use the concentration of the macromolecular component in residue 1 to estimate the corresponding concentration of the component within the micrometeorite fraction of the unprocessed cryoconite used to prepare the residue, is complicated because it is difficult to estimate what proportion of the macromolecular material was supplied by the algae. However, if it is assumed that 50-100% of the macromolecular carbon seen in residue 1 was supplied by the micrometeorites (which is necessary to produce the measured $\delta^{13}C$ value of residue 1), then the concentration in the micrometeorite fraction, (assuming that the unprocessed cryoconite contains *ca.*10ppm of type S material (6.1.)), works out to be at least four orders of magnitude greater than that obtained in the analysis of individual cryoconite micrometeorite samples (5.3.). This suggests that:

(1) The algae supplied a far greater proportion of the residue 1 macromolecular carbon and so possesses a wider range in $\delta^{13}C$ than suggested by the stepped combustion experiments executed in 5.3.

(2) The unmelted micrometeorites, which are not included in the estimation of the micrometeorite content of the unprocressed cryoconite, contain the same macromolecular carbon component as isolated within the spherical type S micrometeorites.

The possibility of a second low-temperature component was indicated by the elevation in $\delta^{13}C$ value at 250°C to -18.1±2.1‰ in figure 6.2.A,. The obscuring effects of the 300-600°C release meant that if this is indeed another component, its exact concentration and isotopic composition could not be determined, so likewise its provenance is undecided.

In the high temperature regime, a further two components might be discernable from the combustion profile of plot A, one at 650-700°C with a $\delta^{13}C$ value of -21.3±1.0‰, the other at 900-1000°C at -21.3±0.9‰. Again the concentration and isotopic composition of the 700°C release was compromised by the much more abundant 300-600°C combusting component. On the other hand, material burning at 1000°C is probably outside the influence of the tail; its concentration is estimated at *ca.*400ppm and the measured $\delta^{13}C$ of *ca.*-20‰ may be close to the true value. The combustion temperature of the 650-700°C component was indicative of either graphite or diamond. The $\delta^{13}C$ value of the 650-700°C release was likewise commensurate with a terrestrial graphite origin (*e.g.* Hoefs, 1987), but although terrestrial diamonds are known to range in $\delta^{13}C$ between *ca.*0 and -30‰, there is a strong bias to $\delta^{13}C$

values of *ca.*-5‰ (Galimov, 1991), and so a terrestrial diamond provenance is not favoured.

6.2.4. The pre-combustion of cryoconite acid-resistant residue 2.

In an attempt to remove the shrouding effects of the 300-600°C release, a second aliquot of residue 1 was combusted overnight (*ca.*12 hours) at 600°C prior to analysis by stepped combustion from 600-1200°C, and the results of this experiment are illustrated by figure 6.2.B. Before elevating the temperature above 600°C several 40 minute combustion steps were executed until the yield of carbon obtained was equivalent to blank levels. In this way it was hoped that the last vestiges of the low-temperture carbon had been removed and that any release obtained >600°C was representative of discrete high stability components. From plot B it was apparent that between 600-1200°C, residue 1 was composed of 656ppm of carbon, and as initially indicated by plot A, this was present as two main releases. Now that the low-temperature carbon has been eliminated, the more abundant high temperature component burns at 700-800°C and accounts for *ca.*400ppm. A less abundant component (*ca.*200ppm) combusts at 1000°C. The release pattern could now be interpreted as the combustion of two components that shared a similar isotopic value of *ca.*-25‰ superimposed on a background that apparently contained heavier carbon. This was illustrated by the flat isotopic pattern seen between 750 and 1000°C, where *ca.*80% of the total high-temperature release occured with corresponding $\delta^{13}C$ values within 2‰ of -25‰, whereas outside of the influence of this carbon the isotope pattern departed to -14.1±0.9‰ at 550-650°C and to -21.7±0.7‰ at 1000-1050°C. Once again elucidating the provenance of the isotopically heavier components was not straightfoward, although it was now evident that the components released between 700 and 1000°C were probably terrestrial, because the isotopic value of -25‰ and combustion temperature was typical of terrestrial graphite (*e.g.* Hoefs, 1987). It was not immediately obvious where such terrestrial graphite could have originated from because the cryoconite samples were collected >20km inland from the Greenland ice margin and so the input of terrestrial contamination would be restricted to the smallest airbourne particulates (see 1.5.5). However, graphite has been found to be a spacecraft debris product (Zolensky *et al.*, 1988) and it was postulated that this provided a source for the graphite, as the Greenland icesheets would act as a collector of refractory spacecraft debris in the same way they concentrate extraterrestrial dust.

6.2.5. The perchloric acid-treated cryoconite residue.

Figure 6.2.C shows a stepped combustion experiment executed on residue 2, where an additional perchloric acid treatment was implemented after the HF/HCl and chromic acid steps. The release profile revealed that the carbon concentration within residue 2 had been reduced to *ca.*0.02wt%. The perchloric acid has removed the macromolecular component seen in residue 1. However, the release of carbon from residue 2 was still dominated by a low-temperature component that constituted *ca.*90% of the total yield with an isotopic signature of *ca.*-30‰ (as indicated by the steps between 200 and 400°C). This low-temperature carbon could be interpreted as organic contamination that had been introduced during sample handling after the acid treatments. The perchloric acid as expected had also removed the high-temperature (graphitic) material seen in plot B, and the resulting isotopic profile between 500 and 1200°C was extremely informative in revealing the identity of the previously shrouded components. In the first instance it was apparent that the lower-temperature (650-700°C) heavy carbon component seen in plot B had also been removed, indicating that it may be graphitic carbon of some description. CI, CM and CR carbonaceous chondrites have been found to contain interstellar graphite that is present in grain sizes ranging from *ca.*20nm to 0.1μm in diameter with accompanying $^{12}C/^{13}C$ ratios between *ca.*10 to 10,000 (Zinner *et al.*, 1990). The effects of the combustion of this material was first seen in acid residues prepared from the Murchison CM2 meteorite where Carr *et al.*, (1983) observed graphite combusting at 650°C with a $\delta^{13}C$ value of +350‰. At face value the release profile in plot B could be the result of analogous meteoritic graphite combusting at slightly lower temperature than the terrestrial graphite release (*i.e.* as a result of the relatively coarser grainsize for the latter component).

After the perchloric acid treatment the peak $\delta^{13}C$ value of the 1000°C component is -7.2±1.1‰, and the overall shape of the isotopic release pattern is consistent with the CO_2 of this isotopic composition being produced by combustion of meteoritic SiC. With the obscuring effects of the terrestrial graphite having been removed by the perchloric acid, it was now possible to estimate the concentration of putative SiC within the micrometeorite fraction of the cryoconite. In the first instance it was neccessary to allow for the blank input to the 1000°C component, and by assuming that the blank approximated 1ng at -30‰, the sample component $\delta^{13}C$ value when

corrected became equal to -2.6‰ with a yield of 4.9ng. On closer examination of the release profile in plot C it was evident that the carbon yield at 1000°C was composed of three components; the blank, SiC and the tail of the lower temperature carbon. From these arguments it could be seen that the blank corrected sample signature was a product of the input from the tail and SiC, and that the following relationship existed;

$$(Y_{BC} \times \delta^{13}C_{BC}) = (Y_T \times \delta^{13}C_T) + (Y_{SiC} \times \delta^{13}C_{SiC})$$

Where; Y_{BC} = Blank corrected sample component yield.
$\delta^{13}C_{BC}$ = Blank corrected sample component $\delta^{13}C$ value.
Y_T = Tail component yield.
$\delta^{13}C_T$ = Tail component $\delta^{13}C$ value.
Y_{SiC} = SiC yield.
$\delta^{13}C_{SiC}$ = SiC $\delta^{13}C$ value.

Solving this equation for Y_{SiC} gave;

$$Y_{SiC} = \frac{(Y_{BC} \times \delta^{13}C_{BC}) - (Y_T \times \delta^{13}C_T)}{(\delta^{13}C_{SiC})}$$

The average $\delta^{13}C$ value of meteoritic SiC is known to be *ca.*+1400‰ (*e.g.* Ash *et al.*, (1991)), leaving the only unknowns in the equation as the yield and istopic composition of the tail component. Assuming the $\delta^{13}C$ value of the tail remained the same as that seen in the peak of the low-temperature combustion, *i.e.* as represented by steps 200 to 400°C, then the isotopic value of the tail could be assumed to be equal to -30‰. Estimating the yield input of this carbon to the overall sample component was not so easy, but it was considered that it most probably lay between 0.5 and 1.5 ng in total, based upon the decay pattern of the contamination combustion profile. By subsituting these values into the equation and using 0.5 and 1.5ng for the outliers of the tail component input, the yield of SiC at 1000°C was found to range between *ca.*23 x 10^{-12}g and 1.5 x 10^{-12}g, and then by taking into account the residue sample mass of 0.0903mg this could be translated into concentrations of 0.25ppm and 0.017ppm. In the preparation of residue 2, the original cryoconite sample mass had been reduced by *ca.*99.84%, so the concentration of SiC within the bulk unprocessed cryoconite could then be estimated to between 0.41ppb and 0.027ppb, and by taking into account that each gram of cryoconite yielded 1 x 10^{-5}g of type S spherule, the concentration of SiC within this spherule component could be estimated to between *ca.*2.7 and 41ppm.

Carbonaceous Chondrites		
Subgroup	SiC (ppm)	Diamond(ppm)
CI	14.1	941
CM2	4.2 to 9.0	360 to 400
CO3	0.3 to 2.0	17 to 165
CV3	0.07 to 0.18	250 to 497
Ordinary Chondrites		
LL3	0.0015 to 1.5	0.5 to 131
L3	<0.04	0.6 to 64
H3	0.006 to 0.11	0.1 to 36
Enstatite Chondrites		
E3 to 5	0.006 to 1.6	0.3 to 67

Table 6.2. Estimated ranges of interstellar silicon carbide and diamond concentrations in bulk samples of primitive chondritic meteorites (after Huss, 1990).

Table 6.1 contains the estimated ranges of the concentration of SiC within the primitive chondritic meteorites. A cursory comparison with the estimated cryoconite type S spherule SiC concentration revealed that a correlation existed between them. In view of the number of assumptions made in the estimation and the possibility that the estimated type S micrometeorite SiC concentration could possibly vary by as much as an order of magnitude, it was not considered viable to make any specific connections to individual meteorite groups, but notwithstanding this, it was believed that the results of the calculation provided good evidence for a meteoritic provenance for the spherules. However, if the SiC concentration did actually fall into the upper limits as suggested by the calculation, then further explanation was required in that either the concentration of type S material had been greatly underestimated, or the other extraterrestrial particles within the cryoconite (*i.e.* unmelted micrometeorites and the spherules <200μm in diameter) also possessed SiC. This was apparent because SiC concentrations greater than a few ppm in the spherules would have manifested themselves in the elevation of $\delta^{13}C$ values in the individual spherule experiments, and this was found not to be the case (5.3.). The conclusion of these arguments was that to balance out the inferred high SiC concentration within the >200mm diameter type S micrometeorites, the smaller dust particles, which although more numerous account for less in total mass (see 1.1.1), would need to yield SiC contents considerably in

excess of the meteoritic values shown in table 6.1. As discussed previously in chapter 1, these higher concentrations of interstellar material would imply that this smaller sized dust fraction was considerably more primitive than the meteorites, an interpretation that is in agreement with a cometary origin.

The $\delta^{13}C$ profile in figure 6.2.C shows a departure at 400-500°C to -34.4±0.4‰. It is interpreted that this represents the combustion of meteoritic interstellar diamond. Swart *et al.*, (1983a) identified the carrier of the anomalous interstellar xenon (Xe-HL) gas component to a carbonaceous species that had been isolated from an acid residue of the Murray CM2 meteorite, and which combusted at 500°C with a $\delta^{13}C$ value between -32 to -38‰. It was not until 1987 that the identity of the species was established by Lewis *et al.*, (1987) as being nanometre-sized diamonds, but similar diamonds have since been isolated from CI and CV3 carbonaceous chondrites, enstatite chondrites and unequilibrated ordinary chondrites (Huss and Lewis, 1989; Alexander *et al.*, 1990), with the realisation that they represent the most abundant interstellar meteoritic component (*e.g.* Huss, 1990). Estimating the concentration of this postulated diamond with respect to the bulk cryoconite (and the micrometeorites within it) was even more problematical than for the SiC, as the $\delta^{13}C$ value at 500°C was the product of diamond, blank, organic contamination and the onset of the combustion of the SiC as illustrated by the elevation of $\delta^{13}C$ to -23.1±0.5‰ by 600°C. Notwithstanding this, an approximation of the possible diamond yield could be made as being between 10 and 20ng of the total *ca.*31ng obtained in the 500°C step. Additionally, from the release profile it was evident that the diamond possessed a $\delta^{13}C$ signature at the light end of the range of -32 to -38‰, because with all of the release not possibly being from the diamond, and with the subsequent mixture of the blank, SiC and organic contamination all pushing the overall value to heavier values, the measured average was still -34.4‰, meaning that the diamond must have been considerably lighter than this. By taking the estimated yield of between 10 and 20ng and by applying the same protocols as applied elucidate the concentration of macromolecular material and SiC in the cryoconite spherule component, the range of diamond concentration within the spherules was estimated to be between *ca.*35500 and 17800ppm.

Comparison to the analogous diamond concentrations in the meteorites in table 6.1 revealed that the correlation was worse than that for the SiC, with the estimated diamond concentration in the micrometeorites being two orders of magnitude greater

than the maximum meteoritic values. However, once again it was considered that after taking into account the increased uncertainties about the absolute yield of diamond from the residue that even this correlation was acceptable. In view that the isotopic signature of the diamond had already been found to vary between -32 and -38‰, it was considered feasible that it could exhibit an even lighter signature, which would again lower the amount of material needed to explain the measured isotopic value from the residue. Even so the concentration of diamond was again shown to be equal or greater than that of the most diamond-rich (primitive) meteorites thus indicating that the smaller micrometeorite grains in the cryoconite were again probably characterised by a high concentration of interstellar material.

6.3. Conclusions of the acid residue study.

The analysis of acid-resistant residues prepared from Greenland cryoconite enabled an assessment of the possibility that interstellar grains maybe present in these deposits (either as discrete grains of from within the micrometeorites).

By comparing the release profiles of residues prepared to slightly different protocols, and by subsequent elimination of terrestrial species that were present as both indigenous phases and contaminants introduced during the handling of the residues, the stepped combustion methods led to the suspicion that minor quantities of isotopically anomalous materials were present. The stepped combustion data can be interpreted to suggest that interstellar graphite, diamond and silicon carbide are all present , and in proportions that are not unreasonable for primitive meteorites, *e.g.* carbonaceous and type-3 ordinary chondrites. Furthermore, the carbonaceous macromolecular material within the residues was found to probably represent a mixture of the previously isolated micrometeoritic and algal components.

Attempts to estimate the relative concentrations of the graphite, diamond and SiC components within the micrometeorite fraction of the bulk cryoconite were problematical due to interfering species in the combustion profiles of the residues, and uncertainties involved with the absolute concentration of micrometeorites in the cryoconite, therefore the results have to be considered as upper limits only. Even allowing for the fact that the micrometeorite concentration in the cryoconite may have been underestimated, the calculated concentration of silicon carbide and diamond in the

>200μm diameter type S micrometeorite fraction of the cryoconite was equivalent, or displayed considerable enrichments, when compared to that found in the primitive meteorites. This result conflicts with the evidence from the studies of individual micrometeorites (chapter 5) >200μm in size, where stepped combustion analyses show no sign of elevated $\delta^{13}C$ values at high temperature or measurements attributable to diamond. This observation suggested that the smaller (<200μm) micrometeorite fraction in the cryoconite might contain interstellar SiC and diamond. Whilst it was not possible to accurately estimate the concentration of SiC and diamond within these smaller micrometeorites, it was suggested that perhaps they possessed higher concentrations than either the larger type S micrometeorites or the most primitive chondritic meteorites, which could possibly infer a cometary provenance.

A mineralogical study of the residues showed the refractory component of the cryoconite to be dominated by spacecraft debris that had presumably become concentrated within the cryoconite by the same mechanisms as the micrometeorites.

Chapter 7

Small Sample Meteorite Pulse-Heating Experiments.

7.1. Introduction.

The stable carbon isotopic results from the analysis of deep-sea, Greenland and Antarctic micrometeorites discussed in chapter 5 suggested that a genetic relationship may exist between the micrometeorites and the meteorites. This conclusion is based upon the observation of components with carbon isotopic compositions which are equivalent in the ordinary and carbonaceous chondrites and micrometeorites. These individual components and the bulk $\delta^{13}C$ value and carbon concentration of the micrometeorites were used to constrain comparisons to the major meteorite groups. The strongest evidence for the asteroidal provenance of the micrometeorites was the identification of a probable meteoritic macromolecular carbonaceous component from the individual sample experiments (5.3).

Within chapter 5 comparisons were made between the bulk micrometeorite isotopic signatures and the conventional meteorite groups to facilitate generic connections between the two. However, the data used for this comparison (table 5.3) were compiled from different investigators who used different analysis protocols and equipment, but more importantly, on large (> milligram) samples taken from much larger aliquots of crushed (homogenised) meteorite. Assuming that the micrometeorites represented random microgram fragments of asteroidal (meteoritic) material produced by collisions either in the asteroid belt or during transit of the parent meteorite to Earth, then analysis of similar sized chips of meteorite would be useful to determine whether the comparisons to the crushed homogenised samples were valid. A second problem affecting the comparisons discussed in chapter 5 is that micrometeorites have all experienced a certain degree of heating during atmospheric retardation. To address this problem it was decided to investigate how carbon

components would behave during pulse-heating. A natural analogue of pulse-heated micrometeorites is meteorite fusion crust. Analysis of fusion crust fragments can also address the hypothesis that the micrometeorites were simply quenched melt droplets from the ablation of much larger (>gram) meteorites.

It must be stressed that the experiments and results presented and discussed within this chapter are only of a preliminary nature. It is recognised that due to natural heterogeneities within the meteorites analysed, experiments ideally need to be duplicated in order to gain a representative picture of carbon abundance and isotopic composition. Likewise it is understood that the parameters used in the pulse-heating experiments need to be extensively varied to fully replicate atmospheric entry heating. Notwithstanding these limitations, this chapter forms an important part of the thesis as a first attempt to address the problems outlined above.

7.1.1. The pulse-heating method.

Many investigators have attempted to model the deceleration of micrometeorites in the atmosphere (*e.g.* Whipple, 1950b, 1951; Opik, 1956; Hawkins, 1964; Hughes, 1978; Fraundorf, 1980; Bonny *et al.*, 1988; Flynn, 1989; Sandford and Bradley, 1989; Love and Brownlee, 1991). As a first approximation to replicate the heating episode experienced by a micrometeorite upon atmospheric entry it was decided to pulse-heat microgram-sized whole-rock meteorite chips to either *ca.*800°C or 1500°C for *ca.*10 seconds. The lower figure was considered to approximate the probable lowest temperature that a microgram sized sample could experience, whereas the upper one was dictated by the limit attainable by the furnace used for the experiment.

The experiment protocol used for the pulse-heating was as follows;

(1) The sample chips were broken from the parent meteorite in the clean room using stainless steel implements. These implements had been pre-cleaned by ultrasonication in a 50:50 mixture of toluene and methanol (AnalaR Grade, BDH Chemicals, Poole, U.K.) and then air-dried at *ca.*100°C overnight.

(2) The meteorite chips were then washed in *ca.*50ml AnalaR grade dichloromethane (CH_2Cl_2) and manipulated into a platinum foil sample envelope.

(3) The sample envelope was then placed into a petri dish (pre-cleaned by combustion in atmosphere at *ca.*600°C for *ca.*1 hour) and removed from the clean room.

(4) The pulse-heating apparatus is illustrated in figure 7.1., and consisted of a resistance wire furnace with thermocouple and a *ca.*15cm length of quartz glass tube (3mm internal diameter). The glass tube had been pre-cleaned by combustion in atmosphere to *ca.*1000°C for *ca.*10 hours. The furnace was preset to either 800 or 1500°C and the glass tube placed in position *ca.*5 minutes before the apparatus was required.

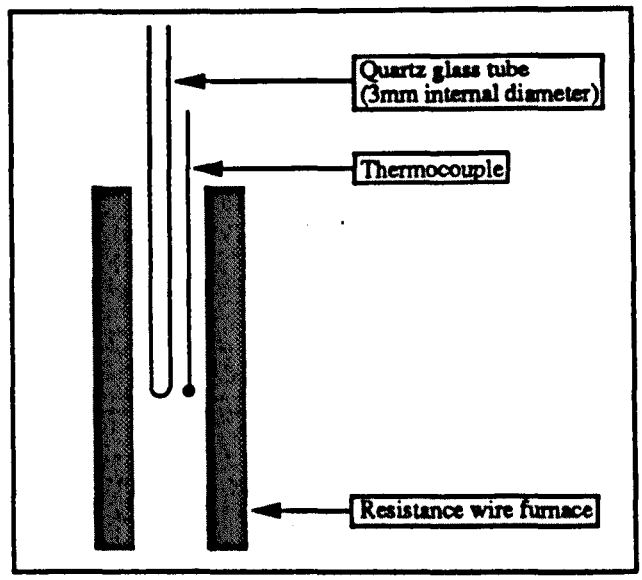

Figure 7.1. The experimental apparatus used for the pulse-heating of microgram-sized meteorite chips.

The sample envelope was dropped down into the glass tube, and after 10 seconds the tube was removed and the envelope tipped into a second pre-cleaned quartz glass tube (5mm internal diameter). This second tube was at room temperature and so facilitated rapid cooling of the sample.

(5) The sample envelope was then loaded into the MS86 gas extraction line as described in 2.3.2.

For comparison purposes to the pulse-heated meteorite chip results, stepped combustion plots for the both 800 and 1500°C pulse-heated blank experiments are reproduced in figure 7.2.

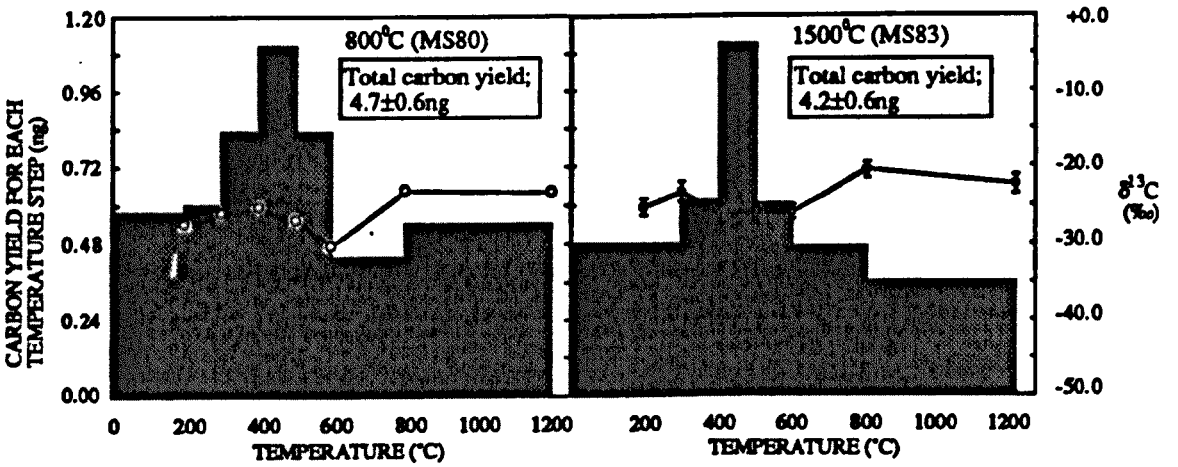

Figure 7.2. Stepped combustion plots of platinum foil sample envelopes that have been pulse-heated to either 800 or 1500°C using the protocol described in the text.

The samples of whole-rock meteorite and fusion crust that were not subjected to pulse-heating were prepared in accordance with steps (1) to (3) above, but before removing from the clean room, the sample envelopes were submerged in CH_2Cl_2. A stepped combustion plot of a blank experiment prepared according to this procedure (protocol D - 4.4.5) is presented in figure 7.3.

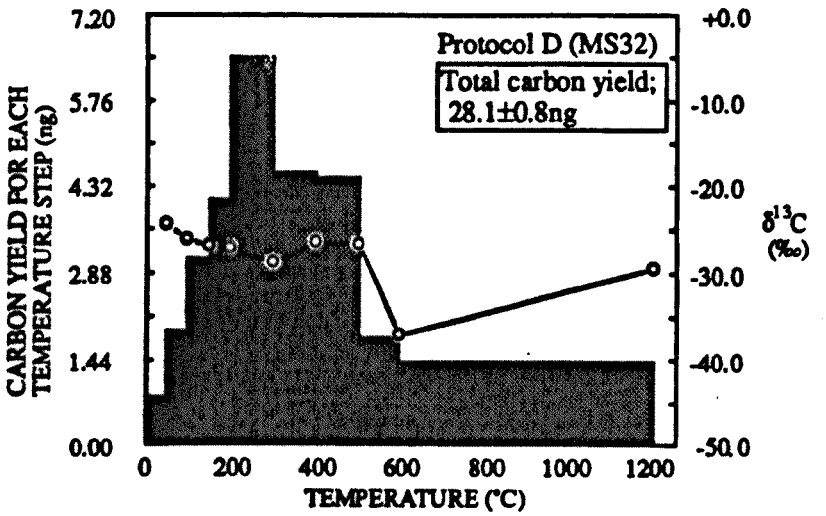

Figure 7.3. A stepped combustion plot of a protocol D experiment blank. This protocol corresponds to that used in the analysis of microgram-sized samples of whole-rock meteorite and meteorite fusion crust.

7.1.2. Meteorite selection.

Three meteorites were chosen for the proposed experiments;

(i) Allende (CV3 carbonaceous chondrite).

(ii) Weston (H4 ordinary chondrite).

(iii) Goalpara (ureilite achondrite).

The meteorites were chosen because they all have a significant carbon abundance, but more importantly, this carbon is present in largely differing forms within each meteorite (7.2). Secondly, for all of the samples it was possible to obtain a small sample of fusion crust which could be analysed for comparison to the artificially heated material. Thirdly, stepped combustion profiles of homogenised samples were available, and this was important so that the heterogeneity of the microgram-sized samples and the survival of carbonaceous species after pulse-heating could be addressed.

7.2. Results.

Table 6.2 shows the bulk blank-corrected results from the analysis of the microgram-sized meteorite samples compared to analogous examples executed on larger homogenised samples taken from the literature.

Sample	Type	Yield(wt%)	$\delta^{13}C$(‰)	Literature analyses		
Weight (μg)				Yield(wt%)	$\delta^{13}C$(‰)	Key
Allende	CV3	0.46	-16.1±0.5	0.27	-18.3	1
54				0.30	-17.3	2
				0.27	-16.4	3
Weston	H4	0.045	-23.3±0.4	0.28	-23.8	1
101				0.27	-27.3	1
				0.28	nm	4
Goalpara	Ureilite	0.055	-4.6±0.4	0.23	-10.03	1
102				0.22	-11.54	1
				1.54	nm	5
				nm	-8.4	6

nm Not measured.
(1) Grady, (1982).
(2) Smith and Kaplan, (1970).
(3) Chang *et al.*, (1978).
(4) Moore and Lewis, (1967).
(5) Wiik, (1972).
(6) Vdovykin, (1970).

Table 7.1. A comparison of the bulk carbon isotopic results obtained from the small meteorite sample experiments with the literature.

The results within table 7.1 show that the isotopic signatures obtained from the analysis of the small samples were in good agreement with the larger homogeneous samples, whereas the carbon yields were in error by as much as an order of magnitude. This observation implied that the generic connections made in chapter 5 between the micrometeorites and meteorites based upon bulk $\delta^{13}C$ values were valid. Goalpara, the one exception in the isotopic correlation, is an achondritic meteorite of the ureilite group, and is known to be composed of mafic silicates set in a carbon rich matrix (Vdovykin, 1970). Within this matrix, graphite and micron sized diamond are the dominant phases, and these are known to possess a $\delta^{13}C$ signature of *ca.*-4‰ (*e.g.* Grady, 1982), so it was apparent that the sample analysed, although reduced in overall carbon content, was relatively enriched in these species as illustrated by the measured bulk isotopic value of *ca.*-5‰.

Subsequent comparison of the bulk blank-corrected $\delta^{13}C$ microgram-sized meteorite results to the analogous data for the Greenland and Antarctic micrometeorites (figure 7.4) revealed that both Weston and Allende could be correlated with the micrometeorites in yield and isotopic composition, but Goalpara was distinct in yield, and more importantly, isotopic composition.

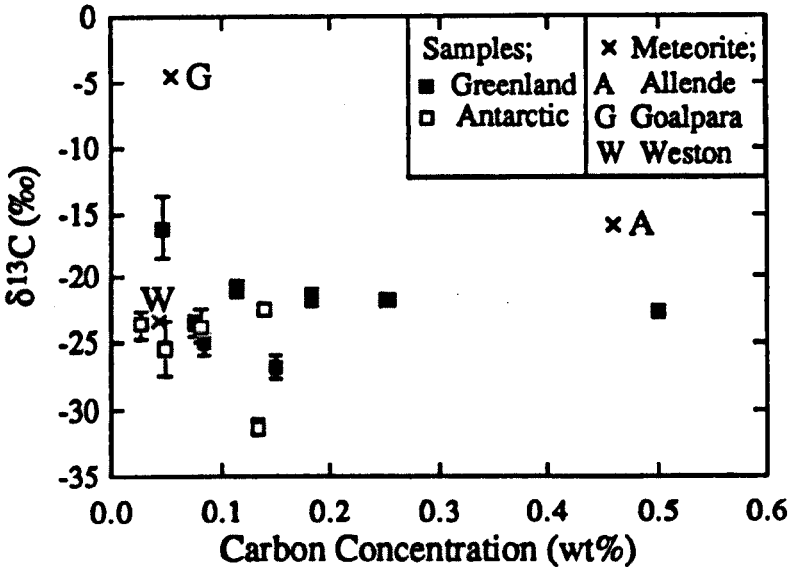

Figure 7.4. Bulk blank-corrected carbon concentrations and $\delta^{13}C$ values for the microgram-sized whole-rock meteorite samples compared to analogous results for the individual Greenland and Antarctic micrometeorites. (The errors in carbon concentration and $\delta^{13}C$ of the meteorite samples are smaller then the symbols).

Figure 7.5 is a version of 7.4 which shows a comparison of the micrometeorites to the meteorite fusion crust experiments. In comparing the two figures it was evident that the isotopic fit of the micrometeorites to the meteorite fusion crusts was closer than to the bulk meteorite results. The total carbon contents of the fusion crusts were measured at 0.63 wt% for Weston, 0.98wt% for Goalpara and 0.25wt% for Allende. It was interesting to note that notwithstanding the observation that the yield measurements had already been shown to be unreliable for comparison purposes to the conventional meteorite groups, all of these yields (apart from Allende) were larger than the literature values for the bulk samples. All of the fusion crust samples were taken from the meteorites at a depth of *ca.*0.5 to 1mm below the outer edge of the crust and so should have been spared contamination from direct handling.

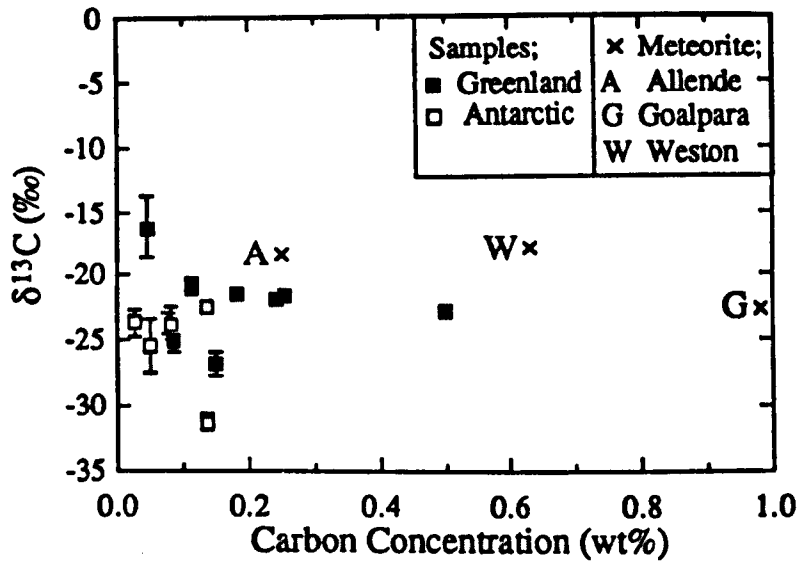

Figure 7.5. Bulk blank-corrected carbon concentrations and $\delta^{13}C$ values for the microgram-sized whole-rock meteorite fusion crust samples compared to analogous carbon results for the individual Greenland and Antarctic micrometeorites. (The errors in carbon concentration and $\delta^{13}C$ of the meteorite samples are smaller then the symbols).

Table 7.2 shows that Allende is the youngest specimen, and being an observed fall is known to have a terrestrial age of only *ca.*20 years. Of equal importance is that Allende was collected and curated within hours of its fall (King *et al.*, 1969) and so has been spared much of the handling that the others have undoubtedly suffered. Within figure 7.5 Allende shows the closest fit to the micrometeorites, and being the freshest sample this observation suggests that a connection could indeed exist with meteorite fusion crusts and the micrometeorites.

Sample	Fall/find	Recovered
Allende	Fall	1969
Weston	Fall	1807
Goalpara	Find	1868

Table 7.2. Details of the collection of the meteorites samples analysed (After Graham *et al.*, 1985).

Figure 7.6 presents a comparison between the micrometeorites and the pulse-heated meteorite samples, but in addition to the previous experiments the bulk isotopic composition of the pulse-heated blank experiments is included.

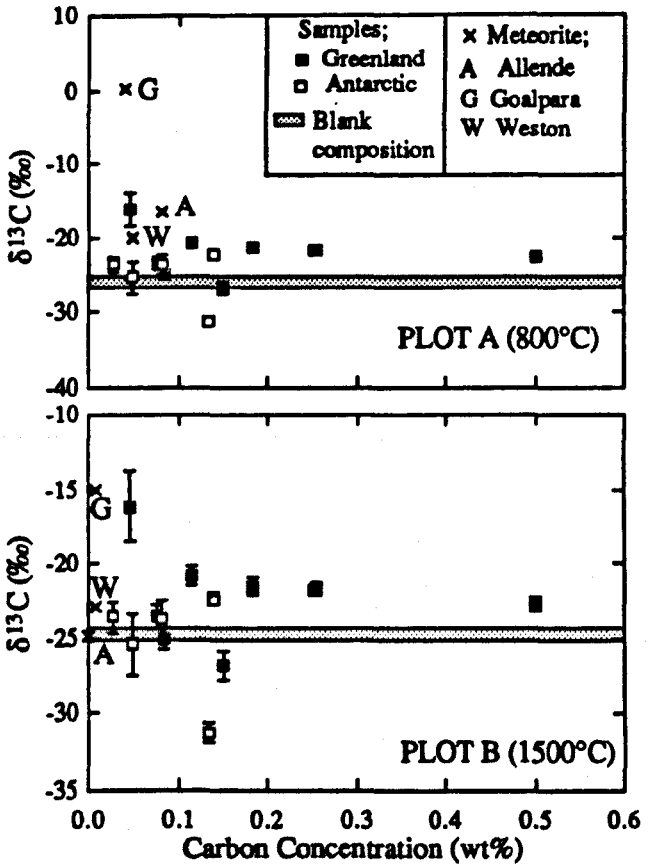

Figure 7.6. Bulk blank-corrected carbon concentrations and $\delta^{13}C$ values for the microgram-sized whole-rock meteorite samples that had been pulse-heated to 800°C (plot A) and 1500°C(plot B) for 10 seconds compared to analogous carbon results for the individual Greenland and Antarctic micrometeorites. (The errors in carbon concentration and $\delta^{13}C$ of the meteorite samples are smaller then the symbols).

The 800°C pulse heated samples of Allende and Weston showed the closest correlation to the micrometeorites of any of the experiments, and so suggest that a generic connection could be made between the two. Also of interest was that Goalpara had retained its heavy isotopic signature, thereby indicating that the diamond and graphite components had survived the heating episode. The results for the 1500°C heated samples indicated that if the micrometeorites were indeed related to macrometeoritic precursors by pulse heating for ten seconds, then the temperature of 1500°C was too high, as in all three samples the carbon concentration was reduced to blank levels. This being said, only Allende and Weston yielded isotopic compositions similar to the blank, Goalpara still retained some heavy carbon, again implying that the diamond/graphite had to some extent survived the 1500°C pulse heating. The experiment temperature of 1500°C was considerably in excess of the normal combustion temperature of these species (*ca.* 600-800°C), so their survival within the sample suggested that the length of the heating episode was also crucial in determining the fate of the components. The behaviour of the carbon inventory of the samples can be investigated more fully by the examination of the individual stepped combustion plots for the meteorite experiments. The stepped combustion plots for the bulk sample, fusion crust and pulse-heated samples of Allende are shown in figure 7.7.

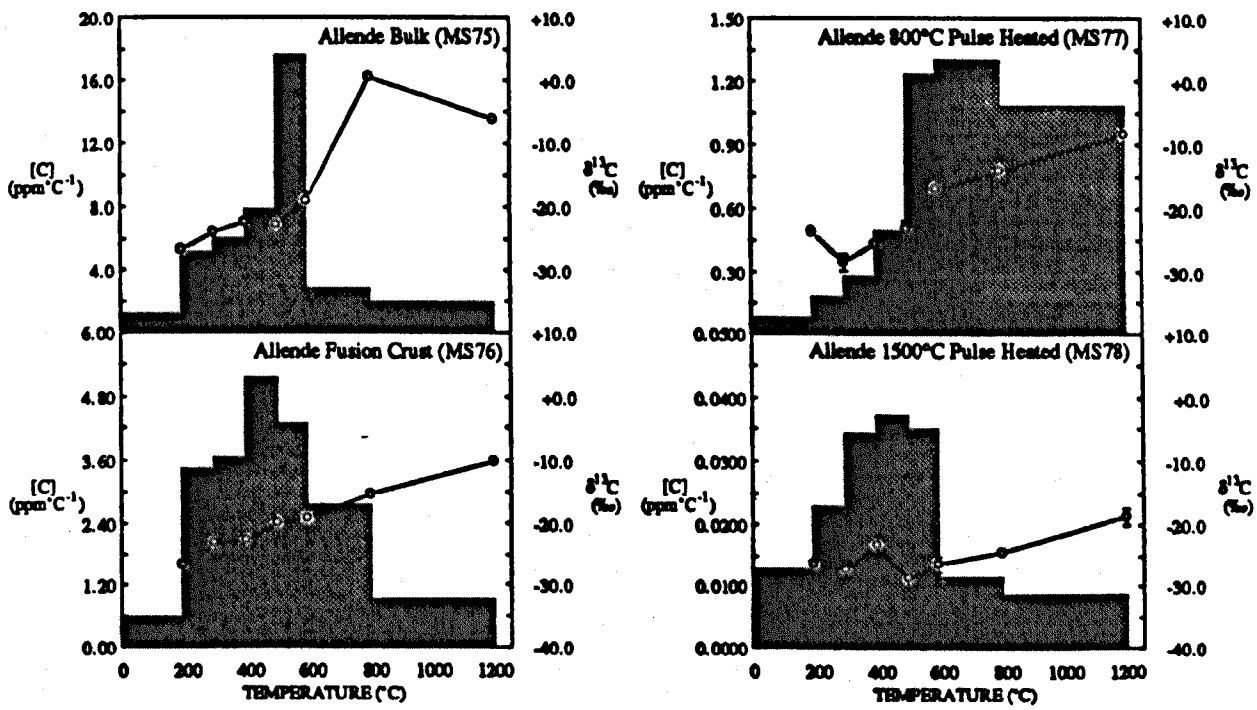

Figure 7.7. Stepped combustion plots for the Allende whole-rock, fusion crust and pulse-heated whole-rock microgram-sized sample experiments.

The carbon inventory of Allende is known to be dominated by a 'poorly crystalline graphitic' component (Smith and Buseck, 1981) which can be seen in the combustion profile of MS75 between 500-600°C. The combustion of this component, along with a minor input of isotopically heavier carbon at higher temperatures which can possibly be attributed to the combustion of interstellar SiC (*e.g.* Ash *et al.*, 1990), gives the sample its bulk (blank corrected) $\delta^{13}C$ value of -16.1±0.5‰. The measured bulk $\delta^{13}C$ value of the fusion crust was -18.3±0.4‰ and this similarity could be attributed to the partial survival of the graphitic component, with the slight lowering of the value probably due to an input of organic contamination with a $\delta^{13}C$ value between -20 to -30‰ at lower temperatures. This observation is extremely important for the survival of the micrometeorite carbonaceous species. The fusion crust represents the final molten material produced during the deceleration of the meteorite before the ablation temperature dropped below its melting point. Blanchard and Cunningham (1974) performed a set of experiments to mimic this ablation process by using an air plasma jet on samples of olivine, and successfully produced material similar in composition to the fusion crust of Allende. Directly determining the temperature at which the ablation had occured within the experiment was not possible, but to melt the olivine it must have been in excess of *ca.*1900°C (the melting point of Mg-rich olivine). Even at these temperatures the stepped combustion experiment carried out on the Allende fusion crust has shown that a proportion of the original carbon inventory of the meteorite had survived, and with apparently little isotopic fractionation. The stepped combustion plot for the 800°C pulse-heated Allende sample showed that although only *ca.*18% of the original carbon inventory remained from the bulk sample (MS75), there had been only a *ca.*50% reduction in the carbon >600°C, again indicating that a proportion of the graphitic carbon had survived the heating episode. The 1500°C heated sample of Allende placed an upper limit for the survival of any indigenous carbon as it yielded results identical to the experiment blank.

The individual stepped combustion plots for Weston are shown in figure 7.8. As previously indicated by the bulk results in figure 7.5, the fusion crust sample of Weston contained an order of magnitude more carbon than the bulk sample. The stepped combustion plot of the fusion crust (MS60) shows how this excess carbon was distributed. Attempting a comparison to the bulk microgram sized sample (MS61) was of little use because it was evident from table 7.1 that the sample was considerably reduced in carbon with respect to the literature values. The overall carbon content of the fusion crust of 0.63wt% was approximately double that of the literature values for

the bulk meteorite, and a comparison to a stepped combustion profile from Grady *et al.*, (1989) showed that this excess occurred in the >600°C release. The fusion crust analysed here contained *ca.*0.4wt% carbon in the 600-1200°C regime whereas Grady *et al.*, (1989) found only *ca.*0.037wt% across the same temperature range, and it is difficult to believe that this enrichment merely reflected sample heterogeneity. Weston is a solar-wind gas-rich breccia, an inhomogenous mixture of clasts of dark and light material, but these clasts have similar carbon contents (*e.g.* Grady, 1982). Weston was collected as a fall in 1807 and so has a terrestrial age of *ca.*185 years, so it could perhaps be expected that after this period of repeated handling and curation in the museum collections that the fusion crust would be contaminated by organics. However, such organic material does not combust at such high temperatures, and to further complicate matters, the excess carbon yielded an isotopic composition between *ca.*-16 to -13‰, which is outside of the range normally encountered in terrestrial contaminants.

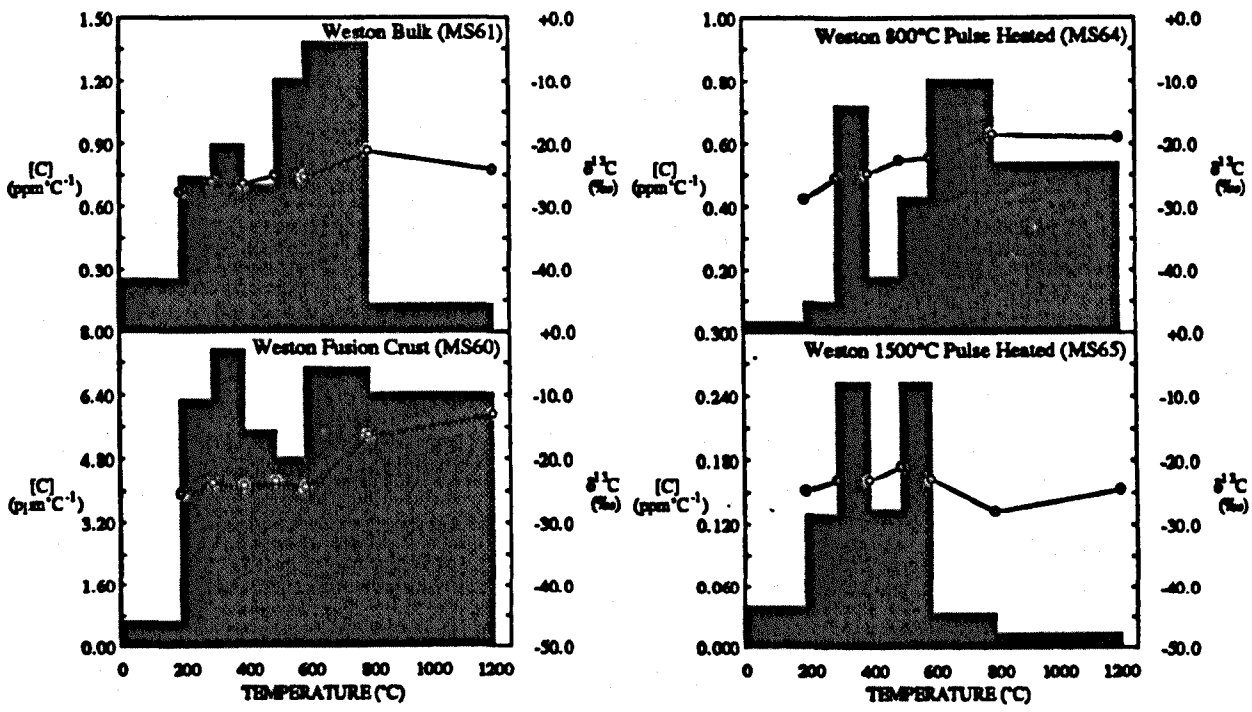

Figure 7.8. Stepped combustion plots for the Weston whole-rock, fusion crust and pulse-heated whole-rock microgram-sized sample experiments.

It is proposed that the following sequence of events could explain the excess carbon in the Weston fusion crust. The fusion crust represents quenched molten material formed during atmospheric entry heating. It is perhaps possible that as the temperature dropped below the melting point of the ablating minerals, the final quenched melt trapped carbonaceous material within it. It is postulated that it is this trapped material that is being released in the fusion crust stepped combustion plot >600°C. The $\delta^{13}C$ value of this trapped material of *ca.*-13 to -16‰ is possibly a result of isotopic fractionation. It is argued that the trapped material in the fusion crust represents low temperature carbon that has preferentially lost ^{12}C by distillation during atmospheric entry heating. Some evidence to substantiate this hypothesis is available in that the 800°C pulse-heated stepped combustion plot of Weston shows carbon >600°C with a higher $\delta^{13}C$ than the bulk sample, and approaching that of the fusion crust. This model can only be regarded as tentative because the Weston experiments have not been duplicated.

Table 7.3 has been constructed to enable interpretation of the pulse-heated samples of Weston and Goalpara. Within the table the yields obtained for the 600-800°C and 800-1200°C temperature steps for the 800°C pulse-heated samples are compared to the same results for the stepped combustions performed on the bulk homogenised meteorites samples by Grady, (1982) and Grady *et al.*, (1989).

Sample	Carbon yields for the high temperature regime (ppm)			
	Grady, (1982)		Pulse-heated	
	600-800°C	800-1200°C	600-800°C	800-1200°C
Weston	504	286	161	215
Goalpara	790	230	264	92

Table 7.3. A comparison of carbon yields obtained from the high temperature regime of stepped combustions performed on the 800°C pulse heated microgram samples of Weston and Goalpara with the analogous results taken from the analyses of milligram-sized samples of homogenous bulk samples by Grady, (1982) and Grady *et al.*, (1989).

The stepped combustion plot of the 800°C pulse-heated sample of Weston (MS64) yielded 161ppm carbon between 600 and 800°C and 215ppm between 800 and 1200°C. The unheated bulk Weston combustion plot (MS61) yielded 270ppm between 600 and 800°C and 50ppm between 800 and 1200°C. This observation

suggests that *ca.*60% of the 600-800°C carbon had survived pulse-heating, but that an enrichment had occured in the 800-1200°C regime. However, comparison to the results for Weston in table 7.3 reveals that this apparent enrichment was probably solely a product of sample heterogeneity; the 800-1200°C Weston yield in table 7.3 is 286ppm which is comparable to the 274ppm obtained from the 800°C pulse-heated sample. Once again, as with Allende, the 1500°C heated sample of Weston produced results similar to the experiment blank.

The fusion crust of Goalpara had also been shown to exhibit excess carbon over both the microgram sample and the literature bulk values, but in contrast to the complicated interpretation of the fusion crust excess in Weston, the plot for the stepped combustion profile for the Goalpara crust (MS70 in figure 7.9) revealed that this excess occurred in the low temperature region with isotopic values of *ca.*-22 to -24‰.

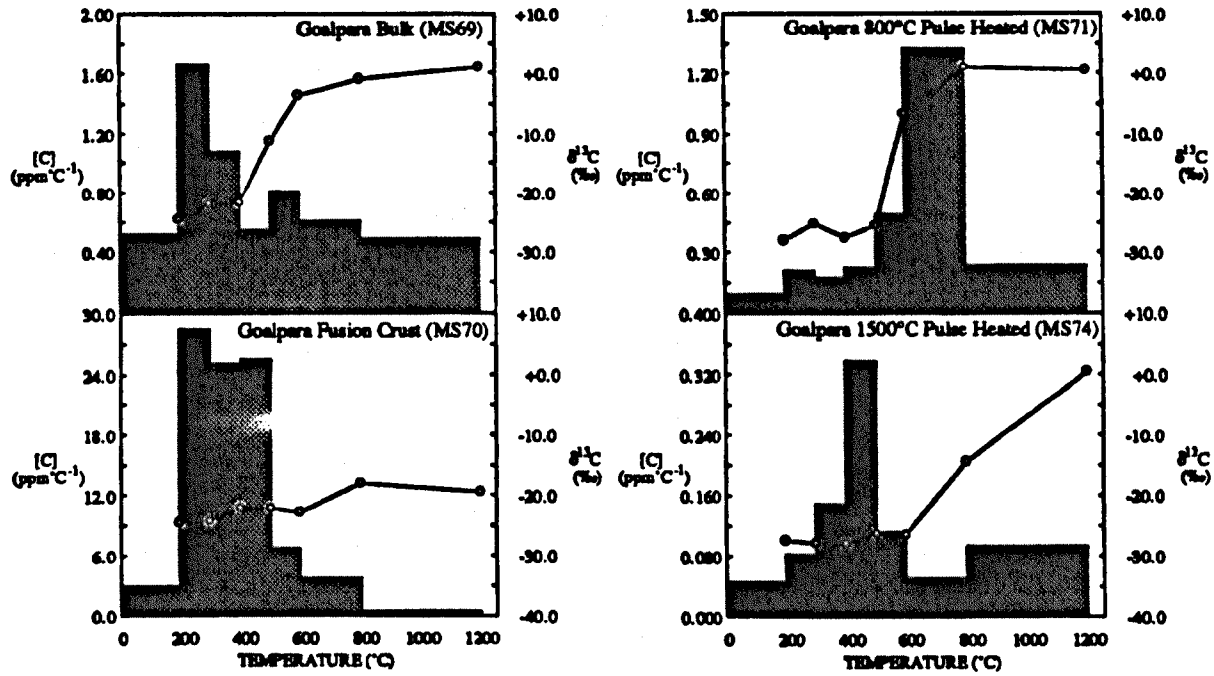

Figure 7.9. Stepped combustion plots for the Goalpara whole-rock, fusion crust and pulse-heated whole-rock microgram-sized sample experiments.

Correspondingly, this excess could be attributed to a terrestrial organic provenance, and was in agreement with its *ca.*124 year terrestrial age. When compared to the unheated microgram-sized bulk sample, the 800°C pulse heated stepwise plot indicated that an apparent enrichment had occured in the 600-800°C regime, but once again this could be explained by sample heterogeneity, as the data in table 7.3, showed that the homogenised sample could yield twice as much carbon across this temperature range.

The 1500°C heated sample stepwise (MS74) showed that even though the yields of carbon had been reduced to blank levels across the combustion plot, the isotopic profile gave evidence for the partial survival of the components responsible for the elevation in $\delta^{13}C$ apparent in the unheated and 800°C pulse heated samples.

7.3. Conclusions.

The analysis of microgram-sized samples of bulk meteorite showed that even though the yields obtained from the experiments did not correlate with equivalent results carried out on much larger aliquots of crushed (homogenous) samples, the isotopic signatures were in good agreement. This result was of considerable importance as it corroborated the genetic interpretations made between the individual micrometeorite bulk sample signatures and the major meteorite groups in chapter 5. More specifically with this meteoritic provenance in mind, in this chapter a comparison between the individual micrometeorite analysis results with the microgram sized bulk meteorite signatures indicated that Weston (H4 ordinary chondrite) and Allende (CV3 carbonaceous chondrite) could be directly correlated to the micrometeorites.

An attempt to investigate the carbon inventory of meteorite fusion crusts to explore a possible genetic connection to the micrometeorites was hampered by the problem of contamination, but Allende, the most pristine and youngest sample in terms of terrestrial age, again exhibited a good correlation in bulk carbon content and $\delta^{13}C$ values. The stepped combustion plot of the Allende fusion crust showed that the graphitic and SiC components had partially survived the ablation process, and even though the exact conditions associated with such ablation were unknown, this observation could be extrapolated to the possible survival of the carbonaceous species within the micrometeorites. The fusion crusts of Weston and Goalpara both showed large carbon enrichments over the literature bulk values. The excess carbon in Goalpara could be interpreted as terrestrial contamination, but the excess in Weston is more difficult to reconcile with this provenance. It was considered possible that the excess carbon in the Weston fusion crust represented carbonaceous species trapped during the last stages of ablation.

The 800°C pulse-heated samples of Allende and Weston showed the closest correlation to the micrometeorite results of all the meteorite experiments. This

observation implied that the carbon inventory of the micrometeorites could be fashioned by such a heating event applied to meteoritic precursor material, and the most plausible scenario for this would seem to be meteoritic dust being heated during atmospheric retardation upon collection by the Earth. However, this model does not explain how the micrometeorites gained their distinctive spherical morphology which is intuitively the result of melting accompanying their atmospheric retardation. A possible explanation would seem to be either that the samples acquired their spherical morpholgies contemporaneously with their original (meteoritic) carbon inventory. It has long been hypothesised that cosmic spherules could exist as entities in the IPM (Parkin *et al.*, 1977), but having been formed by collisions and subsequent melting of asteroids, would not appear to offer a satisfactory solution to the problem. Presper and Palme (1991) found nickle to iridium ratios within melted (spherical) Arctic micrometeorites that indicated the particles were identical, and possibly the precursors to, chondrules within the primitive chondritic meteorites. However, a connection to meteorite chondrules is also perhaps not helpful here, in view that the majority of carbonaceous species are concentrated in the matrix as opposed to the chondrule fraction of the meteorites.

Klock and Beckerling (1991) have shown that *ca.*25% of Greenland spherical micrometeorites are only partially melted, and Maurette *et al.*, (1991) found extraterrestrial neon in a number of completely melted Greenland particles. The almost ubiquitous prescence of the macromolecular component in the micrometeorites discussed in chapter 5 required that such volatile species are retained in all of the samples. It has already been shown in this chapter that the fusion crust of Allende contains residual indigenous carbon, so it is perhaps likely that microgram-sized ablating particles could likewise be melted and still retain much of their original carbon inventory. With the recent discovery of large (*ca.*1mm diameter) ummelted micrometeorites in Greenland and Antarctica (Maurette *et al.*, 1988; Robin *et al.*, 1990) and low-temperature minerals (Bradley and Brownlee, 1991) and undepleted volatile element patterns (Stadermann, 1991) within <50μm diameter unmelted particles indicating that they had not been heated above *ca.*250°C, the original theories constraining the deceleration and heating of extraterrestrial particles devised by Whipple (1950b), which predicted that both of these situations were impossible, have been re-evaluated. Verniani (1969) suggested that the initial deceleration of an incoming particle could be increased, and so the concomittant peak temperatures be reduced, by lowering the average particle density upon initial melting. Bonny *et al.*,

(1988;1991) developed and quantified a similar example to this so-called 'frothing model' where they postulated that the micrometeorites possessed a organic coating that acted as a shield to ablation by pyrolysing upon ablation heating. Such models offer an explanation as to how micrometeorites can enter the atmosphere and suffer less severe heating, but do not help with the production of melted particles with intact carbon inventories.

Of the attempts to re-evaluate the theories and calculations of Whipple (1950b; 1951), the most thorough has been the study by Love and Brownlee (1991). They used improved criteria for the structure of the upper atmosphere and took into account gravitational acceleration and determined numerical solutions for 50,780 examples of impacting micrometeorites between 0.001 and 1mm diameter at entry velocities of 11.2 to 72kms^{-1}. The most relevant of their conclusions to the problem here was that the maximum temperature experienced by a particle had a duration typically less than one second, and the samples that underwent total melting only spent *ca.*2 seconds above their melting points. These conclusions have two major implications for the results discussed in this chapter;

(1) The 10 second period used in the pulse-heating experiments was at least 5 times too long.

(2) If the molten state is only achieved for such a short period, then the situation is increasingly comparable to that of meteorite fusion crust formation.

The pulse-heating experiments using the 10 second heating period have shown that meteoritic carbonaceous species can partially survive within microgram-sized particles at *ca.*800°C. If the duration of the pulse-heating is reduced then it is anticipated that an even higher proportion of the carbon could survive, and that higher tempertures could be used and still yield the same results. The fusion crust experiments showed that indigenous carbon had survived total melting, and so the latter implication (2) suggests that perhaps a pathway exists for both the production of the (spherical) melted micrometeorite morphology and the (partial) survival of the original carbon inventory of the parent body.

Chapter 8

Summary and Future Work.

8.1. Summary.

The aim of this thesis was to undertake a detailed, systematic examination of the content and stable isotopic composition of carbon within micrometeorites. Before the primary objective could be addressed, it was necesssary to devise a scheme of analysis for each micrometeorite that allowed the petrographic type of the sample to be determined whilst minimising any extraneous carbon contamination. This was achieved by cleaving individual micrometeorites by crushing directly onto a clean platinum foil substrate. After a fragment had been removed for petrographic work it was then possible to fashion the foil into a sample envelope ready for introduction into the mass spectrometer carbon dioxide extraction line.

A previous preliminary examination of carbon in individual micrometeorites (Wright *et al.*, 1988) had highlighted two main problems;

(1) Terrestrial contamination largely controlled the yield and $\delta^{13}C$ of the carbon obtained from the samples.

(2) The mass spectrometer used for the analysis of the micrometeorites was not sufficiently sensitive to be able to determine the $\delta^{13}C$ of the nanogram amounts of carbon obtained with sufficient precision to enable separation of indigenous components from contamination, and analytical blank contributions.

Before the successful isolation and identification of indigenous micrometeorite carbon components could be achieved, these problems needed to be solved. An ultra-high sensitivity gas source carbon stable isotope static mass spectrometer built by Mr S.J.Prosser and Dr I.P.Wright (Prosser *et al.*, 1990) offered the opportunity of addressing both questions. A full evaluation of the instrument was carried out as a prelude to a comprehensive study of a stepped combustion experiment protocol and sample handling procedures to minimise carbon contamination (the blank). The new mass spectrometer (MS86) was able to routinely determine the $\delta^{13}C$ of *ca.*1ng of

carbon with a precision of *ca.*<±1‰. The carbon contamination associated with the sample analysis protocol was found to be extremely variable, being constituted of components that could be traced to specific procedural steps during the preparation stage, but also of random contamination events. Notwithstanding this variability in the overall contamination, detailed interpretation of numerous blank experiments enabled the possible range of contaminants to be largely constrained both in absolute amounts of carbon and $\delta^{13}C$, and coupled with the improved mass spectrometer performance it was anticipated that indigenous carbon components could be resolved from contaminants with confidence.

Analyses of the micrometeorite sample fragments removed for petrographic work using an analytical electron microscope (AEM), allowed the samples to be successfully allocated to mineralogic and morphological groups. The major element data acquired by the AEM proved to be of sufficiently high quality so that it could also be used as evidence of extraterrestrial origin and to monitor the effects of algal contamintion in the Greenland micrometeorites.

Stepped combustion carbon analysis of an aliquot of *ca.*20 type S deep-sea micrometeorites on the Triple Collector suggested that a generic connection could be made with the ordinary chondrites. Whilst the bulk carbon signature from a similar deep-sea type I multiple-sample experiment could be interpreted with an iron meteorite provenance, the individual carbonaceous components that constituted the bulk value were difficult to reconcile with such an origin. Stepped combustion analyses of individual Greenland and Antarctic samples on MS86 enabled a more detailed insight into the carbon inventory of the type S micrometeorites. Examination of individual micrometorite stepped combustion profiles and comparison to the results of experiment blanks and analyses of cryoconite algae revealed the possible presence of carbonaceous components indigenous to the micrometeorites. Carbon combusting between 200 and 500°C with a $\delta^{13}C$ of *ca.*-18 to-25‰ was found to be almost ubquitous to the samples, and although a tentative link could be made with similar carbon from the ordinary chondrites, the component could be more closely correlated with carbonaceous chondrite macromolecular material. The concentration of the component in the micrometeorites (*ca.*0.02 to 0.15wt%) was similar to that within the CV and CO carbonaceous chondrites, but with the observation from the small-sample whole-rock meteorite experiments that $\delta^{13}C$ was probably a more reliable tool for

determining the provenance of microgram-sized samples, a connection to the CI, CM or CR chondrites cannot be ruled out. Based on this isotopic evidence it was apparent that the micrometeorites analysed represented either quenched melt droplets from ablating meteorites, or material produced by collisions within the asteroid belt that had then evolved under P-R drag into orbits conducive for collection by the Earth. Contemporary meteorite falls are dominated by the ordinary chondrites (*e.g.* Graham *et al.*, 1985). The asteroid belt is believed to be largely composed of bodies that are believed to represent the parent bodies of the carbonaceous chondrites (*e.g.* Lipschutz *et al.*, 1989). Over half the Earth-crossing asteroids that have been successfully imaged to determine their spectral reflectance type could possibly represent parent bodies of CV and CO chondrites (*e.g.* McFadden *et al.*, 1989). If the cautious interpretation of a predominately CV or CO chondrite micrometeorite provenance is correct, then it is interesting to speculate whether, like contemporary meteorite falls (Graham *et al.*, 1985), the >200μm micrometeorite flux to Earth is derived from these bodies.

The preparation and carbon isotopic analysis of acid-resistant residues of Greenland cryoconite revealed the presence of components that could be linked to pre-solar dust grains of silicon carbide (SiC), graphite and diamond. The presence of pre-solar grains in the micrometerites gave further evidence for a genetic link to the primitive chondritic meteorites.

The postulated survival of a macromolecular carbon species within the apparently melted >200μm diameter micrometeorites prompted an investigation into the effects of the atmospheric entry heating experienced by the samples. This investigation took the form of two sets of experiments;

(1) In an attempt to produce micrometeorite analogues microgram-sized samples of whole-rock meteorite were sujected to pulse-heating to mimic atmospheric entry heating.

(2) The fusion crusts of meteorites were analysed to see if indigenous carbonaceous components had survived ablation.

The results of these experiments are preliminary but revealing. Not only was it shown that pulse-heating of whole-rock meteorites could yield samples with carbon inventories similar in bulk $\delta^{13}C$ and carbon content to the micrometeorites studied, but also there was evidence that the meteorite fusion crusts had retained indigenous

carbonaceous species. Both of these sets of experiments therefore strengthened the hypothesis that the micrometeorites were related to the meteorites.

8.2. Further work.

This section has been divided into the work concerned with general applications of the new ultra-high sensitivity carbon isotope mass spectrometer (MS86), and then that with specific regard to the further study of micrometeorites.

8.2.1. Applications of ultra-high sensitivity carbon isotope mass spectrometery.

During the time that this thesis has been in preparation, the ability of the mass spectrometer MS86 to determine the $\delta^{13}C$ of nanogram amounts of carbon dioxide to precisions of <1‰ has already been utilised to execute small-temperature step (10-50°C) stepped combustion experiments. Interstellar grain components found in meteorite acid-resistant residues (Russell *et al.*, 1991b) have been studied extensively together with whole-rock samples of the SNC meteorites (Hartmetz *et al.*, 1991). It is in such projects, where either sample availability is minimal, or small temperature steps are required in order to resolve between carbonaceous components of not greatly different stability, that MS86 is most useful.

The level of carbon blank within the stepped combustion experiments ultimately controls the size of sample that can be analysed by MS86. Experimentation reported within this thesis showed that even if sample handling contamination was completely removed, then there was a finite input of *ca.*0.3ng per temperature step from the carbon dioxide extraction line (the system blank), and a further *ca.*0.7 to 1ng per step associated with the platinum foil sample envelope. For substantial improvements to be made in overall blank levels it necessary to address these problems. Replacement of the copper oxide as the oxygen source perhaps with a reagent which releases oxygen at a lower temperature could help to alleviate some difficulties. Oxides which liberate oxygen at low temperatures are well known, *e.g.* Ag_2O, PbO, $KMnO_4$ *etc*, but none of these enjoy the reversible properties of CuO so that excess oxygen can no longer be resorbed. Oxygen sources other than CuO (or for that matter any attempt to purify the

oxygen released by CuO) requires an additional valve in the extraction system, which in turn increases its size and potential blank contribution. Such a move might thus be counterproductive since it is already desirable to minitarurise further the gas extraction line as a means of reducing the system blank. Clearly modifications to the oxygen production technique and system size are a trade-off which might not have the desired effect. However, improvements in the cleaning method applied to the platinum foil would perhaps reduce the blank input associated with the sample envelope. With respect to the latter point, further experimentation with the pulse-heating of platinum foil to *ca.*1500°C is required to investigate its cleaning efficacy. A major potential for random contamination could be avoided if the loading section of the gas extraction line was redesigned to avoid the use of teflon stopcock valves.

One of the most important conclusions from the MS86 blank experimentation was that the carbon contamination in any single experiment was extremely variable and not totally controlled by the individual sample preparation protocol used. If the small-sample analysis capability of MS86 is to be fully expoited then it must be stressed that;

(1) Users must co-ordinate experiments so that the presence of otherwise unexpected contaminants are known.

(2) Dedicated clean-room facilities and sample handling equipment are essential.

(3) If solvent cleaning steps are implemented within analysis protocols, then solvents should be dedicated for individual users, frequently checked for contamination and regularly replaced by fresh batches.

8.2.2. The further study of micrometeorites.

The work described within this thesis suggests that the >200μm diameter spherical micrometeorites have an asteroidal provenance. The acid-resistant residues prepared from Greenland cryoconite can be interpreted in favour of the unmelted micrometeorites and the spherical samples <200μm in diameter being primitive and possibly rich in pre-solar material. Bearing in mind that an excess of pre-solar grains could be expected for comets, a circumstantial argument can be made for these cryoconite grains being cometary and hence worthy of much greater scrutiny.

The problem involved with analysis of non-spherical micrometeorites is in isolating extraterrestrial micrometeorites from the myriad of terrestrial particulates that are present within deep-sea sediment, Greenland cryoconite and Antarctic Ice. Proof of extraterrestrial origin of the non-spherical micrometeorites requires specialist techniques, and so it is suggested that a study of these samples would benefit from a collaborative approach. Samples could be initially selected from unprocessed cryoconite using the optical criteria for identifying unmelted micrometeorites of Maurette *et al.*, (1991), and then cleaved using the sample analysis protocol devised in this study. Unmelted micrometeorites in excess of 300μm diameter are readily extractable from cryoconite (*e.g.* Maurette *et al.*, 1991) and so the larger sample mass available for analysis, coupled with their intuitively higher carbon concentrations due to lower atmospheric entry heating temperatures, would allow several fragments to be removed from each crushed sample without comprimising the results of the isotopic work. These sample fragments could then be made available to other investigators whereby either detailed mineralogic studies (*e.g.* Steele, 1991) or the detection of cosmogenic radionuclides (*e.g.* Sarda *et al.*, 1991) could be used to establish the extraterrestrial nature of the samples.

Detailed carbon stable isotopic analysis of the <200μm spherical micrometeorites would require that the improvements in overall blank levels as discussed above in 8.2.1. were realised. However, if as postulated from the acid-resistant cryoconite residues, these grains are characterised by a high (>10ppm) concentration of pre-solar material, then the concomittant high concentration of isotopically anomalous carbon would be recognisable even with the relative increase in carbon contamination.

8.2.2.1. Greenland cryoconite acid-resistant residues.

The study of acid-resistant residues of Greenland cryoconite provides the scope for much further work;

(1) Pre-solar SiC and diamonds are known to be the hosts of isotopically light nitrogen, possessing $\delta^{15}N$ values of *ca.*-625‰ (Russell *et al.*, 1991b) and *ca.*-351‰ (Russell *et al.*, 1991a) respectively. Consequently, stable nitrogen isotopic determination of the residues would hopefully determine whether the conclusions of the carbon work were valid. The concentration of nitrogen within pre-solar SiC and

diamond is much reduced with respect to carbon, *i.e.* Ash *et al.*, (1989) estimated the nitrogen concentration in SiC to be ca.1.7wt% and Russell *et al.*, (1991a) estimated *ca.*3000 to 13,000ppm nitrogen in diamond. However, a new ultra-high sensitivity stable nitrogen isotope mass spectrometer has been built within the Planetary Sciences Unit by Drs I.P.Wright and I.A Franchi, and when fully operational will hopefully enable nitrogen isotopic characterisation of the residues.

(2) Preparation of residues from larger aliquots of unprocessed cryoconite followed by carbon isotopic analysis should enable a better insight into the proposed pre-solar SiC, graphite and diamond components.

(3) Transmission electron microscopy (TEM) could be used to examine the residues to attempt to confirm the presence of the sub-nanometer diameter pre-solar grains.

8.2.2.2. Pulse-heating and fusion crust experiments.

Further experimentation on pulse-heating microgram-sized samples of whole-rock meteorites would enable a much tighter constraint to be placed on the meteoritic provenance of the >200μm spherical micrometeorites, and also provide useful evidence of the fate of various species during atmospheric entry heating. A goal must be to replicate more closely the atmospheric retardation of micrometeorites, experiments using much shorter heating periods (10 to <1second) and higher temperatures (up to *ca.*2000°C). With respect to the conclusions of the individual stepped combustion analyses of Greenland and Antarctic micrometeorites, pulse-heating experiments must be executed on carbonaceous chondrites rich in macromolecular material (*i.e.* the CI or CM chondrites), and ordinary chondrites that span both chemical and petrologic types.

The analysis of meteorite fusion crusts, although hampered by problems of contamination, yielded some unexpected results. The observed survival of apparently indigenous carbonaceous components within the fusion crusts also has important implications for the survival of volatiles in micrometeorites. Careful selection of fresh crust taken from meteorites of varying terrestrial ages followed by carbon isotopic analysis should determine whether survival of volatiles is common, or if it is only the effect of exposure in the terrestrial environment, *i.e.* weathering or curatorial activities

within museums. In particular, analyses of meteorite fusion crusts taken from new finds in areas where biology might not be active, *i.e.* Antarctic and desert meteorites, would be useful.

Appendix A1

Stepped Combustion Data.

A1. Introduction.

The results for stepped combustion data. To facilitate rapid location of individual experiment results from within this appendix, the data tables have been grouped as follows:

(1) Stepped combustion blank experiments. (These have been listed sequentially from protocol A through to H and then finally the 'catastrophic' blanks are presented).
(2) Analysis protocol materials experiments (corresponds to section 4.4.7.).
(3) Multiple particle deep-sea micrometeorite experiments.
(4) Individual particle deep-sea micrometeorite experiments.
(5) Individual Greenland cryoconite micrometeorite experiments.
(6) Individual Antarctic micrometeorite experiments.
(7) Greenland cryoconite algae experiments.
(8) Greenland cryoconite acid resistant residue experiments.
(9) Meteorite small-sample and pulse heating experiments.

Those experiments with run numbers prefaced by T are analyses carried out on the Triple Collector mass spectrometer, whilst those prefaced by MS were carried out on MS86. Temperature steps are accurate to within ±5°C. Carbon yields were determined using a capacitance manometer and have errors of ±0.95ng for the Triple Collector and ±0.13ng for MS86, and sample masses, where included, have errors ±3μg (see appendix A3). The errors quoted on the $\delta^{13}C$ measurements are 1σ instrumental errors. The symbol 'nm' means that either the sample gas was lost or was too small to allow isotopic analysis.

A1.1. Stepped combustion blank experiments.

Protocol A Blank		1-12-88	T606
Temp.(°C)	Yield(ng)	δ13C(‰)	±
150	9.7	-31.2	1.5
200	4.2	-32.5	2.0
225	2.3	-22.2	6.1
250	1.9	nm	
300	3.4	-33.8	5.1
350	3.1	-27.9	4.0
400	2.7	-22.0	4.2
450	0.8	-34.2	10.0
500	1.3	-14.0	9.3
600	1.5	-27.4	7.5
800	1.1	-35.7	6.1
1000	1.1	nm	
1200	0.8	-20.6	6.7

Protocol B Blank		17-12-88	T614
Temp.(°C)	Yield(ng)	δ13C(‰)	±
150	5.0	-32.5	2.4
200	0.6	nm	
250	2.3	nm	
300	3.8	-25.5	2.8
400	5.7	-31.0	1.5
500	4.6	-28.5	1.3
600	0.6	nm	
800	0.6	nm	
1200	0.7	nm	

Protocol C Blank		10-1-89	T620
Temp.(°C)	Yield(ng)	δ13C(‰)	±
100	1.0	nm	
125	1.9	nm	
150	0.4	nm	
175	0.2	nm	
200	1.1	nm	
300	1.0	-33.3	7.7
350	1.5	nm	
400	1.7	nm	
450	1.9	-28.6	8.2
500	1.3	-18.3	6.3
600	1.3	nm	
800	0.4	nm	
1200	0.8	nm	

Protocol C Blank		6-3-90	MS21
Temp.(°C)	Yield(ng)	δ13C(‰)	±
200	7.9	-26.5	0.6
300	6.3	-24.6	0.7
400	4.4	-25.4	0.6
500	1.9	-23.3	1.1
600	2.4	-42.0	0.9
1200	2.2	-29.9	0.9

Protocol C Blank		16-3-90	MS26
Temp.(°C)	Yield(ng)	δ13C(‰)	±
50	0.5	-18.6	0.9
100	1.2	-25.2	1.0
150	1.5	-26.1	0.9
200	1.3	-24.6	0.9
300	4.0	-24.4	0.5
400	4.9	-24.3	0.4
500	8.6	-24.7	0.5
600	4.1	-29.7	0.5
1200	1.4	-27.8	0.9

Protocol D Blank		15-1-89	T636
Temp.(°C)	Yield(ng)	δ13C(‰)	±
100	1.7	-13.6	11.9
200	2.3	-34.5	8.4
300	1.3	nm	
350	1.1	nm	
400	1.0	nm	
500	0.4	nm	
600	0.6	nm	
1200	0.6	nm	

Protocol D Blank		27-3-90	MS32
Temp.(°C)	Yield(ng)	δ13C(‰)	±
50	0.8	-24.6	1.0
100	1.9	-26.4	1.1
150	3.1	-27.1	0.6
200	4.0	-27.2	0.6
300	6.5	-28.9	0.9
400	4.5	-26.6	0.5
500	4.5	-26.7	0.5
600	1.8	-37.2	0.9
1200	1.4	-29.7	0.9

Protocol D Blank		1-6-90	MS50
Temp.(°C)	Yield(ng)	δ13C(‰)	±
200	3.0	-34.2	1.1
300	3.5	-26.8	0.8
400	2.5	-24.3	1.3
500	1.0	-21.6	1.1
600	1.0	-19.9	1.2
800	1.2	-28.4	1.0
1200	0.9	-29.0	1.1

Protocol E Blank	19-5-90	MS44	
Temp.(°C)	Yield(ng)	δ13C(‰)	±
200	2.9	-25.7	1.5
300	3.6	-23.6	0.7
400	4.6	-25.2	0.6
500	3.1	-27.3	1.0
600	1.9	-24.6	1.2
1200	2.1	-28.8	1.2

Protocol E Blank	6-6-90	MS54	
Temp.(°C)	Yield(ng)	δ13C(‰)	±
200	1.6	-27.2	1.0
300	1.8	-24.9	1.0
400	1.3	-24.9	1.0
500	0.9	-23.4	0.9
600	0.6	-22.2	1.0
800	1.1	-23.6	0.9
1200	0.8	-25.5	1.0

Protocol E Blank	16-6-90	MS62	
Temp.(°C)	Yield(ng)	δ13C(‰)	±
200	1.1	-26.5	1.0
300	1.3	-24.7	1.1
400	1.6	-23.0	1.1
500	2.9	-27.9	1.2
600	4.2	-28.4	0.7
1200	3.8	-30.6	0.7

Protocol F Blank	5-10-90	MS88	
Temp.(°C)	Yield(ng)	δ13C(‰)	±
200	4.5	-24.6	1.2
300	1.8	-27.7	1.3
400	1.3	-27.5	1.1
500	1.2	-24.1	1.2
600	0.6	-24.4	1.2
800	0.7	-26.3	1.1
1200	0.4	-17.9	1.2

Protocol G Blank	28-8-90	MS83	
Temp.(°C)	Yield(ng)	δ13C(‰)	±
200	0.5	-25.3	1.1
300	0.5	-23.4	1.3
400	0.6	-26.2	1.1
500	1.1	-25.9	1.0
600	0.7	-26.0	0.9
800	0.5	-20.6	1.0
1200	0.4	-22.5	1.1

Protocol H Blank	10-3-90	MS25	
Temp.(°C)	Yield(ng)	δ13C(‰)	±
200	0.3	-15.8	1.2
300	0.3	-21.6	1.0
400	0.4	-34.0	1.1
500	0.3	-25.9	1.5
600	0.3	-22.1	1.3
1200	0.3	-23.1	1.3

"Catastrophic" Blank	9-3-90	MS24	
Temp.(°C)	Yield(ng)	δ13C(‰)	±
50	0.7	-25.1	1.0
100	1.4	-24.8	1.0
150	3.9	-25.6	0.6
200	3.3	nm	
250	3.1	nm	
300	3.0	-23.7	0.5
350	9.8	-21.9	0.5
400	13.7	-21.7	0.8
450	37.1	-22.5	0.5
500	65.2	-22.7	0.4
600	141.0	nm	

'Catastrophic' Blank	3-6-90	MS51	
Temp.(°C)	Yield(ng)	δ13C(‰)	±
200	3.1	-30.3	0.9
300	2.8	-25.5	1.5
400	5.7	-8.6	1.2
500	21.9	-35.7	0.7
600	11.9	-32.7	0.6
1200	60.2	-32.2	0.5

A1.2. Analysis protocol materials experiments.

Loading Valve Blank	29-9-90	MS84	
Temp.(°C)	Yield(ng)	δ13C(‰)	±
200	2.3	-26.0	1.1
300	7.1	-30.8	1.0
400	17.7	-37.2	0.6
500	43.0	-44.4	0.4
600	8.2	-38.1	0.8
800	4.0	-35.4	1.2
1200	1.3	-32.6	1.2

Furnace P. (0.11mg)	3-10-90	MS86	
Temp.(°C)	Yield(ng)	δ13C(‰)	±
200	2.4	-19.4	1.3
300	1.1	-21.2	1.4
400	1.7	-24.3	1.4
500	1.0	-22.4	1.3
600	1.0	-21.2	1.3
800	0.5	-24.2	1.3
1200	0.4	-18.5	1.4

Al Foil (0.15mg)	1-10-90	MS85	
Temp.(°C)	Yield(ng)	δ13C(‰)	±
200	3.1	-22.4	1.5
300	1.0	-21.3	1.3
400	1.5	-23.9	1.4
500	6.9	-23.6	1.3
600	1.0	-23.1	1.1
800	1.1	-25.2	1.2
1200	1.5	-12.5	1.1

Pyrex Glass (0.32mg)	4-10-90	MS87	
Temp.(°C)	Yield(ng)	δ13C(‰)	±
200	1.3	-24.3	1.5
300	0.9	-23.0	1.4
400	0.8	-23.3	1.5
500	1.8	-32.7	1.3
600	1.7	-33.3	1.3
800	0.5	-25.2	1.2
1200	0.5	-17.4	1.1

A1.3. Multiple particle deep-sea micrometeorite experiments.

Blank	8-5-89	T664	
Temp.(°C)	Yield(ng)	δ13C(‰)	±
100	1.9	nm	
200	0.8	-31.1	14.5
250	2.9	-46.4	6.4
300	5.3	-17.5	2.4
400	3.4	-12.7	3.8
500	1.3	nm	
600	1.1	nm	
1200	1.3	nm	

Type I (0.34mg)	9-5-89	T665	
Temp.(°C)	Yield(ng)	δ13C(‰)	±
100	0.8	nm	
200	26.7	-31.6	3.3
250	26.9	-32.7	3.1
275	6.1	-28.7	1.6
300	2.7	-22.3	6.7
350	5.5	-29.4	2.7
400	4.8	-19.9	2.7
500	8.0	-32.9	1.6
600	3.8	-4.5	6.1
800	0.6	nm	
1200	0.6	nm	

Type S (0.12mg)	11-5-89	T666	
Temp.(°C)	Yield(ng)	δ13C(‰)	±
100	0.4	nm	
200	19.9	-25.7	3.0
225	12.4	-19.2	3.3
250	13.4	-39.5	2.6
275	17.4	-27.2	2.6
350	27.1	-24.8	2.0
400	16.4	-33.9	1.8
500	8.6	-29.6	1.4
600	2.7	-39.8	5.9
1200	0.8	-20.0	9.9

A1.4. Individual particle deep-sea micrometeorite experiments.

Deep-sea KKF (20μg) 9-11-88 T597			
Temp.(°C)	Yield(ng)	δ13C(‰)	±
200	34.7	-27.7	1.7
225	7.1	-30.9	2.6
250	8.0	-29.9	1.4
275	5.9	-26.2	1.8
300	4.2	nm	
325	3.4	-29.6	2.1
350	3.6	-27.2	1.8
375	2.7	nm	
400	1.7	-24.3	5.5
450	3.1	-30.9	2.8
500	3.4	-26.5	2.5
600	1.1	-23.2	5.5
800	1.7	-16.6	9.2
1000	1.0	-8.6	5.2
1200	1.1	+5.3	15.2

Deep-sea KKB (20μg) 10-11-88 T598			
Temp.(°C)	Yield(ng)	δ13C(‰)	±
200	30.2	-31.0	1.3
225	3.2	-26.4	3.0
250	3.6	-17.6	4.5
275	3.2	-28.6	2.5
300	4.4	-30.6	1.8
350	5.7	-26.3	1.7
400	3.1	-27.8	2.4
450	1.7	-24.7	3.9
500	1.0	-19.6	6.7
600	3.8	-24.8	2.3
800	1.1	-29.0	2.3
1000	2.9	-28.4	3.1
1200	0.6	-25.0	6.6

Deep-sea KKE (20μg) 16-11-88 T600			
Temp.(°C)	Yield(ng)	δ13C(‰)	±
200	37.0	-29.3	1.4
225	5.2	-33.3	2.2
250	4.4	-30.0	3.3
275	4.0	-30.9	2.7
300	3.8	-33.3	2.2
350	5.2	-26.9	1.4
400	2.9	-27.4	3.4
450	3.1	-24.3	5.0
500	1.7	-37.0	6.8
600	1.7	-41.6	5.9
800	0.6	-29.1	10.2
1200	1.5	-10.1	12.8

Deep-sea Csp1 (21μg) 11-1-89 T621			
Temp.(°C)	Yield(ng)	δ13C(‰)	±
100	0.2	nm	
200	3.8	-24.2	4.2
300	4.8	-29.5	2.2
350	3.2	-26.0	2.9
400	1.0	-31.8	10.1
500	1.9	-17.5	6.3
600	1.5	-28.4	5.8
800	0.6	nm	
1200	1.2	-26.8	9.7

Deep-sea Csp2 (19μg) 30-1-89 T630			
Temp.(°C)	Yield(ng)	δ13C(‰)	±
100	4.0	-35.9	2.6
200	3.1	-23.7	3.8
250	2.3	-31.8	5.9
300	3.8	-32.0	3.1
350	3.6	-33.4	3.5
400	3.4	-28.7	3.4
500	2.1	-30.4	4.2
600	0.6	nm	
1200	1.3	-20.6	8.3

A1.5. Individual Greenland cryoconite micrometeorite experiments.

SS89M07 (17μg)		9-7-89	T687
Temp.(°C)	Yield(ng)	δ13C(‰)	±
100	0.6	nm	
200	4.8	-29.4	3.0
250	7.6	-36.7	1.7
300	7.9	-33.8	1.6
400	4.2	-26.6	3.8
500	1.5	-26.7	8.0
600	0.7	nm	
1200	1.3	-8.6	13.4

SS89M08 (14μg)		10-7-89	T688
Temp.(°C)	Yield(ng)	δ13C(‰)	±
100	0.1	nm	
200	12.2	-35.2	2.5
250	23.1	-24.0	1.2
300	18.0	-32.3	1.5
400	11.8	-31.9	2.3
500	3.0	-28.9	4.1
600	1.0	-20.3	9.6
1200	1.0	-6.0	16.3

SS89M01 (6μg)		14-2-90	MS13
Temp.(°C)	Yield(ng)	δ13C(‰)	±
200	31.7	-25.6	0.5
300	21.3	-22.2	0.5
350	10.6	-22.9	0.6
400	7.9	-25.5	0.8
450	8.0	-26.5	0.6
500	12.7	-29.5	0.6
600	3.5	-27.9	0.9
1200	3.1	-30.4	0.9

SS89M05 (13μg)		15-2-90	MS14
Temp.(°C)	Yield(ng)	δ13C(‰)	±
200	30.6	-25.2	0.5
300	23.2	-21.6	0.5
350	11.4	-21.2	0.5
400	6.9	-23.4	0.7
450	4.5	-23.8	0.5
500	3.7	-25.9	0.8
600	3.7	-25.8	0.6
1200	4.6	-25.4	0.5

SS89M12 (21μg)		16-2-90	MS15
Temp.(°C)	Yield(ng)	δ13C(‰)	±
200	17.2	-27.8	0.9
300	12.7	-24.5	0.5
350	6.9	-26.1	0.9
400	5.8	-23.4	1.0
450	6.7	-25.5	0.9
500	3.0	-25.2	1.0
600	3.0	-29.8	1.1
1200	3.0	-27.5	1.0

SS89M09 (34μg)		7-3-90	MS22
Temp.(°C)	Yield(ng)	δ13C(‰)	±
200	9.6	-25.2	0.6
300	16.5	-22.6	0.4
400	12.0	-21.8	0.6
500	6.2	-24.8	0.7
600	7.3	-31.8	0.5
1200	2.0	-28.0	1.1

SS89M10 (32μg)		8-3-90	MS23
Temp.(°C)	Yield(ng)	δ13C(‰)	±
200	11.4	-24.2	0.5
300	15.3	-22.2	0.5
400	8.9	-22.4	0.6
500	7.1	-25.5	0.6
600	10.0	-31.7	0.4
1200	1.8	-34.2	1.0

SS89M17 (31μg)		18-3-90	MS27
Temp.(°C)	Yield(ng)	δ13C(‰)	±
200	16.2	-25.2	0.6
300	30.0	-22.3	0.8
400	17.7	-19.2	0.5
500	10.0	-20.4	0.5
600	6.3	-30.9	0.4
1200	3.2	-27.9	0.9

SS89M16 (66µg)		21-3-90	MS30
Temp.(°C)	Yield(ng)	δ13C(‰)	±
200	13.4	-23.5	0.6
300	61.5	-18.6	0.5
350	38.54	-19.2	0.5
400	18.5	-22.0	0.5
450	23.6	-25.5	0.6
500	28.5	-30.1	0.4
600	7.8	-32.0	0.4
800	2.2	-29.6	1.1
1200	1.6	-24.9	1.0

SS89M18 (52µg)		22-3-90	MS31
Temp.(°C)	Yield(ng)	δ13C(‰)	±
200	12.8	-26.1	0.5
300	35.6	-20.9	0.5
400	17.3	-22.2	0.5
500	11.9	-22.1	0.5
600	8.0	-29.9	0.4
800	1.8	-30.5	1.0
1200	0.8	-29.2	1.0

SS89M14 (31µg)		20-3-90	MS29
Temp.(°C)	Yield(ng)	δ13C(‰)	±
200	7.0	-27.2	0.5
300	10.6	-23.4	0.6
400	11.7	-22.3	0.5
500	8.2	-24.0	0.6
600	3.4	-26.7	0.9
800	0.9	-27.3	1.0
1200	0.7	-28.0	1.0

A1.6. Individual Antarctic micrometeorite experiments.

MA1 (23µg)		28-3-90 MS33	
Temp.(°C)	Yield(ng)	δ13C(‰)	±
200	6.4	-26.8	0.4
300	10.8	-26.4	0.5
400	12.4	-25.2	0.5
500	11.2	-24.0	0.5
600	3.2	-37.2	0.8
800	1.5	-30.9	0.9
1200	1.1	-25.7	0.8

MA2 (60µg)		29-3-90 MS34	
Temp.(°C)	Yield(ng)	δ13C(‰)	±
200	11.2	-27.8	0.5
300	32.5	-24.5	0.5
350	22.7	-22.6	0.4
400	18.2	-22.1	0.5
450	12.1	-23.4	0.5
500	6.6	-24.2	0.4
600	5.1	-22.8	0.5
800	1.5	-23.8	0.9
1200	1.4	-23.0	1.0

MA3 (84µg)		30-3-90 MS35	
Temp.(°C)	Yield(ng)	δ13C(‰)	±
200	12.6	-27.7	0.5
300	12.4	-26.4	0.5
350	6.9	-24.1	0.4
400	5.3	-24.0	0.5
500	7.6	-24.4	0.6
600	5.5	-29.1	0.5
1200	0.66	nm	

MA4 (28µg)		12-10-90 MS92	
Temp.(°C)	Yield(ng)	δ13C(‰)	±
200	10.3	-26.9	0.8
300	10.0	-27.6	0.6
350	5.1	-24.7	1.2
400	3.8	-24.5	1.0
500	3.0	-24.1	1.2
600	1.1	-21.8	1.0
800	1.0	-21.5	1.0
1200	1.1	-14.7	1.1

MA5 (57µg)		15-10-90 MS93	
Temp.(°C)	Yield(ng)	δ13C(‰)	±
200	20.7	-28.8	0.5
300	16.6	-31.0	0.5
350	16.3	-31.6	0.5
400	18.2	-32.0	0.4
450	19.6	-30.9	0.5
500	1.8	-23.4	1.1
600	1.8	-24.8	1.1
800	1.4	-22.9	1.0
1200	1.8	-12.8	1.1

A1.7. Greenland cryoconite algae experiments.

Algae (0.028mg)		5-4-90 MS38	
Temp.(°C)	Yield(ng)	δ13C(‰)	±
200	32.4	-26.0	0.5
250	140.9	-23.8	0.4
300	440.1	-21.3	0.4
350	247.4	-21.2	0.5
400	204.3	-23.0	0.4
450	121.9	nm	
500	101.4	-23.0	0.4
550	82.6	-22.7	0.4
600	37.6	-22.7	0.5
800	5.9	-20.9	0.5
1200	3.0	-16.2	1.2

Algae (0.06mg)		19-10-90 MS95	
Temp.(°C)	Yield(ng)	δ13C(‰)	±
200	94.0	-27.8	0.4
300	1008.0	-23.4	0.4
350	341.0	-23.5	0.6
400	274.0	-23.8	0.5
450	166.0	-26.6	0.7
500	156.0	-25.2	0.7
600	95.3	-26.4	0.5
700	1.8	-22.0	1.4
900	4.1	-21.8	0.8
1200	2.4	-14.8	1.4

A1.8. Greenland cryoconite acid resistant residue experiments.

Residue 1 (0.16mg)		11-12-89 T713	
Temp.(°C)	Yield(ng)	δ13C(‰)	±
200	244.4	-25.2	2.2
250	576.7	-18.8	2.1
300	1455.1	-25.7	0.9
350	4678.5	-27.1	0.8
400	10521.9	-23.7	0.8
450	7351.9	-25.6	0.8
500	7008.2	-25.0	0.8
550	4525.8	-25.0	0.7
600	2071.9	-26.4	0.7
650	633.9	-23.4	0.8
700	393.4	-21.3	1.0
750	208.1	-23.9	0.9
800	120.3	-24.2	0.9
850	14.5	-27.2	1.0
900	14.5	-26.6	1.1
1000	42.0	-21.3	0.9
1100	32.5	-27.9	1.0
1200	nm		

1 (pre-comb.) (1.3mg)		13-12-89 T714	
Temp.(°C)	Yield(ng)	δ13C(‰)	±
600	5.7	-25.7	3.1
650	19.3	-14.1	0.9
700	103.3	-15.6	0.8
750	174.3	-24.4	0.8
800	161.4	-23.3	0.8
850	116.7	-25.2	0.8
900	73.9	-26.2	1.0
950	84.6	-25.3	1.1
1000	98.0	-25.4	1.0
1050	24.1	-21.7	0.7
1100	12.9	-31.8	1.0
1200	10.1	-27.6	1.5

Residue 2 (0.09mg)		19-10-90 MS96	
Temp.(°C)	Yield(ng)	δ13C(‰)	±
200	27.5	-29.8	0.8
300	39.5	-30.2	0.5
400	63.4	-28.9	0.4
500	30.9	-34.4	0.4
600	11.6	-23.1	0.5
700	9.8	-22.0	0.6
800	3.0	-20.8	1.2
1000	5.9	-7.2	1.1
1200	2.0	-16.2	1.1

A1.9. Meteorite small-sample and pulse heating experiments.

A1.9.1. Allende.

Sample from British Museum (Natural History) collection. Number; BM1988(M24).

Bulk (0.054mg)		15-9-90 MS75	
Temp.(°C)	Yield(ng)	δ13C(‰)	±
200	11.8	-26.8	0.8
300	27.1	-24.2	0.8
400	31.8	-22.5	1.0
500	41.6	-23.0	0.7
600	94.0	-19.2	0.4
800	29.4	+0.2	0.8
1200	40.2	-6.3	0.8

800°C (0.045mg)		19-9-90 MS77	
Temp.(°C)	Yield(ng)	δ13C(‰)	±
200	0.7	-23.6	1.2
300	0.8	-28.5	1.3
400	1.2	-25.7	1.2
500	2.2	-23.3	1.3
600	5.5	-17.0	0.8
800	11.6	-14.1	0.6
1200	19.2	-8.4	0.6

Fusion Crust (0.15mg)		18-9-90 MS76	
Temp.(°C)	Yield(ng)	δ13C(‰)	±
200	16.5	-26.9	0.5
300	49.9	-23.2	0.5
400	52.8	-22.7	0.6
500	74.9	-20.1	0.7
600	62.2	-19.3	0.5
800	79.7	-15.7	0.5
1200	52.5	-10.4	0.4

1500°C (0.28mg)		20-9-90 MS78	
Temp.(°C)	Yield(ng)	δ13C(‰)	±
200	0.7	-26.3	1.3
300	0.6	-27.3	1.4
400	1.0	-23.3	1.5
500	1.0	-28.7	1.1
600	1.0	-26.4	1.4
800	0.6	-24.3	1.3
1200	1.0	-18.8	1.2

A1.9.2. Goalpara.

Sample from British Museum (Natural History) collection. Number; BM43058.

Bulk (0.102mg)		8-9-90 MS69	
Temp.(°C)	Yield(ng)	δ13C(‰)	±
200	10.4	-24.8	0.6
300	16.9	-21.9	0.6
400	10.9	-21.9	0.6
500	5.5	-11.4	1.2
600	8.2	-3.6	0.7
800	12.4	-1.1	0.6
1200	19.8	+0.8	0.6

800°C (0.055mg)		11-9-90 MS71	
Temp.(°C)	Yield(ng)	δ13C(‰)	±
200	1.0	-28.1	0.9
300	1.1	-25.4	1.0
400	0.9	-27.8	1.0
500	1.2	-25.6	0.9
600	2.7	-6.8	1.0
800	14.6	+0.8	0.4
1200	5.1	+0.3	0.4

Fusion C. (0.162mg)		10-9-90 MS70	
Temp.(°C)	Yield(ng)	δ13C(‰)	±
200	95.8	-24.6	0.4
300	460.0	-24.4	0.4
400	404.0	-22.2	0.4
500	411.0	-22.4	0.6
600	108.0	-23.0	0.3
800	118.0	-18.1	1.0
1200	25.8	-19.6	0.4

1500°C (0.124mg)		13-9-90 MS74	
Temp.(°C)	Yield(ng)	δ13C(‰)	±
200	1.1	-27.5	0.9
300	1.0	-28.0	1.0
400	1.8	-28.0	0.9
500	4.2	-26.4	0.5
600	1.4	-26.6	0.9
800	1.2	-14.4	0.8
1200	4.6	+0.4	1.0

A1.9.3. Weston.

Sample from British Museum (Natural History) collection. Number; BM90254 (dark lithology).

Bulk (0.10mg)		15-6-90	MS61
Temp.(°C)	Yield(ng)	δ13C(‰)	±
200	4.9	-27.9	0.6
300	7.4	-26.2	0.8
400	8.9	-26.4	0.6
500	7.0	-25.3	1.1
600	12.1	-25.6	0.5
800	27.6	-21.2	0.4
1200	5.0	-24.4	0.5

800°C (0.24mg)		29-6-90	MS64a
Temp.(°C)	Yield(ng)	δ13C(‰)	±
200	1.2	-28.9	1.0
300	2.2	-25.7	1.2
400	16.9	-25.0	0.4
500	4.1	-22.7	0.7
600	10.0	-22.2	1.2
800	37.8	-18.8	0.5
1200	50.4	-19.2	0.5

Fusion C. (0.16mg)		14-6-90	MS60
Temp.(°C)	Yield(ng)	δ13C(‰)	±
200	19.9	-25.6	0.4
300	99.8	-23.8	0.4
400	120.0	-24.4	0.4
500	87.6	-23.8	0.4
600	76.8	-24.6	0.3
800	225.0	-16.5	0.6
1200	412.0	-13.1	0.4

1500°C (0.18mg)		30-6-90	MS65
Temp.(°C)	Yield(ng)	δ13C(‰)	±
200	1.3	-24.9	1.2
300	2.3	-23.1	1.2
400	4.5	-23.3	0.6
500	2.4	-21.0	1.2
600	4.5	-22.9	1.1
800	1.1	-28.0	1.1
1200	1.0	-24.7	0.9

A1.9.4. Pulse-heated and microgram-sized meteorite and fusion crust experiment blanks.

Protocol D Blank		27-3-90	MS32
Temp.(°C)	Yield(ng)	δ13C(‰)	±
50	0.8	-24.6	1.0
100	1.9	-26.4	1.1
150	3.1	-27.1	0.6
200	4.0	-27.2	0.6
300	6.5	-28.9	0.9
400	4.5	-26.6	0.5
500	4.5	-26.7	0.5
600	1.8	-37.2	0.9
1200	1.4	-29.7	0.9

800°C Blank		25-8-90	MS80
Temp.(°C)	Yield(ng)	δ13C(‰)	±
200	0.6	-27.4	1.1
300	0.6	-26.0	1.0
400	0.8	-25.4	1.0
500	1.1	-27.0	0.9
600	0.8	-30.3	0.8
800	0.4	-23.2	1.0
1200	0.5	-25.4	0.9

1500°C Blank		28-8-90	MS83
Temp.(°C)	Yield(ng)	δ13C(‰)	±
200	0.5	-25.3	1.1
300	0.5	-23.4	1.3
400	0.6	-26.2	1.1
500	1.1	-25.9	1.0
600	0.7	-26.0	0.9
800	0.5	-20.6	1.0
1200	0.4	-22.5	1.1

Appendix A2

Major Element Chemistry Data Tables.

A2. Introduction.

The results for analytical electron microscope analyses of the major element chemistry of micrometeorites discussed within chapter 3. Data is presented as weight percent element oxide (wt% Oxide), and grouped into tables as follows:

(1) Area analyses of deep-sea micrometeorites.
(2) Area analyses of Greenland cryoconite micrometeorites.
(3) Area analyses of Antarctic micrometeorites.
(4) Spot analyses of deep-sea, cryoconite and antarctic micrometeorite matrix silicate.
(5) Spot analyses of deep-sea, cryoconite and antarctic micrometeorite matrix iron oxide.
(6) Area analyse of micrometeorites presented in table 3.1.

Table A21. Area analyses deep-sea micrometeorites.

Sample	SiO	TiO	Al_2O_3	FeO	MnO	MgO	CaO	Na_2O	K_2O	Cr_2O	NiO	SO_3	P_2O_5	ClO_2	ZrO_2	Sum
KKF*	14.6		5.0	70.5		6.9	0.5			1.2	0.7					99.4
KKB	24.3	0.2	1.1	37.8		20.1	0.2				1.2					84.9
KKE*	22.6	0.3	5.8	50.5		17.4	0.4	0.5	0.5	1.2	0.7					99.9
CSp1	0.3			60.4							0.4					61.1
CSp2	0.3			85.9				0.5		0.2						86.9

* = Totals summed to 100%.

Table A22. Area analyses cryoconite micrometeorites.

Sample	SiO	TiO	Al_2O_3	FeO	MnO	MgO	CaO	Na_2O	K_2O	Cr_2O	NiO	SO_3	P_2O_5	ClO_2	ZrO_2	Sum
SS89M01	38.4	0.2	3.6	10.9		32.7	2.0			0.6						88.4
SS89M05	28.2	0.3	5.1	37.9		7.8	4.3					1.1	0.3	0.1		85.1
SS89M07	20.5		1.5	25.9	0.3	12.9	1.5			0.3						62.9
SS89M08	27.2		0.9	14.8	0.2	17.1	5.6			0.2						66.0
SS89M09	25.4		3.3	25.0		11.4	3.7	0.4	0.1	0.3	0.9					70.5
SS89M10	41.4		2.8	25.1	0.3	30.6	1.5			0.4	1.1					103.2
SS89M12	41.6		2.9	22.2		32.4	1.1			0.4						100.6
SS89M13	33.0	0.3	4.3	20.1	0.3	12.4	9.7	0.6	0.1	0.3		7.5		0.3		88.9
SS89M14	38.9		2.4	29.0	0.4	26.7	3.5									100.9
SS89M16	24.1	0.3	5.3	38.5		2.3	4.4	0.7	0.3	0.6		0.4	0.3	0.3		77.5
SS89M17	22.0	0.3	4.1	32.3	0.3	14.4	1.3			1.2	1.7					77.6
SS89M18	55.3		4.2	18.8	0.4	18.6	3.4		0.2	0.3						101.2

Table A23. Area analyses antarctic micrometeorites.

Sample	SiO	TiO	Al_2O_3	FeO	MnO	MgO	CaO	Na_2O	K_2O	Cr_2O	NiO	SO_3	P_2O_5	ClO_2	ZrO_2	Sum
MA1	35.4		2.4	25.7	0.3	24.8	1.4			0.3						90.3
MA2	39.7	0.4	4.5	23.0		27.9	3.9	0.6		0.3			2.4			102.7
MA3	32.4		5.3	39.8		6.1	2.8									86.4
MA4	21.6	0.2	2.3	37.1		16.1	0.9		0.4							78.6
MA5	35.4			29.6	0.6	6.3										71.9

Table A24. Spot analyses of deep-sea, cryoconite and antarctic micrometeorite matrix silicates.

Sample	SiO	TiO	Al_2O_3	FeO	MnO	MgO	CaO	Na_2O	K_2O	Cr_2O	NiO	SO_3	P_2O_5	ClO_2	ZrO_2	Sum
KKF*	35.5		0.3	41.8	0.4	20.8	0.3	0.3								99.4
KKB	39.7			32.5	0.2	32.4	0.2			0.6	1.8					107.4
KKE*	38.8		0.6	16.8		41.0				0.6	1.8					99.6
SS89M09	37.8	0.3	6.4	26.9		8.2	7.4		0.1				0.4			87.5
SS89M14	40.8		1.3	24.1	0.3	33.0	2.3									101.8
MA3	38.3		5.4	43.5	0.6	4.5	3.1									95.6
MA4	33.3		0.4	13.9		37.3	0.1			0.4	0.5					85.9

* = Totals summed to 100%.

Table A25. Spot analyses of deep-sea, cryoconite and antarctic micrometeorite iron oxides.

Sample	SiO	TiO	Al_2O_3	FeO	MnO	MgO	CaO	Na_2O	K_2O	Cr_2O	NiO	SO_3	P_2O_5	ClO_2	ZrO_2	Sum
KKE*	5.8		2.6	80.4	0.4	6.7				2.7	0.9					99.5
KKB	9.5	0.3	3.6	60.6		9.4				1.7	1.5					86.6
SS89M09	4.7	0.5	4.3	72.8		4.4	0.9			3.4	1.1					92.1
SS89M14	21.6	0.3	3.0	64.8		9.1	2.5			0.3						101.6
MA1	14.9	0.3	4.4	55.5		7.5	0.9			9.8						93.3
MA2	5.7	0.3	1.1	34.4	0.4	0.4	4.1				0.4		0.5			47.3
MA3	1.4	0.4	3.5	80.6		2.1	0.2			0.5	1.0					89.7
MA4	22.2	0.4	5.6	61.3		2.6	3.8						0.5			96.4

* = Total summed to 100%.

Table A26. Area analyses for data presented in Table 3.1.

Sample	SiO	TiO	Al_2O_3	FeO	MnO	MgO	CaO	Na_2O	K_2O	Cr_2O	NiO	SO_3	P_2O_5	ClO_2	ZrO_2	Sum
?13	9.5		1.9	46.4		4.4	0.5			0.3		0.3				63.3
1.1	5.7	1.2	5.2	56.2		2.9	1.3		0.1	0.4	0.7		1.3			75.0
2.6*	7.7	1.1	4.1	79.2	1.2	2.7	0.9			0.5		0.5	1.2	0.2	0.6	99.9
C5	9.1	0.7	2.9	61.7			0.8	0.7	0.2	0.2		0.3	1.1			77.7
4.1	1.2		0.8	70.5	0.4	0.8	0.3	0.4			0.8					75.2

* = Total summed to 100%.

Appendix A3

Summing Individual Stepped Combustion Temperature Steps; a Method for the Estimation of Uncertainties in Average $\delta^{13}C$ and Carbon Concentration.

A3.1. Introduction.

Determination of the absolute yields and isotopic composition of carbon within each sample was carried out by the method of stepped combustion (see Chapter 2 for experimental details), where the sample is combusted from room temperature to 1200°C in discrete temperarture steps typically ranging in size from 10 to 600°C. For purposes of interpretation and discussion of the data from within this thesis, two, or more, individual temperature steps were often summed to produce an average $\delta^{13}C$ value and carbon yield for a wider temperature regime than that represented by the individual steps. Subsequent interpretation of such data made it neccessary to examine error propogation inherent within the summing process to ensure that any interpretations made were valid.

A3.2. Assessment of the errors on the individual temperature step data.

Each temperature step involved the measurement of both the yield and isotopic nature of the the carbon released. Errors in the isotopic determinations were provided directly by the computer software of each mass spectrometer (see Carr, 1985 for details of such error derivations for the Triple Collector, and Prosser *et al.*, 1990 for MS86). These mass spectrometer errors are effectively due to ion counting statistical fluctuations and errors associated with electronic noise *etc.* The errors associated with

the yield measurements required more careful consideration. Actual determination of each yield was executed by measuring the pressure of CO_2 released from each temperature step by utilising a capacitance manometer that had been calibrated previously to allow conversion of the voltage reading obtained to a ng carbon equivalent. Intuitively, there would appear to be two major sources of error within such a measurement;

(1) The ability of the capacitance manometer to measure the correct pressure.

(2) The abilty of the voltmeter to accurately monitor the voltage produced by the manometer and display the correct reading.

The first problem was to ascertain which of these two sources of error controlled the overall error associated with the carbon yield measurement.

In an attempt to determine the general reliability of capacitance manometers, Loriot and Moran (1975) carried out a study where they assessed capacitance manometer performance in measuring the pressure of differing systems of known (calculated) pressure. They concluded that across the pressure range 2×10^{-4} to 5×10^{-6} torr that the capacitance manometer was accurate. Assuming that the lower pressure reading of 5×10^{-6} torr likewise defined the limit of accuracy for the manometers used in the Triple Collector and MS86[10] gas extraction lines (2.3.), it was then necessary to determine what voltage reading this pressure translated to, and if the respective voltmeter in each extraction line could accurately measure the corresponding voltage. For both the Triple Collector and MS86 manometers, a pressure of 5×10^{-6} torr resulted in an output of 5×10^{-5}V. With respect to the voltmeters[11] that monitored this manometer output, the Triple Collector unit was able to measure to $\pm 5 \times 10^{-4}$V, but for MS86 this improved to $\pm 5 \times 10^{-5}$V. Both of these were above the limit of accurate pressure measurement of the manometers, *i.e.* $\geq 5 \times 10^{-5}$V. It was therefore apparent that for each individual measurement of carbon yield by the manometers in the Triple Collector and MS86, the measurement had a error equivalent to the uncertainty in the voltage measurement of the corresponding voltmeter. Each manometer had been

---

[10] Triple Collector = type number 22DBHS-3A2-B-1.

MS86 = type number 39HA-00001.

Both manufactured by MKS Instruments Inc., Burlington, MA, USA.

[11] Both voltmeters were built in-house. (see Carr, 1985 for the Triple Collector, and Prosser *et al.*, 1990 for MS86).

calibrated by admitting known quantities of CO_2 in to the manometer to determine the corresponding voltage output, and by using the resulting voltage to CO_2 (and thence to ng of carbon) conversion factors, the uncertainty in the voltmeters translated into ±0.95ng of carbon for the Triple Collector, and ±0.13ng for MS86.

A3.3. The protocol for summing individual stepped combustion temperature step $\delta^{13}C$ and carbon yield errors.

Having ascertained the individual errors in $\delta^{13}C$ and carbon yield in each temperature step, it was then neccessary to address the method of how to sum these errors when several steps were averaged. Devising a protocol to quantitatively solve this problem proved to be difficult, so instead a protocol to estimate the probable maximum error (PME) was constructed. The PME describes the conditions in which the worse situation is considered in terms of all the individual experiment errors, and the resultant PME defines limits that subsequently encompass every possible result. Generally speaking, because the PME defines the limits for 100% of the results it is approximately equal to a 3 sigma error bar. An example of the PME protocol is presented as follows using the hypothetical summation of three combustion steps;

Step (°C)	Yield* (ng)	$\delta^{13}C_{PDB}$ (‰)	$\pm\delta^{13}C_{PDB}$ (‰)$
400	4.2	-25.6	1.7
500	7.4	-22.4	1.3
600	3.1	-26.7	2.3

(* = Assuming the stepped combustion data has been taken from the Triple Collector, then the error on each measurement will be ± 0.95 ng)

($ = One sigma instrumental errors from the mass spectrometer software)

The method to calculate the average yield and isotopic composition for these steps without taking into account the errors was as follows;

(1) Isotopic average = Each $\delta^{13}C$ value was multiplied by the corresponding yield and then the sum of the three steps was divided by the sum of the yields (Y) *i.e.*

$$\delta^{13}C_{400\text{-}600°C} = \frac{(\delta^{13}C_{400°C} \times Y_{400°C}) + (\delta^{13}C_{500°C} \times Y_{500°C}) + etc.}{(Y_{400°C} + Y_{500°C} + etc.)}$$

(ii) Carbon concentration = The yields were simply summed, and the concentration of carbon within the sample was calculated by dividing by the measured sample mass.

For the set of steps between 400-600°C above, such a calculation produces an average $\delta^{13}C$ value of -24.2‰ and a yield of 14.7 ng of carbon, which with a hypothetical sample massof 20µg translates into a carbon concentration of 735ppm.

To calculate the PME in both the yield and isotopic composition, these calculations were repeated, but after first adjusting the individual $\delta^{13}C$ values and yields by their respective errors, *i.e.* the possible range of values for the yield and isotopic composition for the 400°C step after applying the appropiate errors would become;

Step (°C)	Yield@ (ng)	$\delta^{13}C_{PDB}$ (‰)
400	3.25 to 5.15	-23.9 to -27.3

(@ = If the yield was experimentally measured at < 0.95 ng (or < 0.13 ng for MS86) then a minimum value of 0.1 ng was used within the following calculation)

The isotopic PME was then calculated by repeating the averaging calculation described previously, but using the following yield and isotopic values;

(1) Sum of the maximum yields (Ymax) multiplied by the heaviest isotopes (I+) and divided by Ymax, *i.e.*

$$\delta^{13}C_{400\text{-}600°C} = \frac{((\delta^{13}C_{400°C} + \pm\delta^{13}C_{400°C}) \times (Y_{400°C} + 0.95ng)) + etc.}{(Y_{400°C} + 0.95ng) + etc.}$$

(2) Sum of the minimum yields (Ymin) multiplied by the lightest isotopes (I-) and divided by Ymin, *i.e.*

$$\delta^{13}C_{400\text{-}600°C} = \frac{((\delta^{13}C_{400°C} - \pm\delta^{13}C_{400°C}) \times (Y_{400°C} - 0.95ng)) + etc.}{(Y_{400°C} - 0.95ng) + etc.}$$

(3) Sum of Ymax multiplied by I- and divided by Ymax, i.e.

$$\delta^{13}C_{400\text{-}600°C} = \frac{((\delta^{13}C_{400°C} - \pm\delta^{13}C_{400°C}) \times (Y_{400°C} + 0.95ng)) + etc.}{(Y_{400°C} + 0.95ng) + etc.}$$

(4) Sum of Ymin multiplied by I+ and divided by Ymin, i.e.

$$\delta^{13}C_{400\text{-}600°C} = \frac{((\delta^{13}C_{400°C} + \pm\delta^{13}C_{400°C}) \times (Y_{400°C} - 0.95ng)) + etc.}{(Y_{400°C} - 0.95ng) + etc.}$$

The example used above produces the following results; -22.7‰, -25.7‰, -26.0‰ and -22.5‰. From these results the two extremes (*i.e.* -26.0 and -22.5‰) were used as outliers for the isotopic PME. It must be remembered that these isotopic outliers do not define an error on the average $\delta^{13}C$ value in terms of a gaussian distribution, but define the range of possible $\delta^{13}C$ for the average $\delta^{13}C$ value. It was, however, considered unlikely that the errors in each quantity would combine in the most unfavourable manner as depicted within the calculation, and infact it has been shown that in many cases the standard deviation (σ) is equal to two thirds the value of the PME (*e.g.* Baird, 1962). To gain a less pessimistic idea of the range of $\delta^{13}C$ values produced by the PME, this relationship was implemented by calculating the difference between the outliers, dividing by two, and then multiplying this figure by two thirds to produce a final and hopefully more realistic range in $\delta^{13}C$. For the example used here, this correlates to final value of -25.4 to -23.0‰ (or -24.22 ± 1.2‰).

The PME for the yield was simply calculated by multiplying the number of temperature steps summed by the appropiate manometer derived ± ng of carbon (either 0.95 or 0.13ng), and then using the same arguments as above, multiplying this value by two thirds. Correspondingly, for the three steps here, the ± error is given by 3 x 0.95 ng x 0.67 and is equal to ± 1.9ng.

Finally, when calculating the carbon concentration (C) within the sample, the error in measuring the sample mass was also accounted for. It was found through repeated weighing of a *ca.* 20μg diamond that the balance used (4.2.1.) was accurate to *ca.* ± 3 μg, so to obtain the final outliers for the C, the following was executed;

(1) Highest possible C = (total yield + final error) divided by (mass - 3μg).

(2) Lowest possible C = (total yield - final error) divided by (mass + 3μg).

For the sample used here of mass 20μg, the yield of 14.7± 1.9ng correlates to a range of C between 977 and 557ppm.

A3.4. Specimen calculations.

To illustrate how the protocol performs, this section contains a number of hypothetical examples for the estimation of the range of $\delta^{13}C$ produced in summing a number of stepped combustion temperature steps.

(1)

Example 1			
Temp.(°C)	Yield(ng)	δ13C(‰)	±
800	10.0	+10.0	1.0
900	10.0	+1000.0	1.0
1000	10.0	+1000.0	1.0
1100	10.0	+10.0	1.0

Summing the above data gives an average $\delta^{13}C$ = +505.0±0.7‰.

(2)

Example 2			
Temp.(°C)	Yield(ng)	δ13C(‰)	±
800	10.0	+10.0	1.0
900	100.0	+1000.0	1.0
1000	100.0	+1000.0	1.0
1100	10.0	+10.0	1.0

Summing the above data gives an average $\delta^{13}C$ = +910.0±1.3‰.

(3)

Example 3			
Temp.(°C)	Yield(ng)	δ13C(‰)	±
800	10.0	+10.0	10.0
900	100.0	+1000.0	1.0
1000	100.0	+1000.0	1.0
1100	10.0	+10.0	10.0

Summing the above data gives an average $\delta^{13}C = +910.0 \pm 1.9‰$.

A5.5. Acknowledgements.

Mr Jeremy Higgins is thanked for transforming a rather rambling sequence of hand calculations into an efficient computer program.

References

Abell P.I., fallick A.E. and Pillinger C.T.(1979) Microreduction techniques for conversion of CO2 to CD4 and their potential application for high sensitivity, precise stable carbon isotope measurement. *In; Adv.Org.Geochem., Eds; A.G.Douglas and J.R.Maxwell, Pergamon*, 689-696.

Ahrens L.H. and Von Michaelis H.(1969) The composition of stony meteorites III. Some inter-element relationships. *Earth and Planet.Sci.Letts.*, **5**, 395-400.

Alaerts L., Lewis R.S., Matsuda J. and Anders E.(1980) Isotopic anomalies of noble gases in meteorites and their origin -VI. Presolar components in the Murchison C2 chondrite. *Geochim.et Cosmochim.Acta.* , **44**, 189-209.

Alexander C.M.O'D., Arden J.W., Ash R.D. and Pillinger C.T.(1990) Presolar components in the ordinary chondrites. *Earth and Planet.Sci.Letts.*, **99**, 220-229.

Alexander C.M.O., Swan P.D. and Walker R.M.(1990) The detection of SiC in situ in CM meteorites: a progress report. *Lunar.Planet.Sci.Conf.*, **21**, 11-12.

Allamandola L.J. and Sandford S.A.(1988) Laboratory simulation of dust spectra, *In: 'Dust in the Universe', Eds: Bailey M.E. and Williams D.A., Cambridge Uni.Press*, 229-257.

Allamandola L.J., Sandford S.A. and Wopenka B.(1987) Interstellar polycyclic aromatic hydrocarbons and carbon in interplanetary dust particles and meteorites. *Science*, **237**, 56-59.

Anders E.(1988) Circumstellar material in meteorites: noble gases, carbon and nitrogen,. *In; Meteorites and the early solar system (Eds: J.F.Kerridge and M.S. Matthews), Uni.Arizona Press, Tucson, Arizona*, 927-955.

Anders E. and Grevesse N.(1989) Abundances of the elements: meteoritic and solar. *Geochim.etCosmochim.Acta*, **53**, 197-214.

Anders E., Hayatsu R. and Studier M.H.(1973) Organic compounds in meteorites. *Science*, **182**, 781-790.

Ash R.D.(1990) Interstellar dust from primitive meteorites: a carbon and nitrogen study. *Unpublished Ph.D. thesis, Open University.*

Ash R.D., Arden J.W., Grady M.M., Wright I.P. and Pillinger C.T.(1988) An interstellar dust component rich in ^{12}C. *Nature*, **336**, 228-229.

Ash R.D., Arden J.W., Grady M.M., Wright I.P. and Pillinger C.T.(1990) Recondite interstellar carbon components in the Allende meteorite revealed by preparitive precombustion. *Geochim.et Cosmochim.Acta*, **54**, 455-468.

Ash R.D., Arden J.W. and Pillinger C.T.(1989) Light nitrogen associated with SiC in Cold Bokkeveld. *Meteoritics*, **24**, 248-249.

Ash R.D, Russell S.S., Wright I.P., Pillinger C.T. and Arden J.W.(1991) Minor high temperature carbon components confirmed in carbonaceous chondrites by stepped combustion usiing a new sensitive static mass spectrometer. *Lunar Planet.Sci.*, **22**, 35-36.

Audouze J.(1977) The importance of CNO isotopes in astrophysics, *In; CNO isotopes in astrophysics (IAU Symp.67), Ed; J.Audouze, Reidel, Dordrecht, Holland.*, 3-11.

Aumann H.H.(1984) IRAS observations of nearby main-sequence dwarfs. *Bull.Am.Astr.Soc.*, **16**, 483.

Backman D.E. and Paresce F.(1992) Nearby main sequence stars with cool circumstellar material. *Meteoritics*, **26**, 314.

Bailes M., Lyne A.G. and Shemar S.L.(1991) A planet orbiting the nuetron star PSR1829-10. *Nature*, **352**, 311-313.

Bailey M.E. and Williams D.A.(1988) Dust in the Universe, *Cambridge Uni.Press*, 572pp.

Bailey M.E., Clube S.V.M. and Napier W.M.(1986) The origin of comets. *Vistas Astron.*, **29**, 53-112.

Bailey M.E., Clube S.V.M. and Napier W.M.(1990) The origin of comets. *Pergamon Press*, 577pp.

Baird D.C.(1962) Experimentation: an introduction to measurement theory and experiment design, *Prentice-Hall, New Jersey, USA.*, 198pp.

Bearman G. (Ed)(1989) Ocean chemistry and deep-sea sediments, *Open University course textbook, Pergamon Press, Oxford, UK.*, 134pp.

Beichman C.A.(1987) The IRAS view of the Galaxy and the Solar System. *Ann.Rev.Astron.Astrophys.*, **25**, 521-563.

Bell J.F.(1991) The S-Class asteroid debate: Historical outline. *Meteoritics*, **26**, 315-316.

Belsky T. and Kaplan I.R.(1970) Light hydrocarbon gases, ^{13}C, and origin of organic matter in carbonaceous Chondrites. *Geochim.et Cosmochim.Acta.* , **34**, 257-278.

Bessell F.W.(1836) Bemerkungen uber mogliche unzulanglichkeit der die anziehungen allein berucksichtienden theorie dr Kometen. *Astr.Nach.*, **13**, 345-350.

Bethe H.A.(1939) Energy production in stars. *Phys.Rev.*, **55**, 434-456.

Blanchard M.B. and Cunningham G.G.(1974) Artificial meteor ablation studies: Olivine. *J.Geophys.Res.*, **79**, 3973-3980.

Blanchard M.B.(1972) Artificial meteor ablation studies: Iron oxides. *J.Geophys.Res.*, **77**, 2442-2455.

Blanchard M.B. and Davis A.S.(1978) Analysis of ablation debris from natural and artificial iron meteorites. *J.Geophys.Res.*, **83**, 1793-1808.

Blanchard M.B., Brownlee D.E., Bunch T.E., Hodge P.W. and Kyte F.T.(1980) Meteoroid ablation spheres from deep-sea sediments. *Earth and Planet.Sci.Letts.*, **46**, 178-190.

Blanford G.E., Thomas K.L. and McKay D.S.(1988) Microbeam analysis of chondritic interplanetary dust particles for carbon, oxygen and major elements. *Lunar.Planet.Sci.Conf.*, **19**, 102-103.

Boato G.(1954) The isotopic composition of hydrogen and carbon in the carbonaceous chondrites. *Geochim.et Cosmochim.Acta*, **6**, 209-220.

Bobrovnikoff N.T.(1930) Carbon isotopes in comets. *Publ.Astron.Soc.Pacific*, **42**, 117-124.

Bonny Ph. and Balageas D.(1990) Entry corridor of micrometeorites containing organic material. *Lunar.Planet.Sci.Conf.*, **21**, 111-112.

Bonny Ph., Balageas D. Devezeaux D. and Maurette M.(1988) Atmospheric entry of micrometeorites containing organic materials. *Lunar.Planet.Sci.Conf.*, **19**, 118-119.

Bowell E., Chapman C.R., Gradie J.C., Manson D. and Zellner B.(1978) Taxonomy of asteroids. *Icarus*, **35**, 313-335.

Boyd S.R.(1988) A study of carbon and nitrogen isotopes from the Earth's mantle, *Unpublished PhD thesis, The Open University.*

Bradley J.P. (1988) Analysis of chondritic interplanetary dust thin sections. *Geochim.et Cosmochim.Acta.* , **52**, 889-900.

Bradley J.P. and Brownlee D.E.(1991) An interplanetary dust particle linked directly to type CM meteorites and an asteroidal origin. *Science*, **251**, 549-552.

Bradley J.P. and Brownlee D.E.(1986) Cometary particles: thin sectioning and electron beam analysis. *Science*, **231**, 542-544.

Bradley J.P., Brownlee D.E. and Fraundorf P.(1984) Carbon compounds in interplanetary dust: Evidence for formation by heterogeneous catalysis. *Science*, **223**, 56-58.

Briggs M.H.(1963) Evidence for an extraterrestrial origin for some organic constituents of meteorites. *Nature*, **197**, 1290.

Brophy T.G.(1991) Does debris from the formation of other planetary systems impact Earth?. *Icarus*, **94**, 250-254.

Brownlee D.E , Bucher W. and Hodge P.W.(1971) Micrometeoroid flux from Surveyor glass surfaces. *Proc.Lunar.Planet.Sci.*, **3**, 2781-2789.

Brownlee D.E.(1978) Microparticle studies by sampling techniques. *In: Cosmic dust (Ed: J.A.M. McDonnell), Wiley* 295-336.

Brownlee D.E.(1981) Extraterrestrial components. *In: The Sea (Ed: C. Emiliani)*, **7**, 733-762.

Brownlee D.E.(1985) Cosmic dust: Collection and research. *Ann.Rev.Earth and Planet.Sci.*, **13**, 147-173.

Brownlee D.E.(1987) Interstellar grains in the solar system. *In; Interstellar processes (Eds: D.J. Hollenbach and H.A.Thronson (Jr)), Reidel Publ.Co.*, 513-530.

Brownlee D.E. and Schramm L.S.(1990) The composition of picogram to milligram meteoritic spherules. *Lunar.Planet.Sci.Conf.*, **21**, 134-135.

Brownlee D.E., Bates B.A. and Wheelock M.M.(1984) Extraterrestrial platinum group nuggets in deep-sea sediments. *Nature*, 309, 693-695.

Brownlee D.E., Bates B.A., Pilachowski C.B., Olszewski E. and Siegmund W.A.(1980) Unmelted cosmic materials in deep-sea sediments. *Lunar.Planet.Sci.Conf.*, 11, 109-111.

Brownlee D.E., Blanchard M.B. and Cunningham G.C.(1975) Criteria for identifying ablation debris from primitive meteoritic bodies. *J.Geophys.Res*, 80, 4917-4924.

Brownlee D.E , Bucher W. and Hodge P.W.(1971) Micrometeoroid flux from Surveyor glass surfaces. *Proc.Lunar.Planet.Sci.*, 3, 2781-2789.

Brownlee D.E., Pilachowski L.B. and Hodge P.W.(1979) Meteorite mining on the ocean floor. *Lunar.Planet.Sci.Conf.*, 10, 157-158.

Brownlee D.E., Tomandl D.A., Hodge P.W. and Horz F.(1974) Elemental abundances in interplanetary dust. *Nature*, 252, 667-669.

Brownlee D.E., Tomandl D.A. and Hodge P.W.(1976) Extraterrestrial particulates in the stratosphere. *Lecture notes in physics - 'Interplanetary dust and the zodiacal light' (Eds; Ehlers J. et al.)*, 48, 279-283.

Bruhweiler F.C., Kondo Y. and Grady C.A.(1991) Mass outflow in the nearby proto-planetary system B Pictoris. *Astrophys.J.*, 371, L27-L31.

Bruun A.F., Langer E. and Pauly H.(1955) Magnetic particles found by raking the sea bottom. *Deep-Sea Res.*, 2, 230.

Buchvald V.(1977) The mineralogy of iron meteorites. *Phil.Trans.R.Soc.Lond.*, A286, 453-491.

Buddhue J.D.(1950) Meteoritic dust. *Uni.New Mexico Publ.*, 2, 102pp.

Bunch T.E. and Chang S.(1980) Carbonaceous chondrites - II. Carbonaceous chondrite phyllosilicates and light element geochemistry as indicators of parent body processes and surface conditions. *Geochim.et Cosmochim.Acta.* , 44, 1543-1577.

Caistaing R. and Fredriksson K.(1958) Analyses of cosmic spherules with an X-ray microanalyser. *Geochim.et Cosmochim.Acta.* , 14, 114-117.

Callot G., Maurette M., Pottier L. and Dubrois A. (1987) Biogenic etching of microfractures in amorphous and crystalline silicates. *Nature*, 328, 147-149.

Cameron A.G.W.(1973) Accumulation processes in the primitive solar nebula. *Icarus*, 18, 407-450.

Cameron A.G.W.(1977) Interstellar grains in museums, *In; 'Interstellar dust and related topics', Eds; H.C. Van de Hulst and J.M. Greenberg.*, 545-547.

Cameron A.G.W.(1982) Elemental and nuclidic abundance in the solar system, *In; 'Essays in Nuclear Astrophysics', Eds; C.A.Barnes, D.D.Clayton and D.N.Schramm, Cambridge Uni.Press*, 23-43.

Cameron A.G.W.(1984) Star formation and extinct radioactivities. *Icarus*, 60, 416-427.

Cameron A.G.W. and Truran J.W.(1977) The supernova trigger for the formation of the solar system. *Icarus*, 30, 447-461.

Carr R.H.(1985) High sensitivity stable carbon isotope ratio mass spectrometry: instrument development and applications. *Unpublished Ph.D. thesis, University of Cambridge.*

Carr R.H., Gibson E.K., Rietmeijer F.J.M., Grady M.M., Wright I.P. and Pillinger C.T.(1986a) Characterisation of carbonaceous materials in interplanetary dust particles. *Meteoritics*, **21**, 344-345.

Carr R.H., Grady M.M.,Wright I.P. and Pillinger C.T.(1985b) Martian atmospheric carbon dioxide and weathering products in SNC meteorites. *Nature*, **314**, 248-250.

Carr R.H.,Wright I.P.,Joines A.W. and Pillinger C.T.(1986b) Measurement of carbon stable isotopes at the nanomole level: a static mass spectrometer and sample preparation technique. *J.Phys.E.Sci.Instrum.*, **19**, 798-808.

Carr R.H., Wright I.P. and Pillinger C.T.(1985a) Carbon isotopes in three SNC Meteorites. *Lunar.Planet.Sci.Conf.*, **15**, 664-668.

Carr R.H., Wright I.P., Pillinger C.T., Lewis R.S. and Anders E.(1983) Interstellar carbon in meteorites: Isotopic analysis using static mass spectrometry. *Meteoritics*, **18**, 277.

Chang S., Mack R. and Lennon K.(1978) Carbon chemistry of seperated phases of Murchison and Allende meteorites. *Lunar Planet.Sci.*, **9**, 157-159.

Chevallier P., Jehanno C., Maurette M., Sutton S.R. and Wang J. (1987) Trace element analyses of spheres from the melt zone of the Greenland Ice Cap using synchrotron X-ray fluorescence. *J.Geophys.Res.*, **92**, E649-656.

Clark B., Mason L.W. and Kissel J.(1986) Systematics of the "CHON" and other light element particle populations in Comet Halley. *20th ESLAB Symposium on the Exploration of Halley's Comet, Eds; Battrick B., Rolfe E.J. and Reinhard R., ESA SP-250 III*, 353-358.

Clark L.G., Kinard W.H., Carter D.J. and Jones J.L. (Jr)(1984) The long duration exposure facility (LDEF). Mission 1 experiments. *Nasa Sp-473, Lunar and Planet.Inst, Houston, USA.*

Clayton D.D.(1985) Galactic chemical evolution and nucleocosmochronology: A standard model, *In; Nucleosynthesis, Eds; Arnett W.D. and Truran J.W., Uni.Chicago Press, Chicago*, 308pp.

Clayton D.D.(1988) The relationship between interstellar dust and the isotopic anomalies in meteorites, *In: 'Dust in the Universe', Eds: M.E. Bailey and D.A. Williams, Cambridge Uni.Press*, 145-151.

Clayton D.D. and Ramadurai S.(1977) On presolar meteoritic sulphides. *Nature*, **265**, 427-428.

Clayton R.N., Mayeda T.K. and Brownlee D.E.(1986) Oxygen isotopes in deep sea spherules. *Earth and Planet.Sci.Letts.*, **79**, 235-240.

Clayton R.N., Onuma N., Grossman L. and Mayeda T.K.(1977) Distribution of the presolar component in Allende and other carbonaceous chondrites. *Earth Planet.Sci.Letts.*, **34**, 209-244.

Clube S.V.M. and Napier W.M.(1984) Comet capture from molecular clouds: a dynamical constraint on star and planet formation. *Mon.Not.Roy. Astron.Soc.*, **208**, 575-588.

Combes M.J.P., Mailard J.P. and de Bergh C.(1977) Evidence for a telluric value of the $^{12}C/^{13}C$ ratio in the atmospheres of Jupiter and Saturn. *Astron.Astrophys.*, **61**, 531-537.

Cour-Palais B.G., Brown M.L. and McKay D.S.(1972) Apollo window meteoroid experiment. *NASA SP-315*, 26-1 to 26-10.

Courtin R., Gautier D., Marten A. and Kunde V.(1983) The 12C/13C ratio in Jupiter from the voyager infrared investigation. *Icarus*, **53**, 121-132.

Craig H.(1953) The geochemistry of the stable carbon isotopes. *Geochim.et Cosmochim.Acta.* , **3**, 53-92.

Craig H.(1957) Isotopic standards for carbon and oxygen and correction factors for mass-spectrometric analysis of carbon dioxide. *Geochim.et Cosmochim.Acta*, **12**, 133-149.

Cuzzi J.N., Lissauer J.J., Esposito L.W., Holberg J.B., Marouf E.A., Tyler G.L. and Boischot A.(1984) Saturn's rings: Properties and processes. *In; Planetary rings (Eds: R.Greenberg and A.Brahic), Uni.Arizona Press, Tucson, Arizona.*, 73-199.

Danks A.C., Lambert D.L. and Arpigny C.(1974) The $^{12}C/^{13}C$ ratio in comet Kohoutek (1973f). *Astrophys J.*, **194**, 745-751.

Davis A.M. and Olsen E.(1991) Phosphates in pallasite meteorites as probes of mantle processes in small planetary bodies . *Nature*, **353**, 637-640.

Davis A.M., Clayton R.N., Mayeda T.K. and Brownlee D.E.(1991) Large mass fractionation of iron isotopes in cosmic spherules collected from deep-sea sediments. *Lunar.Planet.Sci.Conf.*, **22**, 281-282.

Dearborn D., Tinsley B.M. and Schramm D.N.(1978) On the origin and evolution of isotopes of carbon, nitrogen and oxygen. *Astrophys J.*, **223**, 557-566.

Dearborn D.S.P.(1977) CNO isotopes in red giants, *In; CNO isotopes in astrophysics (IAU Symp.67), Ed; J.Audouze, Reidel, Dordrecht, Holland.*

Deer W.A., Howie R.A. and Zussman J.(1983) An introduction to the rock forming minerals, *Longman Group Ltd, Harlow, UK*, 528pp.

Deines P.(1980) The isotopic composition of reduced carbon in the terrestrial environment, *In: 'Handbook of environmental isotope geochemistry' (Eds; P.Fritz and J.Ch.Fontes)*, Elsevier, 329-407.

Deines P. and Wickman F.E.(1973) The isotopic composition of 'graphitic' carbon from Iron Meteorites and some remarks on the troilitic sulphur of Iron Meteorites. *Geochim.et Cosmochim.Acta.* , **37**, 1295-1319.

Deines P. and Wickman F.E.(1975) A contribution to the stable isotope geochemistry of Iron Meteorites . *Geochim.et Cosmochim.Acta.* , **39**, 547-557.

Delsemme A.H.(1976) Can comets be the only source of interplanetary dust?. *Lecture notes in physics - 'Interplanetary dust and the zodiacal light' (Eds; Ehlers J. et al.)*, **48**.

Dermott S.F., Nicholson P.P., Burns J.A. and Houck J.R.(1984) Origin of the solar system dust bands discovered by IRAS. *Nature* , **312**, 505-509.

Des Marais D.J.(1978) Carbon, nitrogen and sulphur in Apollo 15,16 and 17 rocks. *Proc.9th Lunar Planet.Sci.Conf.*, 2451-2467.

Des Marais D.J.(1983) Light element geochemistry and spallogenesis in lunar rocks. *Geochim.et Cosmochim.Acta.* , **47**, 1769-1781.

Deuser W.G.(1968) Iron-magnesium-aluminium ralationships in achondrites. *Chem.Geol.*, 3, 81-87.

Dodd R.T.(1969) Metamorphism of the ordinary chondrites: a review. *Geochim.et Cosmochim.Acta*, 33, 161-203.

Dodd R.T.(1981) Meteorites: A petrologic - chemical synthesis. *Cambridge Uni.Press, Cambridge, UK*, 368pp.

Dohnanyi J.S.(1971) Flux of micrometeoroids: lunar sample analyses compared with flux model. *Science*, 173, 558.

Dohnanyi J.S.(1978) Particle dynamics. *In: Cosmic Dust (Ed: J.A.M.Mc Donnell), Wiley*, 527-605.

Draine B.T. and Lee H.M.(1984) Optical properties of interstellar graphite and silicate grains. *Astrophys.J.*, 285, 89-108.

Dufresne E.R and Anders E.(1962) On the chemical evolution of the carbonaceous chondrites. *Geochim.et Cosmochim.Acta.* , 26, 1085-1114.

Elmegreen B.G.(1985) Molecular clouds and star formation: an overview, *In: "Protostars and planets II', Eds: Black D.C. and Matthews M.S., Uni.Arizona Press, Tuscon, Arizona*, 1293pp.

Epstein S. and Taylor H.P.(1970) $^{18}O/^{16}O$, $^{30}Si/^{28}Si$, D/H and $^{13}C/^{12}C$ studies of lunar rocks and minerals. *Science*, 167, 533-535.

Exley R.A., Mattey D.P., Clague D.A. and Pillinger C.T.(1986) Carbon isotope systematics of a mantle "hotspot": A comparison of Loihi seamount and MORB glasses. *Earth Planet.Sci.Letts.*, 78, 189-199.

Fahey A.J., Goswami J.N., McKeegan K.D. and Zinner E.(1987) O^{16} excesses in Murchison and Murray hibonites; a case aginst a late stage supernova injection origin of isotopic anomalies in O, Mg, Ca and Ti.. *Astrophys.J.*, 323, L91-L95.

Fechtig H.(1982) Cometary dust in the Solar System. *In; Comets (Ed; L.L.Wilkening), Uni.Arizona Press, Tucson, Arizona*, 766pp.

Fechtig H., Hartung J.B., Nagel K., Neukum G. and Storzer D.(1974) Lunar microcrater studies, derived meteoroid fluxes, and comparison with satellite-bourne experiments. *Proc.Lunar.Planet.Sci.*, 5, 2463-2474.

Festou M.C., Stern S.A and Tozzi G.P.(1991) Asteroid 4 Vesta: simultaneous visible and ultraviolet IUE observations. *Icarus*, 94, 281-231.

Finkleman R.B.(1970) Magnetic particles extracted from manganese nodules: Suggested origin from stony and iron meteorites. *Science*, 167, 982-984.

Finkleman R.B.(1972) Relationships between manganese nodules and cosmic spherules. *J.Mar.Tech.Soc.*, 6, 34-39.

Fireman E.L. and Kistner G.A.(1961) The nature of dust collected at high altitudes. *Geochim.et Cosmochim.Acta.* , 24, 10-22.

Fireman E.L.and Langway C.C. Jr(1965) Search for aluminium-26 in dust from the Greenland Ice Sheet. *Geochim.et Cosmochim.Acta.* , 29, 21-27.

Fisher C.R., Kennicutt M.C.(II) and Brooks J.M.(1990) Stable carbon isotopic evidence for carbon limitation in hydrothermal vent vestimentiferans. *Science*, **247**, 1094-1096.

Flynn G.J.(1989) Atmospheric entry heating: A criterion to distinguish between asteroidal and cometary sources of interplanetary dust. *Icarus*, **77**, 287-310.

Flynn G.J.(1991) Survival of large micrometeorites on atmospheric entry: Implications for their sources and the flux of cometary dust. *Lunar.Planet.Sci.Conf.*, **22**, 393-394.

Fraundorf P.(1980) The distribution of temperature maxima for micrometeorites decelerated in the Earths atmosphere without melting. *Geophys.Res.Letts.*, **8**, 765-768.

Fredriksson K. and Gowdy R.(1963) Meteoritic debris from the Southern California Desert. *Geochim.et Cosmochim.Acta.* , **27**, 241-243.

Galimov E.M.(1991) Isotope fractionation related to kimberlite magmatism and diamond formation. *Geochim.et Cosmochim.Acta*, **55**, 1697-1708.

Gaffey M.J. and McCord T.B.(1978) Asteroid surface materials: Mineralogical characterizations from reflectance spectra. *Space Sci.Rev.*, **21**, 555-628.

Gardiner L.R.(1978) Static mass spectrometry for the determination of active gases. *Unpublished Ph.D. thesis, University of Bristol.*

Gardiner L.R. and Pillinger C.T.(1979) Static mass spectrometry for the determination of active gases. *Anal.Chem.*, **51**, 1230-1236.

Gast P.W. and Hubbard N.J.(1970) Rare earth abundances in soil and rocks from the Ocean of Storms. *Earth Planet.Sci.Letts.*, **10**, 94-101.

Gibson J.E., Pillinger C.T. and Gibson E.K.(Jr)(1991) Carbon content of silica aerogel: A material proposed as amedium for collection of cosmic dust grains. *Lunar.Planet.Sci.Conf.*, **22**, 441-442.

Giese R.H. and Grun E.(1976) The compatibility of recent micrometeoroid flux curves with observations and models of the zodialcal light. *Lecture notes in physics - 'Interplanetary dust and the zodiacal light' (Eds; Ehlers J. et al.)*, **48**, 135-139.

Gombosi T.I. and Houpis H.L.F.(1986) An icy-glue model of cometary nuclei. *Nature*, **324**, 43-44.

Grady M.M.(1982) The content and isotopic composition of carbon in stony meteorites. *Unpublished Ph.D. thesis, University of Cambridge.*

Grady M.M., Swart P.K. and Pillinger C.T.(1982a) Carbon isotopic compositions of some type 3 Ordinary Chondrites. *Lunar.Planet.Sci.Conf.*, **13**, 277-279.

Grady M.M., Swart P.K. and Pillinger C.T.(1982b) Carbon isotopes in graphite from graphite-magnetite matrix. *Meteoritics*, **17**, 223-224.

Grady M.M., Wright I.P., Carr L.P. and Pillinger C.T.(1986) Compositional differences in enstatite chondrites based on carbon and nitrogen stable isotope measurements. *Geochim.et Cosmochim.Acta*, **50**, 2799-2813.

Grady M.M., Wright I.P. and Pillinger C.T.(1989) A preliminary investigation into the nature of carbonaceous material in ordinary chondrites. *Meteoritics*, **24**, 147-154.

Grady M.M., Wright I.P. and Pillinger C.T.(1991) Comparisons between Antarctic and non-Antarctic meteorites based on carbon isotope geochemistry. *Geochim.et Cosmochim.Acta.* , **53**, 49-59.

Grady M.M., Wright I.P., Swart P.K. and Pillinger C.T.(1988) The carbon and oxygen isotopic composition of meteoritic carbonates. *Geochim.et Cosmochim.Acta*, **52**, 2855-2866.

Graham A.L., Bevan A.W.R. and Hutchison R.(1985) Catalogue of meteorites. *British Museum (Natural History)*, 460pp.

Greenberg J.M.(1988) The interstellar dust model of comets: post Halley. *In; Dust in the universe (Eds: M.E. Bailey and D.A. Williams), Cambridge Uni.Press, Cambridge*, 121-143.

Greenberg J.M. and Chlewicki G.(1984) A far-ultraviolet extinction law: what does it mean?. *Astrophys J.*, **272**, 563-578.

Griffen W.L.,Jaques A.L.,Sie S.H.,Ryan C.G.,Cousens D.R. and Suter G.F.(1988) Conditions of diamond growth: a proton microprobe study of inclusions in West Australian diamonds. *Contrib.Mineral.Pet.*, **99**, 143-158.

Grun E. and Jessberger E.(1990) Dust. *In; Physics and chemistry of comets (Ed: W.F.Huebner), Springer Verlag*, 113-176.

Grun E., Zook H.A., Fechtig H. and Giese R.H. (1985) Collisional balance of the meteoritic complex. *Icarus*, **62**, 244-272.

Gunsalus I.C. and Stanier R.Y. (Eds)(1960) The Bacteria; A treatise in structure and function. Volume I; Structure, *Academic Press*, 513pp..

Gustafson B.A.S. and Misconi N.Y.(1979) Streaming of interstellar grains into the solar system . *Nature*, **282**, 276-278.

Gustafson B.A.S. and Misconi N.Y.(1986) Interplanetary dust dynamics 1. Long term gravatational effects of the inner planets on zodiacal dust. *Icarus*, **66**, 280-287.

Halas S. and Krouse H.R.(1983) Isotopic analysis of nanomole gas samples by means of dynamic flow mass spectrometry. *Rev.Sci.Instrum.*, **54**, 437-443.

Hall D.N.B.(1973) Detection of the ^{13}C, ^{17}O and ^{18}O isotope bands in the infrared solar spectrum. *Astrophys.J.*, **182**, 977-982.

Hallgren D.S. and Hemenway C.L.(1976) Analysis of impact craters from the S149 Skylab experiment. *Lecture notes in physics - 'Interplanetary dust and the zodiacal light' (Eds; Ehlers J. et al.)*, **48**, 270-274.

Halstead R.E. and Nier A.O.(1950) Gas flow through the mass spectrometer viscous leak. *Rev.Sci.Instrum.*, **21**, 1019-1021.

Harding C.(1985) Physics and chemistry of the interstellar medium. *S256 'Matter in the Universe' course textbook, Open Uni. Press, UK*, 81pp.

Hartmetz C.P., Gibson E.K.(Jr) and Blanford G.E.(1991a) Analysis of volatiles present in IDP and stratospheric particles collected on large area collectors. *Proc.Lunar.Planet.Sci.*, **21**, 557-567.

Hartmetz C.P., Wright I.P. and Pillinger C.T.(1991b) Attempts to constrain the carbon isotopic composition of dispersed carbonate in EETA 79001. *Meteoritics*, **26**, 342.

Harvey R.P. and Maurette M.(1990) The best cosmic dust source in the world?: The origin and significance of the Walcott Neve, Antarctica micrometeorites. *Lunar.Planet.Sci.Conf.*, **21**, 467-468.

Harwit M.(1964) Origins of the zodiacal dust cloud II. *Annals N.Y.Acad.Sci.*, **119**, 68-71.

Hauser M.G., Gillet F.C., Low F.J., Gautier J.N., Beichman C.A., Neugebauer G., Aumann H.H., Baud B., Boggess N., Emerson J.P., Houck J.R., Soifer B.T. and Walker R.G.(1984) IRAS observations of the diffuse infrared background. *Astrophys.J.*, **278**, L15-L18.

Hawkins G.S.(1964) Interplanetary debris near the Earth. *Ann.Rev. Astron.Astrophys.*, **2**, 149-164.

Hawkins I. and Jura M.(1987) The 12C/13 C isotope ratio of the interstellar medium in the neighbourhood of the Sun. *Astrophys.J.*, **317**, 926-950.

Hayatsu R. and Anders E.(1981) Organic compounds in meteorites and their origins, *In; 'Topics in current chemistry, cosmo- and geochemistry', Ed; F.L.Boschke, Sringer Verlag, Heidelberg*, 1-37.

Hayes J.M.(1967) Organic constituents of meteorites - a review. *Geochim.et Cosmochim.Acta*, **31**, 1395-1440.

Heiles C.(1976) The interstellar Magnetic field. *Ann.Rev.Astron.Astrophys.*, **14**, 1-22.

Hemenway C.L. and Linscott I.(1964) Preliminary studies of possible cosmic dust impacts on project Mercury vehicle periscope lenses. *Annals N.Y.Acad.Sci.*, **119**, 106-115.

Hemenway C.L. and Soberman R.K.(1962) Studies of micrometeorites obtained from a recoverable sounding rocket. *Astron.J.*, **67**, 256-266.

Hemenway C.L., Hallgren D.S. and Schmalberger P.(1972) Stardust. *Nature*, **238**, 256-260.

Hemenway C.L., Hallgren D.S., Coon R.E. and Bourdillon L.A. (1964) Technical description of the Gemini S-10 and S-12 micrometeorite experiments. *Space Res.*, **8**, 510-520.

Herbig G.H.(1977) Eruptive phenomena in early stellar evolution. *Astrophys.J.*, **217**, 693-715.

Hirao K. and Itoh T.(1986) The Planet-A Halley encounters. *Nature*, **321**, 294-297.

Hodge P.W.(1981) Interplanetary dust. *Gordon and Breach Sci.Publ.*, 265pp.

Hoefs J.(1973) Ein beitrag zur isotopengeochemie des kohlenstoffs in magmatiscen gesteinen. *Contrib.Mineral.Petrol.*, **41**, 277-300.

Hoefs J.(1987) Stable isotope geochemistry, *Springer-Verlag, N.Y., USA*, 241pp.

Horz F., Brownlee D.E., Fechtig H., Hartung J.B., Morrison D.A., Neukum G., Schneider E., Vedder J.F. and Gault D.E.(1975) Lunar microcraters: Implications for the micrometeoriod complex. *Planet.Space Sci.*, **23**, 151-172.

Horz F., Fechtig H. and Janicke J.(1983) Morpholgy and chemistry of projectile residue in small experimental impact craters. *Proc.XIV Lunar.Planet.Sci.(J.Geophys.Res.)*, **88**, B353-363.

Housen K.R. and Wilkening L.L.(1982) Regoliths on small bodies in the solar system. *Ann.Rev.Earth Planet.Sci*, **10**, 355-376.

Huebner W.F.(1990) Introduction. *In; Physics and chemistry of comets (Ed: W.F.Huebner), Springer Verlag*, 1-12.

Huebner W.F. and Mckay C.P.(1990) Implications of comet research. *In; Physics and chemistry of comets (Ed: W.F.Huebner), Springer Verlag*, 305-332.

Hughes D.W.(1978) Meteors. *In: Cosmic Dust (Ed: J.A.M. McDonnell), Wiley*, 123-185.

Hughes D.W.(1980) Cosmic spherules. *Nature*, **287**, 778-779.

Hunter W. and Parkin D.W.(1960) Cosmic dust in recent deep-sea sediments. *Proc.R.Soc.London*, **255**, 382-397.

Hunter W. and Parkin D.W.(1961) Cosmic dust in Tertiary rock and the lunar surface. *Geochim.et Cosmochim.Acta.* , **24**, 32-39.

Huss G.R.(1990) Ubiquitous interstellar diamond and SiC in primitive chondrites: Abundance reflect metamorphism. *Nature*, **347**, 159-162.

Huss G.R. and Lewis R.S.(1989) Interstellar diamonds and SiC from type 3 ordinary chondritic meteorites. *Meteoritics*, **24**, 278-279.

Hutchison R., Bevan A.W.R., Agrell S.O. and Ashworth J.R.(1980) Thermal history of the H-group chondritic meteorites. *Nature*, **287**, 787-790.

Iben I. and Renzini A.(1983) Asymptotic giant branch evolution and beyond. *Ann.Rev.Astron.Astrophys.*, **21**, 271-342.

Irako M.,Oguri T. and Kanomata I.(1975) The static operation mass spectrometer. *Jap.J.App.Phys.*, **14**, 533-543.

Istomin V.G., Grechnev K.V. and Kochnev V.A.(1980) Mass spectrometry of the Venus lower atmosphere. *Paper presented at 23rd COSPAR General Assembly, Budapest, Hungary.*

Jackson A.A. and Zook H.A.(1988) A solar system dust ring: The Earth as its shepherd. *Lunar.Planet.Sci.Conf.*, **19**, 539-540.

Jedwab J.(1971) La magnetite de la meteorite d'Orgueil vue au microscope electronique a balayage. *Icarus*, **15**, 319-340.

Jenkins F.A. and King A.S. (1936) A test of the abundance of carbon in a graphite meteorite . *Publ.Astron.soc.Pacific.*, **48**, 323-325.

Jessberger E.K., Christoforidis A. and Kissel J. (1988) Asects of the major element composition of Halley's dust. *Nature*, **332**, 691-695.

Jones B.(1985) The origin and evolution of planetary systems. *S256 'Matter in the Universe' course textbook, Open Uni. Press, UK*, 87pp.

Kasten F.(1968) Falling speed of aerosol particles. *J.App.Met.*, **7**, 944.

Keeling C.D.(1961) The concentration and isotopic abundances of carbon dioxide in rural and marine air. *Geochim.et Cosmochim.Acta.* , **24**, 277-298.

Kerr F.J.(1962) Galactic velocity models and the interpretation of 21-cm surveys. *Mon.Not.Roy.Astron.Soc.*, **123**, 327-345.

Kerridge J.F.(1983) Isotopic composition of carbonaceous chondrite kerogen: Evidence for an interstellar origin of organic matter in meteorites. *Earth and Planet.Sci.Letts.*, **64**, 186-200.

Kerridge J.F.(1985) Carbon, hydrogen and nitrogen in carbonaceous chondrites: Abundances and isotopic compositions in bulk samples. *Geochim.et Cosmochim.Acta.* , **49**, 1707-1714.

Kerridge J.F. and Matthews M.S. (Eds)(1988) Meteorites and the early solar system. *Uni.Arizona Press, Tucson, Arizona*, 1269pp.

Kerridge J.F., Chang S. and Shipp R.(1987) Isotopic characterisation of kerogen-like material in the Murchison carbonaceous chondrite. *Geochim.et Cosmochim.Acta*, **51**, 2527-2540.

Kessler D.J. and Cour-Palais B.G.(1978) Collisional frequency of artificial satellites: The creation of a debris belt . *J.Geophys.Res.*, **83**, 2637-2646.

Kessler D.J., Zook H.A., Potter A.E., McKay D.S., Clanton U.S., Warren J.L., Watts L.A., Schultz R.A., Schramm L.S., Wentworth S.J. and Robinson G.A.(1985) Examination of returned Solar-Max surfaces for impacting orbital debris and meteoroids. *Lunar.Planet.Sci.Conf.*, **15**, 434-435.

King E.A.(1982) Refractory residues, condesates and chondrules from solar furnace experiments. *J.Geophys.Res.*, **87**, A429-434.

King E.A. and Wagstaff J.(1980) Search for cometary dust in the Antarctic Ice . *Ant.J.US.*, **15**, 78-79.

King E.A. (Jr), Schonfield E., Richardson K.A. and Eldridge J.S.(1969) Meteorite fall at Pueblito de Allende, Chihuahua, Mexico: Preliminary information . *Science*, **163**, 928-929.

King A.S.(1936) A spectroscopic examination of meteorites . *Astrophys.J.*, **84**, 507-516.

King A.S. and Birge R.T.(1929) An isotope of carbon, mass 13. *Nature*, **124**, 127.

Klock W. and Beckerling W.(1991) Bulk composition and mineralogy of micrometeorites from Greenland. *Lunar.Planet.Sci.Conf.*, **22**, 725-726.

Koerberl C. and Hagen E.(1989) Extraterrestrial spherules in glacial sediment from the Transantarctic Mountains, Antarctica: Structure, mineralogy and chemical composition. *Geochim.et Cosmochim.Acta.* , **53**, 937-944.

Krauskopf K.B.(1982) Introduction to geochemistry, *McGraw Hill Int.Series on the Earth and Planet.Sci., UK*, 617pp.

Krinov E.L.(1959) Nonterrestrial dust on the Earth. *Sky and Telescope*, **18**, 617-619.

Kvenvolden K., Lawless J., Pering K., Peterson E., Flores J., Ponnamperuma C., Kapan I.R. and Moore C.B.(1970) Evidence for extraterrestrial amino acids and hydrocarbons in the Murchison meteorite . *Nature*, **228**, 923-926.

Laevastu T. and Mellis O.(1955) Extraterrestrial material in deep-seas deposits. *Trans.Am.Geophys.Union*, **36**, 385-389.

Lambert D.L. and Danks A.C.(1983) High resolution spectra of C2 swan bands from Comet West 1976VI. *Astrophys.J.*, **268**, 428-446.

Langevin Y., Kissel J., Bertaux J.L. and Chassefiere E.(1987) Impact ionisation mass spectrometry of the cometary grains on board Giotto, Vega 1, and Vega 2 spacecraft; preliminary statistical analysis of spectra in compressed modes. *Lunar Planet.Sci.*, **18**, 533-534.

Larimer J.W. and Anders E.(1967) Chemical fractionations in meteorites-II. Abundance patterns and their interpretation. *Geochim.et Cosmochim.Acta*, **31**, 1239-1270.

Larsen E.(1962) The Cavendish Laboratory- Nursery of genius. *Edmund Ward Ltd, London*, 95pp.

Leinert C., Roser S. and Buitrago J.(1983) How to maintain the spatial distribution of interplanetary dust. *Astron.Astrophys.*, **118**, 345-357.

Lewin R.A.(1962) Physiology and biochemistry of algae, *Academic Press*, pp.929.

Lewis R.S., Tang M., Wacker J.F., Anders E. and Steel E.(1987) Interstellar diamonds in meteorites. *Nature*, **326**, 160-162.

Lipschutz M. (1962) Diamonds in the Dyalpur meteorite. *Science*, **138**, 1264-1267.

Lipschutz M.E., Gaffey M.J. and Pellas P.(1989) Meteoritic parent bodies: nature, number, size and relation to present day asteroids, *In: 'Asteroids II' (Eds: R.P.Binzel, T.Gehrels and Matthews M.S.), Uni.Arizona Press*, 740-777.

Lipson H. and Steeple H.(1970) Interpretation of X-ray powder diffraction patterns. *McMillan*, 335pp.

Loriot G. and Moran T.(1975) Reliability of a capacitance manometer in the range 2×10^{-4} - 5×10^{-6} torr. *Rev.Sci.Instrum.*, **46**, 140-143.

Love S.G. and Brownlee D.E.(1991) Heating and thermal transformation of micro-meteoroids entering the Earths' atmosphere. *Icarus*, **89**, 26-43.

Low F.J., Beintema D.A., Gautier T.N., Gillet F.C., Beichman C.A., Neugebauer G., Young E., Aumann H.H., Boggess N., EmersonJ.P., Habing H.J., Hauser M.G., Houck J.R., Rowan-Robinson M., Soifer B.T., Walker R.G. and Wesselius P.R.(1984) Infrared cirrus: New components of the extended infrared emission. *Astrophys.J.*, **278**, L19-L22.

Lyne A.G. and Bailes M.(1992) No planet orbiting PSR1829-10. *Nature*, **355**, 213.

Mackinnon I.D.R. and Carey W.C. (Eds)(1988) Progress towards a cosmic dust collection facility on space station. *LPI Technical Rep.88-01, Lunar and Planet.Inst., Houston*, 81pp.

Marvin U.B.(1963) Mineralogy of the oxidation products of the Sputnik 4 fragment and of iron meteorites. *J.Geophys.Res*, **68**, 5059-5068.

Marvin U.B. and Einaudi M.T.(1967) Black, magnetic spherules fron Pleistocene and recent beach sands. *Geochim.et Cosmochim.Acta.* , **31**, 1871-1884.

Mason B.(1962) Meteorites, *New York, John Wiley and Sons.*

Mathis J.S.(1988) Summary and future prospects. *In; Dust in the universe (Eds: M.E. Bailey and D.A. Williams), Cambridge Uni.Press, Cambridge*, 521-532.

Mathis J.S., Rumpl W. and Nordsieck K.H.(1977) The size distribution of interstellar grains. *Astrophys.J.*, 217, 425-433.

Matsakis D.N., Chui M.F., Goldsmith P.F. and Townes L.H.(1976) Observations of the $^{12}C/^{13}C$ ratios in four galactic sources of formaldehyde. *Astrophys.J.*, 206, L36-66.

Mattey D.P., Carr R.H., Wright I.P. and Pillinger C.T.(1984) Carbon isotopes in submarine basalts. *Earth Planet.Sci.Letts.*, 70, 196-206.

Mattey D.P., Exley R.A. and Pillinger C.T.(1989) Carbon isotopic composition of co-existing fluid and dissolved species in basalt glass. *Geochim.et Cosmochim.Acta.*, 53, 2377-2386.

Maurette M., Hammer C., Brownlee D.E., Reeh N. and Thomsen H.H.(1986) Placers of cosmic dust in the blue ice lakes of Greenland. *Science*, 233, 869-872.

Maurette M., Hammer C., Pourchet M. and Brownlee D.E.(1988) The "Blue lake II" expedition of July-August 1987 in Greenland, and the search for mm-sized unmelted extraterrestrial particles. *Lunar.Planet.Sci.Conf.*, 19, 744-745.

Maurette M., Jehanno C., Robin E. and Hammer C.(1987) Characteristics and mass distribution of extraterrestrial dust from the Greenland Ice Cap. *Nature*, 328, 699-702.

Maurette M., Olinger C., Christophe Michel-Levy M., Kurat G., Pourchet M., Brandstatter F. and Bourdot-Denise M.(1991) A collection of diverse micrometeorites recovered from 100 tonnes of Antarctic blue ice. *Nature*, 351, 44-47.

McFadden L.A., Tholen D.J. and Veeder G.J.(1989) Physical properties of Aten ,Apollo and Amor asteroids, *In; 'Asteroids II', Eds; Binzel R.P., Gehrels T. and Matthews M.S., Uni.Arizona Press, Tuscon, Arizona*, 442-467.

McKeegan K.D.,Walker R.M. and Zinner E.(1985) Ion microprobe isotopic measurements of individual interplanetary dust particles . *Geochim.et Cosmochim.Acta.*, 49, 1971-1987.

McKinney C.R.,McCrea J.M.,Epstein S.,Allen H.A. and Urey H.C.(1950) Improvements in mass spectrometers for the measurement of small differences in isotope abundance ratios. *Rev.Sci.Instrum.*, 21, 724-730.

McNaughton N.J.,Abell P.I.,Wright I.P.,Fallick A.E. and Pillinger C.T.(1983) Preparation of nanogram quantities of deuteromethane for stable carbon isotope analysis. *J.Phys.E.Sci.Instrum.*, 16, 505-511.

McSween H.Y. (Jr)(1987) Meteorites and their parent planets. *Cambridge Uni.Press, Cambridge*, 237pp.

McSween H.Y., Sears D.W.G. and Dodd R.T.(1988) Thermal metamorphism. *In; Meteorites and the early solar system (Eds: J.F.Kerridge and M.S. Matthews), Uni.Arizona Press, Tucson, Arizona*, 102-113.

Millard H.T.(Jr) and Finkelman R.B.(1970) Chemical and mineralogical compositions of cosmic dust and terrestrial spherules from a marine sediment. *J.Geophys.Res.*, 75, 2125-2134.

Millman P.M.(1975) Dust in the Solar System. *In: The dusty universe (Eds: G.B.Field and A.G.W.Cameron), Neale Watson Academic Publ., N.Y.*, 185-210.

Misawa K., Ma S.L., Yamakoshi K., Nogami K. and Nakamura N.(1989) Rare earth element abundances in individual magnetic, stony spherules from deep-sea sediments. *Lunar.Planet.Sci.Conf.*, **20**, 695-696.

Moore C.B. and Lewis C.F.(1967) Total carbon contents of Ordinary Chondrites. *J.Geophys.Res*, **72**, 6289-6292.

Moore C.B., Lewis C.F. and Nava D.(1969) Superior analyses of Iron Meteorites. *In: 'Meteorite Research' (Ed; P.Millman), Dordrecht*, 738-748.

Moore P. and Hunt G.(1990) The atlas of the Solar System. *Mitchell Beazley Int.Ltd, London*, 463pp.

Morrison D.A. and Zinner E.(1977) Distribution and flux of micrometeoroids. *Phil.Trans.R.Soc.Lond.*, **A285**, 379-384.

Mukhin L.M., Dolnikov G.G., Evlanov E.N., Fomenkova M.N., Prilutsky O.F. and Sagdeev R.(1991) Re-evaluation of the chemistry of dust grains in the coma of Comet Halley. *Nature*, **350**, 480-481.

Mullie F. and Reisse J.(1987) Organic matter in carbonaceous chondrites. *Topics in Current Chemistry*, **139**, 83-117.

Muncaster R.(1981) A-level physics. *Stanley Thornes (Publ.) Ltd, UK*, 792pp.

Murata K.J., Freidman I.I. and Madsen B.M.(1967) Carbon-13-rich diagenetic carbonates in Miocene formations of California and Oregon. *Science*, **156**, 1484-1486.

Murphey B.F.(1947) The temperature variation of thermal diffusion factors for binary mixtures of H, D and He. *Phys.Rev.*, **72**, 834-837.

Murphey B.F. and Nier A.O.(1941) Variations in the relative abundance of the carbon isotopes. *Phys.Rev.*, **59**, 771-772.

Murray J.(1876) On the distribution of volcanic debris over the floor of the ocean - its character, source, and some of the propducts of its disintigration and decomposition. *Roy.Soc.Edinburgh.Proc.*, **9**, 247-261.

Murray J. and Renard A.F.(1884) Measurement characters of volcanic ashes and cosmic dust, and their origin in deep-sea sediment deposits. *Proc.Roy.Soc.Edinburgh*, **12**, 474-495.

Murray S. and Renard A.F.(1891) Report of the scientific results of the voyage of H.M.S. Challenger, **3**, *Neill and Co., Edinburgh.*

Mutch T.A.(1964) Extraterrestrial particles in Palaeozoic salts. *Annals N.Y.Acad.Sci.*, **119**, 166-185.

Nagel K., Fechtig H., Schneider E. and Neukum G.(1976) Micrometeorite impact craters on Skylab experiment S149. *Lecture notes in physics - 'Interplanetary dust and the zodiacal light' (Eds; Ehlers J. et al.)*, **48**, 275-278.

Neugebauer G., Habing H.J., Van Duinen R., Aumann H.H., Baud B., Beichman C.A., Beintema D.A., Boggess N., Clegg P.E., De Jong T., Emerson J.P., Gautier T.N., Gillett F.C., Harris S., Hauser M.G., Houck J.R., Jennings R.E., Low F.J., Marsden P.L., Miley G., Olnon F.M., Pottasch S.R., Raimond E., Rowan-Robinson M., Soifer B.T., Walker R.G., Wesselius R.R. and Young E. (1984) The Infrared astronomical satellite (IRAS) mission. *Astrophys.J.*, **278**, L1-L6.

Newman M.J. and Talbot R.J.(1976) Solar neutrinos and solar accretion of interstellar matter. *Nature*, **262**, 559-560.

Ney E.P.(1982) Optical and infrared observations of bright comets in the range 0.5um to 20um . *In; Comets (Ed; L.L.Wilkening), Uni.Arizona Press, Tucson, Arizona*, 766pp.

Nielsen H.P. and Buchvald V.(1981) Roaldite, a new nitride in iron meteorites. *Proc.Lunar.Sci.Conf.*, **XII**, 1343-1348.

Nier A.O.(1940) A mass spectrometer for routine abundance measurements . *Rev.Sci.Instrum.*, **11**, 212-216.

Nier A.O.(1947) A mass spectrometer for isotope and gas analysis. *Rev.Sci.Instrum.*, **18**, 398-411.

Nier A.O. and Gulbransen E.A.(1939) Variations in the relative abundance of the carbon isotopes. *J.Am.Chem.Soc.*, **61**, 697-698.

Nier A.O. and Schlutter D.J.(1988) Helium and neon in individual extraterrestrial particles. *Lunar.Planet.Sci.Conf.*, **19**, 858-859.

Nier A.O., McElroy M.B. and Yang Y.L.(1976) Isotopic composition of the Martian Atmosphere. *Science*, **196**, 68-70.

Nishiizumi K.(1983) Measurement of 53Mn in deep-sea iron and stony spherules. *Earth and Planet.Sci.Letts.*, **63**, 223-228.

Olsson-Steel D.I.(1988) The near Earth flux of microgram dust. *In; Dust in the universe (Eds: M.E. Bailey and D.A. Williams), Cambridge Uni.Press, Cambridge*, 187-192.

Oort J.H.(1990) The orbital distribution of comets. *In; Physics and chemistry of comets (Ed: W.F.Huebner), Springer Verlag*, 235-244.

Opik E.(1937) *Pub.Univ.Tartu.*, **29**, 51.

Opik E.J.(1956) Interplanetary dust and terrestrial accretion of meteoritic matter. *Irish Astron.J.*, **4**, 84-135.

Otting W. and Zahringer J.(1967) Total carbon content and primordial rare gases in chondrites. *Geochim.et Cosmochim.Acta.* , **31**, 1949-1960.

Owen T.(1973) The isotope ratio $^{12}C/^{13}C$ in comet Tago-Sata-Kosaka 1969g. *Astrophys.J.*, **184**, 33-43.

Pagel B.E.J.(1987) Galactic chemical evolution, *In; The Galaxy, Eds; Gilmore G. and Carswell B., NATO AS series C; Mathematical and physical sciences, Reidel.*, **207**, 341-364.

Parkin D.W. and Tilles D.(1968) Influx measurements of extraterrestrial material. *Science*, **159**, 936-946.

Parkin D.W., Sullivan R.A.L. and Andrews J.N.(1977) Cosmic spherules as rounded bodies in space. *Nature*, **266**, 515-517.

Penzias A.A.(1980) Nuclear processing and isotopes in the galaxy. *Science*, **208**, 663-669.

Pettersson H. and Fredriksson K.(1958) Magnetic spherules in deep-sea deposits. *Pacific Science*, **12**, 71-81.

Pillinger C.T.(1984) Light element stable isotopes in meteorites- from grams to picograms. *Geochim.et Cosmochim.Acta.* , **48**, 2739-2766.

Pillinger C.T., Ash R.D. and Arden J.W.(1989) The role of CVD in the production of interstellar grains. *Meteoritics*, **24**, 434.

Piotrowski S.(1953) The collisions of asteroids. *Acta Astronomica*, **5**, 115-136.

Podsiadlowski Ph., Pringle J.E. and Rees M.J.(1991) The origin of the planet orbiting PSR1829-10. *Nature*, **352**, 783-784.

Pompeau G., Rajan R.S., Walker R.M. and Zinner E.(1977) The modern and ancient flux of solar wind particles, solar flare particles and micrometeoroids. *Space Res.*, **17**, 599-604.

Poynting J.H.(1903) Radiation in the solar system: Its effect on temperature and its pressure on small bodies. *Phil.Trans.Roy.Soc.*, **A202**, 525-552.

Presper T. and Palme H.(1992) Are chondrules precursors of some cosmic spherules?. *Meteoritics*, **26**, 386.

Prombo C.A., Nichols R.H., Alexander C.M.O.D., Swan P.D., Walker R.M. amd Maurette M.(1991) SiC in Greenland lake sediments. *Lunar.Planet.Sci.Conf.*, **22**, 1103-1104.

Prosser S.J.,Wright I.P. and Pillinger C.T.(1990) A preliminary investigation into the isotopic measurement of carbon at the picomole level using static vacuum mass spectrometry. *Chem.Geol.*, **83**, 234-246.

Rasio F.A., Nicholson P.D., Shapiro S.L. and Teukolsky S.A.(1992) An observational test for the existence of a planetary system orbiting PSR1257+12. *Nature*, **355**, 325-326.

Ray G. and Hart S.R.(1982) Quantitative analyses of silicates by ion microprobe. *Int.J.Mass Spectrom.Ion Phys.*, **44**, 231-255.

Reinhard R.(1986) The Giotto encounter with Comet Halley. *Nature*, **321**, 313-318.

Reynolds J.H.(1956) High sensitivity mass spectrometer for noble gas analysis. *Rev.Sci.Instrum.*, **27**, 928-934.

Rickman H. and Huebner W.F.(1990) Comet formation and evolution. *In; Physics and chemistry of comets (Ed: W.F.Huebner), Springer Verlag*, 245-304.

Rietmeijer F.J.M. and Mackinnon I.D.R.(1985) Poorly graphitised carbon as a new cosmothermometer for primitive extraterrestrial materials. *Nature*, **315**, 733-735.

Robert F. and Epstein S.(1982) The concentration and isotopic composition of hydrogen, carbon and nitrogen in carbonaceous chondrites. *Geochim.et Cosmochim.Acta.* , **46**, 81-95.

Robertson H.P.(1937) Dynamical effects of radiation in the solar system. *Roy.Astron.Soc.M.N.*, **97**, 423-438.

Robin E., Christophe Michel-Levy N., Bourdot-Denise M. and Jehanno C.(1990) Crystalline micrometeorites from Greenland blue lakes: Their chemical composition, mineralogy and possible origin. *Earth and Planet.Sci.Letts.*, **97**, 162-176.

Robin E., Jehanno C. and Maurette M.(1988) Characteristics and origins of Greenland Fe/Ni cosmic grains. *Proc.Lunar.Planet.Sci.*, **18**, 593-598.

Robin E., Jehanno C., Koerner R.M., Picon J. and Rocchia R.(1990) Discovery of non-contaminated unmelted cosmic dust particles in Antarctica and Northern Canada territories. *Lunar.Planet.Sci.Conf.*, **21**, 1023-1024.

Rogers M.A., van Hinte J.E. and Sugden J.G.(1972) Organic carbon ^{13}C values from Cretaceous, Tertiary and Quaternary main sequences in the North Atlantic, *In 'Initial Reports of the Deep Sea Drilling Project' (Eds: A.S. Laughton and Berggren N.A.)* ,**12**, 1115-1121.

Russell H.N.(1937) Radiation pressure (How The Sun and The Stars, due to the pressure of their light, ultimately clean up the smaller particles in their own immediate neighbourhoods). *Sci.Am.*, **November**, 274-275.

Russell S.S., Arden J.W. and Pillinger C.T.(1991a) Evidence for multiple sources of diamond from primitive chondrites. *Science*, **254**, 1188-1191.

Russell S.S., Ash R.D., Pillinger C.T. and Arden J.W.(1991b) Meteoritic SiC - separate grain population and multiple components revealed by stepped combustion. *Meteoritics*, **26**, 390.

Safronov V.S.(1969) Evolution of the protoplanetary cloud and formation of the Earth and planets, *Nauka, Moscow*, 256pp.

Sagdeev R.Z., Blamont J., Galeev A.A., Moroz V.I., Shapiro V.D., Sherchenko V.I. and Szego K.(1986) Vega spacecraft encounters with Comet Halley. *Nature*, **321**, 259-262.

Sakai H.,Smith J.W.,Kaplan I.R. and Petrowski C.(1976) Micro-determinations of C,N,S,H,He,metallic Fe,$\delta^{13}C$,$\delta^{15}N$ and $\delta^{34}S$ in geologic samples . *Geochem.J.*, **10**, 85-96.

Sandford S.A.(1987) The collection and analysis of extraterrestrial dust particles. *Fundament.Cosmic Phys.*, **12**, 73-1.

Sandford S.A. and Bradley J.P.(1989) Interplanetary dust particles collected in the stratosphere: Observations of atmocspheric heating and constraints on their interelationships and sources. *Icarus*, **82**, 146-166.

Sarda Ph., Staudaucher Th. and Allegre C.J.(1991) Complete rare gas study of a very large unmelted cosmic dust particle fron Greenland. *Lunar.Planet.Sci.Conf.*, **21**, 1165-1166.

Schidlowski M., Hayes J.M. and Kaplan I.R.(1983) Isotopic inferences of ancient biochemistries: carbon, sulphur, hydrogen, and nitrogen, *In: 'Earth's earliest biosphere' (Ed: J.W. Schopf), Princetown Uni.Press*, 149-186.

Schmidt R.A.(1964) Microscopic extraterresrial particles from the Antarctic Peninsula. *Annals N.Y.Acad.Sci.*, **119**, 186-204.

Schmidt R.A.(1965) A survey of data on microscopic extraterrestrial particles. *NASA Rep.TND-2719.*

Schoeller D.A. and Hayes J.M.(1975) Computer controlled ion counting isotope ratio mass spectrometer. *Anal.Chem.*, **47**, 408-415.

Schramm L.S. and McKay D.S.(1986) An impact crater containing meteoritic material in a louver from the solar max satellite: A comparison with experimentally produced craters. *Meteoritics*, **21**, 504-505.

Schramm L.S., Brownlee D.E. and Wheelock M.M.(1989) The elemental composition of interplanetary dust. *Lunar.Planet.Sci.Conf.*, **19**, 1033.

Schwehm G.(1989) Rosetta/CNSR, ESA's planetary cornerstone mission. *Physics and mechanics of cometary materials*, ESA SP-302, 11-15.

Scott E.R.D. and Wasson J.T.(1975) Clasification and properties of iron meteorites. *Rev.Geophys.Space Phys.*, **13**, 527-546.

Scott E.R.D., Brearly A.J., Kiel K., Grady M.M., Pillinger C.T., Clayton R.N., Mayeda T.K., Wieler R. and Signer P.(1988) Nature and origin of C-rich ordinary chondrites and chondritic clasts. *Proc.Lunar Planet.Sci.Conf.*, **18**, 513-523.

Shima M. and Kimoto S.(1966) The black particle found on Mt Nurikura. *Chem.Geol.*, **1**, 77-80.

Shoemaker E.M.(1977) Astronomically observable crater forming projectiles. *In; 'Impact and explosion cratering. Planetary and terrestrial implications' (Eds; Roddy D.J. and Repin R.O.), Pergamon, N.Y.*, 617-628.

Silverman M.P. and Oyama V.I.(1968) Automatic apparatus for sampling and preparing gases for mass spectral analysis in studies of carbon isotope fractionation during methane metabolism. *Anal.Chem.*, **40**, 1833-1837.

Smales A.A., Mapper D. and Wood A.J.(1958) Radioactivation analysis of "cosmic" and magnetic spherules. *Geochim.et Cosmochim.Acta.* , **13**, 123-126.

Smith P.P.K. and Buseck P.R.(1981) Graphitic carbon in the Allende meteorite: A microstructural study. *Science*, **212**, 322-324.

Smith J.W. and Kaplan I.R.(1970) Endogenous carbon in carbonaceous meteorites. *Science*, **167**, 1367-1370.

Solc M., Jessberger E.K., Hsiung P. and Kissel J.(1987) Halley dust composition. *Proc.10th Regional Meeeting of the IAU, Prague*, 47-51.

Spitzer L.(Jr)(1968) Diffuse matter in space. *Interscience Publ., N.Y.*, 262pp.

Stadermann F.J.(1991) Rare earth and trace element abundances in individual IDPs. *Lunar.Planet.Sci.Conf.*, **22**, 1311-1312.

Steele I.M.(1991) Forseritic compositions in Antarctic micrometeorites compared with other extraterrestrial samples. *Lunar.Planet.Sci.Conf.*, **22**, 1321-1322.

Stern S.A. and Shull J.M.(1990) The role of comet clouds in the mass and chemical balance of the interstellar medium. *Astrophys.J.*, **359**, 506-511.

Stern S.A., Stocke J. and Weissman P.R.(1991) An IRAS search for extra-solar Oort Clouds. *Icarus*, **91**, 65-75.

Stewart W.D.P. (Ed)(1974) Algal Physiology and Biochemistry. *Botanical Monographs*, **10**, pp.989.

Swart P.K., Grady M.M., Pillinger C.T., Lewis R.S. and Anders E.(1983a) Interstellar carbon in meteorites. *Science*, **220**, 406-410.

Swart P.K.,Grady M.M. and Pillinger C.T.(1983b) A method for the identification and elimination of contamination during carbon isotopic analyses of extraterrestrial samples. *Meteoritics.*, **18**, 137-153.

Sykes M.V., Lebofsky L.A., Hunten D.M. and Low F.(1986) The discovery of dust trails in the orbits of periodic comets. *Science*, **232**, 1115-1117.

Tang Ming, Lewis R.S., Anders E., Grady M.M., Wright I.P. and Pillinger C.T.(1988) Isotopic anomalies of Ne, Xe, and C in meteorites.I. Seperation of carriers by density and chemical resistance. *Geochim.et Cosmochim.Acta.* , **52**, 1221-1234.

Tauber G.E.(1979) Man's view of the universe. *Crown Publ.Inc., N.Y.*, 352pp.

Telesco C.M. and Knacke R.F.(1991) Detection of silicates in the B Pictoris disk. *Astrophys.J.*, **372**, L29-31.

Thomas K.L., Zolensky M.E., Klock W. and McKay D.S.(1990) Mineralogical descriptions of eight hydrated interplanetary dust particles and their relationships to chondritic matrix. *Lunar.Planet.Sci.Conf.*, **21**, 1250-1251.

Thomas R.M., Whitham P.S. and Elford W.G.(1986) Frequency dependence of radar meteors echo rates. *Proc.Astron.Soc.Aust.*, **6**, 303-306.

Tissot B.P. and Welte D.H.(1984) Petroleum formation and occurence, *Springer-Verlag*, 699pp.

Tomeoka K. and Buseck P.R.(1986) A carbonate-rich, hydrated, interplanetary dust particle: Possible residue from protostellar clouds. *Science*, **231**, 544-546.

Trimble V.(1975) The origin and abundances of the chemical elements. *Rev.Mod.Phys.*, **47**, 877-976.

Trumpler R.J.(1930) Absorption of light in the galactic system. *Publ.Astr.Soc.Pacific*, **42**, 214-227.

Urey H.C.(1948) Oxygen isotopes in nature and the laboratory. *Science*, **108**, 489-497.

Urey H.C. and Craig H.(1953) The composition of stone meteorites and the origin of meteorites. *Geochim.et Cosmochim.Acta.* , **4**, 36-82.

Van der Hulst H.C.(1947) Zodiacal light in the solar corona. *Astrophys.J.*, **105**, 471-488.

Van Schmus W.R. and Wood J.A.(1967) A chemical-petrologic classification for the chondritic meteorites. *Geochim.et Cosmochim.Acta.* , **31**, 747-763.

Vanysek V.(1977) Comets, asteroids and meteorites *(Ed; A.H. Delsemme), Uni.Toledo Press, USA*, 499pp.

Vanysek V. and Rahe J.(1978) The $^{12}C/^{13}C$ isotope ratio in comets, stars and interstellar matter. *The Moon and Planets*, **18**, 441-446.

Vdovykin G.P.(1970) Ureilites. *Sp.Sci.Rev.*, **10**, 483-510.

Verniani F.(1969) Structure and fragmentation of meteoroids. *Space Sci.Rev.*, **10**, 230-261.

Von Michaelis H., Ahrens L.H. and Willis J.P.(1969) The composition of stony meteorites II. The analytical data and an assessment of their quality. *Earth and Planet.Sci.Letts.*, **5**, 387-394.

Wannier P.G.(1980) Nuclear abundances and the evolution of of the interstellar medium. *Ann.Rev.Astron.Astrophys.*, **18**, 399-437.

Wasserberg G.J.(1985) Short-lived nuclei in the early solar system, *In: "Protostars and planets II", Eds: Black D.C. and Matthews M.S., Uni.Arizona Press, Tuscon, Arizona*, 703-737.

Wasson J.T.(1974) Meteorites, *Springer-Verlag, Berlin, Germany*, 316pp.

Watson W.D., Anicich V.G. and Huntress W.T. (Jr)(1976) Measurement and significance of the reaction $^{13}C+ + {}^{12}CO = {}^{12}C+ + {}^{13}CO$ for the alteration of the $^{13}C/^{12}C$ ratio in interstellar molecules. *Astrophys.J.*, **205**, L165-168.

Weast R.C.(1987) CRC handbook of chemistry and physics 1st student edition, *CRC Press Inc., Boca Raton, Florida, USA*, 1916pp.

Weiss-Wrana K.(1983) Optical properties of interplanetary dust; Comparison with light scattering by larger meteoritic and terrestrial grains. *Astron.Astrophys.*, **126**, 240-250.

Weissman P.R.(1985) The origin of comets: Implications for planetary formation, *In: 'Protostars and Planets II', Eds: D.C.Black and M.S.Matthews, Uni.Arizona Press, Tuscon*, 895-920.

Weissman P.R.(1986) Are cometary nuclei primordial rubble piles?. *Nature*, **320**, 242-244.

Weissman P.R.(1990) The Oort Cloud. *Nature*, **344**, 825-830.

Wetherill G.W.(1985) Asteroidal sources of Ordinary chondrites. *Meteoritics*, **20**, 22-Jan.

Wetherill G.W.(1991) Occurence of Earth-like bodies in planetary systems. *Science*, **253**, 535-536.

Wetherill G.W. and Stewart G.R.(1989) Accumulation of a swarm of small planetesimals. *Icarus*, **77**, 330-357.

Whipple F.L.(1950a) A comet model.1. The acceleration of Comet Encke. *Astrophys.J.*, **111**, 375-375.

Whipple F.L.(1950b) The theory of micro-meteorites. Part 1. In an isothermal atmosphere. *Proc.Natl.Acad.Sci.US.*, **36**, 687-695.

Whipple F.L.(1951) The theory of micrometeorites, part II: in heterothermal atmospheres. *Proc.Natl.Acad.Sci.US.*, **37**, 19-30.

Whipple F.L.(1967) On maintaining the meteoritic complex. *NASA Sp-150 (Zodiacal light and the interplanetary medium)*, 409-426.

Whipple F.L.(1978) Comets. *In: Cosmic Dust (Ed: J.A.M. McDonnell). Wiley*, 73-1.

Whipple F.L.(1987) A review of cometary sciences. *Phil.Trans.R.Soc.Lond.*, **A323**, 339-347.

Wiik H.B.(1972) The chemical composition of the Havero meteorite, and the genesis of the Ureilites. *Meteoritics*, **7**, 553-557.

Williams D.A.(1988) Chenical effects of dust. *In; Dust in the universe (Eds: M.E. Bailey and D.A. Williams), Cambridge Uni.Press, Cambridge*, 391-402.

Wood J.A.(1967) Chondrites: their metallic minerals, thermal histories and parent bodies. *Icarus*, **6**, 1-49.

Wood J.A. and Morfill G.E.(1988) A review of solar nebula models. *In; Meteorites and the early solar system (Eds: J.F.Kerridge and M.S. Matthews), Uni.Arizona Press, Tucson, Arizona*, 329-347.

Wong W.W., Benedict C.R. and Kohel R.J.(1979) Enzymic fractionation of the stable isotopes of carbon dioxide by vibulose-1,5 biophosphate carboxylate. *Plant.Physiol.*, **63**, 852-856.

Wright I.P.(1984) $\delta^{13}C$ measurements of smaller samples. *Trends in Anal.Chem.*, **3**, 210-215.

Wright I.P. and Pillinger C.T.(1989) Carbon isotopic analysis of small samples by the use of stepped-heating extraction and static mass spectrometer. *In: New frontiers in stable isotopic research: Laser probes, ion probes, and small-sample analysis. US Geological Survey Bulletin 1890*, 9-34.

Wright I.P.,Carr R.H. and Pillinger C.T.(1988) Carbon stable isotope analyses of individual deep-sea spherules. *Meteoritics*, **23**, 339-349.

Wright I.P.,McNaughton N.J.,Fallick A.E.,Gardiner L.R. and Pillinger C.T.(1983) A high precision mass spectrometer for stable carbon analysis at the nanogram level. *J.Phys.E.Sci.Intsrum.*, **16**, 497-504.

Wyckoff S., Lindholm E., Wehinger P.A., Peterson B.A., Zucconi J-M. and Festou M.C.(1989) The $^{12}C/^{13}C$ abundance ratio in Comet Halley. *Astrophys J.*, **339**, 488-500.

Yang J. and Epstein S.(1984) Relic grains in the Murchison meteorite. *Nature*, **311**, 544-547.

Yates P.D., Wright I.P. and Pillinger C.T.(1992) Application of high-sensitivity carbon isotope techniques - a question of blanks. *Chem.Geol.(Isotop.Geosci.Sect.)*, **101**, 81-91.

Zinner E.(1988) Interstellar cloud material in meteorites. *In; Meteorites and the early solar system (Eds: J.F.Kerridge and M.S. Matthews), Uni.Arizona Press, Tucson, Arizona*, 956-983.

Zinner E. and Epstein S.(1987) Heavy carbon in individual oxide grains from the Murchison CM meteorite. *Earth Planet.Sci.Letts.*, **84**, 359-368.

Zinner E. and McKeegan K.D.(1984) Ion probe measurements of hydrogen and carbon isotopes in interplanetary dust. *Lunar.Planet.Sci.Conf.*, **15**, 961-962.

Zinner E., Amari S. and Lewis R.(1991) Silicon carbide from a supernova?. *Meteoritics*, **26**, 413.

Zinner E., McKeegan K.D. and Walker R.M.(1983) Laboratory measurements of D/H ratios in interplanetary dust. *Nature*, **305**, 119-121.

Zinner E., Wopenka B., Amari S. and Anders E.(1990) Interstellar graphite and other carbonaceous grains from the Murchison meteorite: Structure, composition and isotopes of C, N, and neon. *Lunar.Planet.Sci.Conf.*, **21**, 1379.

Zolensky M.E. and McSween H.Y.(Jr)(1988) Aqueous alteration. *In; Meteorites and the early solar system (Eds: J.F.Kerridge and M.S. Matthews), Uni.Arizona Press, Tucson, Arizona*, 114-164.

Zolensky M.E., Webb S.J. and Thomas K.L.(1988) The search for refractory interplanetary dust particles from pre-industrial aged Antarctic Ice . *Proc.Lunar.Planet.Sci.*, **18**, 599-605.